# Ophiolites of the eastern Vardar Zone, N. Greece.

**Panagiotis T. Zachariadis**

geboren in Thesssaloniki, Griechenland

Mainz, Juli 2007

# Foreword

This PhD thesis has started in winter 2003 in Mainz under the supervision of Prof. Dr. T. Reischmann. Results of this study have been presented in international conferences and resulted in the publication of the following abstracts so far:

*Zachariadis P., Kostopoulos D., Reischmann T., Himmerkus F., Matukov D., Sergeev S., (2006). U–Pb ion-microprobe zircon dating of subduction-related magmatism from northern Greece: The ages of the Guevgueli, Thessaloniki and Chalkidiki igneous complexes. Geophysical Research Abstracts, Vol. 8, 05560*

*Zachariadis P., Reischmann, T.; Kostopoulos, D., (2007a). The Thessaloniki Ophiolite. A Middle Jurrassic supra-subduction zone ophiolite between the Vardar Zone and the Serbomacedonian Massif, N. Greece. EGU General Assembly 2007". EGU2007-A-10069.*

*Zachariadis P., Kostopoulos D., Reischmann T., Sklavounos S., (2007b). Petrogenesis and tectonic setting of the Oraeokastro Ophiolite, N. Greece: Petrological, geochemical and isotopic constraints. EGU General Assembly 2007. EGU2007-A-10034.*

The writer of this thesis had been involved in other research projects during this period. The results of those projects were also presented in international conferences. A list is given below.

*Himmerkus F., Zachariadis P., Reischmann T., Kostopoulos D., (2005). The mafic complexes of the Athos-Volvi-Zone – a suture zone between the Serbo-Macedonian Massif and the Rhodope Massif? Geophysical Research Abstracts, EGU05-A-10240.*

*Kostopoulos D., Zachariadis P., Godelitsas A., Reischmann T., Baltatzis E. and. Papanikolaou D. (2006). First report on post-Miocene rhyolitic volcanism from Ikaria Island, central Aegean, Greece. NECAM 2006, International conference on Neogene Magmatism of the Central Aegean and Adjacent areas.*

*Boudi D., Prophitis E., Zachariadis P., Kostopoulos D., Baltatzis E., and Chatzitheodoridis E, (2007). Petrology, geochemistry and geotectonic setting of the Titaros Ophiolite and associated Pelagonian basement rocks in the area of Mt. Olympos. Bulletin of the Geological*

# **Abstract**

In the frame of the present thesis the geochemistry, petrology and geochronology of ophiolites that are located in North Greece was studied in order to give insights on the geochemical and geodynamic processes that lead to their genesis and evolution.

Northern Greece is a geologically complex area where continental blocks of different provenance and age came together. These continental blocks, or terranes, are separated by zones of low-grade to amphibolite facies rock associations of both sedimentary and igneous origin. From east to west the metamorphic continental block of the Rhodope Massif comes into contact with that of the Serbo-Macedonian Massif along the Athos-Volvi-Thermes suture zone. In turn, the Serbo-Macedonian Massif is bordered to the west by the Peonias subzone of the Vardar Zone. Their interface is a narrow belt of rocks consisting of limestones, metasedimentary and volcanosedimentary rocks, as well as granitic rocks and ophiolite complexes which has been termed the Circum-Rhodope Belt. From north to south these are the Guevguely, Oraeokastro, Thessaloniki, and Chalkidiki ophiolites. The importance of those ophiolites is that they mark a subduction zone in the easternmost border of the Vardar Ocean, suggesting that there was an active margin along the southernmost border of the Serbo-Macedonian and Rhodope massif. A detailed study aiming to investigate the formation of these ophiolites would add up important information on the evolution of the Vardar Ocean and allow us to understand the processes that took place at the active margin where the suture of this system took place.

The aim of this thesis was accomplished through detailed studies on the mineral as well on the whole rock geochemistry using high-precision analytical equipment. Additionally the results obtained from the major and trace element chemistry were coupled Nd and Sr isotopic data. In order to precisely place the evolution of these ophiolites in time, U-Pb geochronology on zircons was conducted using a SHRIMP-II.

The chemistry of the ophiolites has in variable proportions typical characteristics of subduction zone magmatism (e.g. Nb anomalies, Th enrichment). Normalised to normal mid-ocean ridge basalt (N-MORB) high field strength element patterns vary from depleted to sub-parallel to the N-MORB line. Rare earth element patterns (REE) normalised to C1-chondrite have a flat heavy-REE section suggesting shallow regime of source melting for all the ophiolites. The majority of the samples have light-REE depletes patterns. $^{87}Sr/^{86}Sr$ isotopic ratios are in cases influenced by alteration. The $\varepsilon_{Nd}$ values recalculated for Middle Jurassic are positive but lower than N-MORB and depleted mantle. With exception to the Thessaloniki ophiolite that has a uniform chemical character, the rest of the ophiolites show twofold chemistry consisting of rocks of that are similar to the N-MORB with minor subduction zone characteristics and rocks with more pronounced subduction zone characteristics. Tectonomagmatic discrimination schemes classify the samples as island arc tholeiites and

back-arc basin basalts or N-MORB. Melting modelling applied to evaluate the source properties and the degree of melting verifies the twofold nature of the ophiolites.

As deduced from geochemical and petrological investigations, the ophiolites from the Guevguely complex, Oraeokastro, Thessaloniki, and Chalkidiki represent relics of supra-subduction zone ophiolites that have formed in succeeding stages of island arc rifting and back-arc spreading. The geochronological studies made in the frame of this thesis place the formation of these ophiolites between 160 and 169 Ma.

The possible evolution of these ophiolites would include an eastward subduction of the Vardar Ocean in an intra-oceanic setting during the Middle Jurassic. In the first stages of the supra-subduction zone development (170-165 Ma) the formation of the low-$K_2O$ acidic magmatism that we meet now in some Paikon andesites, the rhyolites in Mikro Dasos and in parts of the Chortiatis Magmatic Suite took place. Contemporaneously, generation of mafic magmatism occurred, as we find it in the western part of the Guevguely ophiolite (Skra), Thessaloniki, probably in Oraeokastro (represented by a low $TiO_2$ group of mafic extrusives) and in less extend in Kassandra. As the subduction continued the arc was rifted further as a result of subduction rollback and asthenosphere upwelling, and the formation of the eastern part of the Guevguely ophiolite (Evzonoi), Oraeokastro (represented by a high $TiO_2$ group of mafic extrusives), and Kassandra ophiolites (161-155 Ma) took place in a setting resembling the Marianas. Synchronously we have the initiation of an eastward subduction that resulted in the closure of this back arc basin probably below the Chortiatis – Mikro Dasos arc and the evolution of the Sithonia ophiolite in the fore-arc region.



**Schematic representation of the progressive ophiolite evolution in the eastern Vardar Ocean.**
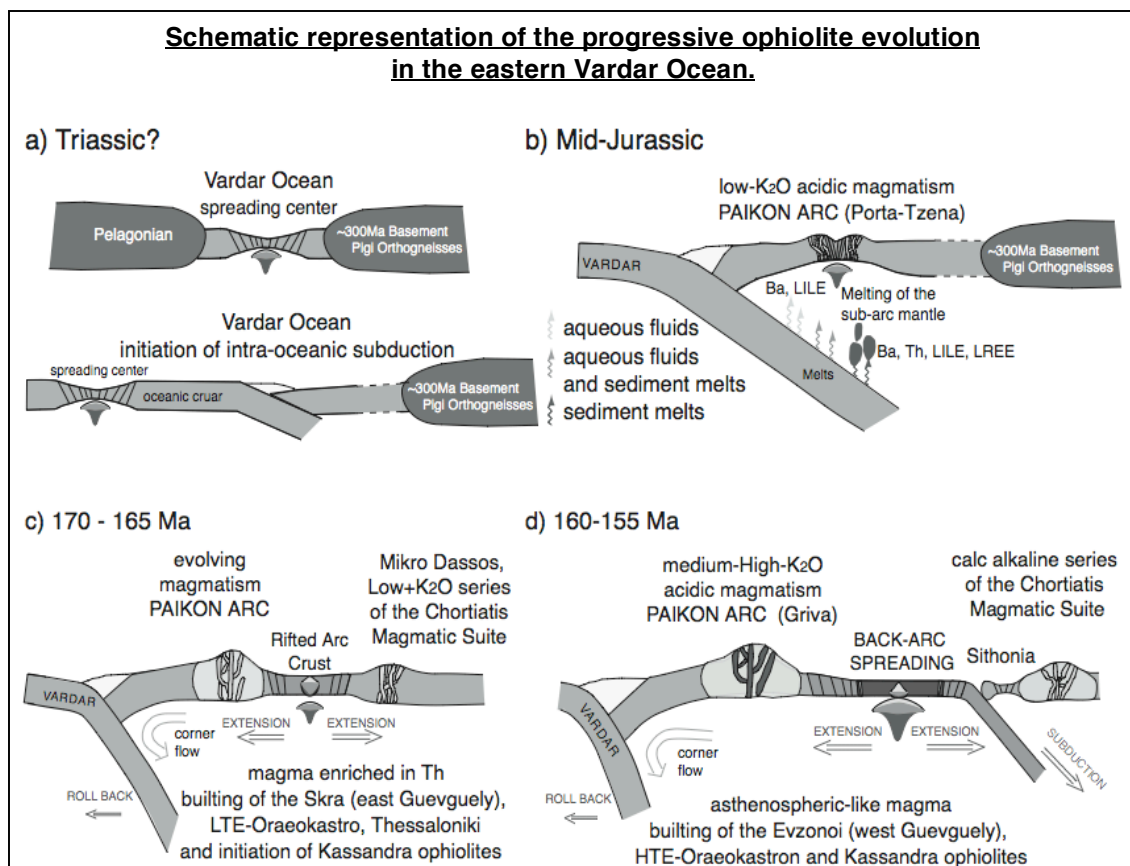
# Zusammenfassung

Im Rahmen dieser Arbeit wird die Geochemie, Petrologie und Geochronologie der Ophiolithe Nordgriechenlands untersucht, um einen Einblick in die Prozesse Ihrer Entstehung und Entwicklung zu bekommen.

Das Gebiet Nordgriechenlands umfasst ein geologisch komplexes Areal, zusammengesetzt aus kontinentalen Blöcen verschiedenartiger Herkunft und unterschiedlichen Alters. Diese kontinentalen Blöcke, oder „Terranes", sind voneinander durch Bereiche niedriggradiger bis amphibolithfazieller Gesteinsassoziationen, sowohl sedimentären als auch vulkanischen Ursprungs, getrennt. Im Verlauf von Ost nach West liegt entlang der Athos-Volvos-Thermes-Sutur der metamorphe kontinentale Block des Rhodope-Massivs in Kontakt mit dem Block des Serbisch-Makedonischen Massivs. Dieses grenzt seinerseits im Westen an die Peonias-Subzone der Vardar-Zone. Diese Nahtstelle, bezeichnet als Circum-Rhodope-Belt, besteht aus einem schmalen Gürtel aus Karbonaten, meta- und vulkanosedimentären sowie granitischen Gesteinen und Ophiolithen. Von Norden nach Süden lassen sich diese Ophiolithe in die Guevguely-, Oraeokastro-, Thessaloniki- und Chalkidiki-Ophiolithe unterteilen.
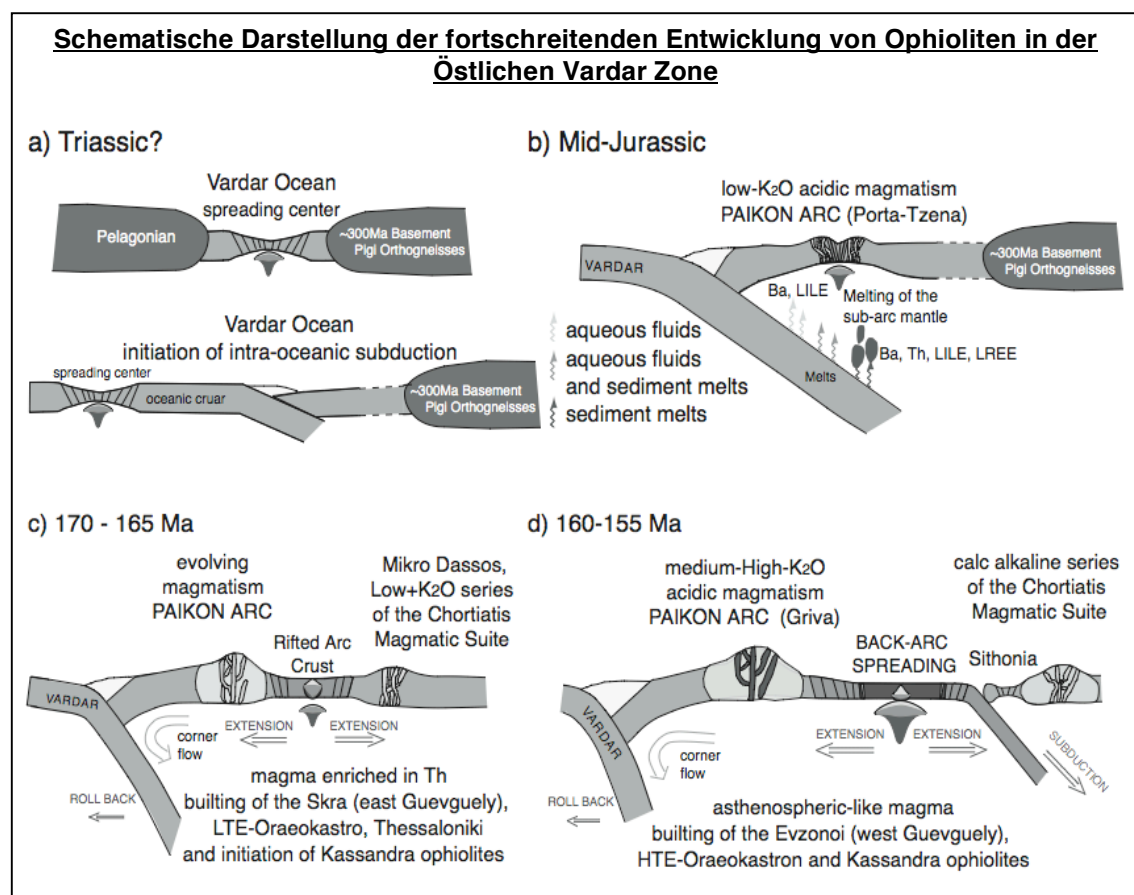
Die Bedeutung dieser Ophiolithe liegt darin, dass sie eine Subduktionszone im östlichsten Bereich des Vardar-Ozeans und damit einen aktiven Plattenrand entlang der südlichsten Grenze des Serbo-Makedonischen und Rhodope-Massivs dokumentieren. Die Erforschung der Entstehungsgeschichte dieser Ophiolithe gibt wertvolle Informationen über die Entwicklung des Vardar-Ozeans und trägt damit zum Verständnis der Prozesse am aktiven Kontinentalrand entlang der Sutur dieses Systems bei.

Die Untersuchungen wurden anhand detaillierter Analysen der Mineral- sowie Gesamtgesteinschemie mittels hochpräziser Messmethoden durchgeführt. Darüber hinaus wurden die Sm-, Nd- und Sr-Isotopie analysiert. Um die Entwicklung der Ophiolithe zeitlich genau einordnen zu können, wurde U-Pb-Geochronologie an Zirkonen mittels eines SHRIMP-II vorgenommen.

Die chemischen Eigenschaften der einzelnen Ophiolithe (wie z.B. Nb-Anomalien und Th-Anreicherungen) sind in unterschiedlichem Maße charakteristisch für Subduktionszonen-Magmatismus. Normalisiert auf normalen Mittelozeanischen Rücken-Basalt (N-MORB) zeigen die High Field Strength –Elemente Variationen von verarmten bis N-MORB-subparallelen Mustern. Die Seltenen Erden (REE)-Muster aller Ophiolithe, auf den C1-Chondrit normalsiert, besitzen im Bereich der schweren REE einen flachen Verlauf, der für Schmelzbildung in geringer Tiefe typisch ist. Die größte Zahl der Proben zeigt eine Verarmung an leichten REE. $^{87}Sr/^{86}Sr$-Verhältnisse weisen in einigen Fällen Einflüsse von Alterationen auf. Die $\varepsilon_{Nd}$-Werte, errechnet für das Mittlere Jura, sind positiv, aber geringer als die Werte für N-MORB und verarmten Mantel. Mit Ausnahme des Thessaloniki-Ophioliths, der eine einheitliche

chemische Charaktersitik besitzt, sind die übrigen Ophiolithe aus Gesteinen aufgebaut, die zum Einen N-MORB-Eigenschaften mit geringem Subduktionszonen-Einfluss, zum Anderen aber ausgeprägte Subduktionszonen-Charakteristik aufweisen. Tektonomagmatisch lassen sich die Gesteine demnach in Inselbogentholeiite, Back-Arc-Becken-Basalte oder N-MORB unterscheiden. Schmelzmodelle zur Errechnung der möglichen Magmenquelle und entsprechende Schmelzgrade bestätigen den bimodalen Charakter der Ophiolithe.

Aus den geochemischen und petrologischen Untersuchungen lässt sich ableiten, dass die Guevguely-, Oraeokastro- Thessaloniki- und Chalkidiki-Ophiolithe Reste von Supra-Subduktionszonen-Ophiolithen darstellen, die sich während der verschiedenen Stadien des Inselbogen-Riftings und Back-Arc-Spreadings gebildet haben. Die geochronologischen Analysen dieser Studie ergeben, dass diese Ophiolithe vor 160 bis 169 Ma entstanden sind.

## Schematische Darstellung der fortschreitenden Entwicklung von Ophioliten in der Östlichen Vardar Zone

a) Triassic?

Vardar Ocean spreading center

Pelagonian — ~300Ma Basement Pigl Orthogneisses

Vardar Ocean initiation of intra-oceanic subduction

spreading center — oceanic cruar — ~300Ma Basement Pigl Orthogneisses

b) Mid-Jurassic

low-$K_2O$ acidic magmatism PAIKON ARC (Porta-Tzena)

VARDAR — ~300Ma Basement Pigl Orthogneisses

Ba, LILE — Melting of the sub-arc mantle

aqueous fluids
aqueous fluids and sediment melts
sediment melts

Ba, Th, LILE, LREE

Melts

c) 170 - 165 Ma

evolving magmatism PAIKON ARC

Mikro Dassos, Low+$K_2O$ series of the Chortiatis Magmatic Suite

Rifted Arc Crust

VARDAR

corner flow — EXTENSION — EXTENSION

ROLL BACK

magma enriched in Th builting of the Skra (east Guevguely), LTE-Oraeokastro, Thessaloniki and initiation of Kassandra ophiolites

d) 160-155 Ma

medium-High-$K_2O$ acidic magmatism PAIKON ARC (Griva)

calc alkaline series of the Chortiatis Magmatic Suite

BACK-ARC SPREADING — Sithonia

VARDAR

corner flow — EXTENSION — EXTENSION — SUBDUCTION

ROLL BACK

asthenospheric-like magma builting of the Evzonoi (west Guevguely), HTE-Oraeokastron and Kassandra ophiolites

Die hier vorgestellte Entwicklung der Ophiolithe schließt eine ostwärtige Subduktion des Vardar-Ozeans in einem Intraozeanischen Setting während des Mittleren Jura ein. Im ersten Stadium der Evolution der Supra-Subduktionszone (170 – 165 Ma) wurden saure, niedrig-$K_2O$-Magmatite gebildet, die heute als Paikon-Andesite, Rhyolithe in Mikro Dasos und in Teilen der magmatischen Chortiatis-Folge zu finden sind. Zeitgleich fand die Entwicklung des mafische Magmatismus statt, wie er im westlichen Teil des Guevguely-Ophioliths (Skra), Thessaloniki, wahrscheinlich in Oraeokastro (in Form einer niedrig-$TiO_2$-Gruppe der mafischen Extrusiva) und, weniger ausgeprägt, in Kassandra vorliegt. Die fortlaufende

Subduktion, der damit verbundene Roll-Back der subduzierten Platte und der Aufstieg der Asthenosphäre resultiert in der Entwicklung eines Riftsystems im Bereich des Inselbogens. In diesem Setting, vergleichbar mit dem der Marianen, bildeten sich vor 161 - 155 Ma der östlicher Teil des Guevguely-Ophioliths (Evzonoi), der Oraeokastro (vertreten durch eine hoch-$TiO_2$-Gruppe mafischer Vulkanite)- und Kassandra-Ophiolith. Synchron beginnt die ostwärtige Subduktion, die mit der Schließung des Back-Arc-Beckens, wahrscheinlich unterhalb des Chortiatis-Mikro Dasos-Bogens, und der Entwicklung des Sithonia-Fore-Arc-Ophioliths im Bereich des Fore-Arcs endet.

# Contents

## Chapter 1. Geology of Grecce

## Chapter 2: Methods

## Chapter 3. The Guevguely Ophiolite

## Chapter 4. The Oraeokastro Ophiolite

## Chapter 5. The Thessaloniki Ophiolite

## Chapter 6. The Kassandra – Sithonia Ophiolite

## Chapter 7. Synthesis

## Literature

## Appendixes

## PHOTOS

    Guevguely

    Oraeokastro

    Thessaloniki

    Sithona-Kassandra

# Glossary

Here is a list of abbreviations used in the following text.

## Chemistry

**LILE**: large ion lithophile elements, include elements that have monovalent or divalent ions, like K, Rb, Ba, Cs

**HFSE**: high field strength elements, include elements whose ions have charge greater or equal to 3. This group includes the lanthanides, Sc, Y, Th, Pb, Zr, Hf, Ti, Nb and Ta

**REE**: rare earth elements. Group of elements that have atomic numbers from 51-71. This group includes the elements known as lanthanides.

**LREE**: light rare earths, include the elements La, Ce, Pr, Nd and Pm

**MREE**: middle rare earths, include the elements, Sm, Ey, Gd, Tb, Ho

**HREE**: heavy rare earths, include the elements Er, Tm, Yb, Lu

**CI**: carbonaceous chondrite

**N-MORB**: mid-ocean ridge basalt

**OIB**: ocean-island basalt

**IAT**: island arc tholeiites

**WPB**: within-plate basalts

**IA**: island arc

**VA**: volcanic arc

**MOR**: mid-ocean ridge

**UC**: Upper continental crust

**MC**: Middle continental crust

**LC**: Lower continental crust

**GLOSS**: Global oceanic subducted sediment

**BSE**: Bulk silicate earth

**D(M)M**: Depleted (MORB) mantle

## Minerals

**Cpx**: clinopyroxene

**Opx**: orthopyroxene

**Ol**: olivine

**Plg**: plagioclase

**Hb**: hornblende

**Tit**: titanite

**Act**: actinolite

**Ep**: epidote

**Chl**: chlorite

**Sp**: spinel

**Ser**: serpentinite

## Geology

**CRB**: Circum-Rhodoe-Belt

**SSM**: Serbomacedonian Massif

**RHM**: Rhodope Massif

**VZ**: Vardar Zone

**GVL**: Guevguely

**EYZ**: Eyzonoi

**ORK**: Oraeokastro

**MLF**: Monolofos

**THS**: Thessaloniki

**CR**: Circum Rhodope

**SIT**: Sithonia

**KAS**: Kassandra

# Introduction to the thesis and problematic

Northern Greece is a geologically complex area where continental blocks of different provenance came together now separated by zones of low-grade to amphibolite facies rock associations of both sedimentary and igneous origin.

From east to west the metamorphic continental block of the Rhodope Massif comes into contact with that of the Serbo-Macedonian Massif along the Athos-Volvi-Thermes suture zone, (Dixon and Dimitriadis 1984, Himmerkus et al. 2005). In turn, the Serbo-Macedonian Massif is bordered to the west by the Peonias subzone of the Vardar Zone. Their interface is a narrow belt of rocks consisting of alpine limestones, metasedimentary and volcanosedimentary rocks, as well as granitic and metamafic rocks, which has been termed the Circum-Rhodope Belt (Kaufmann 1976). At its western margin the Vardar Zone overrides the Pelagonian Zone along a series of complex nappes composed mainly of ophiolitic rocks.

In the present thesis, the geochemistry, petrology and geochronology of mafic and ultramafic rocks that outcrop between the eastern part of the Peonias subzone of the Vardar Zone and the Serbo-Macedonian Massif along the Circum-Rhodope Belt will be examined in detail. Bebien and co-workers studied these outcrops in the 1980's and concluded that they represent ophiolitic fragments generated in an ensialic back-arc basin and coined the term Innermost Hellenic Ophiolite Belt (IMHOB) (Bebien et al. 1986). Ophiolites that belong to IMHOB are the Guevguely (Bebien 1982,1987), the Oreokastron (Haenel-Remy and Bebien 1985), and the Sithonia and Kassandra complexes (Mussalam and Jung 1986, Jung and Mussalam 1985, Mussalam 1991). The Samothraki ophiolite (Tsikouras 1990, Tsikouras and Katzipanagiotou 1998) as well as the Evros ophiolite (Magganas 2002) are also considered members of the IMHOB but they were not included in this study.

While there has been a number of basic field and structural/petrological investigations of the IMHOB bodies there is a marked paucity of high-quality geochemical studies (trace-elements and isotopes) and a lack of radiometric age dating. Inferred from stratigraphic criteria the genesis of these mafic bodies has been placed in the Jurassic. Only Spray et al (1984) have so far published well-documented radiometric ages for the Guevguley ophiolite. Danelian et al (1996) inferred an Oxfordian age for the same ophiolite based on radiolarian fauna they discovered within the extrusive sequence of the eastern part of the complex. A mid-Jurassic age on a gabbroic rock from central Chalkidiki occurs as personal communication between Mussalam and Jung (1986) and Kreuzer without accompanying information on the isotopic ratios, errors or measuring conditions and therefore cannot be fully evaluated.

In the following chapters the genesis and relations between the IMHOB complexes are examined in detail using high-quality geochemical and radiometric data. The first chapter is an introduction to the general geology of the area compiled using previous studies. Then

each ophiolitic complex is dealt separately with ample discussion of field relations and whole-rock major- and trace-element geochemistry. At the end the whole-rock isotopic and zircon geochronological data are combined with the geochemical results towards an evolutionary scenario for these mafic complexes.

However, before moving on to present the results of this study, an introduction to the definition of the term ophiolite as well as an analysis of the geodynamic significance of the occurrence of such rock complexes is deemed necessary.

## The definition of the term "ophiolite"

Before we move on it is necessary to give a definition of the term ophiolite and how it evolved from the original founding to the Penrose conference -were it was first introduced -to the modern times. This would be helpful in order to give a reference point to what we will use during our study when characterizing a mafic complex as ophiolite, or when we discard an already characterized ophiolite. A detailed description of the term ophiolite is given in Coleman (1977). In the following paragraphs there will be a short synopsis of the evolution of the term ophiolite.

The word ophiolite derives from the greek word "όφις" (ophis) that means snake. The term was first introduced by Brongniart (1827) to describe serpentinites because of the shiny mottled and greenish appearance of such rocks. The word ophiolite is found in "a textbook of mineralogy" by Dana (1949) along with other terms to describe varieties of serpentinites.

Steinman (1926) expanded the term ophiolite to include peridotites, diabase spillites and other related rocks. Steinman was the first to point out the close relation of the ophiolite with associated sediments of deep water such as radiolarian cherts and clays. From this point the term ophiolite was appointed to describe a rock association rather than a single rock type and was named "Steinman Trinity".

"As ophiolites one must characterize only the consanguineous association of predominately ultrabasic rocks of which the principal one is always peridotite (serpentinite) with subordinate gabbro, diabase, spillite or norite and related rocks. The name ophiolite is not permissible for those rock groups that consist only of diabse-like rocks of quite similar composition and structure." (source Coleman, 1977)

In 1972 the participants of the international conference of the Geological Society of America's Penrose Conferences conclude to an accepted definition of the term ophiolite that would also be linked to use of this term by the European geologists. The definition of term ophiolite as used in the Penrose Conference 1972 refers to a distinctive assemblage of mafic to ultramafic rocks. It is marked that it should not be used as a rock name or as lithologic unit in mapping. In a completely developed ophiolite (Fig. A), the rock types occur in the following sequence, starting from the bottom and going up:

**Ultramafic complex**, consisting of variable proportions of harzburgite, lherzolite and dunite, usually with a metamorphic tectonic fabric (more or less serpentinized).

**Gabbroic complex**, ordinarily with cumulus textures commonly containing cumulus peridotites and pyroxenites and usually less deformed than the ultramafic complex.

**Mafic sheeted dyke complex**

**Mafic volcanic complex, commonly pillowed.**
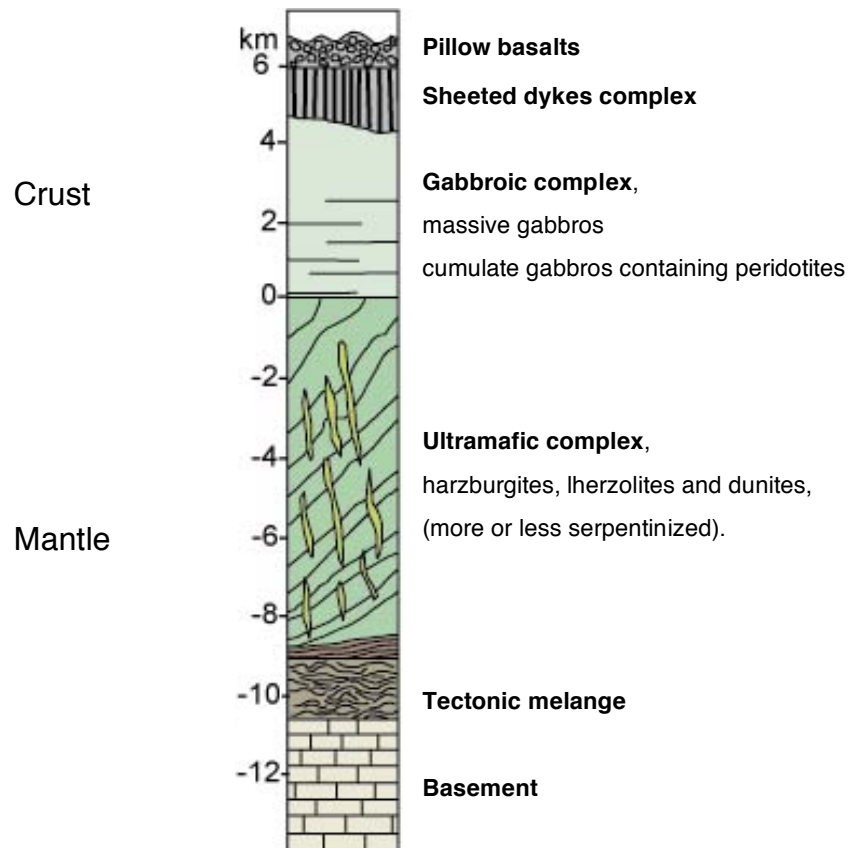


 **Fig. A**. Simplistic stratigraphic column of an ophiolitic sequence

**Associated rock typea,** include:

a) an overlying sedimentary section typically including ribbon cherts, thin shale interbeds, and minor limestones.

b) podiform bodies of chromites generally associated with dunite.

c) sodic felsic intrusive and extrusive rocks.

Faulted units between mapable units are common. Whole sections may be missing. An ophiolite may be incomplete, dismembered or metamorphosed. Although an ophiolite is generally interpreted to be a fragment of oceanic crust and upper mantle, the use of the term should be independent of its supposed origin. Moores 1982 suggested that the tectonic melange and the metamorphic sole observed at the bottom of some ophiolites should be included in the term "ophiolite".

# Geodynamic significance of the Ophiolites

Before 1960, the common occurrence of 'ophiolitic rock types' had been recognised and linked to submarine processes and thereby to the geosyncline concept. Moores (1969) and later Moores and Vine (1971) in Vourinos and Troodos ophiolites respectively, recognised the similarity of the ophiolite startigraphy they were observing to the oceanic lithosphere. Miyashiro in 1973 reported that there were rocks in the Troodos that have silica content that is more than 52.5% and geochemically belong to the calc-alkaline series, suggesting that the Troodos Massif was probably formed in an island arc. This observation was followed by an answer of Moores (1975) that the calc alkaline chemical characteristics that Miyashiro describes could have been the result of metasomatic alteration and by Gass (1975) who suggests that the 120 km continuous sheeted dykes complex was not compatible to the arc theory of Miyashiro. Pearce and Cann (1973) collected analyses from basalts that erupted in different tectonic settings and observed a chemical variability between many of them and basalts that have erupted in mid-ocean ridges (MOR). Robinson and Malpas (1990) studied the chemistry of glasses from Troodos and suggested a subduction related origin. Pearce et al. (1984) suggested that most of the up to then studied ophiolites have been formed in an supra-subduction zone setting (SSZ). It has to be noted that by suprasubduction zone setting

It is characterised the positions on the upper plate of the subduction system where an extensional regime is evolved. These positions can be the fore-arc and the back arc, and in cases (e.g. Mariannas, Crawford et al. 1981) the rifting of an arc.

Stern and Bloomer (1992), proposed that subduction could have been initiated within the ocean possibly due to sink of old, dense oceanic lithosphere into the asthenosphere. The part of the lithosphere adjacent to the sinking lithosphere moves towards the sinking lithosphere creating an extensional regime were fluids released form the sinking plate and decompression, induce melting of the mantle wedge which provides the magmatism for the formation of new mafic crust. Hamilton (1985), Flower and Dilek (2003), Dilek and Flower (2003), suggested that mantle flow beneath the mantle wedge and subduction rollback play a major role to the formation of SSZ ophiolites.

In spite of the growing popularity of the supra-subduction setting as a possible setting for the development of an ophiolite, many scientists continued to support an ocean ridge setting for all ophiolites (e.g. Coleman 1981, Boudier and Nicolas 1985, Nicolas 1989). Boudier and Nicolas 1985 divided the ophiolites in two subtypes. The Harzburgite Ophiolite Subtype (HOS) and the Lherzolite Ophiolite Subtype (LOS). Later the two groups were renamed HOT and LOT replacing the word subtype with simply type. The criterion of the division used by Boudier and Nicolas 1985 is the nature of the ultramafic rocks. In a HOT ophiolite the ultramafic complex consists dominantly of harzburgite with layers of

orthopyroxenite and dunite. The abundance of dunite increases when one goes to higher parts of the stratigraphy. In LOT ophiolites the ultramafic complex consists of plagioclase lherzolites with layering of websterite. The only significant presence of dunite is restricted to the upper parts of the section (≤2km). Boudier and Nicolas, (1985) assigned the differences in the ultramafic section to the spreading rate, discarding the SSZ origin of the ophiolites. Slow spreading centers (10-15mm/yr) show smaller degrees of melting thus they exhibit a mantle section dominated by lherzolites, whereas fast-spreading (1cm/yr) centers would be have a more depleted mantle section (hurzburgites). Nicolas and Boudier (2003), expressed their scepticism over the SSZ origin of the ophiolites and suggested that there should be a turn towards detailed structural studies on ophiolites.

In this study we will accept the general consensus that ophiolites form in both mid-ocean ridge (MOR) and suprasubduction zone setting (SSZ), without overlooking the theory of Nikolas and Boudier, to explain the formation and development of the studied ophiolites.


## Why are ophiolites important?


Ophiolites are pieces of oceanic crust generated either in mid-ocean ridges or in supra-subduction zone settings and are tectonically emplaced on continental margins. Just the first part gives the scientists a great chance to:


A.      Study the structure of the ocean floor and investigate the tectonic, magmatic, hydrothermal processes that take place in the ocean floor, either in mid-ocean ridges or in island arcs.

B.      Study the processes that happen in the mantle beneath such areas and understand the evolution of Earth's mantle.


As mentioned before, ohiolites are tectonically emplaced on continental margins. Emplacement of ophiolites happens during the closure of oceans or during exhumation processes where material from deeper places of the crust is transported on the surface of the earth (eclogites). This is very important in defining paleo-geotectonic environments, identifying suture zones and investigate tectonic processes that take place in the crust (exhumation), all these being very important for palinspastic reconstructions of ocean basins and mountain belts

Ophiolites are very often associated with ore deposits. The mantle section of ophiolites is host of chromite, nickel, platinum-group elements (PGE). Massive sulphide deposits often hosting precious metal deposits (Au,Ag) and associated stockwork mineralisation are usually only found throughout the volcanic section above the sheeted dyke

complex. Understanding the formation of ophiolite complexes and therefore the oceanic crust can help us in both understanding the formation of these ores and aiding to the exploration of such deposits.

## Description of the contents

In the first chapter there will be introduction to the geology of Greece with emphasis to the geology of the area of study and the immediate adjacent geological units, namely the Vardar Zone, the Circum-Rhodope Belt and the Serbomacedonian Massif.

Chapter 2 is divided to three parts. In the first part there will be a review on the characteristics of subduction zone magmatism. The second part will be focused on presenting and explaining the melting modelling that will de used for the petrogrnnetic investigation of each ophiolite. The third part will include decription of the methods used in this study.

In chapters 3-6 the geochemical and geochronological results obtained for the studied ophiolites will be presented. Each ophiolite will be included in one chapter where field observations, sample description, whole-rock major and trace elements and isotopic analyses will be presented and discussed.

In chapter 7 there will be the synthesis of all the colleted information in order to present a comprehensive story on the evolution of these ophiolites and the adjacent area.

At the end, the literature used in the frame of this study as well the appendices section will be listed. The appendices section will include a complete record of the geochemical and geochronological analyses, description and location of the samples, as well as outcrop photos.

# Chapter 1. Introduction to the geology of Greece and of the study area

_____

## 1.1  The geological subdivision of Greece

Greece is positioned within a huge and complex orogenic system that extends from the Pyrenees in Spain to the Tibetan plateau and further east (Fig. 1). This orogenic system is known as the Alpine – Himalayan orogenic belt. During the Mesozoic and Cenozoic times the Greek orogenic system, or the Hellenides as it is widely known, was part of the Dinaride-Tauride branch of the Alpine system.
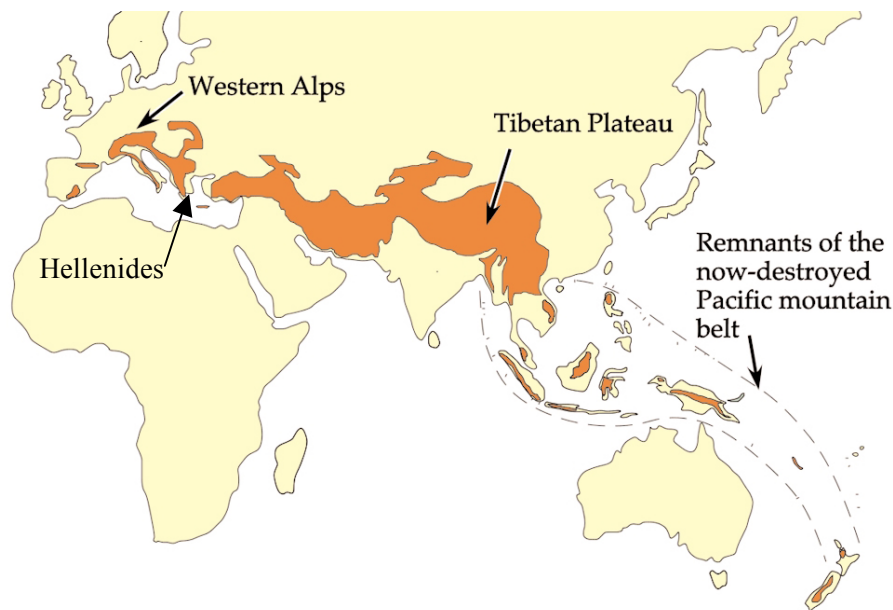


**Fig. 1.** Schematic map of the Alpine – Himalayan orogenic system and the position of the Hellenides. (after Lister et al., 2001)

The Hellenides have been subdivided into several geotectonic zones on the basis lithological and geotectonical structural characteristics (Fig. 2). (Aubouin 1965, Jackobshagen 1985, Mountrakis 1983, Papanikolaou, 1986). These zones form three major groups, the External Hellenides, the Internal Hellenides and the Hellenic Hinterland. The division between External Hellenides and Internal Hellenides is based upon the observation that the zones making up the external Hellenides have not been affected by Upper Jurassic – Lower Cretaceous compression that is observed to have taken effect in the Internal Hellenides. The Hellenic Hinterland is mainly built up of pre-alpine metamorphic rocks, exception is the Upper tectonic Unit of Rhodope which is built up of Jurrasic rocks. The zones that belong to the Hellenic Hinterland are the Serbo-Macedonian and the Rhodope Massifs.

The Internal Hellenides comprise, from east to west, the Circum-Rhodope, the Vardar (Axios), the Pelagonian, the Attic-Cycladic and the sub-Pelagonian Zones (see Fig. 2). The

Vardar zone is further subdivided, from east to west, into the Peonias, the Paikon and the Almopias sub-zones respectively. The sub-Pelagonian and the Vardar Zones contain the two main ophiolite belts of the Hellenides. The Internal Hellenides are built up of metamorphic rocks of pre-alpine protoliths, alpine sediments and igneous rocks that have been formed from Mesozoic to Palaeogene magmatic activity.

**Border between Internal Hellenides and the External Hellenides**

**Border between Hellenic Hinterland and the Internal Hellenides**

**Hellenic Hinterland**
- RHODOPE MASSIF
- SERBOMACEDONIAN MASSIF

**Internal Hellenides**
- CIRCUM-RHODOPE BELT
- VARDAR ZONE

- PELAGONIAN ZONE
- ATTIKOCYCLADIC ZONE
- MESO-HELLENIC TROUGH
- PINDOS ZONE
- **Ophiolites**

**External Hellenides**
- PARNASSOS-GKIONA ZONE
- GAVVROVO - TRIPOLIS ZOINE
- IONIAN ZONE
- PAKSON (PROAPOULIAN) ZONE

**Fig. 2**. Simplified map of the Hellenides. (modified after Geological Map of Greece, IGME (1983) and Mountrakis 1984)

The zones constituting the External Hellenides are, from west to east, the Paxon (pre-Apulian), Ionian, Gavrovo-Tripolis, Olonos-Pindos and Parnassos-Ghiona Zones respectively (see Fig. 2). With the exception of the Olonos-Pindos Zone which represents a deep turbidite basin (Neumann & Zacher, 2004), the remainder of External Hellenide Zones are characterised by thick platformal carbonate sedimentation. A striking difference between the

External and the Internal Hellenide / Hellenic Hinterland Zones is the ubiquitous presence, in the former, of HPLT metamorphism (Phyllite-Quartzite Unit of Peloponnese and Crete) (Theye et al. 1992)

The ophiolites that are the focus of this study are located at the border between the Internal Hellenides and the Hellenic Hinterland, in the area between the Vardar Zone and the Serbo-Macedonian Massif. In the ensuing text special emphasis will be placed on the regional geology, but also the specific geological features of the Vardar Zone, the Circum Rhodope belt and the Serbo-Macedonian Massif.

## 1.2 Ophiolites of Greece

The ophiolites of Greece have been regarded as parts of the Tethyan system, a system of oceans that extends from the present-day Atlantic to the Pacific oceans, and have been classified as Tethyan ophiolites. Tethys was first mentioned by Suess (1893, 1909) to describe the ocean that evolved during the Mesozoic separating Eurasia from Gondwana. Tethyan ophiolites can be traced from Western Europe (Alps) to central Asia (Zagros Mountains) and further east into Tibet.



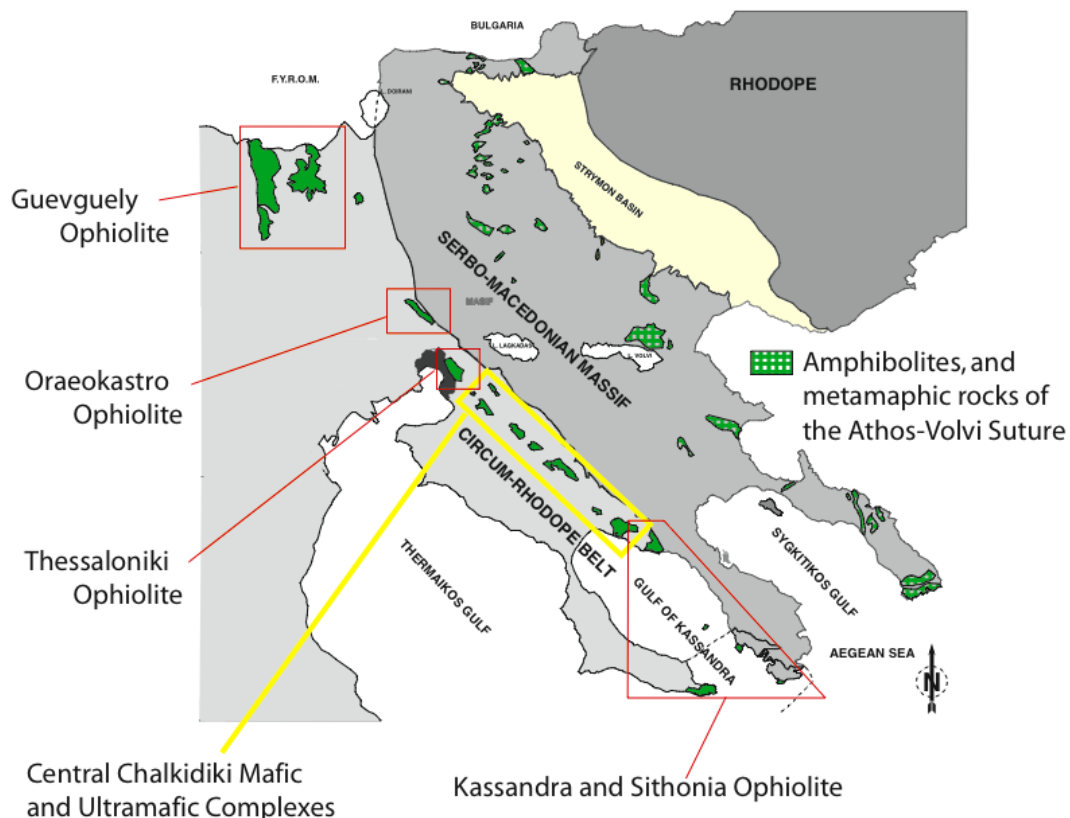**Fig. 3.** Map of the central part of N. Greece showing the position of the study areas and the investigated ophiolites in relation to the major geologic divisions of N. Greece. In the yellow box we see the locations of the mafic and ultramafic complexes of central Chalkidiki, which were not part of this study. To the east we see the location of the complexes that built up the Athos Volvi Suture (Himmerkus et al. 2005).

In Greece there are two major belts of ophiolites which are separated by the Pelagonian Zone. The eastern ophiolite belt comprises the ophiolites of the Vardar Zone (sensu stricto) and those of the so-called Innermost Hellenic Ophiolite Belt (Haenel-Remy Bebien 1984), i.e. the bodies of Guevguely, Oraeokastro, Thessaloniki, Chalkidiki (Fig. 3). The western ophiolitic belt includes the complexes of Vourinos, Pindos, Koziakas, Orthrys and Argolis. The Evros and Samothraki ophiolites, which border the eastern margin of the Greek Rhodope Massif, is regarded as part of the eastern ophiolite belt.

Both ophiolite belts described above can be traced northwards into the Balkans. The western ophiolite belts continues into the Mirdita Zone of Albania, bends along the Scoutari-Peč line and then follows the Dinaride ophiolite belt while the eastern ophiolite belt continues into F.Y.R.O.M. and Serbia up to the Pannonian Basin.

Further details on the geochemical characteristics and the geotectonic setting of the Greek ophiolites will be presented in the Synthesis Chapter were they will be discussed and compared to those of the bodies studied in detail here.

## 1.3 The Vardar Zone

The Vardar Zone is situated between the Pelagonian Zone and the Serbo-Macedonian Massif. It forms an elongated NNW-SSE trending belt (Fig. 1.1a), characterised by numerous ophiolitic bodies and is regarded as a suture zone (e.g. Mercier et al. 1975; Brown & Robertson 2004). The Greek part of the Vardar Zone has been subdivided by Mercier 1966 into three sub-zones. From east to west these sub-zones are the Almopias, Paikon and Peonias sub-zones (Fig. 4).

The Peonias sub-zone, is further subdivided, from west to east, into the Propeonias and the Eastern Peonias Units. The Propeonias Unit consists of Tithonian limestones and psammites, the Guevguely ophiolite and the Fanos Granite, the Oraeokastro ophiolite, Late Jurassic fossiliferous limestones, phyllites, mica schists and volcanosedimentary rocks (reference). The Eastern Peonias Unit is built up of two series of rocks namely, an unmetamorphosed sedimentary sequence of Middle Triassic to Early Jurassic (Lias) age consisting of limestones and a sequence consisting of metamorphosed sediments (psammites, cherts, quartzites) and minor greenschist-facies mafic rocks (reference). The two units are separated by a tectonic contact.

The Paikon sub-zone, according to Mercier 1966, consists of Triassic neritic marbles, clastic sediments, mica schists and a sequence of volcanic rocks that exhibit a wide range of compositions from rhyolite to basalt. The age of the latter has been determined as Late Jurassic (~155 Ma, Anders et al. 2005). The Almopias sub-zone consists of ophiolites and meta-volcanic and meta-sedimentary rocks of Triassic to Jurassic age. On top there is a

series of Cretaceous to Late Jurassic (Maastrichtian) sedimentary rocks, which resembles the structure of flysch.
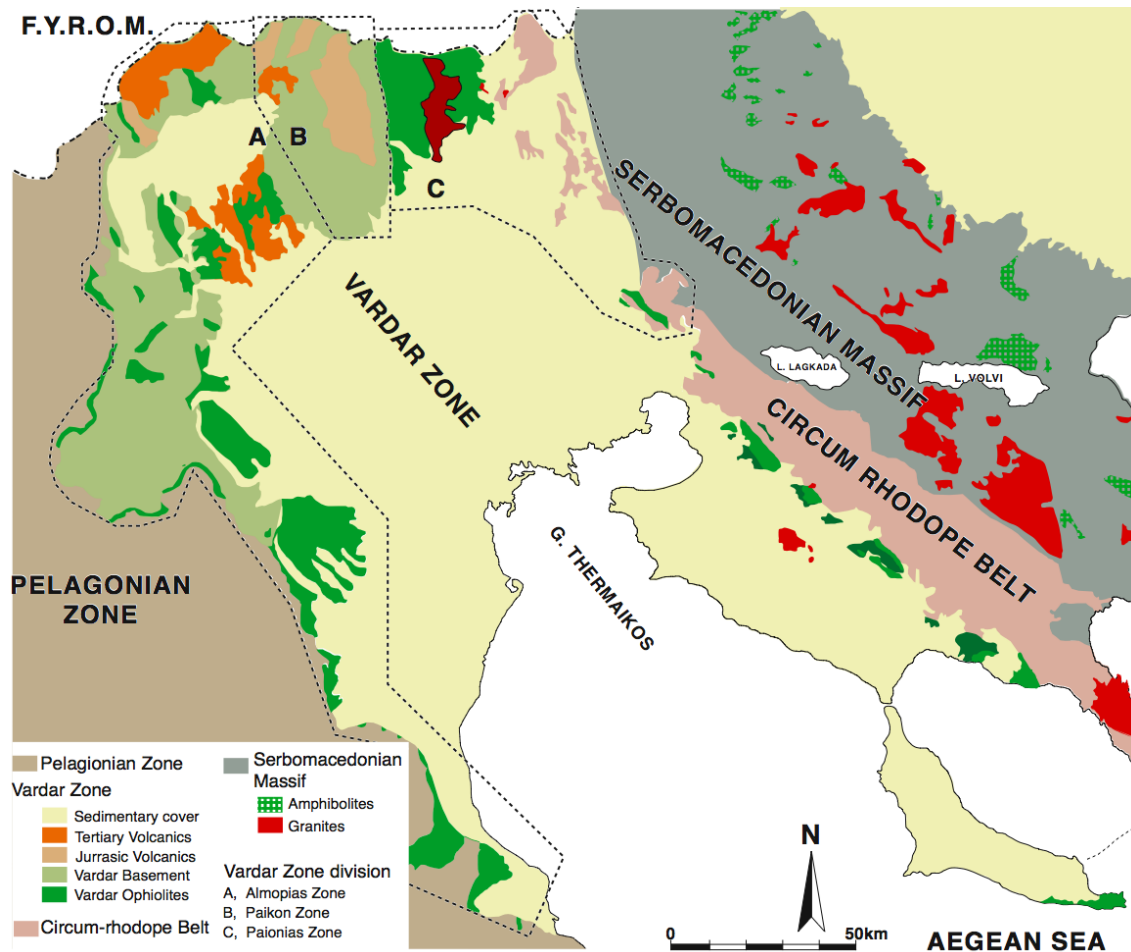


**Fig. 4**. Map of the Vardar zone the subdivision and adjacent geological zones. (Modified after the Geological Map of Greece, IGME 1983)

Here is a brief description of the geotectonic evolution of the Vardar Zone. The Almopias sub-zone is interpreted as a former ocean basin that subducted underneath the Serbo-Macedonian Massif to form the Paikon volcanic arc in Mid-to Late Jurassic times. During the Late Jurassic, ophiolites from this ocean were obducted westwards onto the Pelagonian Zone (Mercier et al. 1975; Brown & Robertson 1994, 2003, 2004; Bébien et al. 1994; Sharp & Robertson 1994). During the Cretaceous, however, an ocean basin existed in this area, either as a remnant ocean that had escaped Jurassic obduction or as a small Cretaceous pull-apart basin (Sharp & Robertson 1994). Final closure of the ocean is assumed to have occurred during the Tertiary, accompanied by thrusting of ophiolites eastwards onto the Paikon sub-zone (Sharp & Robertson 1994; Brown & Robertson 2004). A different interpretation of the Paikon sub-zone as a tectonic window (Godfriaux & Ricou 1991; Ricou & Godfriaux 1991, 1995; Ferrière et al. 2001) is highly controversial (e.g. Mercier & Vergély 1994). The Guevgueli ophiolite in the western part of the Peonias sub-zone is considered to

have formed in an ensialic back-arc basin opening behind (to the east of) the Paikon arc (Bébien 1982; Brown & Robertson 2003). It was then thrusted westwards onto the Paikon sub-zone (Mercier et al. 1975; Brown & Robertson 1994). Evidence for subduction activity in the eastern Vardar Zone was reported from the Paikon and the eastern Peonias sub-zones by Baroz et al. (1987) and Michard et al. (1994) respectively, where they found high-Si phengite- and glaucophane-bearing rocks.

## 1.4 The Circum-Rhodope belt

Located between the Serbo-Macedonian Massif and the Vardar Zone there is a narrow belt of rocks consisting of alpine limestones, sedimentary and volcanosedimentary sequences, as well as metamafic and granitic rocks. The metamorphic conditions are in the range of the greenschist facies although some scarce examples of higher grade rocks can be found. Due to this reason this belt was defined by Kauffmann et al. (1976) as a separate geotectonic unit in comparison with the nearby Vardar Zone and the Rhodope and Serbo-Macedonian Massifs, and was named the Circum-Rhodope belt (Fig. 5).

The Circum-Rhodope belt is a 10-20 km wide, northwest-southeast trending zone along the western border of the Vardar Zone with the Serbo-Macedonian Massif. In the Greek territory this zone extends from the Hellenic-F.Y.R.O.M border to the Chalkidiki peninsula (see Fig. 5). Low-grade metasedimentary units (mainly phyllites) fringing the eastern margin of the Rhodope Massif have also been assigned a Circum-Rhodope belt origin.

The Circum-Rhodope belt is subdivided into three units which, from east to west, are the Deve Koran – Doubia Unit, the Melissochori – Cholomon Unit and the Aspri Vrissi – Chortiatis Unit.

The Deve Koran – Doubia Unit consists of quartzites, meta-sandstones, quartzite-schists and Permian meta-conglomerates, known as the Examili Formation. Higher in the pile a volcanosedimentary sequence of Permian to Early Triassic age is observed. At the top there is a Middle Triassic to Middle Jurassic neritic carbonate series, built up by recrystallised limestones interlayered with marls and clays.

The Melissochori – Cholomon Unit is the largest of all three Circum-Rhodope belt units. Its lower parts comprise Middle to Late Triassic pelagic marbles and recrystallised limestones with interlayers of graphite and sericite schists. Moving up stratigraphy there is a clearly phyllitic horizon 400 m thick, consisting of common, quartzitic, and graphitic phyllites. In the higher parts of this Unit we observe the so-called Svoula Formation (reference). It represents an Early to Middle Jurassic turbidite flysch sequence with scarce olistholiths of Triassic marbles.

The Aspri Vrissi – Chortiatis Unit is composed, in its lower parts, of neritic sediments similar to those of the Deve Koran – Doubia unit. The upper part of the Unit is characterised

by deep-sea sedimentation attested to by red clay schists, black graphitic phyllites, marls and quartz schists. Ophiolitic rocks (mainly mafic and ultramafic cumulates and harzburgite tectonite) and a sizeable complex of volcanoplutonic acidic rocks, the latter known as the Chortiatis Magmatic Suite (reference) also occur within this Unit.
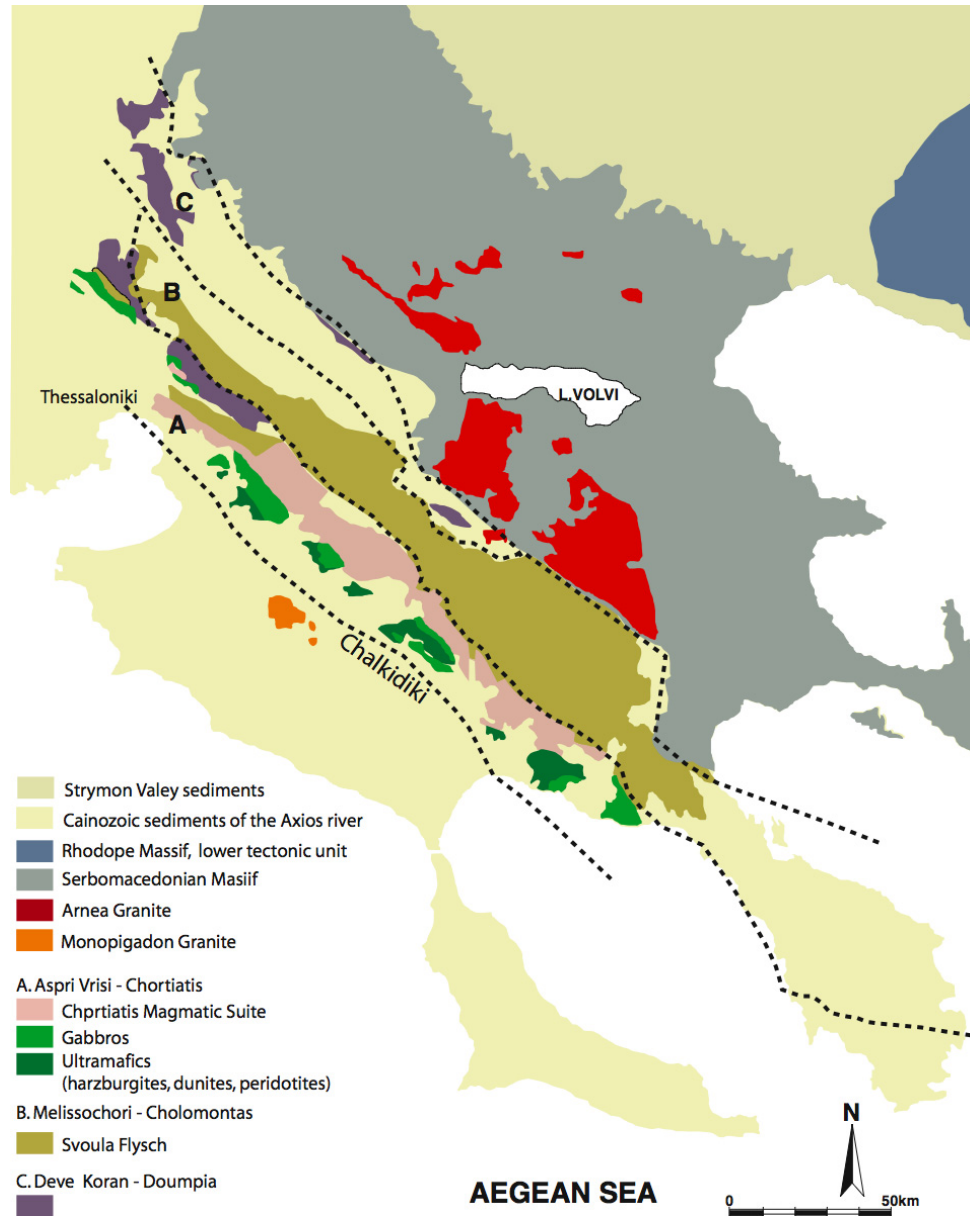


**Fig. 5.** Simplified map of the Circum-Rhodope belt, the subdividion of it in units and adjacent zones. (modified After Kockel et al. 1977, and Mounrakis 1984).

The phyllitic unit that outcrops along the south-eastern margin of the Rhodope Massif cannot be directly related to any of the three units mentioned above, although it is considered to be part of the Apri Vrissi – Chortiatis unit because of the existence of ophiolitic rocks among the phyllites.

The Circum-Rhodope Belt is thought to represent the continental margin of the Hellenic hinterland (Serbo-Macedonian and Rhodope Massifs) below which the oceanic crust of the Vardar Zone was subducted.

## 1.5 The Serbo-Macedonian Massif

The Serbo-Macedonian Massif (SMM), first defined by Dimitrievic (1957), is an elongated basement sliver, 30 to 60 km wide, west of the Rhodope Massif, stretching for about 300 km from SW Bulgaria in the north to the central Chalkidiki peninsula of northern Greece in the south (see Fig. 6). The Greek part of the SMM extends from the Kerkini Mountains at the border with Bulgaria to the peninsula of Chalkidiki (Kockel et al, 1977). The SMM is situated between the Vardar Zone (Mercier, 1968) and the Pelagonian Zone (Mountrakis, 1986, Anders et al., 2002, 2003) in the west, and the Rhodope Massif in the east (Turpaud 2006, Burg et al 1996 Jacobshagen, 1986, Ricou et al 1998).
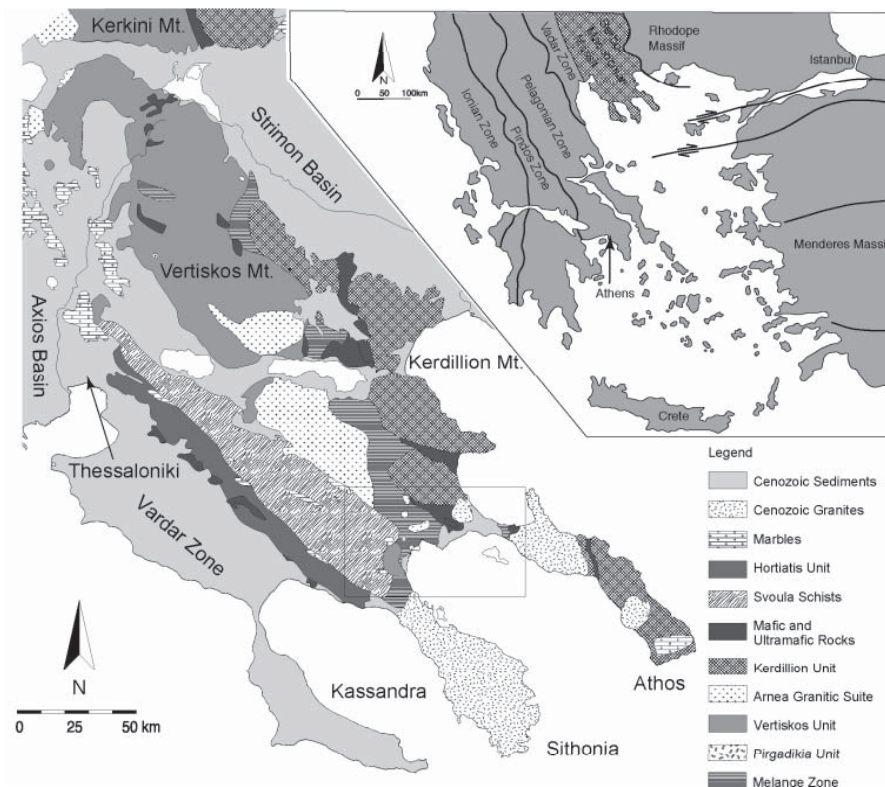


**Fig. 6.** Simplified geological map of the Serbo-Macedonian Massif from the Chalkidiki Peninsula in the south to the Kerkini Mountains in the north (modified after Kockel & Mollat 1977). The tectonic position in the Hellenic orogen is shown in the inset. The SMM and the Rhodope Massif form the metamorphic hinterland of the Hellenides. Together with the Pelagonian Zone they form the Internal Hellenides, which are mainly constructed of granites and gneisses. The Vardar and Pindos Zones are remnants of oceanic basins and the external Hellenides mainly consist of Mesozoic carbonates (from Himmekus et al. 2006).

The central and eastern parts of the SMM are largely composed of granitic basement rocks, which, in places, are associated with meta-sediments and amphibolites. The SMM is subdivided into two main units, the structurally overlying Vertiskos Unit in the north-west and the underlying Kerdillion Unit in the east (Kockel et al, 1977).

The basement of the Vertiskos Unit is mostly built up of orthogneisses, which occur in synformal structures associated with amphibolites and metasediments (Himmerkus et al, 2003). This Unit is intruded by Triassic leucocratic granites, associated to the Arnea Granite (e.g. De Wet, 1989), which is characterised by a within-plate signature (Kostopoulos et al., 2001; Himmerkus et al., 2004).

The SMM and the Rhodope Massif form the metamorphic hinterland of the Hellenides. Together with the Pelagonian Zone are mainly constructed of granites and gneisses. The Vardar and Pindos Zones are remnants of oceanic basins and the External Hellenides mainly consist of Mesozoic carbonates (from Himmekus et al. 2006).

Himerkus et al. (2006) defined the Vertiskos Terrane as a Silurian continental magmatic arc, which was intruded by within-plate granitoids in Triassic times (Himmerkus et al. 2005). The Kerdillion Unit consists of banded biotite gneisses and forms three major gneiss domes (Kockel et al. 1977; Himmerkus et al. 2002). The two units of the Serbo-Macedonian Massif are divided by a mélange zone comprising ophiolitic material (Volvi Complex) (Dixon & Dimitriadis, 1984; Himmerkus el al. 2004). Low-grade metasediments are only present at the western border of the SMM with the Vardar Zone, along the Circum-Rhodope Belt (Kaufmann et al., 1976).

# Chapter 2. Methods

## 2.1 Introduction

Before we proceed in discussing the geochemistry of the ophiolites, it is necessary to give an introduction to some characteristics of the subduction zone magmatism and the differences in comparison to the mid-ocean ridges. In Tatsumi and Eggins (1985), Shervais (2001), Hawkesworth et al., (1993) among others, one can find a detailed examination on the characteristics of subduction zone magmatism. In the following paragraph there will be a reference to the most important ones.

Subduction zone magmas are generally enriched in large ion lithophile elements (LILE) like K, Rb, Cs, Th, compared to HFSE (Hawksworth et al.1979, Saunders et al. 1980) and the light rare earth elements, (LREE) relative to normal mid-ocean ridge basalts (NMORB). This enrichment is attributed to aqueous fluids or melts expelled from the subducting slab [e.g. Hawksworth and Powelll 1980 McCulloch and Gamble 1991, H. Keppler 1996, Pearce, 1982; Wood, 1980]. Some LILE (e.g., K, Rb, Ba) tend to be soluble in aqueous solutions or melts during slab dewatering reactions; others (Th, LREE) are relatively immobile during alteration.

On the other hand the rocks formed in supra subduction zone settings show depletion in the high field strength elements (HFSE) like Ti, Nb, Ta, Hf. relative to N-MORB, which are generally caused by larger fractions of partial melting, also in response to aqueous fluids or melts expelled from the subducting slab [e.g. Münker et al. 2004 and references therein, Pearce, 1982, 1995, Pearce and Norry, 1979; Shervais, 1982; Wood, 1980]. Volcanic rocks in supra-subduction zone ophiolites show systemically low Ti/V ratios. V partitioning is controlled by $fO_2$ during melting, whereas Ti partitioning is independent of the oxidation state [Shervais, 1982] therefore higher oxygen fugacities will be as reflected by low Ti/V ratios.

Magmas in suprasubduction zones show enrichment in the radiogenic isotopes of Sr and Pb, resulting in higher radiogenic ratios, and depletion in radiogenic Nd, resulting in lower $^{143}Nd/^{144}Nd$ ratios, relative to MORB [e.g., Cohen and O'Nions, 1982; Hamelin et al., 1984, 1981; Hanan and Schilling, 1989; Ito et al., 1987; Jacobsen and Wasserburg, 1979; McCulloch and Cameron, 1983; McCulloch et al., 1980).

The particular characteristics of the subduction zone magmas are reflected by differences in the rock types and the chemistry of minerals we observe in those settings. Clinopyroxene crystallizes before plagioclase during the crystallization of the magma, resulting in a crystallization sequence, where olivine is the first mineral to crystallize (if present, relatively rare in SSZ-ophiiolites), followed by clinopyroxene while plagioclase comes later, instead of the typical MORB crystallization sequence were olivine crystallizes first and plagioclase precedes the crystallization of clinopyroxene [Cameron et al., 1980; Hebert and Laurent, 1990]. Mineral compositions in the volcanic and mantle section are refractory compared to those found in oceanic basalts and abyssal peridotites, e.g., Cr spinels with high

Cr/Al ratios and low Mg/Fe ratios [Cameron, 1985; Crawford et al., 1989; Dick, 1989; Dick and Bullen, 1984; Umino et al., 1990]. Plagioclase is calcic and orthopyroxene appears in some cumulate plutonic rocks caused by changes on phase equilibria during hydrous melting and crystallization [e.g., Beard, 1986; Hebert and Laurent, 1990].

Subduction zone magmas demonstrate a compositional diversity, and the products of these magmas are more evolved in composition than in any other tectonic settings. Characteristic of subduction zone magmatism is the appearance of boninite series volcanics, which are second stage melts with high MgO, high silica, and high LILE content. [Crawford et al., 1989; Ernewein et al., 1988; Juteau et al., 1988a, 1988b; Malpas, 1990; Robinson and Malpas, 1990].

The mantle has refractory composition, comprising harzburgite tectonites and dunite in contrast to the more fertile abyssal lherzolites commonly found with oceanic crust (e.g., Dick, 1989; Dick and Bullen, 1984).

# 2.2 Petrogenetic modelling of the ophiolites.

## 2.2.1 Descricption of compatible vs incompatible element model (Ti/Cr).

Pearce (1975, 1980, 1982) and Pearce et al (1984, 1986) have shown that plots of the concentration of a compatible versus the concentration of an incompatible element can provide valuable information on the melting of the source of basalts.

In order to quantify the source and melting properties we use the co-variation of a compatible vs. an incompatible element. The reason for that is that melting of a mantle source will deplete the source in the incompatible element while in the same time the compatible element will be barely affected.  As a consequence of that, in a bivariate diagram, the partial melting trends of the source will be presented as lines sub-parallel to the incompatible-element axis. By contrast, fractionation of mineral phases will result in the rapid depletion of the melt in its compatible element content, and thus in trends nearly sub-parallel to the compatible-element axis. By extrapolating the fractionation trend that fits through our samples back to the melting line we can make an estimation of the source and the degree of melting required. For the studied ophiolite complexes the melting modelling will be based on compatible vs incompatible element non-modal equilibrium melting modelling of Ti and Cr. In this model no more that 1wt% of melt can be rest in the source and the source composition is recalculated after the extraction of each fraction of melt. The equation describing the melting model can be found in Shaw (1979) and Frey (1985)

As a starting source we have chosen a FSL ($Ol_{57.6}Opx_{25.6}Cpx_{14.4}Sp_{2.4}$). DSL is the FSL after being melted by 15%.

|      | Ol   | Opx | Cpx | Sp  |
| ---- | ---- | --- | --- | --- |
| Ti   | 0.02 | 0.1 | 0.4 | 0.5 |
| Cr   | 1    | 3   | 6   | 250 |

**Table 1.** Partition coefficients of Ti and Cr for Ol, Opx, Cpx,Sp. (taken from Kostopoulos 1988)

## 2.2.2 Description of the REE model

The petrogenesis of the extrusive rocks from the ophiolite of Oraiokastro will be investigated in this thesis by modelling REE concentrations using a non-modal equilibrium partial melting model applied to variably depleted asthenospheric mantle compositions (lherzolite to harzburgite) both prior to and after adding variable amounts of enriched components. The latter include bulk continental crust (BCC), ocean-island basalt (OIB) and global oceanic sediment (GLOSS) compositions. Details of the modelling procedure can be found in Kostopoulos and Murton (1992). In short, the enriched component infiltrates the mantle source and forms an intergranular thin film without further interaction with the matrix. This mechanism is known as cryptic metasomatism (Reisberg and Zindler 1986, Suzuki 1987, Zindler and Jagoutz 1988, Drury and van Roermund 1988, Witt and Seck 1989). Upon subsequent melting the enriched component will be extracted in the first melt fractions.

According to the melting scheme employed, the source is melted in 1% steps, the melt is extracted and the residue recalculated to 100% and melted again by 1% and so on. Individual fractions of 1% are pooled, their compositions averaged and normalised to that of carbonaceous chondrite before being plotted on a variation diagram (Fig. A, the normalisation values used are from Boynton 1984).

We will now examine the effects of melting an unmodified source and of melting a modified source by variable component addition, on the REE patterns of the melt. As possible sources we will consider a fertile spinel lherzolite (FSL) and a depleted spinel lherzolite (DSL; see below) since there is no evidence for deep melting or residual garnet (Grt) in the source of the volcanics from whole rock chemistry. We will start by taking a fertile spinel lherzolite ($Ol_{57.6}Opx_{25.6}Cpx_{14.4}Sp_{2.4}$) as the initial source, similar to the depleted MORB mantle (DMM) composition. The proportion of each mineral in the melt will be 0.2 for Olivine (Ol), 0.3 for Orthopyroxene (Opx), 0.5 for Clinopyroxene (Cpx) and 0 for spinel (Sp) (Shaw 2000). Four

possible DSL sources will also be used, calculated as follows: FSL-5% melting, FSL-11% melting, FSL-16% melting, FSL-21% melting. The modal mineralogy of these possible DSL sources is described as:

**FSL-5% :** $Ol_{59.5}Opx_{25.4}Cpx_{12.6}Sp_{2.5}$

**FSL-11% :** $Ol_{62}Opx_{25.1}Cpx_{10.2}Sp_{2.7}$

**FSL-16% :** $Ol_{64.2}Opx_{24.8}Cpx_{8.2}Sp_{2.8}$

**FSL-21% :** $Ol_{66.4}Opx_{24.6}Cpx_6Sp_3$

Each of the four DSL compositions will be treated as the initial source with variable additions (0.1%, …… ) of the enriched components mentioned above.

The REE composition of the FSL is taken from the DMM values of Workmann and Hart (2005), bulk crust (BC) is from Rudnick, R.L. and Gao, S. (2004), and GLOSS is from Plank, T. and Langmuir, C.H. (1998).
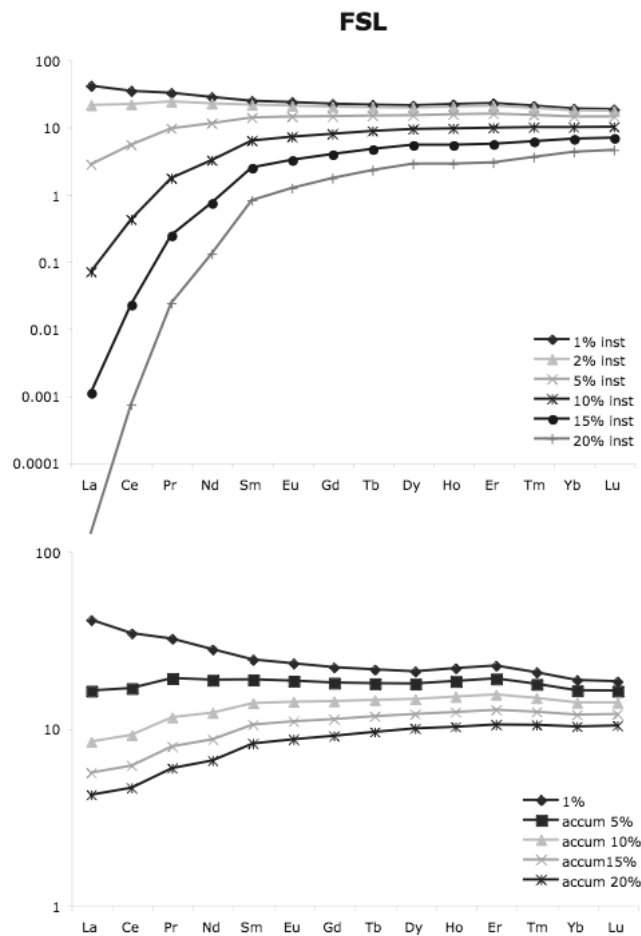


**Fig. A**. Instantaneous and accumulated melts produced by non-modal equilibrium partial melting of a FSL.

## 2.2.3 Results of the REE melting models

For the petrogenetic modelling we will examine the behaviour of the REE under different properties of melting. The REE partition coefficients for Ol, Opx, Cpx and Sp are quoted from Shaw (2000) and are listed in table 2. The results of the melting model will be visualised on chondrite normalised multielement diagrams. The values used to normalise the concentrations of the REE are taken from Boynton 1984.

In Fig. B and C we see the result of 0.1 % addition of OIB, Bulk Crust, and GLOSS to a FSL as well as variably depleted FSL as an example of the model

|     | Ol | Opx | Cpx | SP |
|-----|------|------|------|------|
| La | 0.000053 | 0.000044 | 0.0536 | 0.00002 |
| Ce | 0.000105 | 0.00014 | 0.0858 | 0.00003 |
| Pr | 0.000251 | 0.00033 | 0.137 | 0.0001 |
| Nd | 0.000398 | 0.00052 | 0.1873 | 0.0002 |
| Sm | 0.00065 | 0.0016 | 0.291 | 0.0004 |
| Eu | 0.0008 | 0.0033 | 0.329 | 0.0006 |
| Gd | 0.0015 | 0.005 | 0.367 | 0.0009 |
| Tb | 0.0021 | 0.0067 | 0.405 | 0.0012 |
| Dy | 0.0027 | 0.0084 | 0.442 | 0.0015 |
| Ho | 0.005 | 0.0127 | 0.415 | 0.0023 |
| Er | 0.01 | 0.017 | 0.387 | 0.003 |
| Tm | 0.016 | 0.025 | 0.409 | 0.0038 |
| Yb | 0.027 | 0.033 | 0.43 | 0.0045 |
| Lu | 0.03 | 0.041 | 0.433 | 0.0053 |

**Table 2.** Mineral/Melt partition coefficients for REE used in the present melting modelling. The coefficients are from, Gurenko and Chaussidon (1995), Hart and Dunn (1993), Johnson et al. (1990) Jones (1995), Ozawa and Shimizu (1995), Yang et al. (1998), Zack et al. (1997).
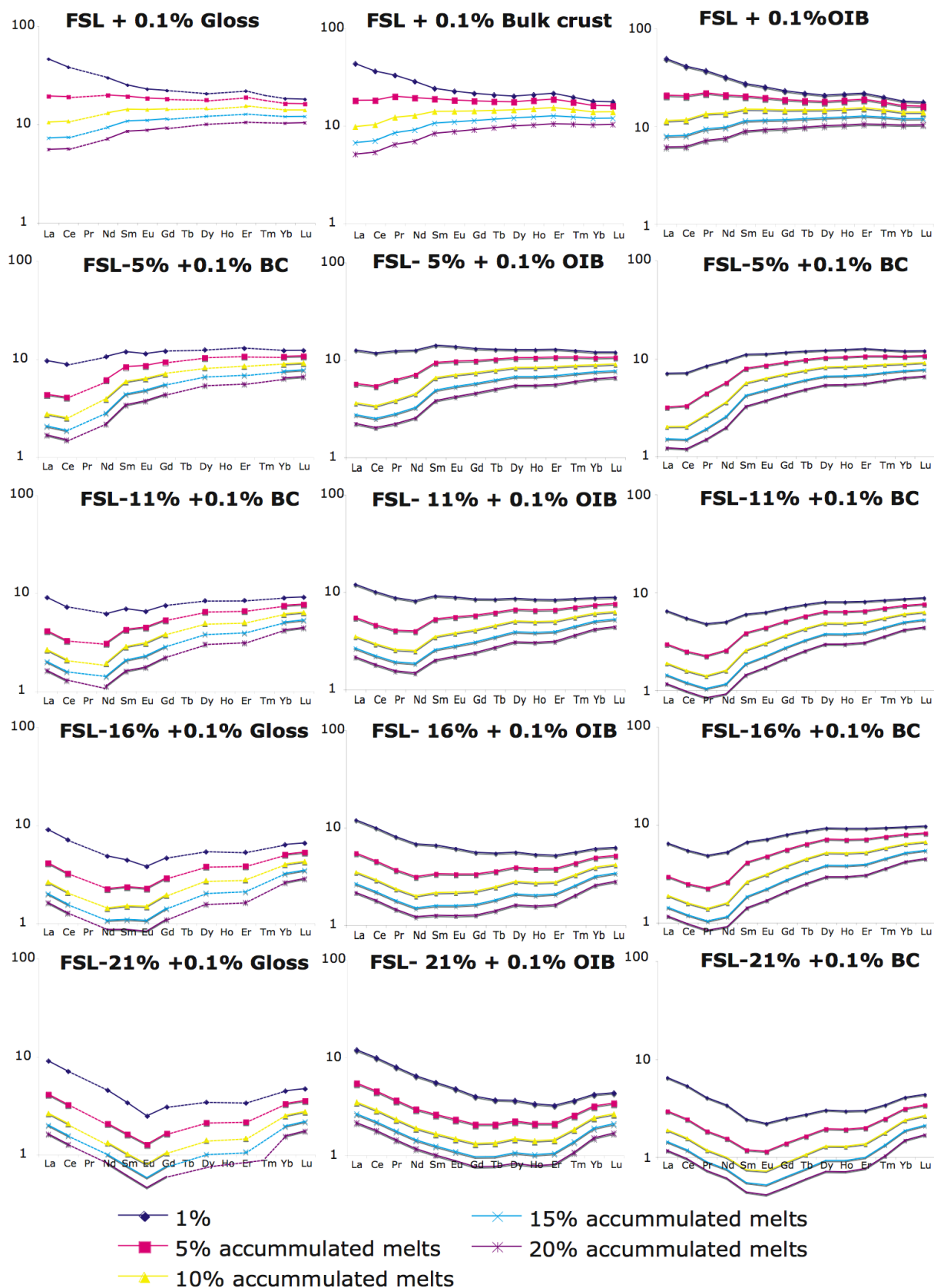
**Fig. B**. REE patterns of accumulated melts produced by non-modal equilibrium partial melting of a FSL, FSL-5%, FSL-11%, FSL-16% and FSL-21% source that has been modified by the addition of 0.1% BC and OIB.

# 2.3 Sample Preparation and analytical techiques

**Mineral analyses**

**Thin section preparation**

The rocks were cut in small blocks and then sliced in suitable size for the thin section. The surface was worked with different polishing materials on rotating surfaces and the finalisation of the preparation was achieved when the thin section reached the thickness of 40µm using a 600/2 diamond paste.

**Mineral chemical analyses**

Mineral analyses were carried out in the dedicated microprobe laboratories in Mainz. A minor amount of mineral analyses from samples from the Oraikastro ophiolite have been taken from Zachariadis (2002). The analytical equipment in Mainz was a WDS Jeol Superprobe JXA 8900R. Prior to entering the microprobe the samples were carbon-coated under vacuum and then degassed for 5 hours in a vacuum chamber. The measuring conditions were, beam diameter of 2µm, accelerating voltage of 15 kv, 12 nA current. The total measuring time for each spot was nearly 2 min for the silicates and the analytical program was SilIUMainz The time was increased to 4 minutes per spot for the spinels and olivines and the program used was SpinellUMainz and UltraUMainz

## Whole-rock analyses

**Sample preparation**

The samples were reduced in size using a hydraulic press and a jaw crusher. Rock bits were carefully hand picked, with intention to select the freshest ones and avoid alteration effects and veining, thus being representative of the sample. The selected rock pieces were washed in an ultrasonic bath with distilled water supplied from a Millipore system, and then powdered in an agate mill.

**Glass Pellets**

The fusion disks were prepared by mixing lithium tetraborate in 6:1 ratio with sample powder. The amounts of materials used were 0.8000±50mg sample and 4.8000±50mg lithium-tetraborate. The melting procedure took place in platinum crucibles applying 5 min

pre-heating and 5 min heating over bulsen lamps. The platinum crucibles were cleaned in a ultra-sonic bath using a mild solution of water and HCl (1/10 ratio).

**L.O.I. (loss on ignition)**

Loss on ignition was calculated on 2gr of powdered sample. The sample was weighted in ceramic crucible and then inserted into the oven. The process included 1 hour step up heating to 1000°C, and 2 hours staying on maximum heat (1000°C). The L.O.I. was calculated on the weight difference before and after the heating stage.

**Powder Pellets**

The powder pellets were prepared by mixing 6gr of sample with 15 drops of Scandiplex resin and 10 drops of Scandiplex hardener inside an agate mill. The mixture was homogenised for approximately 10 min and then inserted in a mould that had the same dimensions as the XRF sample holder. Pressure of 8 Atm was applied on the mixture for 20 seconds. This amount of pressure was important for the matrix correction during the X.R.F. analysis. After that, the pressed material was inserted into an oven for 4 hours (preferably overnight) at temperature of 55°C for the resin and the hardener to cure down.

**X.R.F.**

Whole rock analyses for major and trace elements were performed using partly a Phillips PW 1404 and a Philips Magic X Pro spectrometer based on the principles of X-Ray fluorescence. The measurement conditions are described on the webpage of the laboratory (http://www.uni-mainz.de/FB/Geo /Geologie/EMSRFA/RFA.html).

**LA-ICPMS**

Further trace element analyses were carried out in the department of geochemistry of Max-Planck-Institute in Mainz, using an Finnigan Element 2 high-resolution single-collector ICP-MS in conjunction with a laser ablation facility (213 nm Merchantek). The samples were melted on an Iridium stripe by applying high current of 120A for 20 secs, and cooled down using Ar gas. The amount of sample used for the preparation was 40mg. Three spot analyses per sample were made on each fused glass. The instrument was calibrated against NIST612 using the reference values proposed by Jochum *et al.* (2000). $^{43}$Ca isotope was used as the internal standard, based on CaO concentration determined by the XRF. Spot size was 20μm and the counting time was 30s for the blank-background and 80s the sample analyses.

**Isotopic investigations**

For whole-rock Sr- and Nd-isotope composition analyses, very fine grained sample powders were dissolved in acidic inside Savillex beakers on heating plates. 50 mgr of sampled was weighed in the Zavilex beaker and left for one day to be digested with HF. After that the Hf was evaporated and the dissolving continued with the digestion of the sample with small amounts of HF and $HClO_4$ and then left to evaporate on heated plates. The final dissolution was achieved adding 5ml 6N 2* HCl and then evaporating it. Before the seperation of the Sr and Nd, the sample was dissolved in 1,2ml 2,5N HCl 2* and centrifuged. In cases of felsic samples, the dissolving took place in Teflon bombs using five steps of digestion with acids. In the three steps the samples was attacked with an solution consisted of 1/3 $HNO_3$ and 2/3 Hf. The two were carried out using 6N HCl.

The Sr and REE chromatographically separated using 5 ml cation-exchange resin columns, following standard procedures (White & Patchett 1984), including a second clean-up step for Sr using 1 ml resin columns. Nd was collected from the REE fraction with HDHP-coated Teflon columns. 200ngr of Sr was loaded with $TaF_2$ on W filaments, whereas Re filaments in double configuration were used for Nd measurements. Isotopes were measured with a Finnigan MAT261 thermal ionization mass spectrometer (TIMS) in multicollector mode. Mass fractionations were corrected to $^{146}Nd/^{144}Nd=0.7210$ and $^{86}Sr/^{88}Sr=0.1194$. International standards were also measured over the period of measurements. For La Jolla, the measured $^{143}Nd/^{144}Nd$ ratio was $0.511819\pm9$ (= 16), whereas for NIST SRM 987 (formerly NBS 987) an $^{87}Sr/^{86}Sr$ ratio of $0.710234\pm12$ (=16) was obtained.

# Geochronology

**Zircon separation**

To separate the zircons from a rock chunk a reduction of the rock size to the grain level is necessary. For this reason we process the sample according to following procedure. We wash the sample thoroughly to prevent contamination from minerals that have been transported to the sample from another source and that are hidden now in cracks or on the surface dirt. For reducing the sample size we use a configuration consisting of jaw crushers, rotating mills and drum-mills. After every step we use the 500mμ sieve to take the fraction that is below the limit. We do that to avoid over-crushing the minerals of the sample so in the end we take entire crystals. We pass the product of the crushing stage through a hydro-mechanical separation stage using a shaking stage supplied with water which is known as Wilfley table. At this stage we get rid of the clay minerals together with most of the very light mineral fraction of our sample. The fraction obtained from the hydro-mechanical separation is let to dry out. After that we introduce the sample to a magnetic separation stage. Here we

make use of the paramagnetic properties of the minerals by applying a magnetic field on their direction of movement.  The result of that is that minerals follow separate ways according to whether a mineral is magnetic under the given magnetic field. Zircons are non-magnetic minerals. To separate them we usually keep the fraction from the separator that is not magnetic to 1.2A. In some cases we can go up to 1.8A. By doing so we remove the metamictic and the zircons that have inclusions. In this stage all the metallic minerals such spinel, chromite and Fe-oxides as well as mafic minerals such olivine, pyroxene hornblende, and amphibole are separated from the rest. The non-magnetic fraction that is collected goes under density separation using liquids that have high density. The principle here is to seperate the minerals that have lower density than zircons from the zircons. For that reason we choose to use the "heavy" liquids bromoform  that has a density of 2.8kg/cm$^{-3}$ and then methylene-iodide that has a density of 3.37kg/cm$^{-3}$. Zircons have density of 4.6-4.7kg/cm$^{-3}$. In this stage we remove all the non-magnetic minerals that have lower that 3.37kg/cm$^{-3}$ density like feldspars and quarz. The heavy fraction that was produced after the above-mentioned separation stages except from the zircons also contains other heavy minerals such as apatitite and titanite. The final separation of zircons is achieved through careful hand picking using binoculars and making use of the crystallographic properties of the mineral. Zircons can distinguished from other mineral from the shape, and brightness and colour.

The zircons were prepared in mounts using resin and harder. The mounts were left to cure down for 5 days at room temperature and normal pressure before further processing. Further processing included polishing until the half width of the zircon grains.

**CL-imaging**

CL-imaging was applied to the separated zircon populations prior to geochronology, for identifying the inner structure of zircons and distinguish between different crystal domains and multistage crystal growth. The information collected was used to deduce the evolution history of the zircon grains and select the exact place of the spots to be analysed. CL pictures of the analyzed zircon crystals were also produced after the SHRIMP analyses to verify the points and prevent possible misleading conclusions. The equipment used for that reason was a Cameca Camscan MX2500, equipped with a Bentham CL-detector, located in the Centre of Isotopic Research (CIR) at VSEGEI in St. Petersburg, Russian Federation. The scanning electron microscope was operating at accelerating voltage of15kV and at 5nA current. Before beeng inserted to the analytical equipment the mounts were Au-coated in vacuum for 1sec at 20mA.

**SHRIMP**

In-situ U–Pb analyses were performed on a SHRIMP-II in the Centre of Isotopic Research (CIR) at VSEGEI, applying a secondary electron multiplier in peak-jumping mode

following the procedure described by Compston et al (1984) Williams (1998), Compston (1999), and Larionov et. al, (2004). A primary beam of molecular oxygen was employed to bombard zircon in order to extract secondary ions. A 70 µm Kohler aperture allowed focusing of the primary beam so that the ellipse-shaped analytical spot had a size c. 27 x 20µm, and the corresponding ion current varied from 3.7 to 4.5nA. The sputtered secondary ions were extracted at 10 kV. The 80µm wide slit of the secondary ion source, in combination with a 100µm multiplier slit, allowed mass-resolution M/$\Delta$M $\geq$ 5000 (1% valley); thus, all the possible isobaric interferences were resolved. One minute rastering over a rectangular area of c. 35 x 30 µm was employed before each analysis in order to remove the gold coating and possible surface common Pb contamination.

The following ion species were measured in sequence: $^{196}Zr_2O$–$^{204}Pb$–background (c. 204 AMU)–$^{206}Pb$–$^{207}Pb$– $^{208}Pb$–$^{238}U$–$^{248}ThO$–$^{254}UO$ with integration time ranging 2 to 14 seconds. Five cycles for each analyzed spot were acquired. Apart from 'unknown' zircons, each fifth measurement was carried out on the zircon Pb/U standard TEMORA 2 (Black et al., 2004). It has an accepted $^{206}Pb/^{238}U$ age of 416.75 ±0.24 Ma. The SL13 zircon with U concentration of 238 ppm and a $^{206}Pb/^{238}U$ age of 572.1 ±0.4 Ma (Claoue-Long et al. 1995) was applied as "U-concentration" standard.

**Data reduction and processing**

Data reduction of the SHRIMP data was carried out using the SQUID 1.12 excel add-in developed by Ludwig 2005a. Data plotting was done with the help of the ISOPLOT/Ex 3.22 excel add-in developed also by Ludwig 2005b.

# Chapter 3. The geochemistry and petrology of the Gevguely ophiolite.

## 3.1 Introduction

The Guevguely ophiolite is situated in the southern part of the Balkan Peninsula in Greece and F.Y.R.O.M. In this study we will focus our interest in the southern part of this ophiolite, located in the territory of Greece.
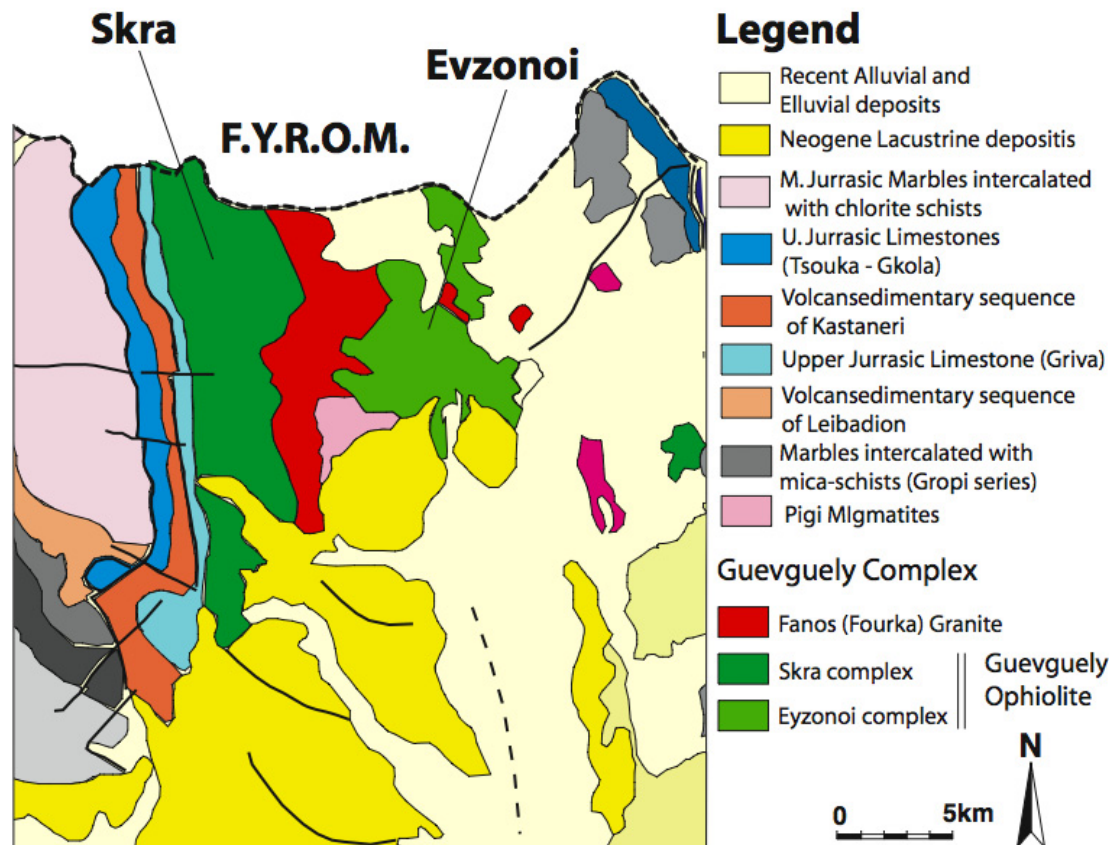


**Fig. 1**. Simplified map of the geology of the Guevguely ophioite and the surrounding area. The ophiolite is marked by the green colour. The eastern part of the ophiolite is the Skra complex and the west part is the Evzonoi complex. (modified after Bornovas and Rondogianni 1983)

The Gevguely ophiolite outcrops at the eastern border of the Vardar Zone to the Circum-Rhodope Belt (Kaufmann 1976) and the Serbomacedonian Massif (Himmerkus et al., 2005). The mafic complex is divided in two parts by the intrusion of the Fanos granite (Christofidis et al. 1990, Soldatos et al. 1993) in some parts of the literature the Fanos granite is referred to as the Fourka granite. For making the reference to each part easier the western part of the Guevguely ophiolite will be hereafter referred to as the Skra complex whereas the

eastern part will be referred to as the Evzonoi complex. To the west the ophiolite is thrusted onto the Paikon arc while the rest is surrounded by the sediments of the Axios-Vardar river.

The western part namely the Skra complex consists of parts of the gabbroic complex and extrusive rocks (sample photos from the outcrops can be seen in Appendix G). Bebien (1982) reports the presence also of ultramafic rocks, which could not be found and therefore they have not be sampled. The cumulate rocks are composed of Ol-gabbros and gabbros. The extrusives are mainly massive lavas and dykes. Within the gabbroic complex it was possible to spot locally some ponds of felsic differentiates that have been collected for purpose of the age determination of the Gevguely complex.

The Evzonoi complex is composed of pillow lavas, massive lavas and a sheeted dykes complex. Within the sheeted dykes it is possible to find acidic volcanic (rhyolites) dykes cross-cutting the mafic dykes, containing in places xenoliths of the adjacent mafic rock. The margins of these rhyolitic dykes against the mafic dykes as well as to the xenoliths are very sharp. The xenoliths have sharp boundaries and undeformed shape suggesting that the intrusion of the felsic volcanics took place after the cooling of the mafic rocks. Fieldwork was also extended into the Fanos granite in order to examine whether there is evidence of post-granitic mafic magmatism present in the granitic body. During the fieldwork it was possible to identify rare occurrences of mafic dykes intruding in the Fanos granite. These dykes were sampled and examined aiming to identify the nature of their chemistry and deduce information on their formation, in an attempt to identify the episodes of magmatism in this area and investigate whether the ophiolite formation has preceded the granite crystallisation or it belonged to a latter magmatic event.

In this chapter I present the geochemical and the radiometric data obtained for the Guevguely complex. The sampling was especially focused on the extrusive sequence of the Guevguley complex. We will then interpret these data to define the petrological and petrogenetic characteristics of this complex investigate the relation between the two parts of the Guevguely complex and construct a model for the geotectonic evolution of the area.

## 3.2 Geochemistry

### 3.2.1 Major and trace element analyses

The chemical composition of the rocks from the Skra and Evzonoi complex are presented in appendices D,E,F. The samples forms Skra are marked as GVL samples while the samples from Evzonoi as EYZ.

The samples from both the Skra and Evzonoi complexes appear to be altered to greenschis- facies metamorphism. Clinopyroxenes have been mainly altered to chlorite and actinolite. Calcic-Plagioclase is altered to albite. Secondary minerals occurring in the samples are chlorite, titanite, epidote, and variable amounts of quartz. Relics of unaltered

clinopyroxene that was possible to be found have been analysed by microprobe and have augitic composition.
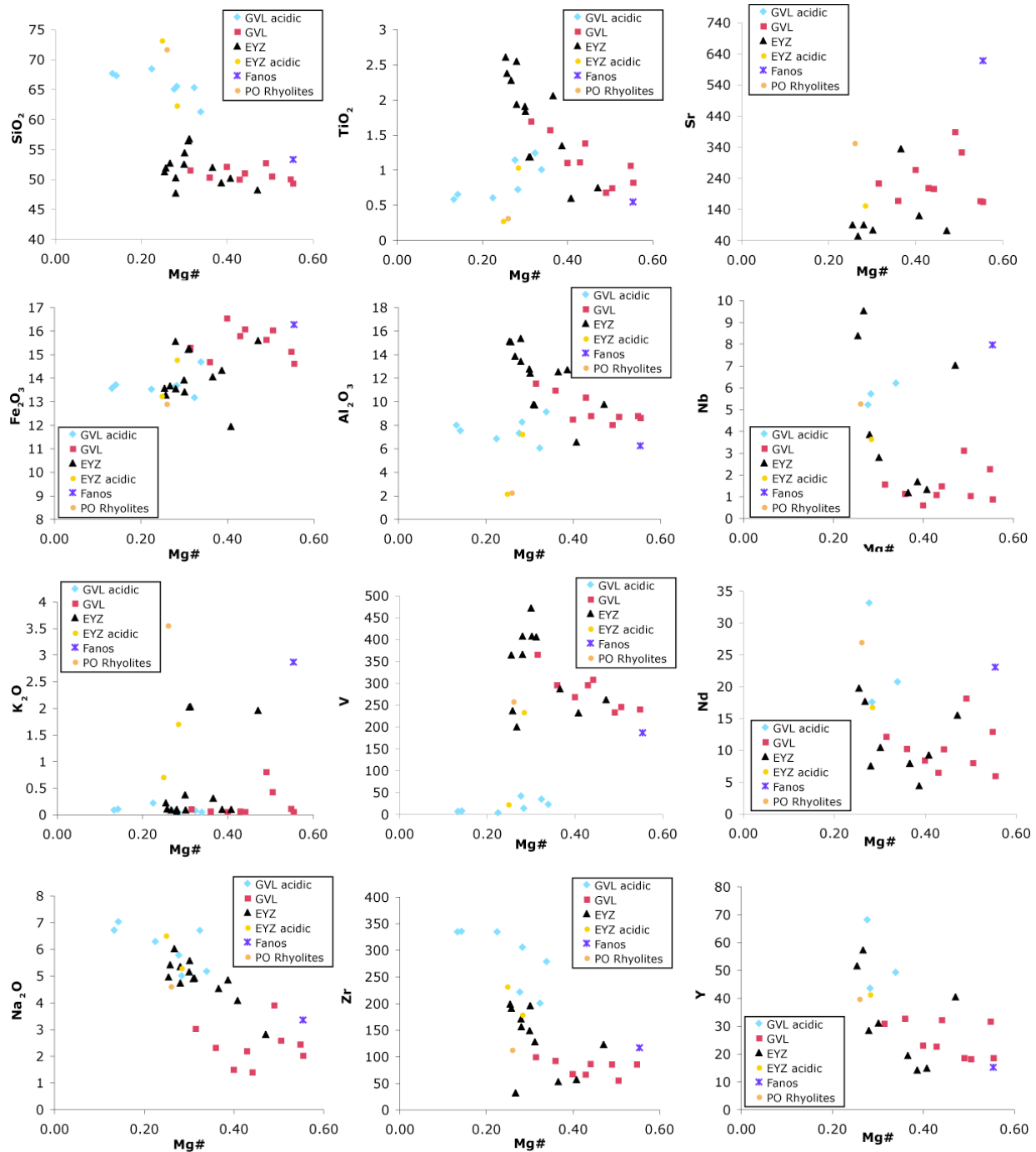


**Fig. 2.** Element versus Mg# for the mafic and acidic samples from the Evzonoi and Skra complexes. GVL: samples from SKRA, EYZ: samples form Evzonoi, FA: mafic dykes from fanos, PO Rhyolites: post-ophiolitic rhyolites.

In Fig. 3 variation diagrams of major and the trace elements against Mg# are presented. In most of the diagrams there is an irregular and unclear variation of the elements against Mg#. This could the result of element mobility during alteration. For that reason we have examined the co-variation of elements vs Zr. The plots are shown in Appendix F.
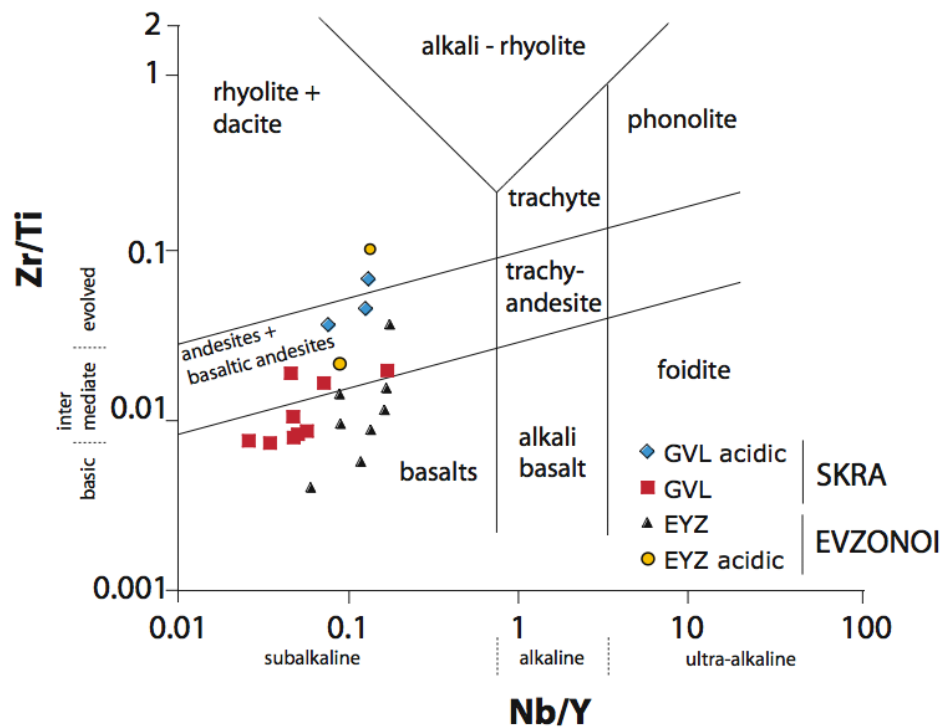


**Fig. 3.** Zr/Ti versus Nb/Y for the volcanic samples from the Skra and Evzonoi complex of the Guevguely ophiolite. (after Winchester and Floyd (1977) revised after Pearce et al 1996)

These diagrams are used to evaluate the influence of the alteration on the elemental mobility. The choice of Zr as index is justified by the fact that Zr is general regarded as an immobile during alteration element. It becomes immediately apparent from the major element versus Zr diagrams that the mafic and the acidic samples from Skra (shown as GVL samples) correlate well with Zr adundances suggesting that these samples and by implication the Skra complex hava been least affected by alteration.  In all diagrams the acidic and the mafic samples have the same kind of behaviour except form the TiO$_2$ versus Zr diagram. In this diagram the mafic samples have positive correlation with Zr whereas the acidic ones have negative correlation. This could be ascribed to titanomagnetite fractionation in the acidic samples that lowers the concentration of Ti in the more differentiated compositions while leaving the concentration of Zr unaffected By contrast the samples from the Evzonoi area show a less uniform behaviour than the samples from Skra. TiO$_2$ and Fe$_2$O$_3$ seems to be relative undisturbed by alteration while the rest of the major elements do not seem to correlate with Zr. Most of the trace-element concentrations for both Skra and Evzonoi samples

correlate well with that of Zr. Sr however seems to be highly disturbed by alteration. The acidic samples form Skra are highly depleted in V relative to the rest of the samples and are very well correlated towards Zr. As mentioned above, this is due to titanomagnetite fractionation that strongly fractionates V in addition to Ti. Sample GVL 15 deviates systematically towards higher concentration in all elements versus Zr plots, except Y, Yb and Hf. For the petrogennetic investigations of the Skra and Evzonoi complexes we will make use of the most undisturbed by alteration elements according to the plots, namely $TiO_2$, Y, Nb, Zr, Yb, Ta, Th, and Hf.

   ***Skra Complex:*** The Skra complex is characterised by the occurrence of bimodal magmatism. The extrusive part of the complex is built up of both mafic and acidic rocks that have a compositional gap in silica between 52.71wt% and 61.22wt%. The acidic rocks are located in the southern part of the Skra complex. The mafic rocks are classified as subalkalic basalts according to the Winchester and Floyd (1977) classification scheme (modified by Pearce (1996), Fig. 3.) whereas the acidic rocks are classified as andesites and dacites.
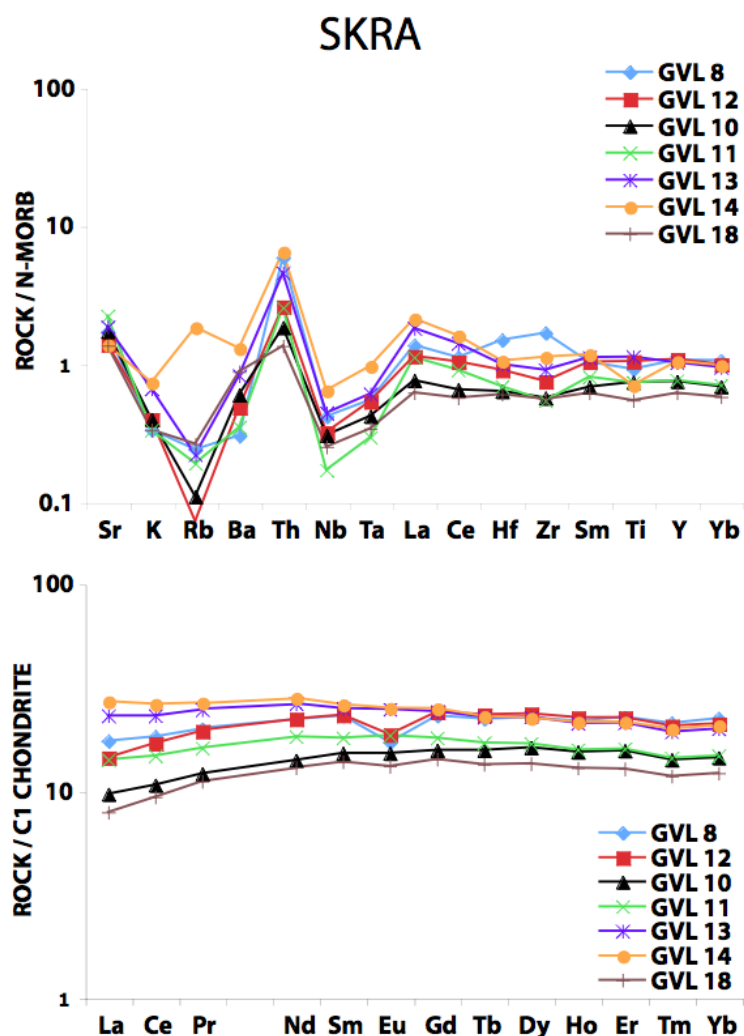


**Fig. 4.** REE diagrams for the Skra samples normalised to C1 chondrite. Normalised to N-MORB multielement "spiderdiagramms" for the same samples. Normalising values for N-MORB are from Pearce (1982, 1983) and C1 after and from McDonough and Sun (1995).

The mafic extrusives from the Skra complex have $SiO_2$ 49.31wt% - 52.71wt%, MgO 4.77wt% - 9.65 wt% and $TiO_2$ 0.68wt% - 1.69wt%. Relative to N-MORB they are depleted in LILE except for Sr (Fig. 4). Th is enriched, forming a positive anomaly while there is a negative Nb anomaly. Generaly there is a depletion trend in the HFSE from Yb to Nb suggesting that these rocks were most probably derived from a previously depleted source. Some samples show a slight enrichment in La and Ce. Samples GVL 15 and GVL 16 are enriched in the LILE and they have a pronounced enrichment in La and Ce (Fig. 6). The mafic samples from Skra have variably-depleted LREE patterns relative to carbonaceous chondrite (Fig. 4). Most of the samples have slight to no Eu anomalies and relatively flat HREE normalised to carbonaceous chondrite patterns suggesting only moderate (if any) plagioclase fractionation in the source and no involvement of garnet during melting of the source of the rocks thus shallow melting above the garnet lherzolite field. The LILE enriched samples (GVL15 and GVL 16) have are LREE-enriched patterns (Fig.6). Sample GVL 15 has a fractionated pattern (La/Yb>5) suggesting different conditions of genesis compared to the rest of the samples from Skra complex. The steep slope from La to Yb can be the result of garnet present in the source, which suggests that the melting of the source has taken place at greater depths than of the rest of the samples. GVL 16 has a less fractionated pattern (La/Yb=2) with nearly flat HREE, which resembles the HREE patterns of the rest of the Skra samples (Fig. 4).
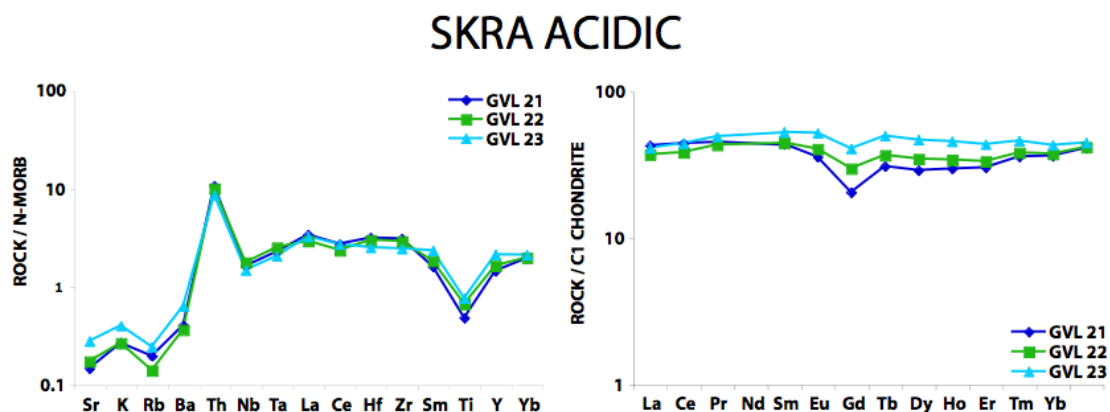


**Fig. 5.** Normalised to C1 chondrite REE diagrams for the acidic samples from Skra. Normalised to N-MORB multielement "spiderdiagramms" for the same samples. Normalising values like in Fig 4.

The rocks that form the acidic rock suite have $SiO_2$ 61.22wt% - 68.41wt%, MgO 1.11wt% - 4.22 wt% $K_2O$ 0.04wt% - 0.21wt% $TiO_2$ 0.58wt% - 1.24wt%. These low-K andesites and dacites are depleted in the LILE relative to N-MORB. There is a distinctive positive Th anomaly and negative Nb and Ti ones. They also display a negative Ti anomaly. The Nb/Yb ratio is less than one but the HFSE patterns are subparallel to the N-MORB axis. In chondrite-normalised diagrams the acidic samples from Skra are LREE-depleted, they have a negative

Eu anomaly and flat HREE to slightly enriched HREE patterns suggesting similar shallow melting conditions for their source as the mafic samples from Skra. The REE patterns of the acidic rock suite form the Skra complex resemble the REE patterns of the andesites and dacites from the Tonga- Kermadec system (Ewart and Hawkesworth 1987).
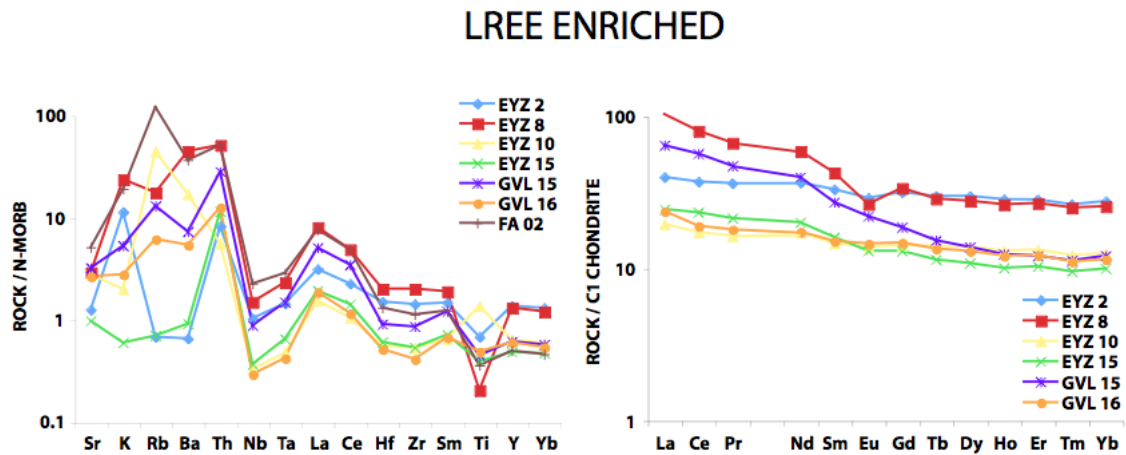


**Fig. 6.** REE diagrams for the acidic and LREE-enriched mafic samples from the Skraa and the Evzonoi complexes normalised to C1 chondrite. Normalised to N-MORB multielement "spiderdiagramms" for the same samples. Normalising values for C1 after and for N-MORB like in Fig 4.

The mafic and the acidic samples from the Skra complex cannot be directly genetically correlated to each other. This is clearly evident in the Mg# versus $SiO_2$ diagram of Fig. 7. On this diagram, the two groups of samples form two distinctly different trends that cannot be related via crystal fractionation processes. The most differentiated mafic sample has the same Mg# value as the least differentiated acid sample, but the compositional gap between them in terms of $SiO_2$ content precludes any possible genetic link between them.



**Fig. 7.** Mg# versus $SiO_2$ for the mafic and acidic samples from the Skra complex of the Guevguly ophiolite. Mg#=Mg/(Mg+0.9$Fe_2O_3$). Red squares represent the mafic samples whereas the blue rhombus reprents the acidic samples.

***Evzonoi complex:*** The Evzonoi complex is characterised by the occurrence of mafic and intermediate rocks. A minor presence of acidic rock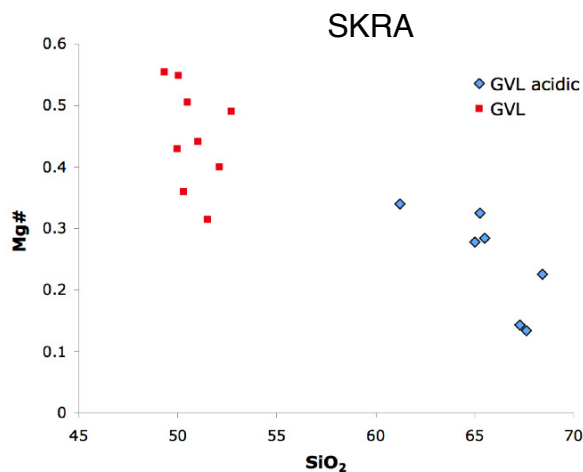s is related to the intrusion of rhyolitic dykes in the mafic outcrop. These rhyolitic dykes, as described in the introduction of this chapter belong to a later magmatic event and therefore cannot be genetically related to the mafic samples. These rhyolites have $SiO_2$ content between 71.65wt% and 73.13wt%, MgO contents between 0.64wt% and 0.71wt% contents between $TiO_2$ 0.27wt% and 0.31wt%. The rhyolites (EYZ8) are enriched in LILE and Th relative to N-MORB, they have negative Nb anomaly and negative Ti. They also display an enrichment trend in the HFSE from Yb to Nb. In chondrite-normalised diagrams these rocks have LREE-enriched patterns, negative Eu anomalies and nearly flat HREE patterns
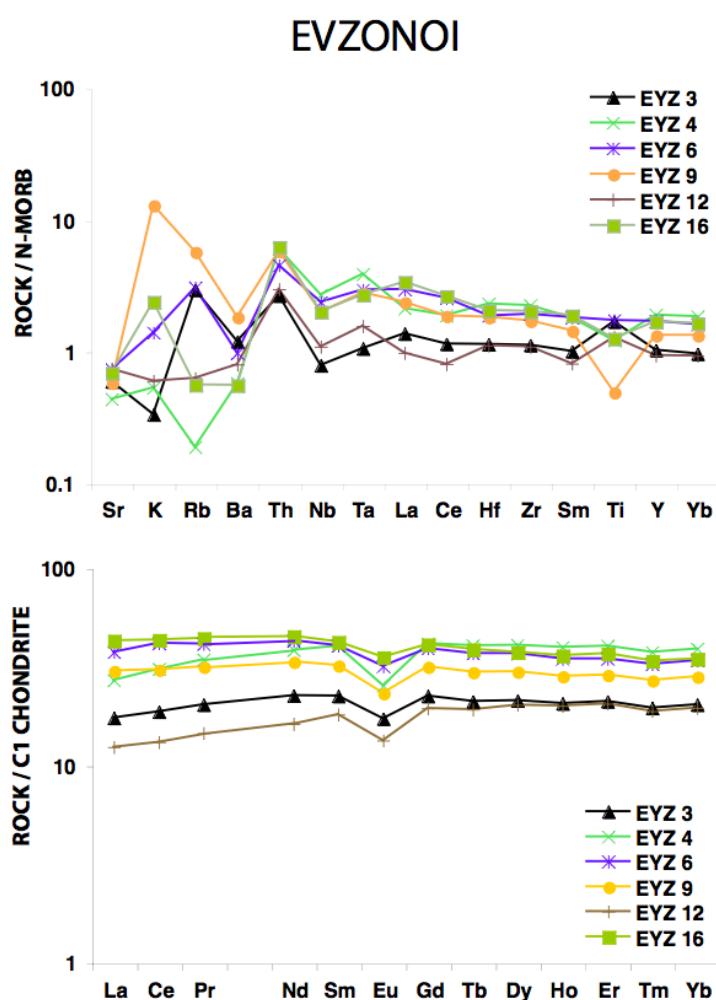


**Fig. 8.** Normalised to C1 chondrite REE diagrams for the Evzonoi samples. Normalised to N-MORB multielement "spiderdiagramms" for the same samples. Normalising values for CI after and for N-MORB as in Fig 4.

The mafic and intermediate rocks have $SiO_2$ content between 48.13wt% and 56.68wt%, MgO 3.94wt% - 7.22wt% and $TiO_2$ 0.59wt% - 2.54wt%. In normalised to N-MORB

spiderdiagrams, the majority of the samples show irregular patterns in the LILE. These rocks are neither significantly enriched nor depleted like their Skra counterparts in LILE. All samples show a positive Th and a negative Nb anomaly and nearly flat HFSE patterns from Nb to Yb. The mafic rocks from the Evzonoi complex show typically LREE-depleted patterns to almost LREE-flat, negative Eu anomalies while the HREE patterns remain flat similar to those of the Skra mafic samples suggesting shallow a melting regime. The mafic rocks that were sampled in contact to the rhyolite intrusions (EYZ 10 and EYZ 9) are enriched in the LILE, they have fractionated LREE patterns, a feature that can be attributed to influence of the rhyolitic intrusion.

As mentioned before, I tried to identify any possible intrusion of mafic dykes in the body of the Fanos granite. Such dykes (e.g. FA02, Fig. 6) were identified and sampled. The multielement diagrams as well as the chondite normalised REE patterns are presented in Fig. 7. FA02 has $SiO_2$ content of 53.24wt%, MgO =6.98wt% and $TiO_2$ =0.54wt%. The same sample has a strongly fractionated normalised to C1-chondrite REE patterns, with a dominant enrichment of the LREE relative to the HREE. The La/Yb is higher than 9. The shape of the patterns is compatible with residual garnet in the source of this rocks suggesting melting in the garnet stability field. This sample has a high enrichment in the LILE , and an enrichment of the HFSE but it also has negative Nb and Ta anomaly. The later is typical of subduction-zone magmatism, as mentioned in the introduction of this part.

## 3.2.2 Sr and Nd Isotopes

The Sr and Nd-isotope data for the Gevguely ophiolite are presented in appendix E. The initial ratios as well as the $\varepsilon_{Nd}$ are recalculated at 165 Ma and the chonditic values used are $^{143}Nd/^{144}Nd$= 0.512638 (Goldstein et al. 1984) and $^{147}Sm/^{144}Nd$= 0.1967 (Jacobsen and Wasserburg 1980, Peucat et al. 1988).

All samples from both the Skra and the Evzonoi complexes have positive $\varepsilon_{Nd(165)}$ values, which is typical for rocks of mantle origin (Fig. 10). In the Skra complex the values range from 2.4 to 6.8 whereas in the Evzonoi complex the values span between 0.62 and 6.5. The $^{87}Sr/^{86}Sr$ values measured are between 0.703206 and 0.705330 for the Skra and between 0.704665 and 0.712489 for the Evzonoi complex.These values have been recalculated to Middle Jurassic like for the $\varepsilon_{Nd(165)}$ before plotted on the diagrams. The acidic samples from Skra have very high $\varepsilon_{Nd(165)}$ values (~ 6), similar to those of sample EYZ 2 a similar acidic sample from Eyzonoi complex. The rhyolites from Evzonoi have the lowest $\varepsilon_{Nd(165)}$ values (0.62) and the highest $^{87}Sr/^{86}Sr$ (0.712489) among the rest of the samples. The post-ophiolitic rhyolites from Evzoni have the lowest εNd values (0.62) and the highest $^{87}Sr/^{86}Sr$ (0.712489) values of the rest of the samples.

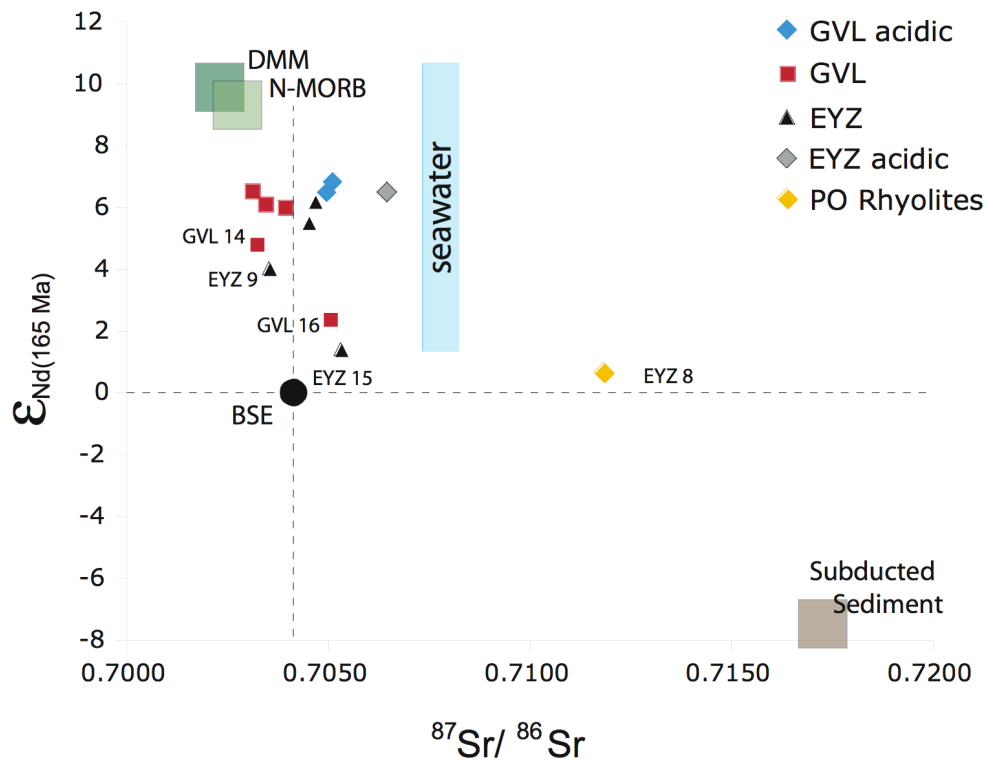**Fig. 10.** $\varepsilon_{Nd}$ versus $^{87}Sr/^{86}Sr$ for the samples from both complexes of the Guevguely ophiolite. BSE: Workman and Hart (2005), DMM :Rehkamper and Hofmann (1987), and Klein (2004), MORB:Kelemen et al. (2004) and Seawater values after from Burke et. al (1982).
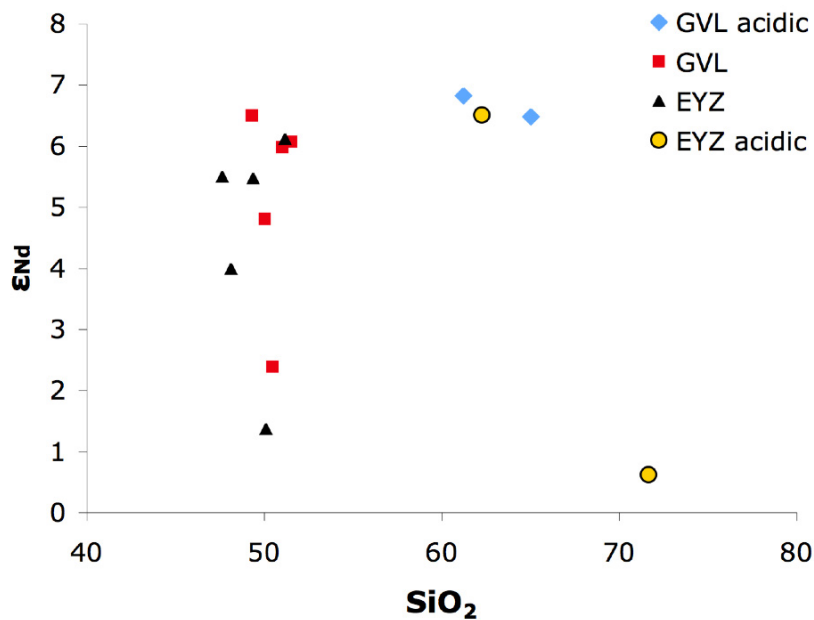


**Fig. 11.** Plot of the $\varepsilon_{Nd}$ versus $SiO_2$ for the samples from the Skra and Evzonoi complexes of the Guevguely ophiolite

The mafic samples from Guevguely have positive correlation of the $\varepsilon_{Nd(165)}$ and the $^{87}Sr/^{86}Sr$ (Fig. 9). Sample GVL 14 and 16 are displaced to lower $\varepsilon_{Nd(165)}$ values for the Nd and $^{87}Sr/^{86}Sr$ isotopes compared to the rest of the mafic samples. Sample GVL16 shows LREE-enriched patterns while GVL 14 has relatively flat C1-chondrite normalised patterns (see Fig. 4). The andesites from Skra are displaced from the main trend of the mafic Skra samples towards slightly higher Sr for the same $\varepsilon_{Nd}$ adding up argument to the assumption we made based on the major elements that these samples derived from different processes. The $\varepsilon_{Nd}$ values for all the samples from the Guevguely ophiolite are lower than those of mid-ocean ridge basalts for that time (165 Ma), suggesting that their source was isotopically modified from an enriched component.

As can be see from Fig. 11 the $\varepsilon_{Nd}$ values of the mafic samples decrease independently of the SiO2. This means that a process like AFC could not possibly influence the magmatic evolution of these rocks. The sample EYZ 2 has a high $\varepsilon_{Nd}$ values and a high SiO2 content, this can be ascribed to the influence of the later rhyolitic dykes on the chemistry of some of the mafic rocks.
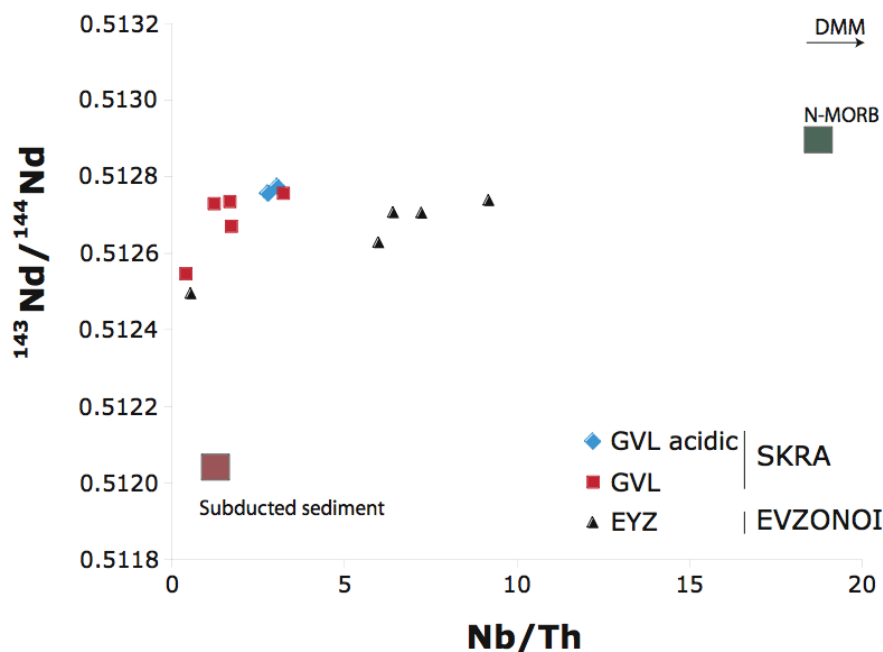


**Fig. 12.** plot of Nd isotopes versus Nb/Th for the samples from the Skra and Evzonoi complexes of the Guevguely ophiolite

$^{143}Nd/^{144}Nd$ is positively correlated with the Nd/Th ratio (Fig. 12). Skra and Evzonoi complexes follow two different trends that can be the appointed to different ratios of mixing between a subducted sediment source and a N-MORB or DMM, or due to different Nb/Th of the sediment component that mixes with the mantle source of each complex.

## 3.2.3 Melting model

In order to quantify the source and melting properties of the Guevguely ophiolite we use the co-variation of a compatible vs. an incompatible element as described in the methods paragraph (Fig. 13).
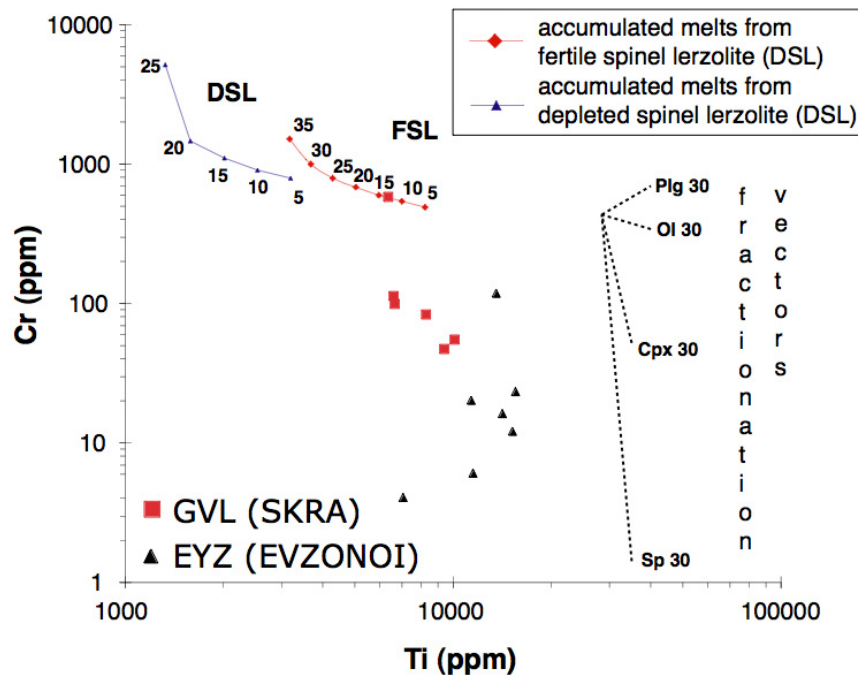


**Fig. 13.** Ti versus Cr diagram for GVL and EYZ samples from the Guevguely ophiolite. (GVL: Skra complex, EYZ: Evzonoi).

The fractionation vectors on Fig. 13 correspond to 30% crystallisation of olivine, plagioclase, clinopyroxene and spinel phases. Accumulated melts represent the mixture of melt fractions of 1wt% that were pooled of the source and mixed together. Examining the Cr vs Ti diagram (Fig. 13) we can infer that the rocks from Evzonoi require very low degrees of melting (<5%) of a fertile spinel lherzolite, while those of from Skra require higher degrees of melting (5-15 %) of the same source.

## 3.3 Tectonomagmatic discrimination

According to the Ti versus V diagram (Fig. 14) proposed by Shervais (1982), the samples from Skra show a positive correlation between V and Ti forming a trend starting from

the overlapping area between the IAT and the MORB-BABB fields to the field of the MORB-BABB. The Evzonoi samples do not uniformly plot in one field, a group of three samples plot in the field of the IAT whereas the majority of the samples plot in the field of MORB-BABB having higher Ti/V values than the Skra samples.
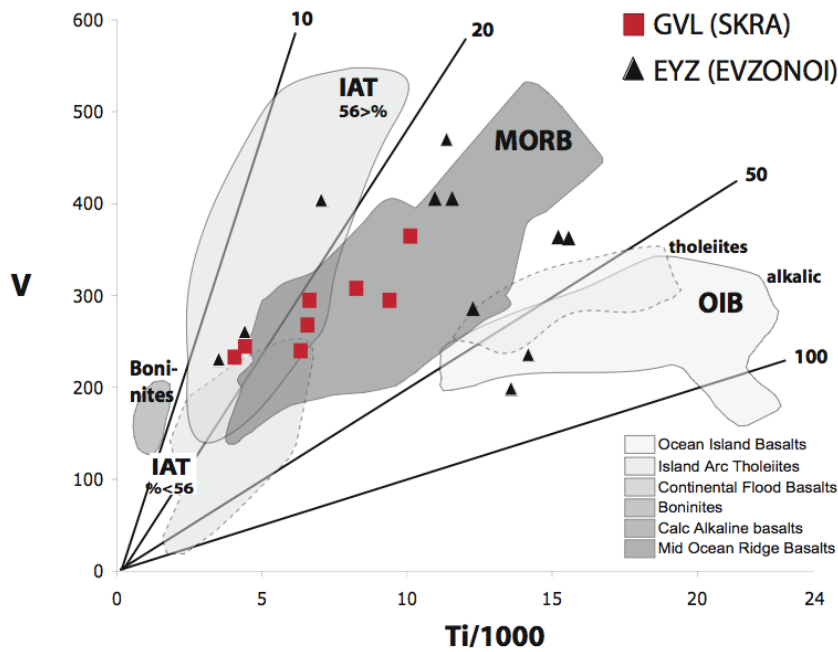


**Fig. 14.** Ti versus V diagram showing the samples from the Skra and Evzonoi complexes After Shervais (1982). The acidic samples are only ploted as indications.
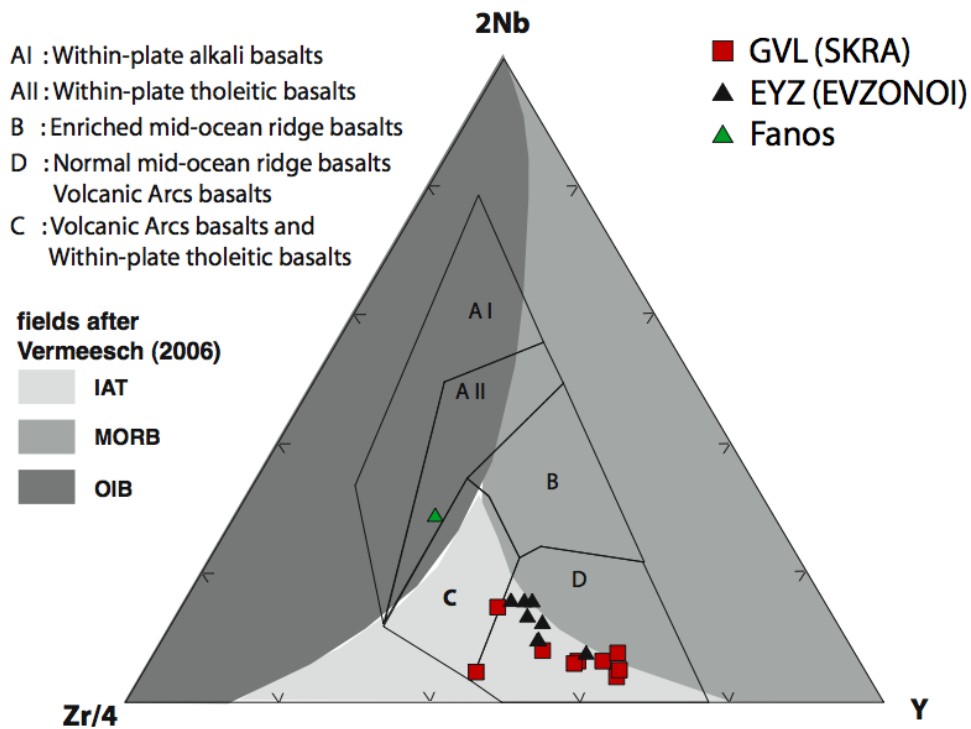


**Fig. 15.** Zr- Nb-Y diagram showing the samples from the Skar and Evzonoi complexes of the Guevguely ophiolite ophiolite. After Meschede (1986).

Pearce and Norry (1979) examined the Ti, Zr, and Y characteristics from basalts erupted at different settings. Nb can be used to investigate the mantle differentiation processes, and the Zr/Nb ratio can be used as a proxy for enrichment or depletion processes in the mantle (Meschede 1986 and references therein), while Zr/Y can be used to investigate long term source heterogeneities and to distinguish between basalts erupted in within-plate settings and basalts erupted in mid-ocean ridges and volcanic arcs (Pearce and Norry 1979 and references therein). Using the same elements Meschede (1986) proposed the Zr-Y-Nb triangular diagram for the classification of mafic extrusive rocks. The samples from Skra plot in the field of N-MORB and VAB (Fig. 15). The samples from Evzonoi plot in the same field as the samples from Skra. None of the samples plot in the field of within-plate basalts suggesting that these samples have not been influenced by within-plate enrichment
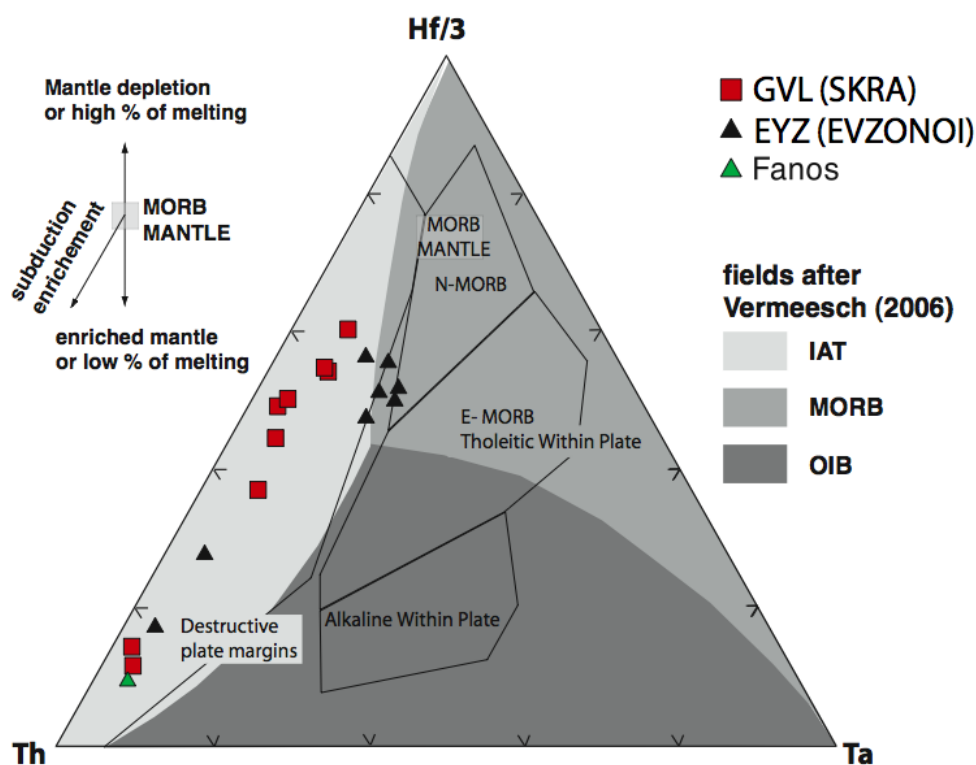


**Fig. 16.** Hf/3-Th-Ta diagram showing the samples from Skra (GVL samples) and Evzonoi (EYZ samples) complexes from the Guevguely ophiolite. After Wood (1980).

On the Th / Hf / Ta diagram proposed by Wood (1980) (fig.16), the samples from Skra plot outside the MORB array and in the field of the destructive plate margin basalts, forming a trend towards higher Th. This trend is discontinuous. Two of the samples (GVL 15, GVL 16) plot towards much higher Th concentrations than the rest. These samples have the lowest Nd highest Sr isotopic values and have LREE-enriched patterns. The majority of the samples

from Evzonoi plot between the field of N-MORB and the field of destructive plate basalts. Two of the samples plot clearly in the field of destructive plate basalts. These samples have the highest LREE enrichment among the Evzonoi sampes. The sample with the highest Th enrichment (EYZ 15) has also the lowest $\varepsilon_{Nd}$ values among the mafic samples from the Evzonoi complex.

## 3.4 Petrogenesis

Th is a strongly incompatible elements and is abundant in pelagic sediments, thus it it is enriched in subductions zones. It can be used as a proxy to identify subduction-zone influence in volcanic rocks (Spandler et al. 2004, Pearce 1982, Wood 1980). Ta on the other hand can be used as a proxy for the source fertility. Normalising Th and Ta against Yb could eliminate the effects of pheno - cryst accumulation.
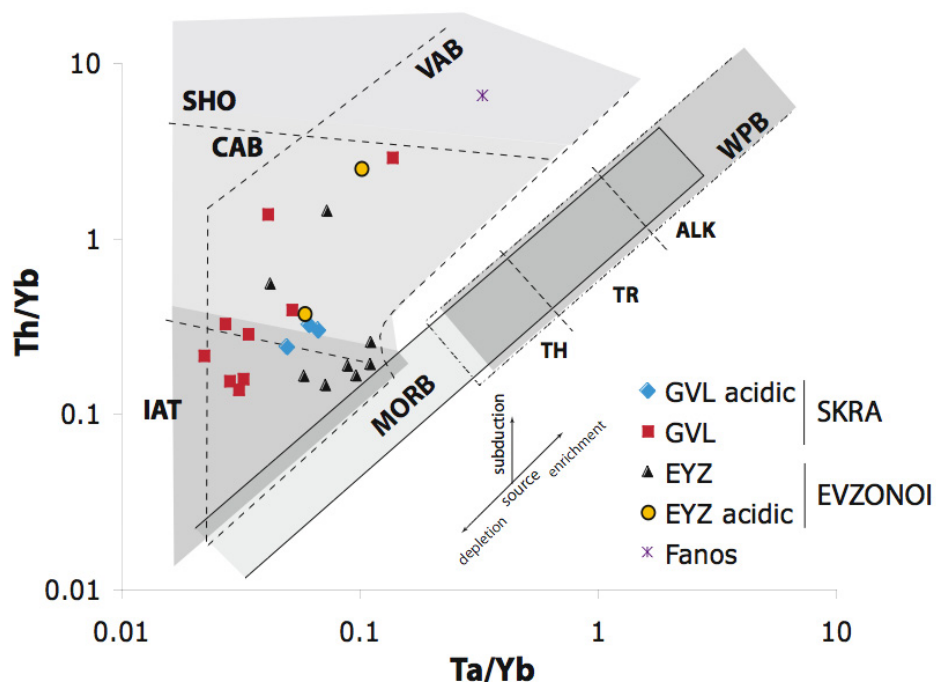


**Fig. 17.** Th/Yb versus Ta/Yb diagram for the Skra (GVL) and Evzonoi (EYZ) samples from the Geuvguely ophiolite. (after Pearce 1982). CAB: calc-alkaline basalts, VAB: volcanic-arc basalts, IAT: island-arc tholeiites, SHO: shoshonites. WPB: within-plate basalts, MORB:mid-ocean ridge basalt.

On the Th/Yb versus Ta/Yb diagram (Fig. 17; Pearce, 1982), all the samples plot above the mantle array suggesting that they all have been enriched in Th, thus their chemistry has been influenced by a subduction derived component. The LREE-enriched samples from Skra and Eyzonio plot in the field of the continental arc volcanics. The LREE-depleted samples from Evzonoi and the Skra complex plot in the field of island-arc tholeiites. The samples from Skra specifically plot very close to the mantle array. Pearce (1982) explaining

the petrogenetic properties of this diagram suggested that by extrapolating the subparallel vector of the subduction enrichment back to the MORB array we could make estimates on the source characteristics.

The samples from both complexes from the Guevguely ophiolite are displaced from the mantle array towards higher Th/Yb ratios. Skra and Evzonoi are forming two different and distinct groups. Back projecting these two groups to the mantle array we can assume that the Skra complex must have derived from a more depleted source that the Evzonoi complex. The LREE-depleted andesites have also elevated vaues of Th/Yb compared to the mantle values and plot between the fields of the IAT and CA. The LREE-enriched mafic samples have the highest Th/Yb values among the samples from the Guevguely complex. The mafic sample that intrudes the Fanos granite (FA02), is displaced towards the highest Th/Yb and Ta/Yb ratios among the rest of the samples.
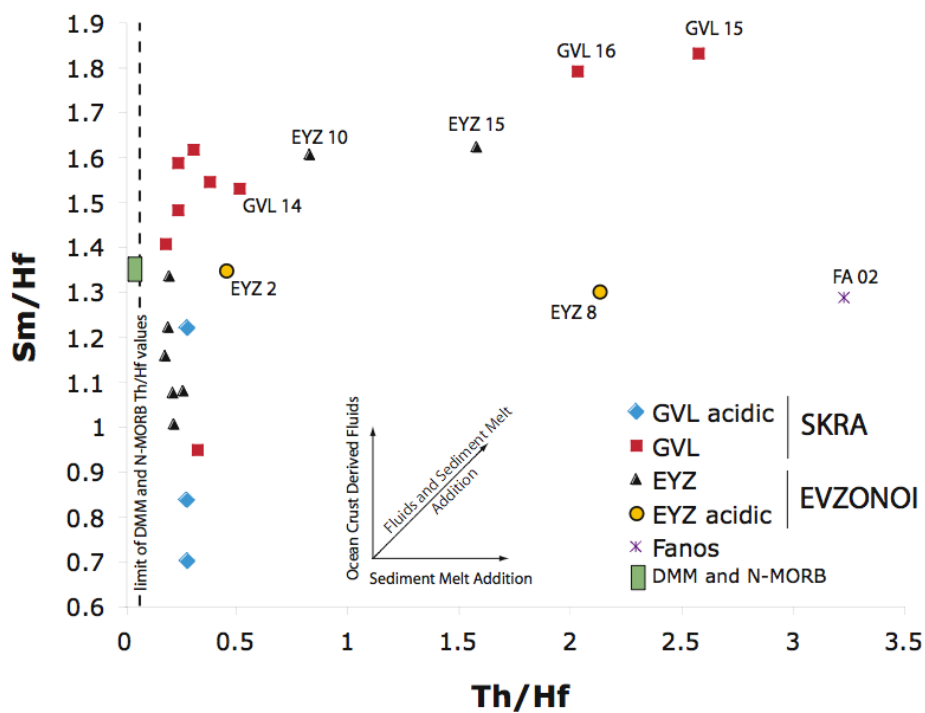


**Fig. 18.** Sm/Hf vs. Th/Hf for the samples from the Guevguely ophiolite. (after Barry et al. 2006, modified)

The LREE-depleted samples from both Skra and Evzonoi complexes show increase in Sm/Hf for a narrow window of Th/Hf values (Fig. 18). The reverse is true for the acidic samples and dyke FA02 that show a spread in Th/Hf values for relatively constant Sm/Hf values The LREE samples show a positive correlation between Sm/Hf and Th/Hf ratio values. Compared to DMM and N-MORB, the LREE-depleted mafic samples possess Th/Hf ratio values that are 3-8 times higher, whereas the LREE-enriched mafic samples possess Th/Hf ratio values that are 20-35 times higher. The LREE-depleted andesites from Skra have Th/Hf

ratios around 4. The rhyolites and the mafic dykes that intrude the Fanos granite have the highest Th/Hf ratios. The enrichment in Sm is possibly caused as a result of aqueous fluid transfer form the slab to the sub-arc mantle or by a low-T melt (Pearce et al. 1995, Barry et al. 2006). The rhyolitic intrusion EYZ 8 and the dyke FA02 as mentioned before are enriched in Th but not in Sm. This can be attributed to sediment melt rather than fluid addition. The LREE-enriched mafic samples follow a positive trend between Sm/Hf and Th/Hf which can be caused by the combined effect of fluid and melt addition.
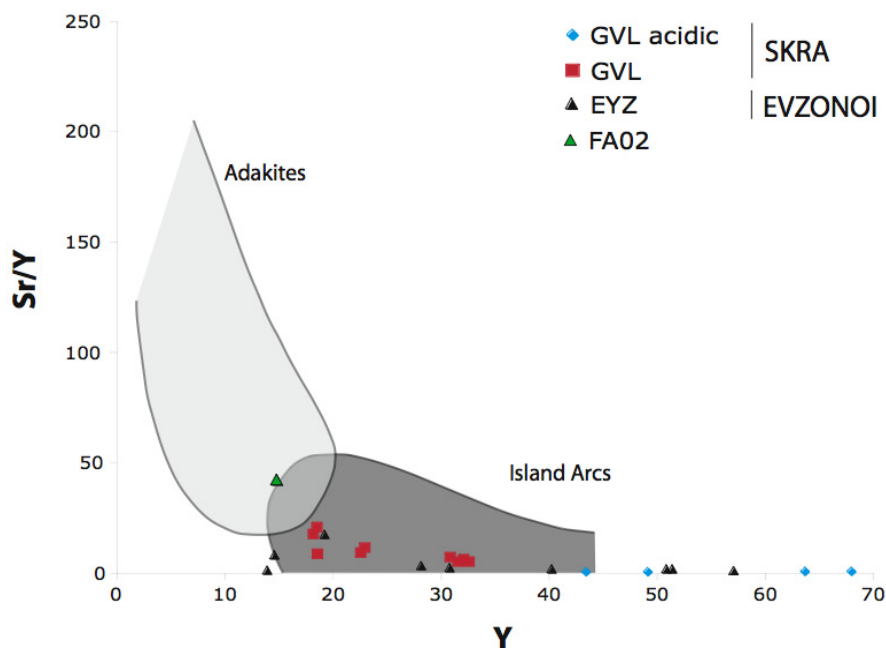


**Fig. 19.** Sr/Y vs. Y for the samples from the Guevguely ophiolite. (after Defant and Drummond 1990)

The melt component that is involved in the genesis of the Guevguely complex is more likely to have been derived from the sediments of the subducted slab only, rather than to be a product of both sediment and slab melt. This is evident from the low Sr/Y values that range from 0-20 (Fig. 19). Slab melts have been connected with the occurrence of adakites and they are characterised by high Sr/Y ratios (Defant and Drummond 1990). The Y concentration is above 10 ppm for all the samples studied here.

# 3.5 Geochronology

The only radiometric age determinations existing so far for the Guevguely ophiolite complex are those of Spray et al. (1984). These authors applied the $^{40}Ar/^{39}K$ method on biotite and kaersutite separates from gabbros and diorites of the complex and suggested a formation age between 149±3 and 163±3 Ma. Danielian et al. (1996) extracted radiolarians from the

deep-sea sedimentary cover directly overlying the ophiolitic extrusives in the Evzonoi complex and determined an Oxfordian age (161.2-155.7 Ma); they suggested an early Late Jurassic age for the formation of both the Skra and Evzoni complexes.
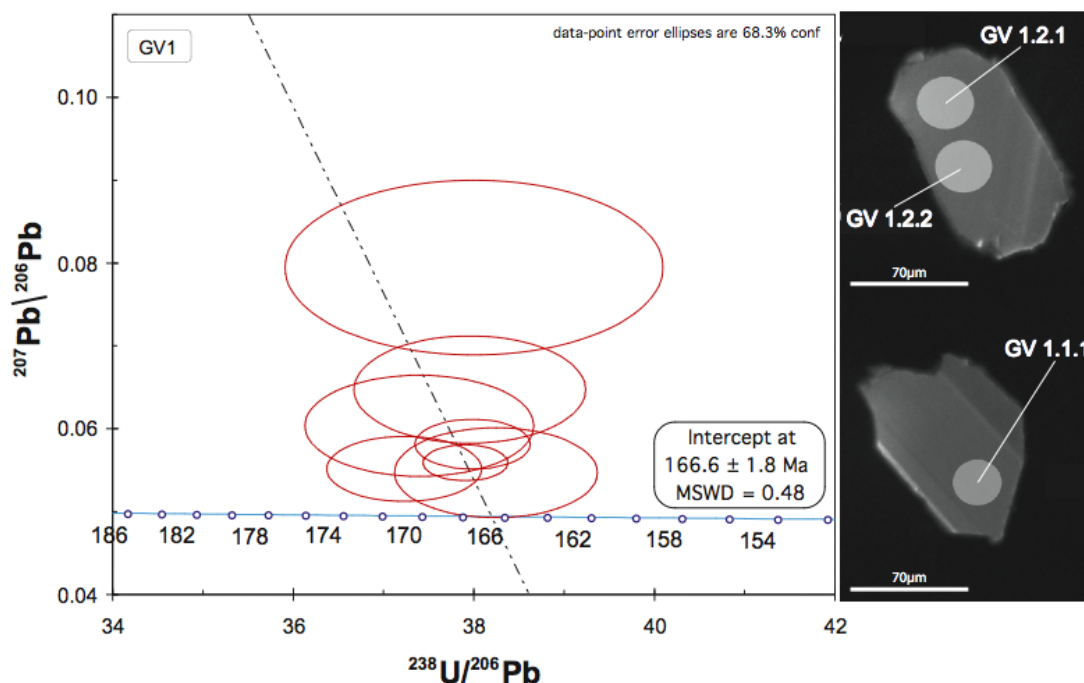


**Fig. 20.** Tera Wasserburg diagram for the Guevguely plagiogranite and representative CL images of zircons. The whitish circles represent individual spot analyses by SHRIMP.

For the purpose of age determination of the Guevguely complex a plagiogranite (trondhjemite) pond within high level gabbros was sampled. The zircons separated are subidiomorphic to allotriomorphic and occasionally broken. They consist of a single domain and do not show any signs of inheritance. Their size varies between 60μm and around 135μm. Cathodo-luminescence (CL) imaging revealed broad to no- developed oscillatory zoning (Fig. 19). U/Th of the zircons is between 0.53 and 0.84 excluding a metamorphic origin. A total of eight spot analyses on seven different crystals were made. One crystal was analysed both at the rim and the core; the ages obtained are identical within error. The measured zircons (Fig. 20) when plotted on a Tera-Wasserburg diagramm yield a $^{238}$U/$^{206}$Pb age of 166.6±1.8 Ma (MSWD=0.48), interpreted here as the crystallization age of the plagiogranite, thus the intrusion age of the Guevguely complex.

The difference between the age proposed in this study and that proposed by Spray et al. (1984) can be ascribed to Ar loss from the amphibole separates used by the latter authors for the age determination.

## 3.6 Conclusions

Based on the petrological and geochemical characteristics, the Greek part Guevguely ophiolite can be divided in two complexes namely the Skra and the Evzonoi complexes. The Skra complex occupies the western part of the Guevguely ophiolite while the Evzonoi complex occupies the eastern part as it is divided by the Fanos granite.

The Skra complex is characterised by bimodal magmatism. Two rock suites were recognised : one is dominated by mafic rocks with $SiO_2$ content ranging up to 52 wt%, the other is composed of acidic rocks having $SiO_2$ content between 61 and 66wt%. The acidic samples are low-K, LILE and LREE-depleted. The depletion in LILE can be attributed to hydrothermal circulation that took place after the formation of these rocks and resulted in leaching the samples from the LILE. The depletion in REE is clearly a magmatic phenomenon; the samples closely resemble the andesites and dacites that erupt in the Tonga - Kermadec arc (Ewart 1973). Th is enriched in all samples. Nb and Ta form negative anomalies in the multielement profiles. The mafic samples have mainly LREE-depleted patterns. Slightly LREE-enriched samples are also present. HREE patterns are all flat suggesting melting in the spinel lerzolite field.

The Evzonoi complex is built up from mafic rocks. Scarce rhyolitic dykes cross cut all the mafic dykes and can be was assigned to a later event that had nothing to do with the ophiolite genesis.  Some rare andesites are found to cross cut the mafic dykes. The samples from Evzonoi have a variable LILE content. Th is slightly enriched while in some samples it very difficult to distinguish this enrichment. Nb and Ta form slight negative anomalies. The HFSE form patterns subparralel to the N-MORB line. The LREE are depleted and the HREE have flat patyterns resembling the patterns of the Skra samples. The rhyolite have fractionated REE patterns. LREE are highly enriched relative to the HREE and the HREE patterns are flat.

The isotopic systematics of the samples, are characterized by positive $\varepsilon_{Nd(165Ma)}$ values that are lower than the DMM or N-MORB values, suggesting that these samples have derived from a mantle source that has been isotopically modified by an enriched component. This enriched component as deduced by the co-variation between Nd isotopes with $SiO_2$ or Nb/Th is most probably a subduction-derived hydrous fluid and/or melt; rather than AFC processes. The samples from both complexes have been derived from a mantle source that has previously experienced melt extraction and that has been modified by the addition of fluids and melts derived from the sedimentary cover of the subducted slab. Evzonoi show lower enrichment from the subducted slab component than the Skra complex.

The chemistry of the samples from the Guevguely ophiolite have  typical charcterstics of subduction-zone magmatism. Tectonomagmatic discrimination based on Ti/V and Zr/4-Y-2Nb systematics classifies the samples from Skra and Evzonoi as MORB and VAB or IAT

whereas tectonomagmatic discrimination based on Th-Hf/3-Ta systematics classifies the samples as having derived from destructive plate margins while on the same diagram the samples from Evzonoi plot between the fields of N-MORB and basalts from destructive plate margins. Compatible vs incompatible element non-modal equilibrium melting modelling suggest that the sanples from Skra complex could be explained by 15-10% of melting of a FSL while the Evzonoi complex could explained by less than 5% of melting of similar source.

There is evidence of mafic magmatism intruding the Fanos granite. This episode of magmatism is characterised by high in $K_2O$, highly fractionated REE patterns and the highest enrichment in LILE observed among the rest of the investigated samples. Ta and Nd are depleted, typical of subduction-zone magmatism. Zr, Nb and Y systematics suggests that these samples show a within plate enrichment. These samples have distinct chemistry from the rest of the mafic samples. The chemical signature they carry suggest a more mature arc activity in contrast to the Skra and Evzonoi complexes that point towards more primitive arc system.  This suggests that the intrusive mafic magmatism observed in the Fanos Granite followed the granite emplacement.
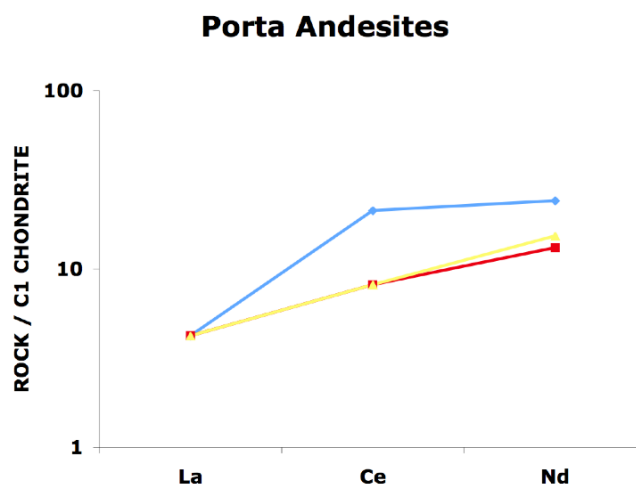


**Fig. 21.** REE diagrams for the Porta andesites (Paikon) normalised to C1 chondrite. Normalising values for C1 after and from McDonough and Sun (1995). The analyses are from Brown and Robertson (2005).

As a conclusion I will try suggest a possible geotectonic scenario for the evolution of the Geuvguely ophiolitic complex as well for the surrounding area. When one tries to identify the contact of this ophiolite with the country rocks and evaluate the nature and mode of its emplacement, one finds out that the eastern and southern parts are concealed by the Neogene sedimentary cover of the Axios-Vardar basin that leaves no visible site of the contact of the Evzonoi complex to the surrounding rocks. The western border of the Evzonoi complex is restricted by the intrusion of the Fanos Granite. The Skra complex is thrusted onto the rocks that built the Paikon Unit. The thrust is characterised by mylonitised rocks of

volcanic origin. Anders et al (2005) made a gechronologcal and a geochemical study on the acidic magmatism as well as on basement rocks that outcrop in this area. Starting with the basement Anders et al (2005) estimated the age of the orthogneisses of Pigi, which are in contact to the ophiolite to 320Ma. Monazites from the same rock yield ages of around 158Ma Anders et al. (2005). Anders et. al (2005) also provided radiometrical ages for the Mikro Dassos volcanics as well as of the Griva mylonites. The Skra myllonites contains mica-feldspar-quartz and are located in the western part of the ophiolite complex. The age of these rocks have been dated by Anders et. al (2005) as 155±2Ma. These mylonities were posibly formed during the obduction of the Guevguley complex onto the Paikon massif. The Mikro Dassos rhyolites are located in the eastern part. The age of these rhyolites has been estimated as 164±4Ma. In the same study the age of the Fanos granite was determined as 158±1Ma. It is evident that during the middle Jurassic there was extensive magmatic activity in this area. Examining the chemical analyses Brown and Robertson (2005) provide for magmatic rocks from the area we see that the andesites and dacites from Porta are low- $K_2O$ andesites that have depleted LREE C1-chondrite normalised patterns (Fig. 21). Combining all the pieces of information so far we could tie all the magmatic episodes described above in the following scenario (Fig. 22):

An eastward intra-oceanic subduction is initiated within the Vardar ocean. In the early stages of this subduction system, suprasuduction-zone magmatism evolved on the overriding plate. In this stage the eruption of the andesites from the Skra complex take place. The subduction continues and an extensional regime is evolved on the overriding plate as a result of the subducted plate rollback. As a result there is splitting of the proto-arc (mechanism similar to that described by Karig 1971, 1977) and a basin begin to evolve. In this stage the Skra complex evolves at 167±2Ma (this study). The extension continues and asthenospheric material rises as a result of cornel flow. The rise of the asthenosphere causes the eruption of more fertile magmas as before, still having some traces of the subduction magmatism. In this stage the Evzonoi complex evolves. (156-161Ma Danelian 1996, Oxfordian radiolarian fauna in from sediments within the lava section)

The subduction of the Vardar Ocean below the Paikon arc continues, the magmatism evolves and the arc passes to a more mature stage. The extrusive rocks have typical characteristics of volcanic arc magmatism. Behind the Paikon arc the back-arc basin closes below the eastern margin that is represented by the Mikro Dasos arc suite and the Pigi migmatites. Blocks of the Guevguly ophiolite get obducted onto the continental margin and the intrusion of evolved extrusives (as represented by the rhyolites that intrude the Evzonoi complex e.g. sample EYZ 8) and the 158Ma Fanos Granite (Anders et al 2005) takes place. On the side of the Paikon arc the

## a) Triassic?

Vardar Ocean

spreading center

Pelagonian

~300Ma Basement
Pigi Orthogneisses

## b) Mid-Jurassic

low-K$_2$O acidic magmatism
**Paikon Arc** (Porta-Tzena)
initiation of **Guevguely ophiolite**

VARDAR

~300Ma Basement
Pigi Orthogneisses

Ba, LILE  Melting of the
sub-arc mantle

Ba, Th, LILE, LREE

Melts

aqueous fluids

aqueous fluids
and sediment melts

sediment melts

## c) ~167 Ma

evolving
magmatism
**Paikon Arc**

Rifted Arc
Crust

**Mikro Dassos,**

VARDAR

~300Ma Basement
Pigi Orthogneisses

EXTENSION        EXTENSION

corner
flow

magma enriched in Th
builting of the **Skra complex,**

ROLL BACK

## d) ~160 Ma

**Paikon Arc**

BACK-ARC
SPREADING

**Mikro Dassos,**

VARDAR

~300Ma Basement
Pigi Orthogneisses

EXTENSION   EXTENSION

SUBDUCTION

corner
flow

asthenospheric-like magma
builting of the **Evzonoi complex,**

ROLL BACK

## e) 158-155 Ma

Mikro Dassos

Medium-High-K$_2$O
acidic magmatism
**Paikon Arc** (Griva)

VARDAR

~300Ma Basement
Pigi Orthogneisses

Rhyolites

Fanos Granite

**Fig. 22**. Schematic approach of the evolution of the Guevguely complex from 167-158 Ma.

# Chapter 4. Geochemistry and petrology of the Oraeokastron Ophiolite, N. Greece.

## 4.1 Regional geology

The Oraeokastron ophiolite is situated in northern Greece in the prefecture of Macedonia, about 5 km north-northwest of the city of Thessaloniki. It occupies an area 12 km long and 2.5 km wide, trending NW-SE (Fig. 1). To the east, the ophiolite is in contact with a series of phyllites and Triassic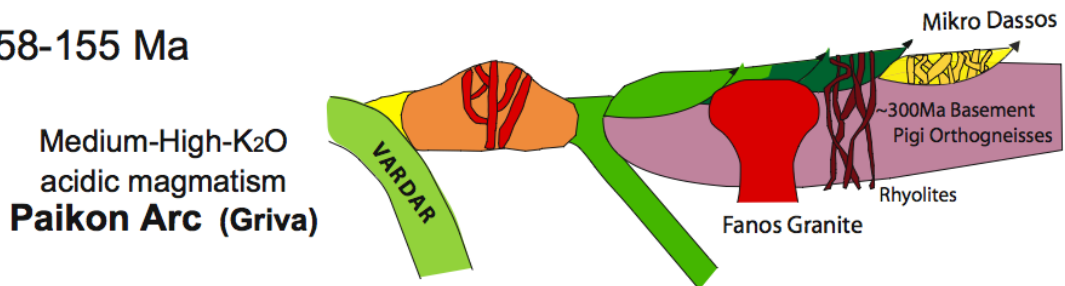 limestones (Stais 1993). The limestones have been thrusted on top of the ophiolite. As inferred by the brittle deformation phenomena observed, the contact between the limestones and the ophiolite is of tectonic nature. Along the contact we observe phyllites that are composed of elongated plagioclase minerals in a very fine-grained dark green matrix. The absence of quartz suggests that these phyllites have had a mafic protolith, and probably they represent ophiolitic material that was tectonized during the emplacement of the limestone. Photos from the outcrops can be seen in Appendix G.

To the west the ophiolite is in contact with a Tithonian fossiliferous conglomerate (Mercier 1966, Kockel 1977). This conglomerate consists of sandstone and other sediment pebbles. Some mafic rock pebbles were also found. The matrix of the conglomerate is calcareous and the fossils found are mainly corals. There is a gradient drop in the pebble size and their abundance in the conglomerate towards the south. The same conglomerate is also found in contact with the ultramafics south of the Petroto village. In that area, the pebbles are much bigger and very irregular in size. Field observations suggest an increase in the deposition depth of the conglomerate towards the southeast.

Fieldwork in the wider Oraeokastro area revealed the possible extension of the ophiolite body beyond its previously known northern limit of the northern limestone (Kastro limestone). Pockets of undeformed mafic material as well as minor occurrences of severely altered ultramafic material were observed inside highly sheared matrix that continues north of the main body towards the villages of Petroto and Monolofos. The matrix ,as said before, Is highly sheared and is not very easy to distinguish the composition of it. Nevertheless after looking very closely to it we were not able do distinguish any quartz, suggesting that the protolith was a mafic rock, most probably from the Oraeokastro ophiolite.

The Oraeokastron ophiolite could better be described as an incomplete ophiolitic sequence with respect to the Penrose conference definition (Anonymous 1972) of an ophiolitic sequence. A well-exposed sheeted-dyke complex as well as a detailed cumulate section are absent.

Ultramafic rocks consisting of harzburgite tectonite occur as a small isolated body, detached from the main outcrop some 2 to 3 km further northeast in between the villages of Petroto and Monolofos (Fig. 1). The country rocks surrounding these ultramafics plus the ultramafics themselves are sheared and foliated close to their contact.

Microgabbros, and isotropic gabbros built up the major outcrop of the Oraeokastron ophiolite forming in places magmatic breccias and magma mingling phenomena. The gabbros

consist mainly of Cpx and Plg but also some differentiated coarse-grained hornblende-plagioclase are present. The gabbros are in places foliated and in many cases micro-shear zones are distinguishable.
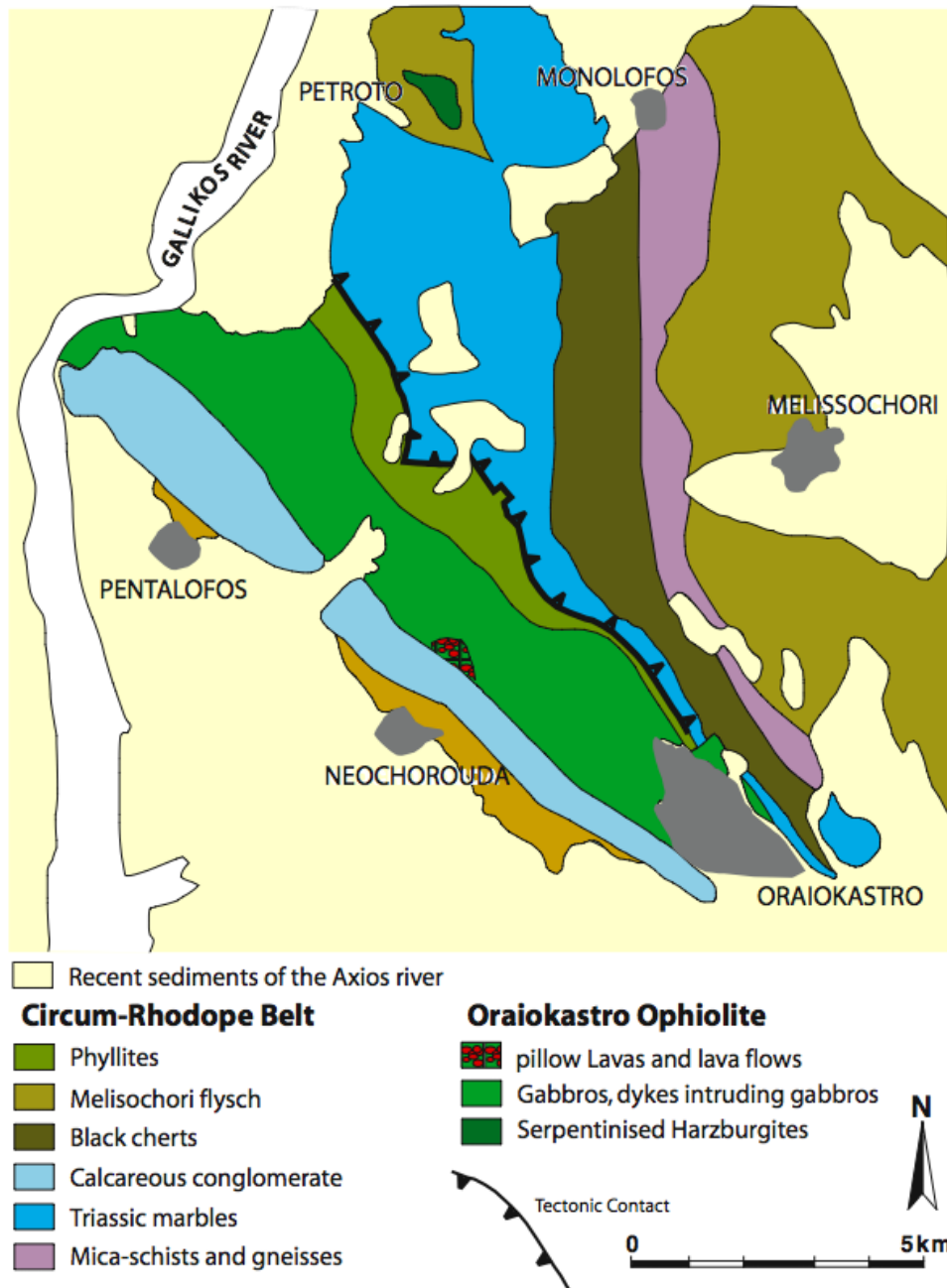


**Fig. 1.** General geological map of the Oraeokastron ophiolite and the surrounding Circum-Rhodope Belt formations.

Dykes can be found as single intrusions in gabbros and as small outcrops of dyke swarms. The extrusive part of the ophiolite can be seen along the western border and consists of lavas, in pillow and flow forms and rare hyaloclastites. The major exposure of lavas is located north of the village of Neochorouda close to a small water dam. The lavas are fine-grained and vesicular and contain inter-pillow sediments, probably lmestones.

Evolved rock types, such as plagiogranites, have been found to outcrop as lenses or intrusions inside the gabbros. An exposure of a dioritic intrusion has also been found among the basaltic material in the south border close to the village of Pentalofos.

## 4.2 Mineralogy

The primary mineralogical assemblage observed in the lavas and dykes is plagioclase + clinopyroxene in variable proportions, set in a micro (or crypto-) crystalline matrix. Clinopyroxene has been partially preserved fresh; plagioclase and possibly olivine occur as pseudomorphs after secondary minerals. Altered plagioclase, clinopyroxene and hornblende are the only minerals observed in the gabbroic rocks. Secondary minerals are albite, actinolite, chlorite, epidote, pumpellyite, sphene, magnetite, and in one case, a single grain of xenocrystic zircon. This zircon was found in glassy lava.
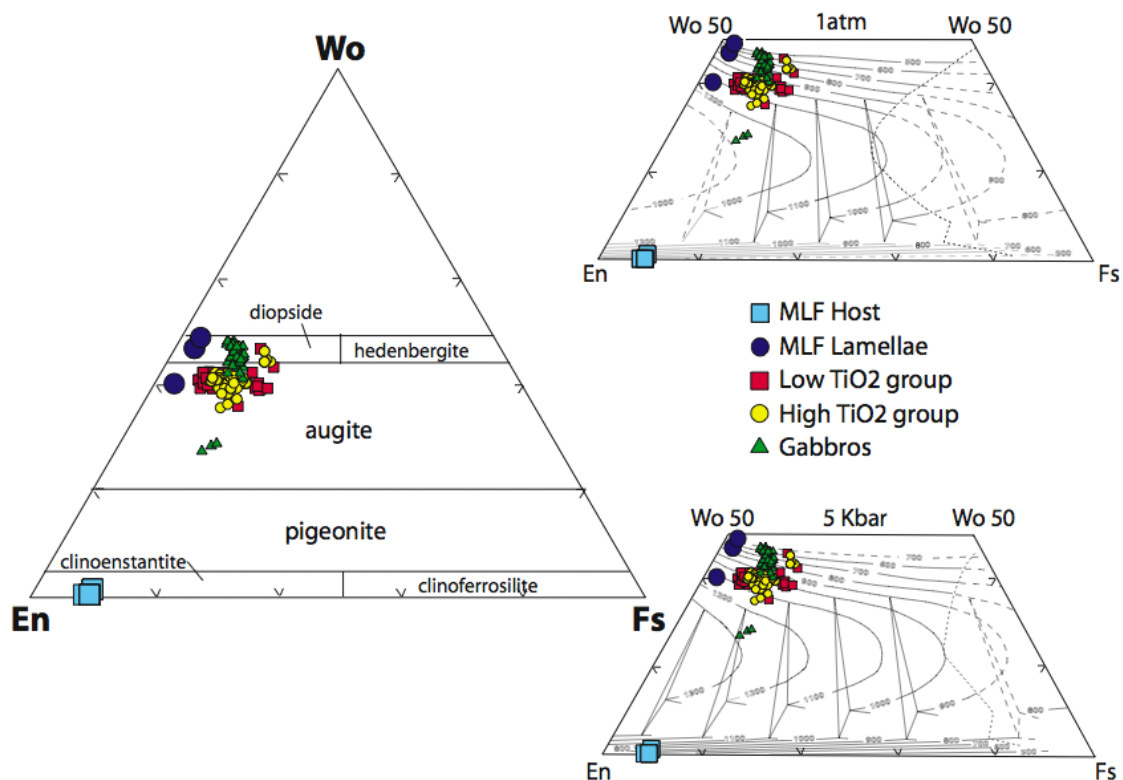


**Fig. 2**. Standart classification triangle of pyroxenes (after Morimoto 1988) and parts of it with the isotherms proposed by Lindsley (1983).

The clinopyroxenes have typical augite compositions (Fig. 2). Their average composition is $En_{52}Fs_8Wo_{40}$. The augites appear to have been altered to actinolite, chlorite and in some cases to calcite. The plagioclases have lost almost all of their Ca and have been

altered to albite. Their average albite content is now $Ab_{96}$. The plagioclases also appear in some cases kaolinized and saussuritised. Clinopyroxene barometry based on the empirical barometer proposed by Nimis (1995, 1995), iterated with the thermometer proposed by Bertrand & Mercier (1985) applied to augite phenocrysts from dyke and lava samples yielded crystallization temperatures in the range $1095\pm22^{\circ}C$ to $1130\pm22^{\circ}C$ and pressures from $1.9\pm0.6$ to around $3.3\pm1.4$ kb.
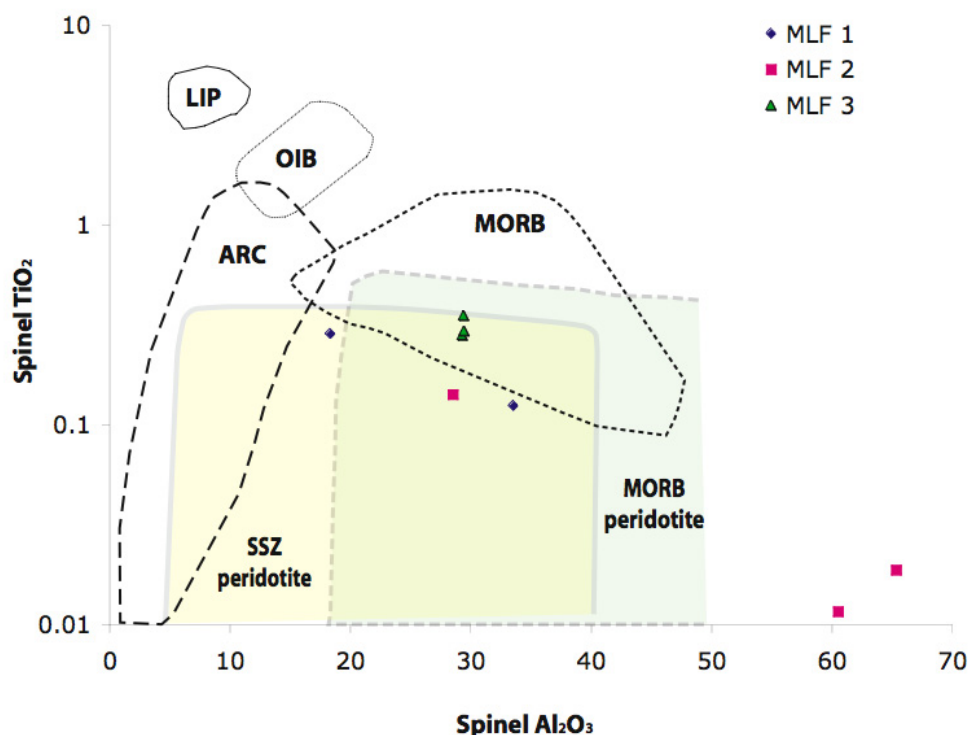


**Fig. 3**. $TiO_2$ vs $Al_2O_3$ diagram showing the spinels from Monolofos area. MLF 1,2,3 are the analyses from the three different thin sections from sample MLF3. LIP, OIB. MORB nd ARC areas mark the field of volcanic spinels. Fields after Kamenetcky (2001).

The constituent minerals of the ultramafic rocks are olivine, orthopyroxene, clinopyroxene and spinel. Olivine is mostly altered to serpentinite and chlorite. Clinopyroxene, often altered to actinolite, occurs both as free grains and also as exsolution lamellae in orthopyroxene. Spinel is mainly Cr-eriched having Cr number (Cr#= Cr/(Cr+Al)) that vary from 0.420 to 0.575 and Mg number (Mg#= Mg/(Mg+0.9Fe)) from 0.530 to 0.920. In cases, it appears to be zoned showing a depletion in MgO, MnO, Cr2O3, and FeO towards the rim, followed by a consecutive increase of the $Al_2O_3$ content. The very high Mg# that is observed in one case is assigned to the very core of a spinel crystal. Except from the Cr-spinels, it was also possible to spot Al-spinels.

High-Al-spinel occurs as overgrowths on Cr-spinel rims. This type of spinel has Cr# values less than 0.1 and Mg# between 0.781 and 0.797. On the $TiO_2$ vs $Al_2O_3$ diagram (Fig. 2), the spinels from the Oraeokastro harzburgite are projected in an area where the fields of

the supra-subduction zone (SSZ) and the mid-ocean ridge (MOR) peridotites overlap (Fig. 3). The high-Al spinels plot clearly in the field of the MOR peridotites.

# 4.3 Geochemistry

## 4.3.1 Major and trace elements.

The tables presenting the geochemical analyses are located in Appendix D and E. Based on their geochemical characteristics the extrusive rocks are divided into two groups, a high-$TiO_2$ group that will hereafter named after HTE and a low-$TiO_2$ group that will be referred to as LTE. In Fig. 3 we see element vs Mg# variation diagrams. It is clear that for elements like $SiO_2$ $Al_2O_3$ and $TiO_2$ the HTE-group does not follow the general linear correlation trend as it is set by the LTE and the gabbros. In order to examine if this is a primary feature or an artifact due to alteration we investigated the covarioation of element versus Zr. Comparing the major-element composition of the samples to Zr (Appendix. F.), used as an index of mobility during metamorphism, we observe that the major elements are disturbed in variable degrees except for $TiO_2$ and $P_2O_5$. The HTE seems to be affected more by hydrothermal circulation than the LTE and the gabbros. Trace elements, with exception of Ni and Cr, also seem to be disturbed and the REE show a very good correlation to Zr. Macroscopic observations of the HTE rock specimens reveal a network of epidotisation veins that we do not observe in the LTE group with the same intensity.
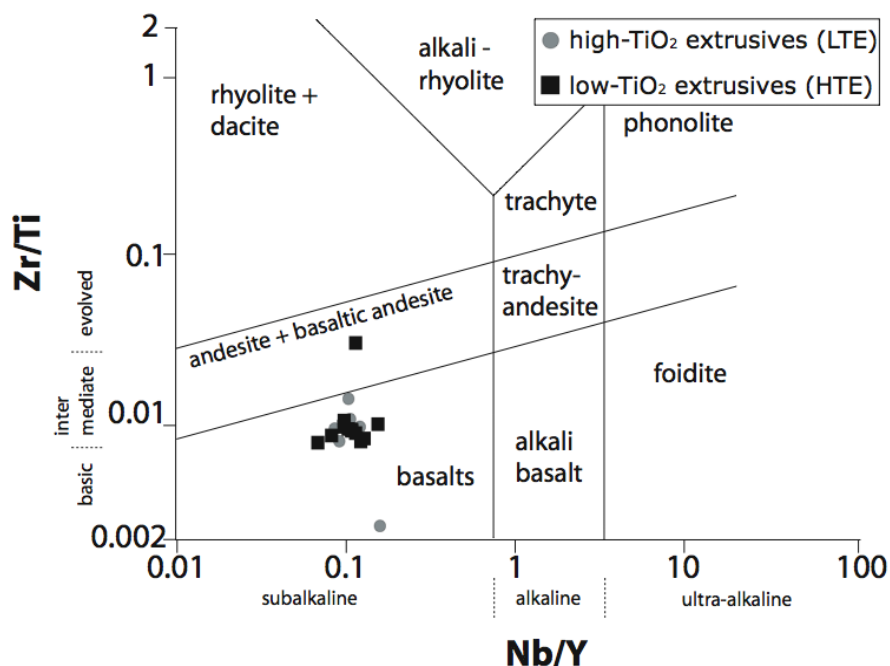


**Fig. 4.** Zr/Ti versus Nb/Y for the volcanic samples from Oraiokastro ophiolite. (after Winchester and Floyd (1977) revised after Pearce et al 1996)

On the Zr/Ti versus Nb/Y classification diagram (Winchester and Floyd 1977, revised after Pearce et al. 1996; Fig.4), the volcanic samples from the Oraeokastro ophiolite plot in the field of basalts and basaltic andesites.

The dykes of the LTE contain $SiO_2$ between 51.92wt% and 53.85wt%, $TiO_2$ between 0.48wt% and 0.70wt%, MgO between 5.78wt% and 8.35wt% and total $Fe_2O_3$ between 8.11wt% and 9.27wt%. The lavas of this group have higher $SiO_2$ (around 55.60wt%) and $TiO_2$ (0.80wt% - 0.76wt%) contents but their MgO and the total $Fe_2O_3$ values are within the variation observed for the dykes. The Zr content of the LTE rocks varies between 27 and 42 ppm, that of Y between 14.8 and 21 ppm and that of V between 241 and 285 ppm.
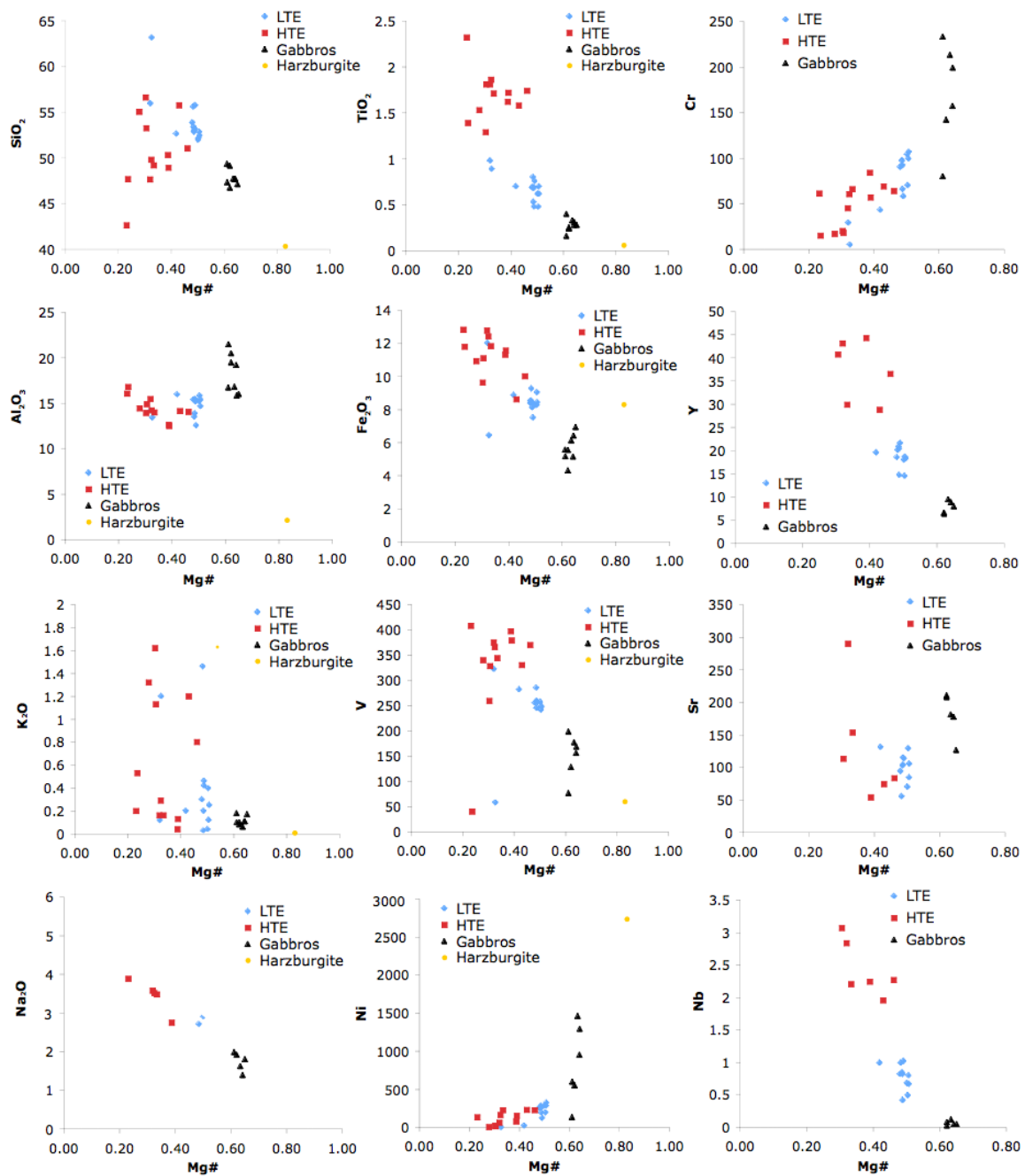


**Fig. 5.** Element versus Mg# for the mafic and ultramafic samples from the Oraeokastro Ophiolite

52
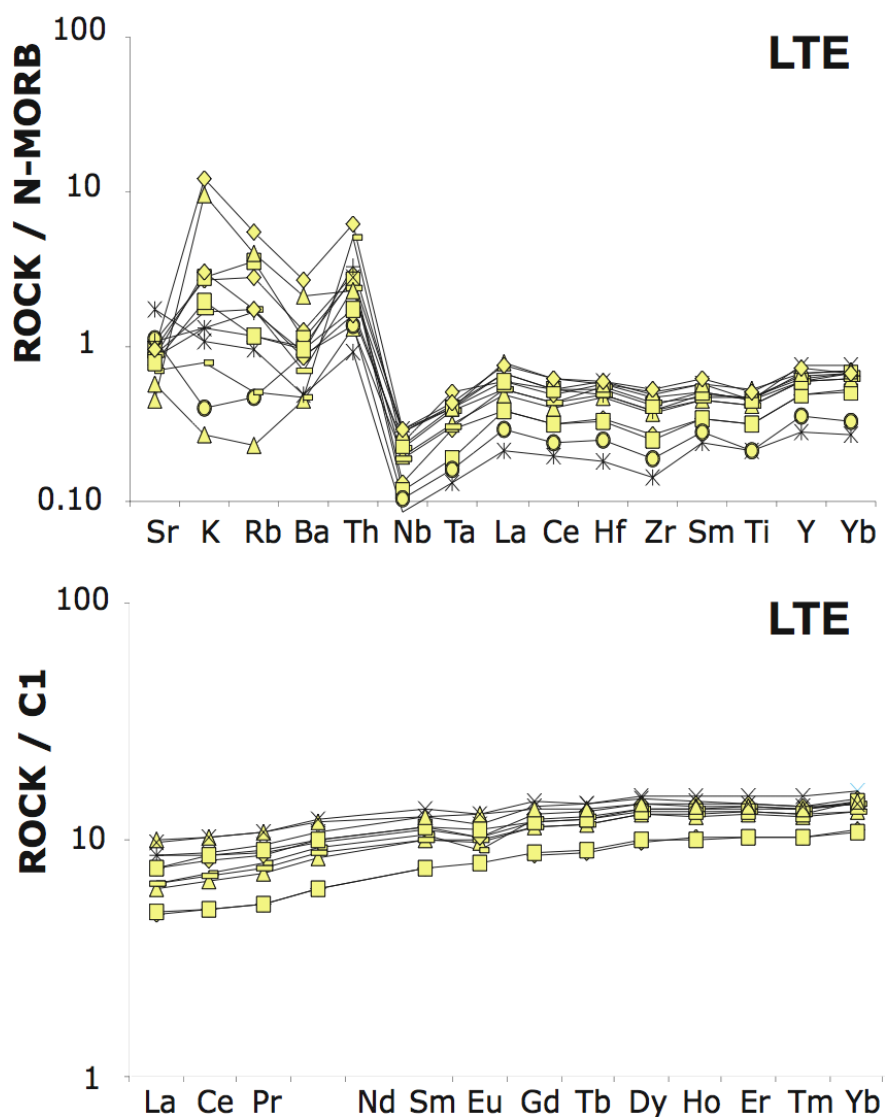
**Fig. 6. A**. Normalised to N-MORB multielement "spiderdiagramm" for the LTE group. **B** normalised to C1 chondrite REE diagrams for the same group. Normalising values for C1 after McDonough and Sun (1995) and for N- MORB after Pearce (1982, 1983).

Examining multi-element profiles (Fig. 5) normalised to N-MORB for the LTE rocks we observe that these samples have highly variable LILE and HFSE concentrations. The samples are mainly enriched in these elements; Ba shows a negative anomaly, Th shows a positive one, whereas Sr, K, and Rb show an irregular behaviour being mostly enriched relative to N-MORB. Thorium appears to be enriched in all samples (1-8 x N-MORB), particularly in ORK6, in which it displays an enrichment factor of 30 relative to N-MORB. There is also a distinct negative Nb anomaly and a slight positive Ce anomaly. All samples of the LTE are depleted in REE, Y, $TiO_2$, Zr and Nb and show a progressive depletion from Yb to Nb, which implies that they were derived from a depleted mantle source to which a (La,Ce)-enriched fluid was added. LREE-depleted (La/Yb <1) and flat HREE patterns suggest that

melting of the source took place above the garnet stability field; negative Eu anomalies further imply plagioclase fractionation before eruption

The HTE is characterised by higher $TiO_2$, $Fe_2O_3$ and HFSE values compared to the LTE. $SiO_2$ concentration varies between 46.11wt% and 56.61wt%, $TiO_2$ between 0.98wt% and 2.32wt%, MgO between 4.60wt% and 7.75wt% and total $Fe_2O_3$ between 9.63wt% and 12.82wt%. The lavas of this group have the same chemistry as the dykes. The Zr content of this group varies between 3 and 113 ppm, Y values are between 6 and 45 ppm and V values are between 121 and 408 ppm. These large variations are attributed to the effects of alteration and episotisation.
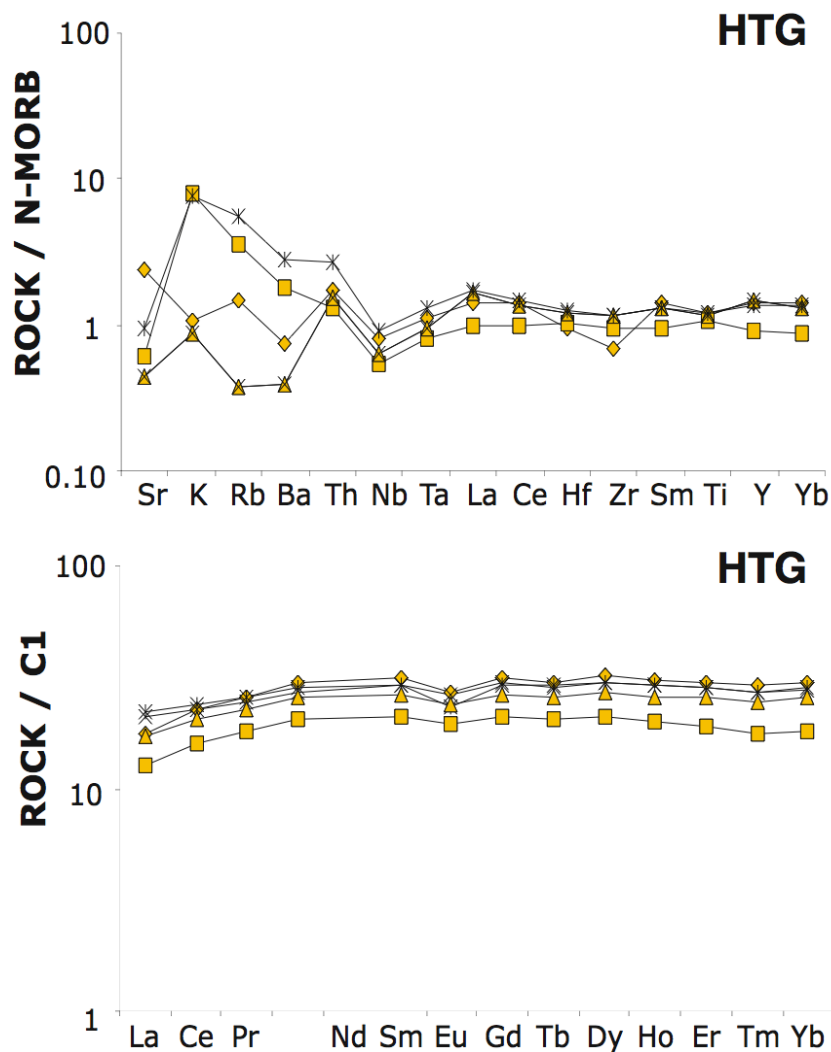


**Fig. 7. A** Normalised to N-MORB multielement "spiderdiagramm" diagrams for the HTE. **B**. normalised to C1 chondrite REE for the same group. Normalising values for C1 after McDonough and Sun (1995) and for N- MORB after Pearce (1982, 1983).

As can be seen from Fig. 6, LILE concentrations are enriched compared to N-MORB and there is also a slight negative Nb anomaly. The concentration of Th is also enriched but

only slightly compared to the LTE. The normalised concentrations of Y, $TiO_2$, Zr, Ce and Nd of this group, allowing for minor fluctuations, are similar to those of N-MORB, forming patterns sub-parallel to the N-MORB line. The samples of the HTE do not demonstrate the same depletion trend of the HFSE as the samples of the LTE, suggesting that their source is not depleted in these elements as it is in the case of the LTE.

The HTE rocks have LREE-depleted patterns (Fig. 6) resembling those of N-MORB (La/Yb <1). This, coupled with the presence of flat HREE patterns, suggests that melting of the source took place in the stability field of spinel lherzolite; negative Eu anomalies further imply plagioclase fractionation before eruption. The total REE content of the HTE is higher than that of the LTE suggesting that the HTE rocks have been derived from a more enriched source compared to the LTE ones.

The $SiO_2$ content of the gabbros range from 45.71 to 49.78 wt.wt% and the $TiO_2$ content between 0.1wt% and 0.40 wt.wt%. The Mg# (calculated as $MgO/[MgO+0.85Fe_2O_3]$) of these samples ranges between 0.62 and 0.66. The Oraeokastron gabbros seem to be genetically related more to the LTE rather than to the HTE as seen on the $TiO_2$ versus Mg# diagram (Fig. 7).
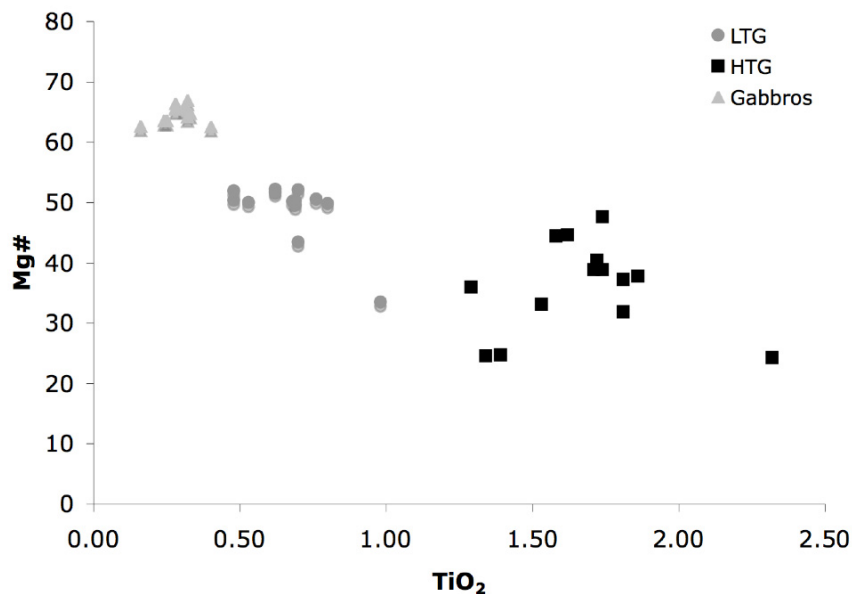


**Fig. 8.** Mg# versus $TiO_2$ for the samples form the Oraiokastro ophiolite.

The gabbros show low total REE contents, much lower than those of their related volcanics. They are characterised by. LREE-depleted and flat HREE-patterns and by a strong positive Eu anomaly that suggests accumulation of plagioclase (Fig. 8).
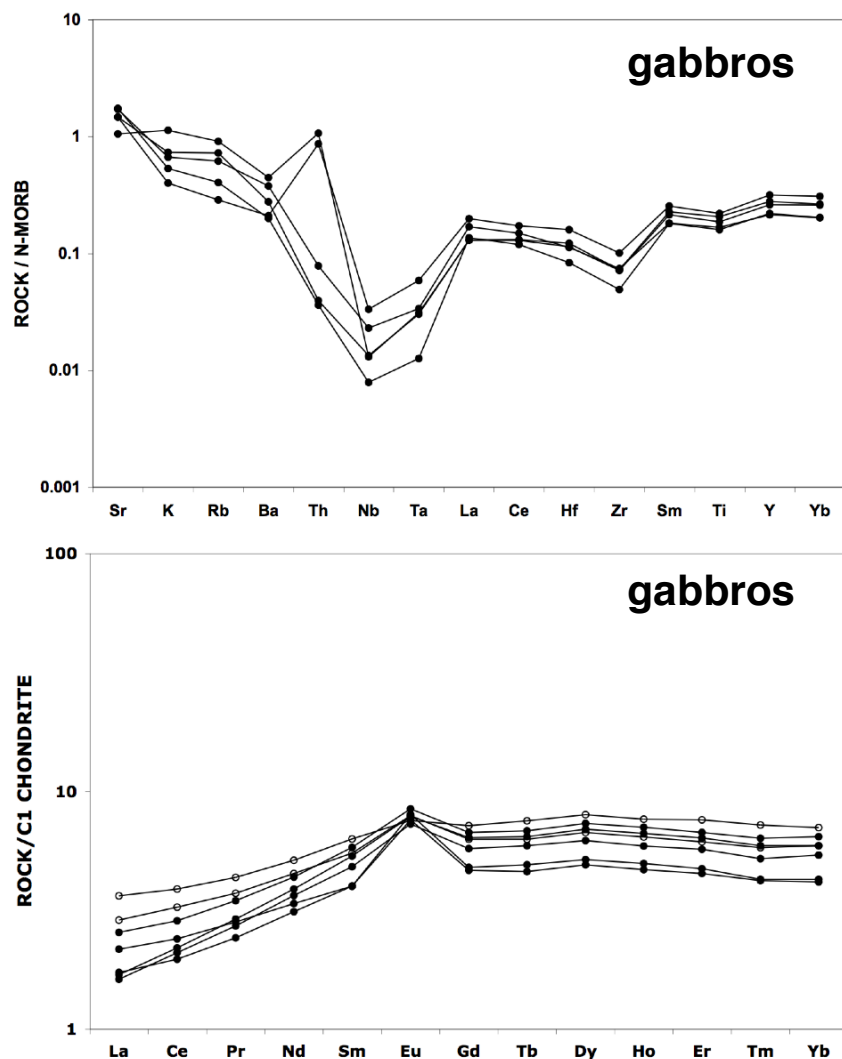
**Fig. 9.** Normalised to C1 chondrite REE for the gabbros from Oraeokastro Normalising values for C1 after McDonough and Sun (1995) and for N- MORB after Pearce (1982, 1983).

Except for mafic rocks, fractionated rock types were also encountered and sampled during fieldwork. Such samples come from both the extrusive and the plutonic suite of the ophiolite. Two plutonic, leucocratic outcrops were sampled. The first has very high $SiO_2$ (83.29 wt.wt%), very low $TiO_2$ (<0.1 wt.wt%), low $Al_2O_3$ (9.21 wt.wt%) and very low trace-element content. According to the Rb vs. Y/Nb tectono-discriminant diagram of Pearce et al. 1984, it can be classified as ocean-ridge granite. The second has much lower $SiO_2$ content (70.66 wt.wt%) and much higher $TiO_2$ (0.36 wt.wt%) and $Al_2O_3$ (13.76 wt.wt%) contents. In this sample the concentration of Zr is 283 ppm, that of Sr is 234 ppm but Rb appears to be low (2 ppm). This rock is peraluminous and shows a clear volcanic-arc character as suggested by the Rb vs. Y/Nb diagram (Fig. x). The fractionated extrusive rocks are andesites and dacites and were sampled from lava-dominated outcrops. Their $SiO_2$ content ranges between 62.07 and 65.81 wt.wt%, that of $TiO_2$ between 0.35 and 0.89 wt.wt% and that of

$Al_2O_3$ from 12.77 to 17.23 wt.wt%. Concentrations of Zr, Sr and Nb are in the range 162-207, 117-206 and 5-12 ppm respectively.

## 4.3.2 Sr and Nd isotopes

Sr and Nd isotope data for samples from the Oraeokastron ophiolite are presented in Appendix F. $^{143}Nd/^{144}Nd$ initial ratios and $\varepsilon Nd$ values have been calculated at 165 Ma. Chondritic values used are $^{143}Nd/^{144}Nd=0.512638$ and $^{147}Sm/^{144}Nd=0.196700$. Analysed samples from the LTE have Sm and Nd concentrations between 1.097 and 1.7 and between 2.8 and 4.4 ppm respectively, whereas those from the HTE have Sm and Nd concentrations between 3.8 and 5. and between 11.34 and 15.98 ppm respectively. The rocks from the HTE are isotopically more depleted than those of the LTE. The HTE rocks have $^{143}Nd/^{144}Nd$ values between 0.513008 and 0.512985, $\varepsilon_{Nd(165Ma)}$ values between 6.37 and 7.06 and $^{86}Sr/^{87}Sr$ values between 0.7042 and 0.7056, whereas the rocks belonging to the LTE have $^{143}Nd/^{144}Nd$ values between 0.512983 and 0.512898, $\varepsilon Nd$ between 6.13 and 3.98 and $^{86}Sr/^{87}Sr$ between 0.7042 and 0.7054. The gabbros have initial $^{143}Nd/^{144}Nd = 0.512949$ that correspond to $\varepsilon_{Nd(165Ma)}=7.14$ and $^{86}Sr/^{87}Sr= 0.7034$.
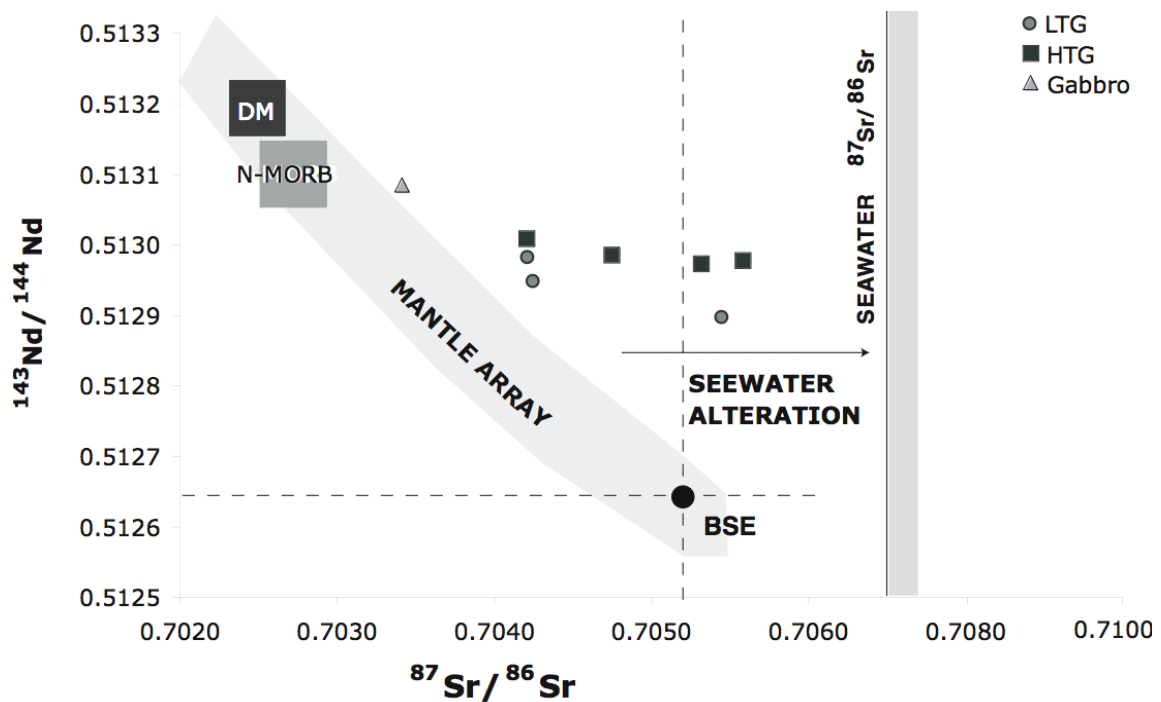


**Fig. 10.** $\varepsilon_{Nd}$ recalculated to 165 Ma versus $^{87}Sr/^{86}Sr$ for the Oraiokastro samples. BSE: Workman and Hart (2005), DMM :Rehkamper and Hofmann (1987), and Klein (2004), MORB:Kelemen et al. (2004) and Seawater values after the Sr-Isotope evolution curve from Burke et. al (1982).

The $^{143}$Nd/$^{144}$Nd values are lower than the values of the depleted mantle and the middle ocean ridge basalts, suggesting that the source of these rocks was isotopically modified from an enriched component. Examining the co-variation of the isotopic systems (Fig. 10.) we recognise two different trends. The first one corresponds to the HTE and is characterised by a shift towards higher $^{87}$Sr/$^{86}$Sr as the εNd remains relatively constant. This can be explained as the result of seawater/rock interaction, which is caused by hydrothermal circulation. The second trend includes the LTE and shows a strong coupling of the two isotopic systems interpreted either as the combined effect of the hydrothermal circulation and contamination of the source from subduction released aqueous fluids or melts.

## 4.4 Tectonomagmatic discrimination

The lavas from the LTE have Ti/V values between 18 and 19. The dykes from the same group have lower values between 11 and 18. According to the Ti versus V diagram (Fig. 11) proposed by Shervais (1981), both the lavas and the dykes plot in the field of island arc tholeiites (IAT). The HTE demonstrates significantly higher Ti/V values. The samples of this group have higher Ti/V ratios than the LTE that are between 27.21and 33.08 for the lavas, and between 30 and 34 for the dykes. All the samples from HTE plot in the field of mid-ocean ridge basalts (MORB) and back-arc basin basalts (BABB) on the same diagram.
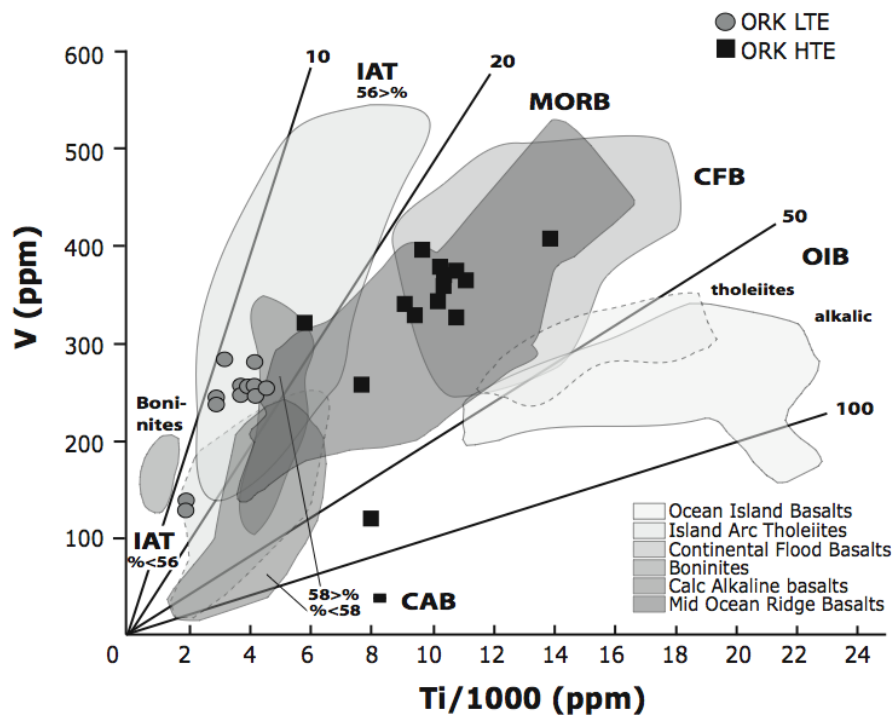


**Fig. 11.** Ti versus V diagram showing the HTE and LTE samples from the Oraiokastro ophiolite. (after Shervais, 1981)

On the Th-Hf/3-Ta diagram proposed by Wood (1980) (Fig.12), all the samples plot outside the MORB array and in the field of destructive plate-margin basalts, forming two different trends towards higher Th. All the samples from LTE plot clearly in this field whereas the samples from the HTE are less enriched in Th and have slightly higher Ta. Some of the samples belonging to the HTE plot on the division line between the IAT and the MORB fields.
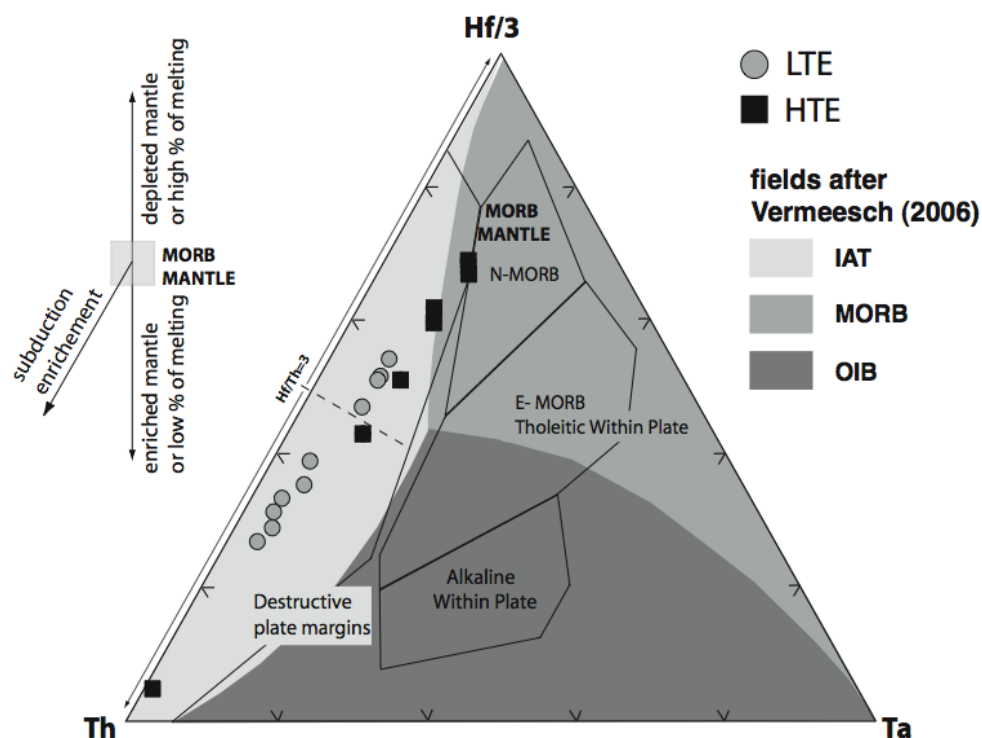


**Fig. 12.** Hf/3-Th-Ta diagram showing the HTE and LTE samples from the Oraeokastro ophiolite. (after Wood, 1980)

In Pearce and Norry (1979) there is an extended presentation of the Ti, Zr, and Y characteristics from basalts erupted in different settings. Nb can be used to investigate the mantle differentiation processes, the Zr/Nb ratio can be used as a proxy for enrichment or depletion processes in the mantle (Meschede 1986 and references therein), while the Zr/Y ratio can be used to investigate long term source heterogeneities thus to distinguish between basalts erupted in within-plate settings and basalts erupted in mid-ocean ridges and volcanic arcs (Pearce and Norry, 1979 and references therein). On the Zr/4-Y-2*Nb triangular diagram proposed by Meschede (1986) the rocks belonging to the HTE and the LTE plot in the fields of the normal mid-ocean ridge and volcanic-arc basalts and they do not demonstrate any within-plate enrichment (Fig. 13).
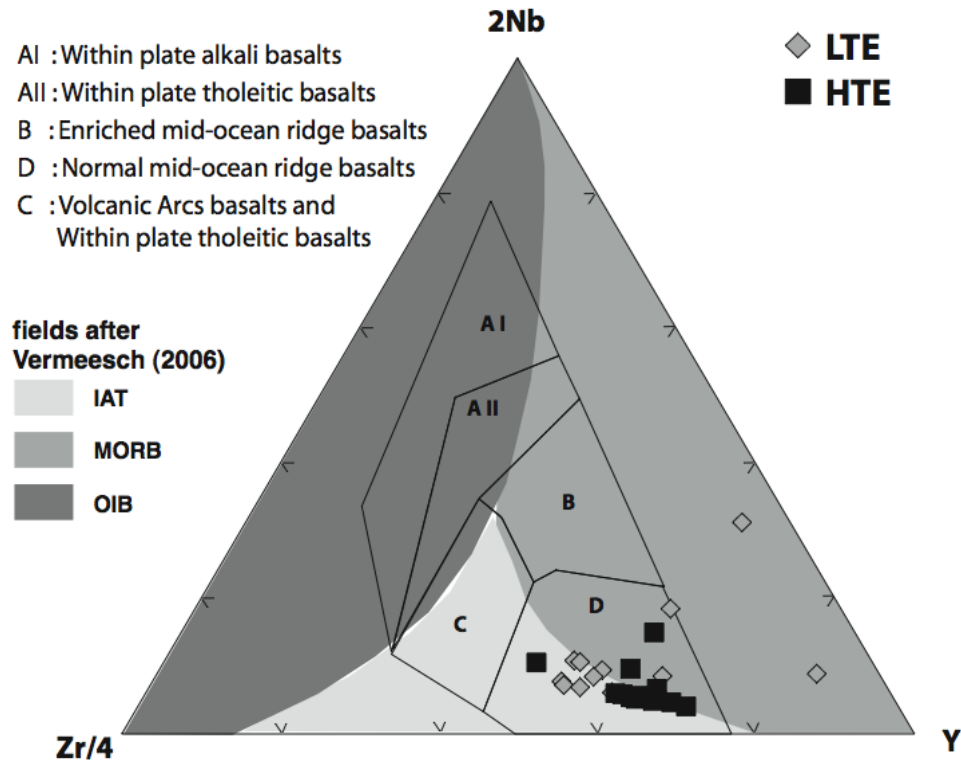
**Fig. 13.** Zr/4- 2*Nb-Y diagram showing the HTE and LTE samples from the Oraeokastro ophiolite. (after Meschede 1986)
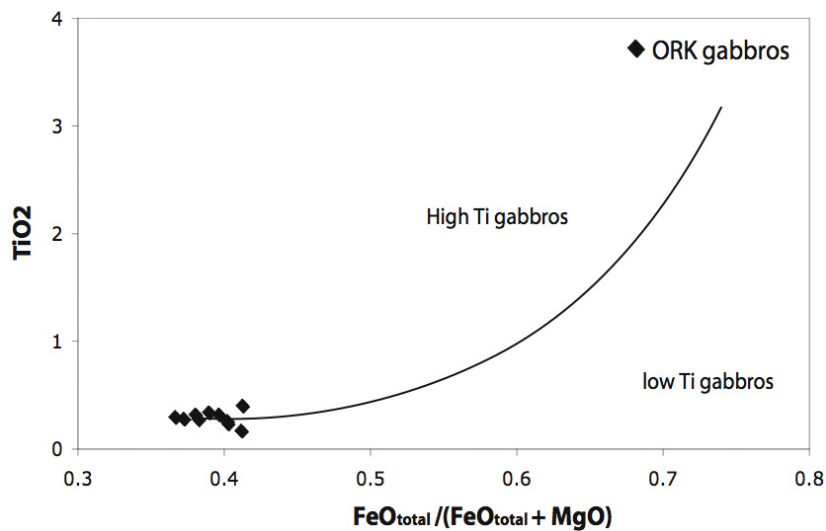


**Fig. 14.** $TiO_2$ versus mafic index fro the gabbroic samples from Oraiokastro ophiolite. (after Serri 1984)

Based on the TiO2 content and the mafic index M.I (MI: Fe# = molar FeO/(FeO+MgO)), as proposed by Serri (1981), the gabbros exhibit a mixed low-Ti to high-Ti magmatic affinity. The samples plot around the empirical line that divides the low- from the high-Ti fields (Fig. 14). Serri (1981) in his study correlated high Ti gabbros to high $TiO_2$

ophiolites, the latter being similar to oceanic crust formed along mid-ocean ridges. For the low $TiO_2$ gabbros he suggested that they occur within low $TiO_2$ ophiolites which represent magmatism associated with the remelting of a previously depleted mantle source, induced by infiltration of hydrous fluids and/or silicate melts derived from the sedimentary cover of a subducting slab, implying a supra-subduction zone origin for the low $TiO_2$ gabbros.

As discussed earlier in this chapter there are also some acidic plutonic and volcanic rocks that outcrop with the ophiolitic body. Following the discrimination scheme proposed by Pearce (1984) (Fig. 15), we observe, that the trondjemite that was sampled from the gabbroic section is classified as volcanic arc granite, while the later dioritic intrusion as ocean ridge granite. The volcanic rocks are plotted on this diagram only as indications since this diagram is applicable only to granitic rocks.
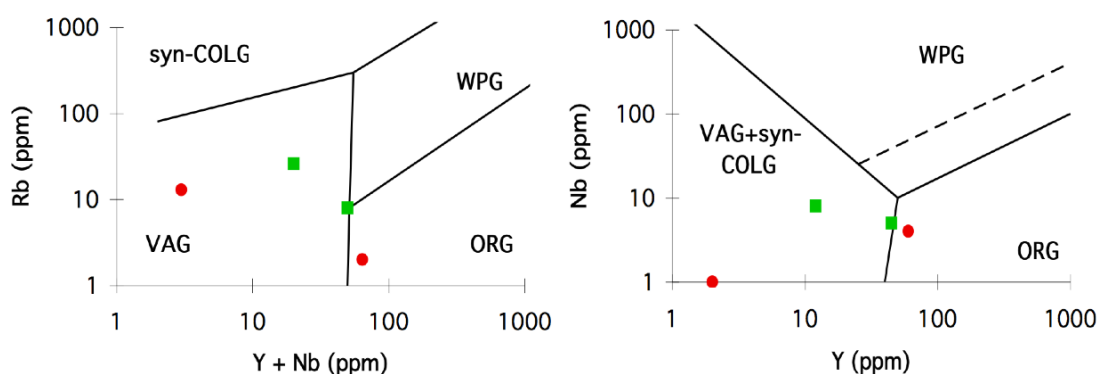


**Fig. 15.** tectonomagmatic discrimination diagrams for granitic rocks. The red dots represent the granitic samples from Oraiokastro, while the green squares stand for the volcanic rocks which are ploted as idicatitives. (after Pearce, 1984)

## 4.5 Petrogenesis

It is known that Th is enriched in subductions zones (reference) so it can be a good proxy to identify subduction zone influence in rocks.

On the Th/Yb versus Ta/Yb diagram (Fig. 16), the samples from HTE plot in the field of island-arc tholeiites, while the samples from LTE extend from the field of IAT into the field of calc-alkaline basalts. Pearce (1982) explaining the petrogenetic properties of this diagram suggested that by extrapolating the subparallel vector of the subduction enrichment back to the MORB array we could make estimates on the source characteristics. Tantalum can be used as a proxy for the source fertility. Examining the behaviour of the samples from Oraeokastron we see that both groups plot above the mantle array forming two different vertical to the Ta/Yb axis vectors, caused by Th enrichment. By back-projecting these two vectors to the mantle array we can deduce that the LTE rocks must have been derived from a

depleted lehrzolite source while those of the HTE from a less depleted peridotite, similar to the MORB source.
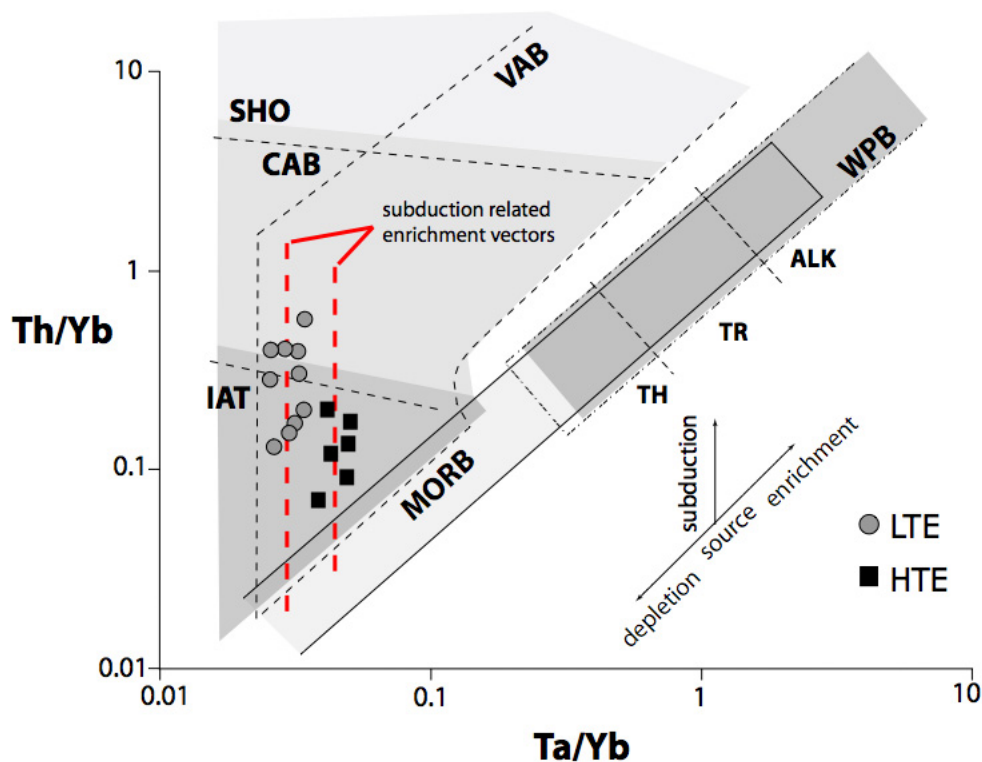


**Fig. 16.** Th/Yb versus Ta/Yb diagram for HTE and LTE samples from the Oraeokastro ophiolite. (after Pearce, 1982).

In order to quantify the source and melting properties we use the co-variation of a compatible vs. an incompatible element. The reason for that is that melting of a mantle source will deplete the source in the incompatible element while in the same time the compatible element will be barely affected.  As a consequence of that, in a bivariate diagram, the partial melting trends of the source will be presented as lines sub-parallel to the incompatible-element axis. By contrast, fractionation of mineral phases will result in the rapid depletion of the melt in its compatible element content, and thus in trends nearly sub-parallel to the compatible-element axis. By extrapolating the fractionation trend that fits through our samples back to the melting line we can make an estimation of the source and the degree of melting required. For Oraeokastron the melting modelling will be based on compatible vs incompatible element non-modal equilibrium modelling of Ti and Cr (Fig. 17). In this model no more that 1wt% of melt can be rest in the source and the source composition is recalculated after the extraction of each fraction of melt. The equation describing the melting model can be found in Shaw (1979) and Frey (1985). The crystallisation vectors on Fig. 17 correspond to 30wt% crystallisation of olivine, plagioclase, clinopyroxene and spinel mineral phases.  Accumulated melts represent the mixture of melt fractions of 1wt% that were pooled of the source and

mixed together. Examining the Cr vs Ti diagram (Fig. 17) we can infer that the rocks from the HTE require very low degrees of melting (<5wt%) of a fertile spinel lherzolite, while those of the LTE require higher degrees of melting (~25wt%) of the same source. The LTE can be alternatively explained by ~5wt% melting of a depleted spinel lherzolite.
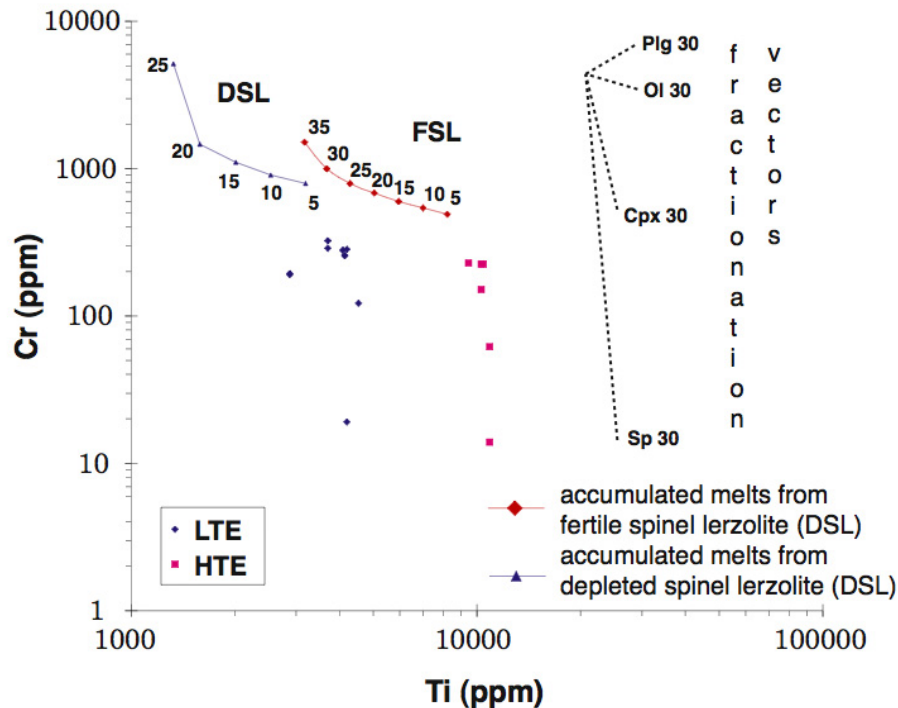


**Fig. 17.** Ti versus Cr diagram for HTE and LTE samples from the Oraiokastro ophiolite. Disussion in text.

Hellebrand (2002) proposed an empirical equation that links the Cr# of spinel from residual peridotites to the degree of fractional melting as follows: $F=10*\ln(Cr\#)+24$. Application of this equation to the Cr-spinels from the Oraeokastron harzburgites, resulted in degrees of fractional melting ranging between 15 and 19 (Fig. 18). The Al-spinels from the same rocks yield peculiarly low degrees of fractional melting that are less than 1wt%. In the case of zoned spinels, the degree of melting is also showing zonation decreasing form the core to the rim of the crystal.

The differences in the degrees of melting that were obtained by the two generations of the spinels namely the Al- and the Cr- spinels can be related to the results obtained from the non-modal equilibrium modelling. The results obtained for the LTE can be correlated to the results obtained for the Cr-spinels whereas the very low degrees of partial melting obtained from the HTE is in concordance to the very low degrees of melting that the Al-spinels yielded. Combining it with the fact that the Al rich generation of spinels is later than the Cr rich, we can infer that the LTE preceeded the formation of the HTE.
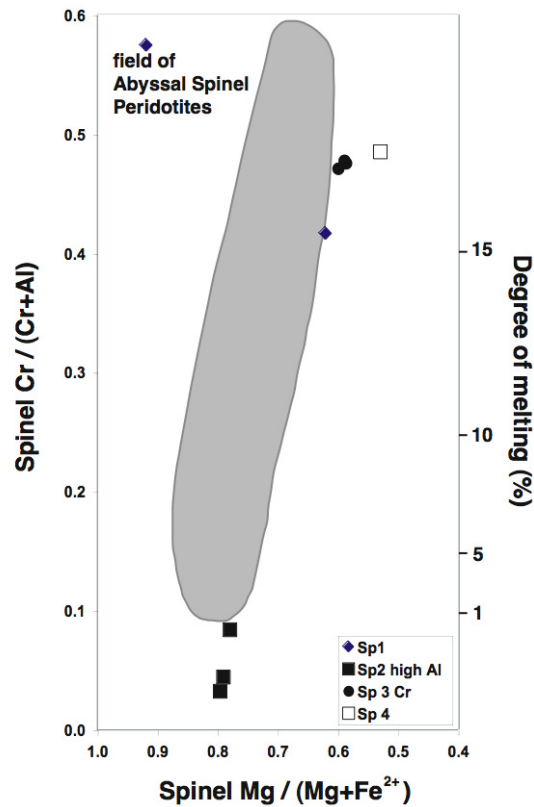
**Fig. 18.** Cr# versus Mg# from spinels fron the serpenitinised harzburgites from the Oraiokastro area sampled near the Monolofos village.  Abyssal Spinel peridotite field after Dick and Bullen (1984) and the meliting axis from Hellenbrand (2002).

Non-equilibrium melting modelling (Fig. 19, modelling parameters and explanations are given in the beginning of Part B) of the REE suggests that the HTE could have derived from ~3wt% of melting of a FSL source. The LTE group could have derived from the accumulation of 1-5wt% of melts from a FSL source that has previously experienced a 5wt% melt extraction and that has been modified by the additon  0.1wt% of subducted sediment.
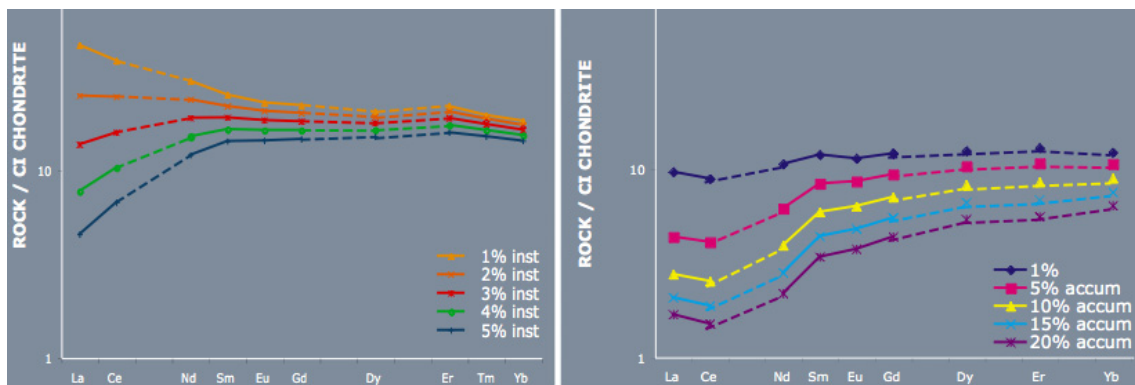


**Fig. 19.** Non-equilibrium REE melting modelling of the REE for the a) HTE and b) LTE

# 4.6 Conclusions

The Oraeokastron ophiolite is an incomplete ophiolite. A well-exposed sheeted dyke complex and cumulate ultramafics are not present. The main exposure consists of gabbroic rocks. A pillow lava section is well exposed in one location near the village of Neochorouda. Dykes only occur as intrusions in gabbros. More evolved lavas, plagiogranite stocks as well as a granitic intrusion were also found.

The mafic rocks from the Oraeokastron ophiolite have undergone metamorphism as a consequence of hydrothermal circulation and regional metamorphism, in the range of greenschist facies. As a result of that only pyroxenes, of augitic composition, out of the primary minerals have been preserved fresh. Plagioclase is altered to albite. The metamorphic assemblage is chlorite + actinolite + albite + epidote ± quartz ± pumpellyite ± magnetite ± pyrite.

Major element chemistry of the samples is disturbed from the metamorphic and hydrothermal processes. Most of the immobile trace-element content of these rocks as well as the REE content has been retained intact and is thus representative of the initial composition.

The extrusive rocks of the ophiolite are classified as basalts and basaltic andesites. There are two groups of mafic extrusive samples that can be distinguished on the basis of their major element chemistry and especially their $TiO_2$ content that is pretty unaffected by metamorphic processes. A high $TiO_2$ and a low $TiO_2$ group. Thorium is found to be enriched in both groups, being more enriched in the low $TiO_2$ group. Th follows distinct enrichment vectors for each groups towards higher Th/Yb ratios suggesting that the influence of the subduction component is different for the two groups. Multi-element diagrams show that both groups have been affected by contamination of the magma source, probably due to subduction zone fluids. REE systematics suggest that the low- $TiO_2$ group is derived from a depleted, relative to the N-MORB source, whereas the high- $TiO_2$ group is derived from a similar to the N-MORB source. The two groups are also distinguished on the basis of their isotopic characteristics. Samples from both groups plot outside the mantle array suggesting that the Sr isotopic system was modified by seawater alteration. The samples from the LTE appear to have an additional source enrichment vector, which can be distinguished from that of the HTE group.

Tectonic setting discrimination diagrams indicate a subduction zone environment for the LTE and a middle ocean ridge or back-arc basin environment for the HTE. Th/Yb versus Ta/Yb diagram reveals that both groups have a subduction component addition. The gabbros have a complex behaviour, plotting around the line that discriminates between low and high-Ti gabbros. Acidic samples plot in the volcanic-arc field, except for an intrusive diorite rock which was classified as ocean-ridge granite.

Petrogenetic modelling suggests that the rocks from the HTE require very low degrees of melting (~5wt%) of a fertile spinel lherzolite, while those of the LTE require higher degrees of melting (~25wt%) of the same source. The LTE can be alternatively explained by <5wt% melting of a depleted spinel lherzolite. Cr-spinels from serpentinised harzburgites yield degrees of melting between 15 and 19 wt%, while the later generation of Al-spinels from the same rocks yield degrees of melting less than 5wt%.

Combining all the above pieces of information, we conclude that the Oraeokastron ophiolite was formed in a setting above an intra-oceanic subduction zone. The coexistence of two different magmatic groups (BABB - IAT) can better be explained within the frame of the evolution of a back arc rifting. It is well documented by many examples from modern supra-subduction zone settings, that in late stages of rifting of an island arc or during the evolution of a back arc basin we observe the coexistence of MORB-like and IAT-like magma types. In the case of Oraeokastron, we favour the back-arc basin evolution scenario. The absence of a well-documented sheeted complex and the size of the ophiolite can be explained within the scenario of the rifting of a pre-existing island arc (Fig. 20). Unfortunately the lack of radiometric data on the age of the ophiolite make is it very hard to place the evolution in time.
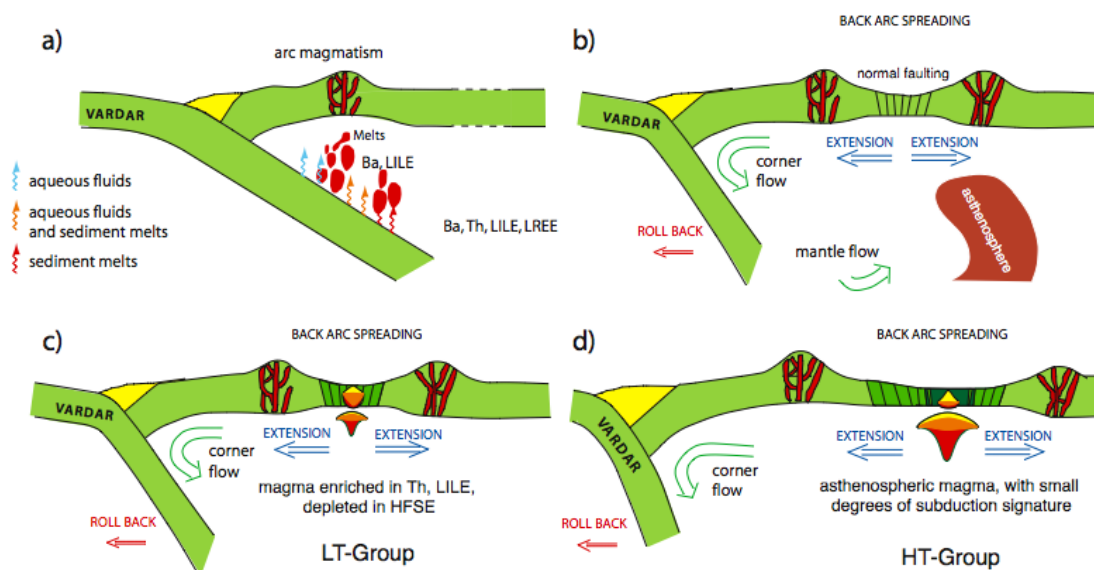


**Fig. 20.** Schematic cross sections of the evolution of the Oraeokastro Ophiolites

# Chapter 5. Geochemistry and petrology of the Thessaloniki ophiolite, N. Greece.

## 5.1 Regional setting

Thessaloniki is the capital city of Macedonia in northern Greece and is located on the borderline between the Vardar Zone to the west and the Circum-Rhodope Belt to the east (fig. 1). The excavation activity for the construction of the ring road of the city brought to light the upper part of a previously unrecognised volcanic system. The importance of this new volcanic system is the key position it occupies between the Vardar zone and the Serbomacedonian massif.
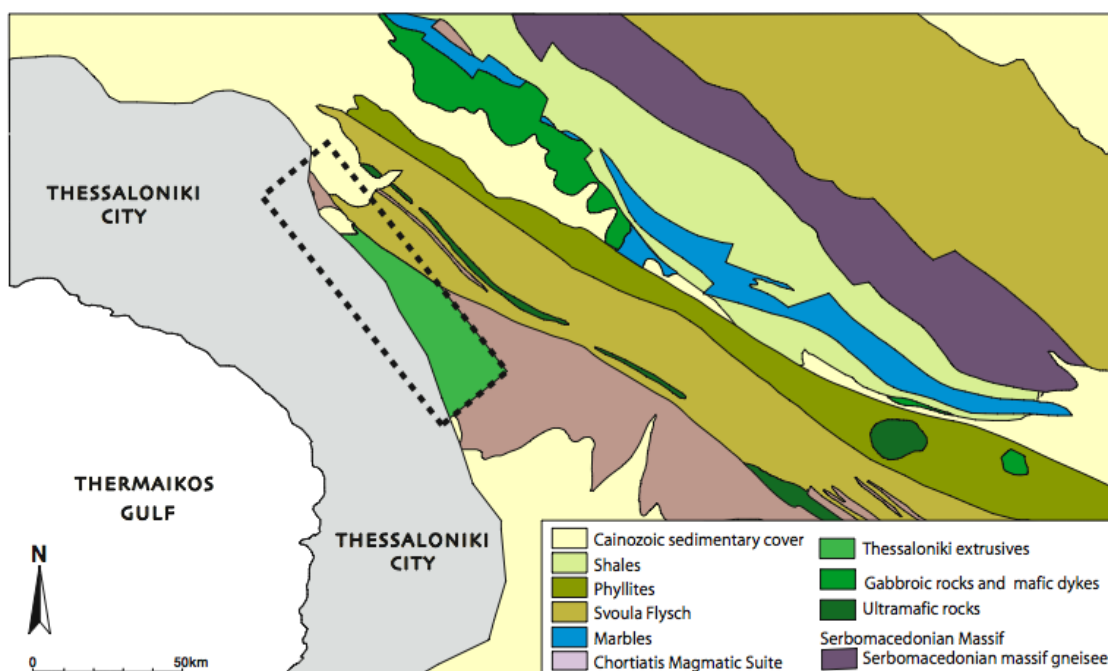


**Fig. 1.** Simplified geological map of the area around the city of Thessaloniki. The dashed line encompasses the study area. (after Kockel 1978, modified)

The only reports that were made on the rocks from this area are from Sapountsis (1979) and the discussion of the report of the later by Dimitriadis (1980). Sampountzis studied the gabbroic rocks from the wider area of Thessaloniki. In his study he concludes that these rocks bear similarities to basic and ultrabasic rocks found in Precambrian terrains, quoting a Precambrian K-Ar age for these rocks. No further details on the age are given at any point of his manuscript. Dimitriadis (1980) wrote a comment on that paper to the same journal that had been published suggesting that the same rocks could be part of an ophiolitic sequence, commenting also on the reliability of the dating for these rocks taken into account the low $K_2O$ of the gabbros. He quotes the indirect methods of geochronological determinations made by Mercier (1961,1968), Mercier et al. (1975) and Kockel (1971, 1977) who suggested that the Thessaloniki gabbros were formed during the Mesozoic probably during L. Jurassic.

In this chapter, the geochemistry, petrology, geotectonic evolution and geochronology of this newly exposed magmatic system will be examined in detail.

## 5.2 Sample description

The Thessaloniki magmatic system is built up mainly of dykes and less commonly of lavas. The lavas occur predominantly as flows and to a lesser extent as pillows. Minor outcrops of pillow lavas were found in construction sites at the foundations of buildings in the northern suburbs of the city. There is a spatial distribution in lavas and dykes such that the lavas outcrop systematically south of the dykes. The dykes mainly occur as sheeted swarms. In places among the dykes we observed magma mingling phenomena, where fine grained extrusive magma mingle with gabbroic liquid. Epidotite and epidosite veins are also present. Fresh samples were collected from major road cuts Among them, 25 were selected for geochemical investigation. A diorite outcropping among the high-level intrusives was selected for dating of the Thessaloniki arc. Photos from the outcrops can be found in Appendix G.

## 5.3 Geochemistry

### 5.3.1 Major and trace elements.

Whole-rock XRF, LA-ICP-MS and isotopic analyses are presented in appendices D, E and F respectively. The samples from Thessaloniki have been altered to greenschist facies metamorphism. The major magmatic minerals, clinopyroxene and plagioclase have been transformed to chlorite / actinolite and albite respectively. Secondary minerals include titanite, epidote, and variable proportions of quartz. The presence of minor magnesio-hornblende suggests transition to lower amphibolite facies conditions. Although intended, it was not possible to identify the chemistry of minerals from the primary mineralogical assemblage due to the intense alteration. During our microprobe study it was only possible to identify the chemical composition of the metamorphic minerals.

In Fig. 3 we see element vs Mg# variation diagrams for the samples from thessaloniki as well as from cumulate rocks from the surrounding area. As we see elements like $SiO_2$, $TiO_2$ $Na_2O$ Sr, have generally negative correlations with Mg# while $Al_2O_3$, Cr, Ni show a linear positive ones. The behaviour of element versus Mg# is compatible with the normal differentiation trend of basalts. The cumulates in most cases seem to genetically linked to the samples from the ophiolite. As it has been evident from the mineral-assembalge the samples from Thessaoniki are altered to greenschist facies. To examine the effects of alteration on whole-rock chemistry we will examine the co-variation of each element against Zr, used as an

alteration index (Appendix F.). As can be seen from the variation diagramms most major element concentrations have been variably disturbed while certain trace elements (e.g. Y, Nb, Ba, Hf, Ta, Th and the REE) appear to have been immobile. Only immobile elements will be used in petrogenetic modelling and interpretations
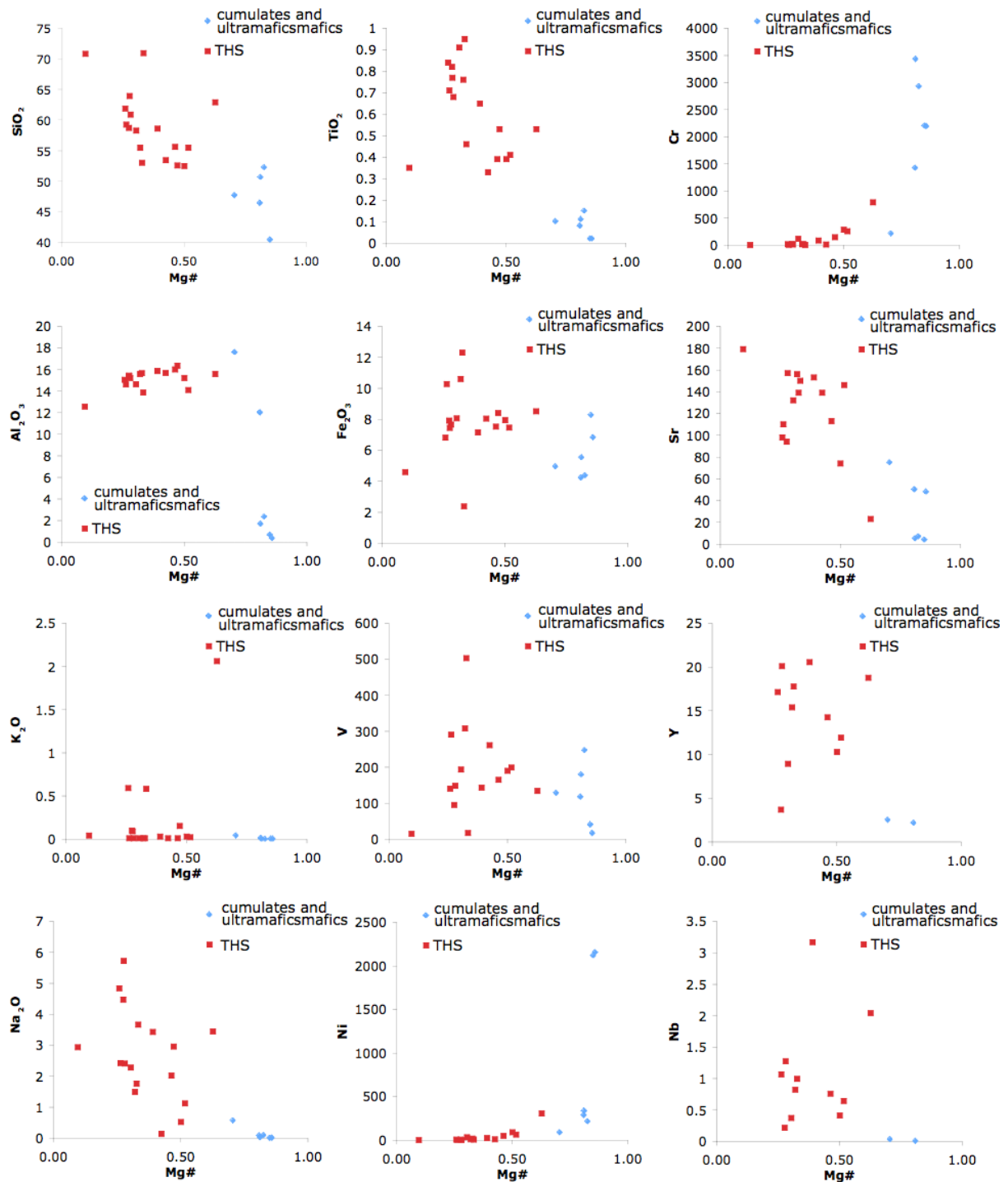


**Fig. 2.** Element versus Mg# for the mafic and acidic samples from the Thessaloniki ophiolite and the surounding mafic cummulates and ultramafic rocks.

Lavas and dykes from the Thessaloniki ophiolite classify as subalkalic basalts to andesites while one sample plots close to the field of dacites (Fig. 3, after Winchester and Floyd, 1977, modified by Pearce, 1996). The $SiO_2$ content of the samples exhibits a wide and continuous range from 52-70 wt.wt%. The $TiO_2$ content is always less than 1 wt.wt% and spans between 0.35 and 0.95 wt.wt%. The samples are low in $K_2O$ having concentrations between 0.01-0.58 wt.wt%, excepting sample THS 16 which contains around 2 wt.wt% $K_2O$. All major-element oxides show large variations. MgO ranges between 0.44 and 7.19 wt.wt%, $Fe_2O_3$ between 2.37 and 12.30 wt.wt% and $P_2O_5$ between 0.01 and 0.09 wt.wt%. The trace elements also show large variations in their concentrations. Y ranges between 3.7 and 20.5ppm, Zr between 9 and 81ppm and Nb between 0.21 and 3.17ppm.
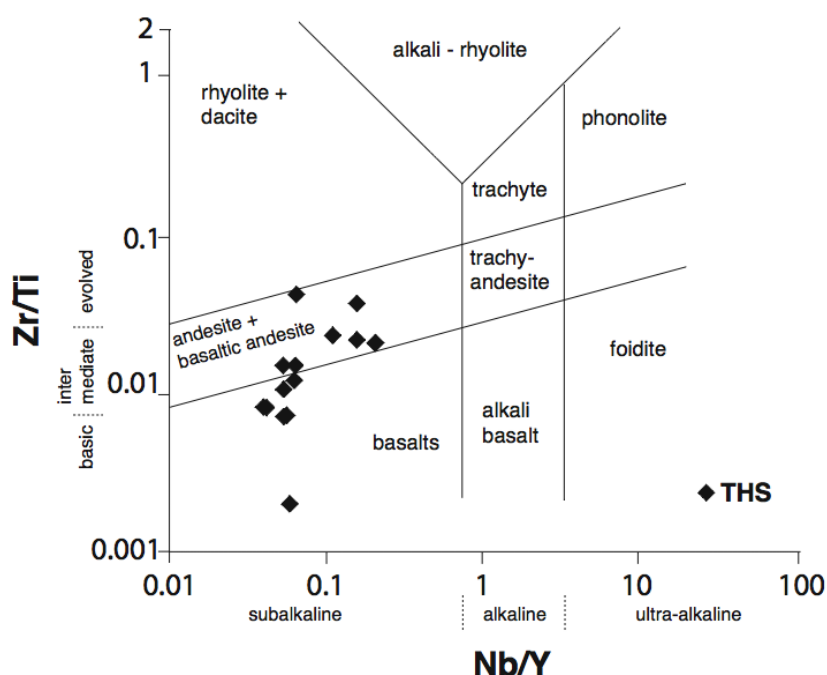


**Fig. 3.** Zr/Ti versus Nb/Y for the volcanic samples from the Thessaloni ophiolite. (after     Winchester and Floyd (1977) revised after Pearce et al 1996)

Compared to normal mid-ocean ridge basalts, the samples from Thessaloniki are depleted in K and Rb while Sr and Ba are closer to MORB concentrations. (fig 4). Taking into consideration the covariation of these elements with Zr, examined earlier, we can attribute the observed depletion to alteration rather than to a primary source feature. As discussed in the beginning of Chapter 2, LILE are mobile during dehydration of the subducting slab and are characteristically enriched in magmas erupted in subduction zones. The depletion observed here can be best explained by hydrothermal processes that leached the rocks from these elements. Sample THS 16 has typical enriched LILE patterns. Thorium is enriched up to 10 times MORB in the majority of the samples. Samples THS 16 and THS 15 have even higher Th up to around 30 times MORB. There is a distinct negative Nb anomaly in all samples. The

majority of the samples show depleted HFSE patterns with increasing depletion from Yb to Nb suggesting that these rocks have derived from a depleted source. Samples THS 16 and THS 15 show an enrichment trend in the HFSE. All samples show a selective enrichment in La and Ce compared to the remainder of the HSFE; this can be explained by the addition of a component enriched in La and Ce to the source of these rocks.
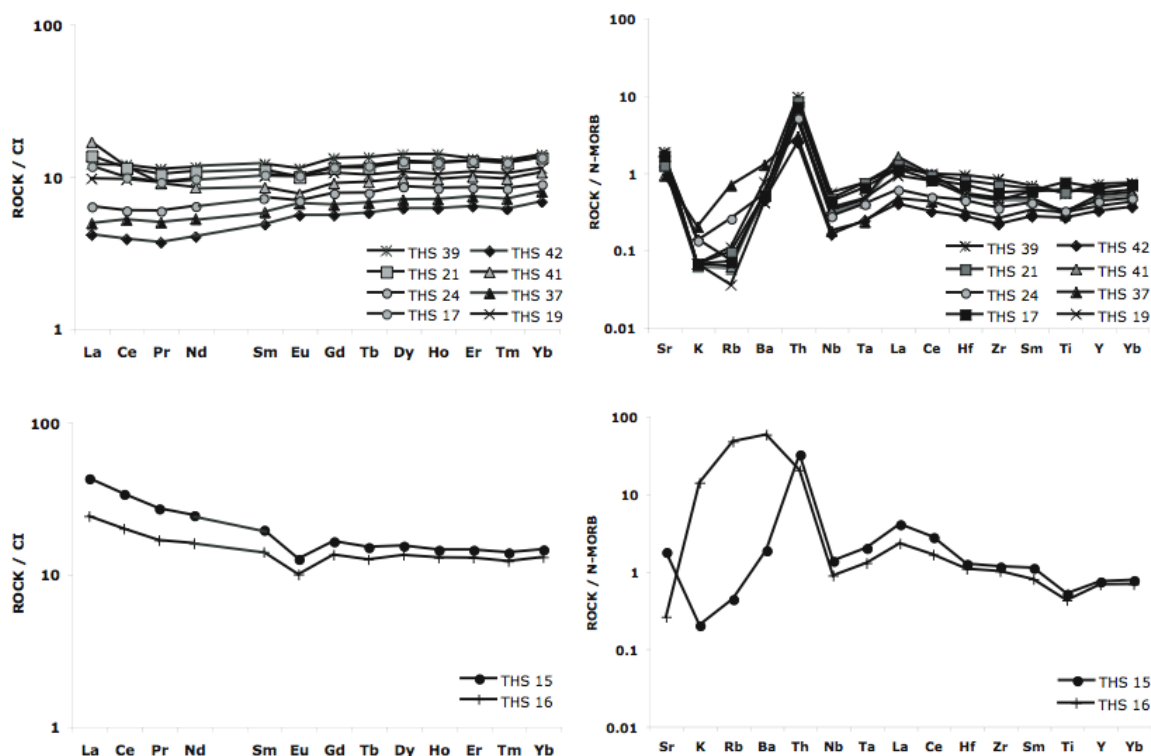


**Fig. 4.** Normalised to C1 chondrite REE diagrams for the Thessaloniki samples. Top La/Yb<1, bottom La/Sm >1. Normalised to N-MORB multielement "spiderdiagramms" for the same samples. Normalising values for N-MORB are from Pearce (1982, 1983) and C1 after and from McDonough and Sun (1995).

Chondrite-normalised REE patterns are shown in Fig. 4. The samples from Thessaloniki show a variable behaviour in the LREE. The majority of the samples show depleted to flat LREE patterns (La/Yb≤1), while samples THS 16, 15 and 41 have LREE enriched patterns (La/Yb>1). Addressing again the element versus Zr plots we see that the high La concentration of sample THS 41 appears to be the result of alteration and does not represent a primary magmatic feature. Nearly all samples display negative Eu anomalies suggesting plagioclase fractionation; sample THS 42 however has no Eu anomaly and THS 37 has a slightly positive Eu anomaly. The HREE patterns are flat implying shallow melting of the source above the garnet stability field. The REE patterns of LREE-depleted samples are parallel suggesting they are the result of fractional crystallisation of similar degrees of melting of the same source. The variable La and Ce abundances in the same group of rocks can be attributed to variable contamination of the magma by subduction-zone derived components.

## 5.3.2. Sr- Nd Isotopes

The Sr and Nd isotope data for the Thessaloniki ophiolite are presented in Appendix F. All Nd initial ratios and εNd values are recalculated at 167 Ma. Chondritic values used are: $^{143}Nd/^{144}Nd=0.512638$ (Goldstein et al. 1984) and $^{147}Sm/^{144}Nd=0.196700$ (Jacobsen and Wasserburg 1980, Peucat et al. 1988). The samples have Sm and Nd concentrations between 1.126 and 2.746ppm and 3.099 and 10.41ppm respectively. Calculated $\varepsilon_{Nd(167)}$ values are higher than $\varepsilon_{Nd\ CHUR)}$ (excepting sample THS 16) and range between 5.41 and -0.67. $^{87}Sr/^{86}Sr$ ratios range between 0.711218 and 0.704944.

Time-corrected εNd values are lower than those of mid-ocean ridge basalts; this, coupled with the observed negative trend in Fig. 5 suggest that the source of the Thessaloniki rocks was a depleted mantle peridotite that was isotopically modified by an enriched component, possibly due to crustal contamination or sediment-related mass transfer in a subduction-zone setting.
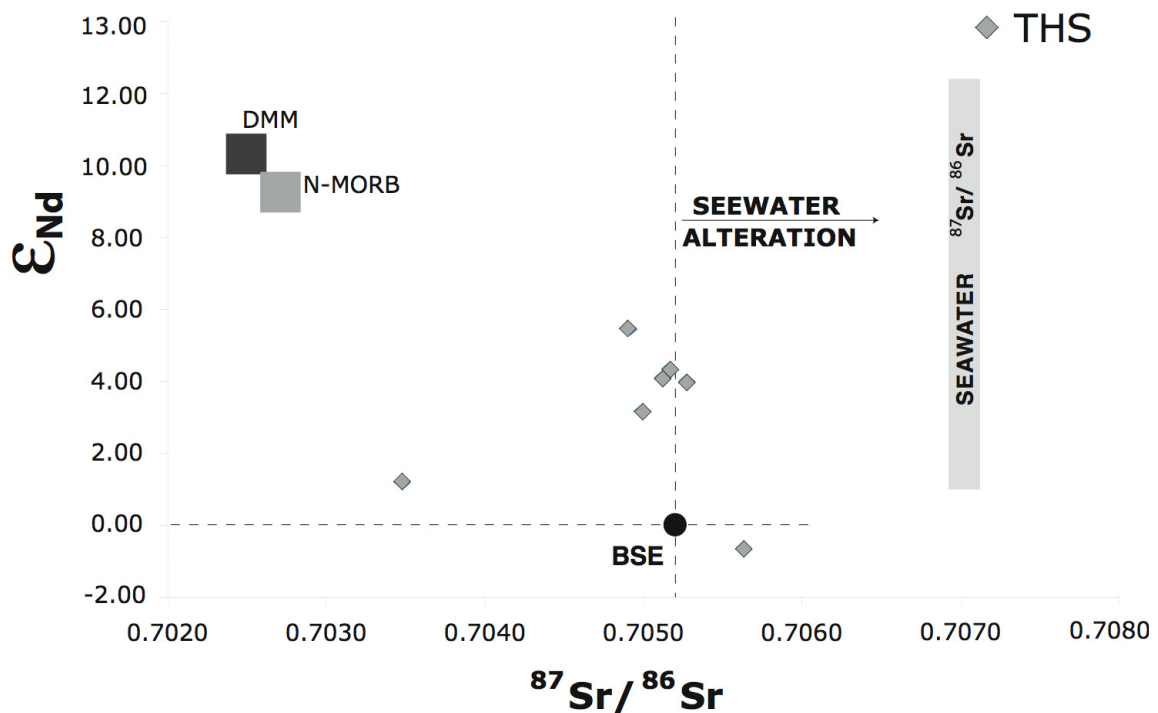


**Fig. 5.**    recalculated to 165 Ma versus $^{87}Sr/^{86}Sr$ for the Thessaloniki samples. BSE: Workman and Hart (2005), DMM :Rehkamper and Hofmann (1987), and Klein (2004), MORB:Kelemen et al. (2004) and Seawater values after Palmer and Edmond (1989).

Time-corrected $\varepsilon_{Nd(167)}$ values and $^{87}Sr/^{86}Sr$ ratios are negatively correlated for all samples from Thessaloniki with the notable exception of sample THS16. This sample is

displaced towards much higher $^{87}Sr/^{86}Sr$ values thus deviating significantly from the trend defined by the other samples. This, coupled with its unique enrichment in LILE implies that this sample has "seen" not only the strongest enrichment but also an enrichment of, perhaps, a different nature. The displacement to considerably higher $^{87}Sr/^{86}Sr$ ratios is not followed by a commensurate displacement in εNd. Sample THS 37 that has a cumulate-like REE pattern has the higher $ε_{Nd(167)}$ value, while the samples with LREE enrichment have the lowest $ε_{Nd(167)}$ ratios. The remainder of the samples define a coherent group that shows only a minor negative correlation between $ε_{Nd(167)}$ and $^{87}Sr/^{86}Sr$ ratio values.
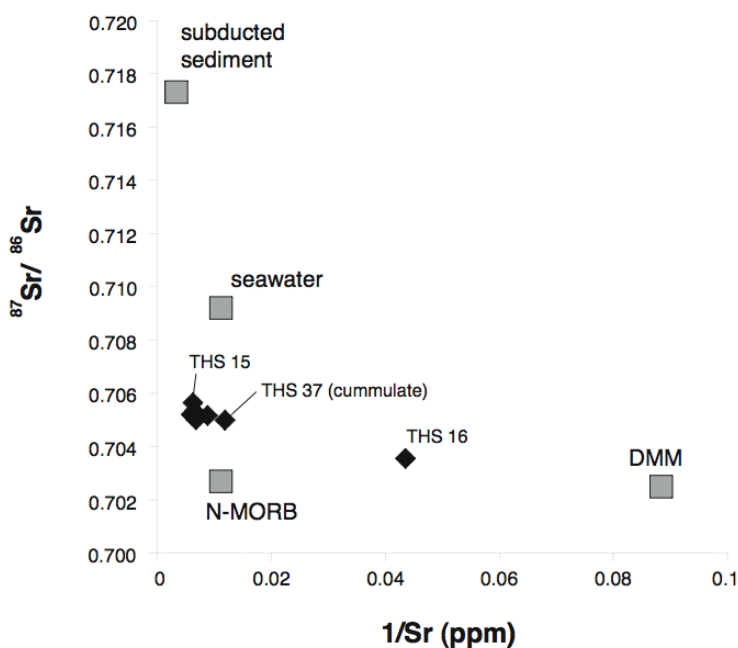


**Fig. 6.** $^{87}Sr/^{86}Sr$ vs 1/Sr plot for the Thessaloniki samples. Values for subducted sediment, DMM, and N-MORB as in Fig. 5. Seawater values are from Palmer and Edmond 1989.
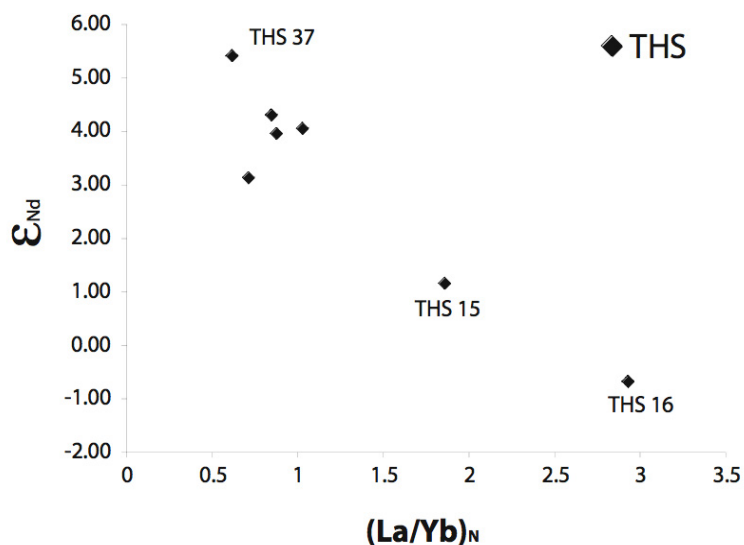


**Fig. 7.** $ε_{Nd}$ vs. $(La/Yb)_N$ for the Thessaloniki ophiolite samples

In Fig. 6, we see a plot of $^{87}Sr/^{86}Sr$ verssus 1/Sr ratio values. The rationale behind such a diagram is that samples fractionating from the same source should have constant radiogenic Sr ratios for increasing Sr concentration. The mafic samples from Thessaloniki cluster in a group with relatively uniform 87Sr/86Sr and low 1/Sr ratio values. The cumulate sample, THS 37, has higher 1/Sr but is in the same range of $^{87}Sr/^{86}Sr$ as the mafic extrusives. The two acidic samples are displaced to higher $^{87}Sr/^{86}Sr$ than the rest. THS 15 has similar Sr concentration as the mafic, but THS 16 is displaced towards higher 1/Sr values. As was the case in the $\varepsilon_{Nd(167)}$ vs. $^{87}Sr/^{86}Sr$ plot, sample THS16 plots away from the all the other Thessaloniki samples towards much higher $^{87}Sr/^{86}Sr$ and 1/Sr ratio values.

Fig. 7 shows a negative correlation between $^{143}Nd/^{144}Nd$ and (La/Yb)n ratio values. This suggests that the process leading to lower Nd isotope ratios is also responsible for the enrichment in LREE. The considerable variation in the εNd values from +5 to -0.7 precludes dynamic (continuous) melting as the cause of the trend seen in Fig. 7 but favours source enrichment by OIB-like and/or sediment melts (see Kostopoulos & Murton, 1992).

## 5.3.3 Melting Model
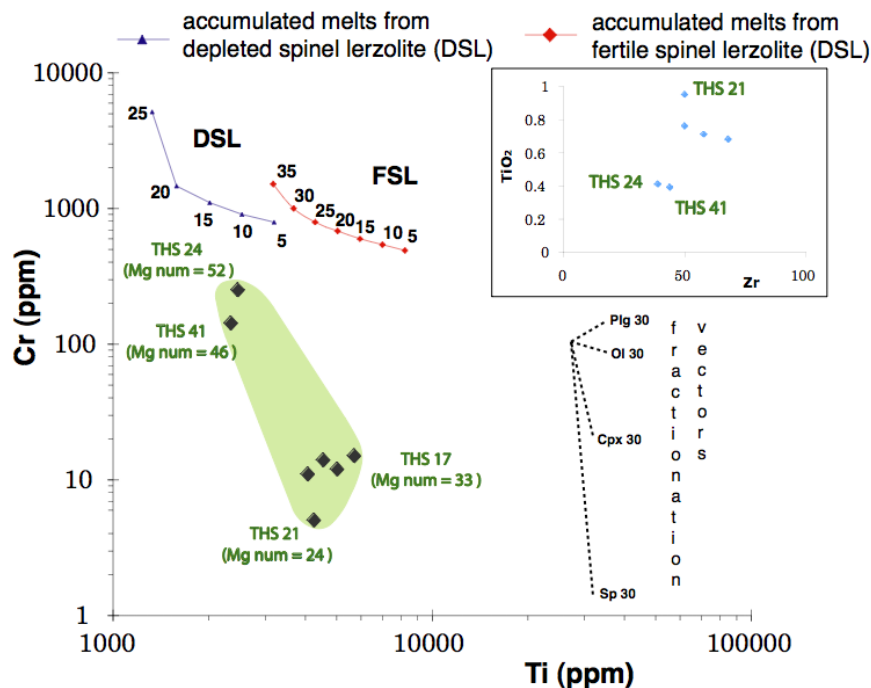


**Fig. 8.** Ti vs Cr diagram for the Thessaloniki ophiolite. In the inlet diagram we see the variation of the samples to Zr, used in this case as alteration index.

Same as for the previously investigated ophiolites, so in the case of the Thessaloniki ophiolite we will use the co-variation of a Cr and Ti as described in the methods paragraph in

order to quantify the source and melting properties(Fig. 8). The fractionation vectors on Fig. 8 correspond to 30wt% crystallisation of olivine, plagioclase, clinopyroxene and spinel phases. Accumulated melts represent the mixture of melt fractions of 1wt% that were pooled of the source and mixed together. Examining the Cr vs Ti diagram (Fig. 8) we see that samples THS24 and THS41 are have very low $TiO_2$ contents and seems that they have derived from a DSL source by 10-15% melting. The rest of the samples plot in higher $TiO_2$ concentrations and seem to have derived from a 15-25% melting of a FSL source. Checking the $TiO_2$ vs Zr diagram for these samples (Fig. 8) we see that ssamples THS24 and THS41 are displaced from the main trend of the rest of the samples, feature that could be attributed to mobilisation of $TiO_2$ due to alteration.

## 5.4 Tectonomagmatic discrimination

Reference to Appendix F and the element vs Zr plots for the Thessaloniki samples demonstrates that some trace elements that are considered important for tectonomagmatic discrimination such as Ti, V and Sr appear to have been mobilized during alteration. Only elements that appear to have been undisturbed (Y, Nb, Hf, Th, Yb, Ta, and Zr) will be used hereafter to discriminate between different tectonic settings.
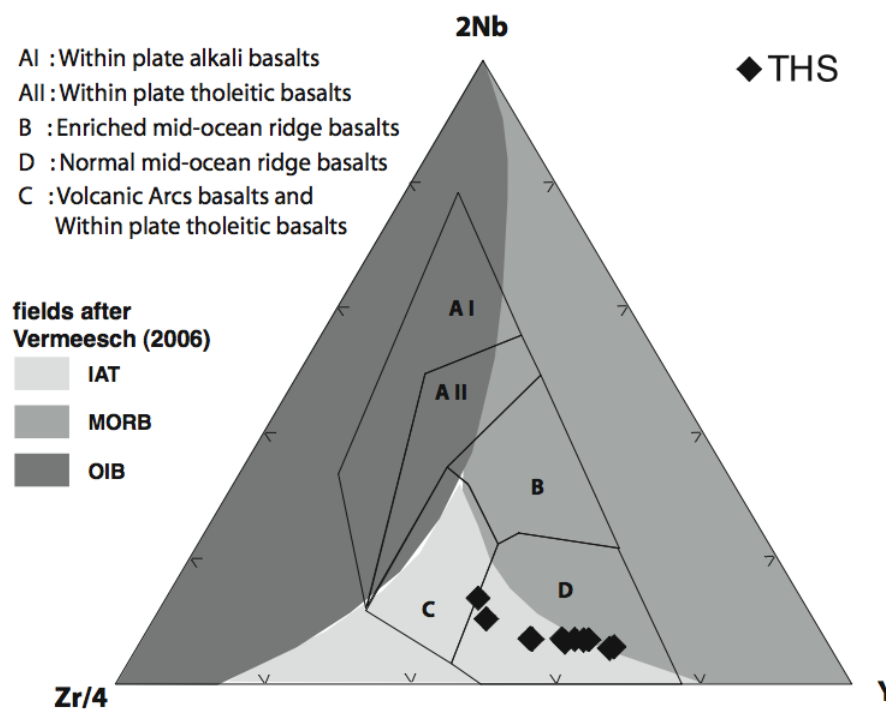


**Fig. 9.** Zr/4-2*Nb-Y diagram showing the classification of samples from the Thessaloniki ophiolite Fields after Meschede (1986).

Meschede (1989) utilized the elements Zr, Y, and Nb to discriminate between within-plate basalts (WPB), N-MORB and island-arc basalts (IAB). Niobium can be used as an index of mantle differentiation, and the Zr/Nb ratio can be used as a proxy for enrichment or depletion processes in the mantle (Meschede, 1989 and references therein), while the Zr/Y ratio can be used to investigate long-term source heterogeneities thus distinguish between basalts erupted in within-plate settings and basalts erupted in mid-ocean ridges and volcanic arcs (Pearce and Cann, 1973 and references therein, Pearce and Norry, 1979). Plotting the Thessaloniki samples on Zr/4-2*Nb-Y diagram of Fig. 9 we observe that they fall in the fields of N-MORB and volcanic-arc basalts, and that there is no evidence for a within-plate enriched mantle signature in the source region of these rock
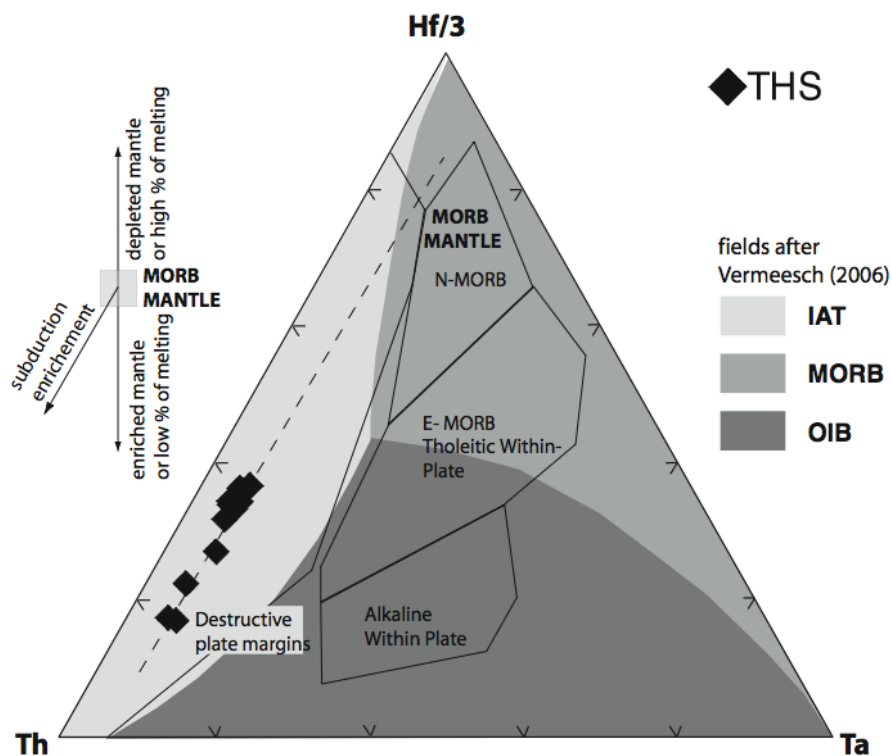


**Fig. 10.** Hf-Th-Ta diagram showing the distribution of samples from the Thessaloniki ophiolite. Fileds after Wood (1980).

Thorium is considered to be immobile to temperatures up to 600°C and its concentration is typically enriched in subduction zones (Wood 1979). Examining the behaviour of Th relative to that of Zr we can assume that the concentration of Th has not been modified by alteration and metamorphism. Therefore the Th concentration is considered as a primary feature of the rocks. Based on the discrimination diagram Th-Hf/3-Ta (Fig. 10) proposed by Wood (1980) the samples from Thessaloniki plot in the field of rocks from destructive plate margins forming a trend towards higher Th concentrations. The samples are

displaced towards low Ta values implying that these rocks have derived from a depleted source.

## 5.5 Examining the contamination component

As shown in the previous paragraphs the samples from Thessaloniki have been derived from a mantle source that has been modified by an enriched component in a supra-subduction zone setting. In this paragraph we will try to investigate the characteristics and infer the origin of this component.
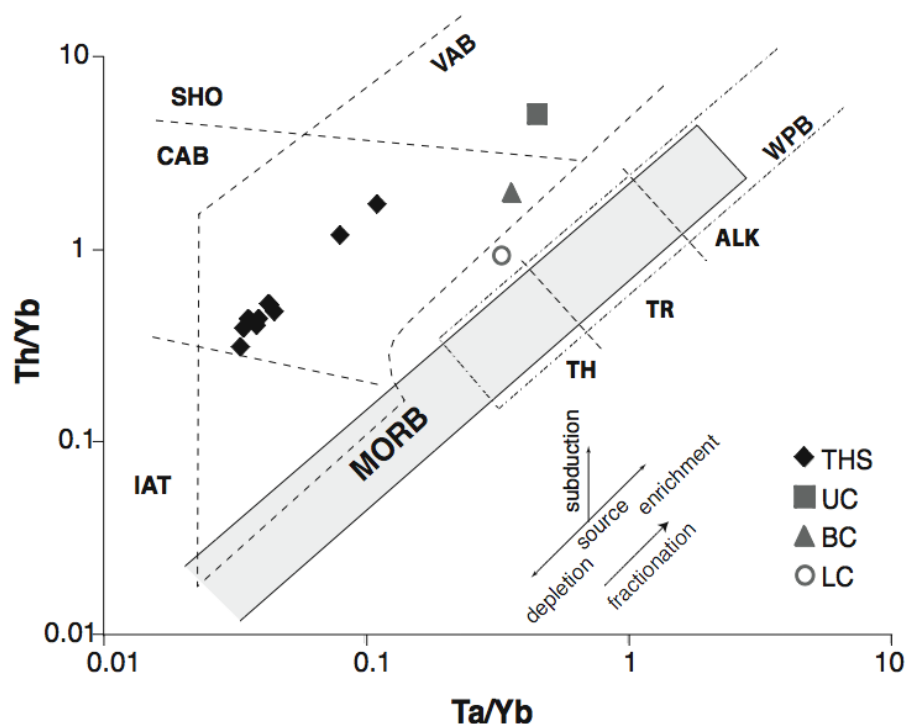


**Fig. 11**. Th/Yb versus Ta/Yb diagram for the samples from the Thessaloniki ophiolite (after Pearce 1982). BCC: Bulk Continental Crust; UCC: Upper Continental Crust; LCC: Lower Continental Crust (values from Rudnick & Gao 2004).

Pearce et al. (2005) used the elements Th, Ta, Ba and Nb to identify the subduction components that contributed to the arc magmatism of the Marianas arc-basin system. All the elements were normalised to Yb in order to diminish the effect of fractional crystallisation and phenocryst accumulation. Ytterbium is compatible with garnet; however, since there is no evidence either of residual garnet or deep melting as deduced from the HREE patterns nor of mobilisation due to alteration, normalisation to Yb will produce reliable results.

On a Th/Yb vs. Ta/Yb diagram (Fig. 11) the samples are displaced from the MORB-OIB array to higher Th/Yb ratios. This enrichment in Th is caused by fluids or sediment melts

released from the subducted slab at depths between 70-150km (Spandler et al. 2004). The displacement of the Th/Yb ratio towards higher values than the MORB-OIB array is defined by Pearce et al. (2005) as the Ba-Th component that is supposed to have been derived from the subducted slab in deep parts of the subduction zone. Johnson & Plank (1999) defined experimentally the sediment solidus to $>750^{o}C$ and suggested that Th can be mobilised for conditions above the solidus and only by a silicate melt. Ta/Yb is positively correlated with Th/Yb for all the samples.
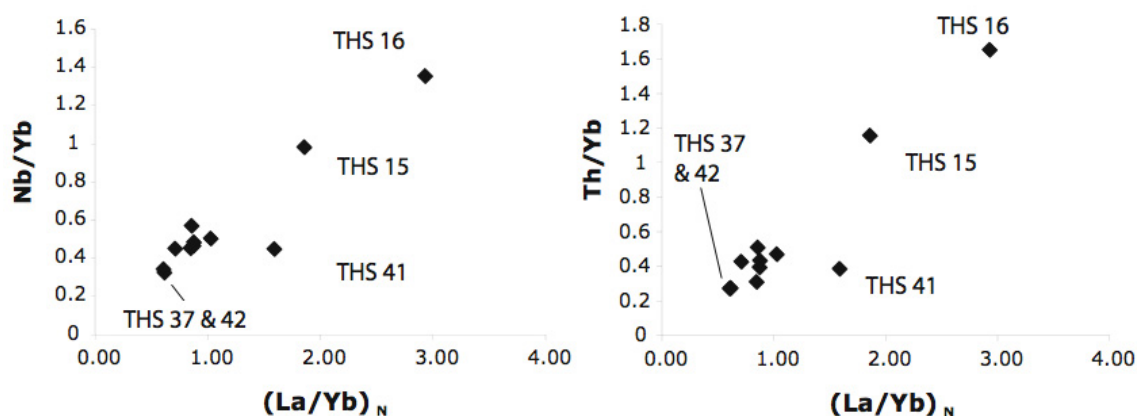


**Fig. 12.** **a)** Nb/Y aversus (La/Yb)$_N$ and **b)** Th/Yb versus (La/Yb)$_N$ for the Thessaloniki ophiolite

The LREE-enriched samples are characterised by much higher Th/Yb and Ta/Yb values compared to the LREE-depleted samples suggesting that they have been affected more from the subducting slab. Th/Yb is positively correlated with (La/Yb)$_N$ (Fig. 12a), which means that the component that caused the Th enrichment is also responsible for the LREE enrichment in the samples THS 15 and 16. The rest of the samples show a general increase of the Th/Yb as the La/Yb increases but within a small window of (La/Yb)$_N$ values.

## 4.5 Geochronology

Mussalam and Jung (1986) have reported (as personal communication with Kreuzer) a K-Ar age of 174±4.8 Ma for a hornblende gabbro from the "Thessaloniki Ophiolite". However, details on sample locality and measured isotope ratios were not reported, therefore a full evaluation of the meaning of this age cannot be made.

With regard to the Thessaloniki complex, a sample from a dioritic outcrop situated among high-level intrusives was selected for geochronological investigation. The rock is situated at the outskirts of the city of Thessaloniki along the north slope of the city's ring road. The zircons separated were typically idiomorphic and their CL images revealed a purely

igneous structure attested to by very well-developed oscillatory zoning (Fig. 13). U/Th ratios span from 0.14 to 0.41 excluding metamorphic origin.

The size of these zircons ranges between 250µm for the largest and 70µm for the smallest. A total of nine spot analyses on eight different zircon grains was performed. One crystal was analysed both at the rim and the core; the ages obtained are identical within error. The analysed zircons yielded a concordia age of 169±1 Ma (MSWD=0.16), which is interpreted as the crystallisation age of the diorite (Fig. 13). It has to be noted that the age obtained in our study is similar within error with the age reported by Mussalam and Jung (1986).
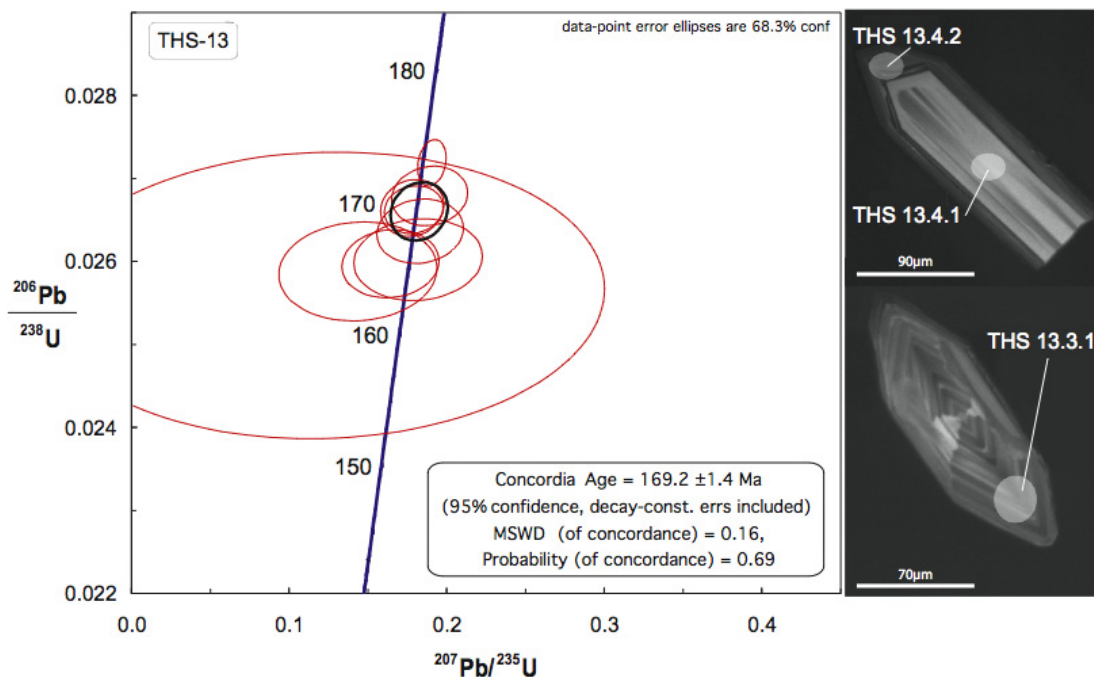


**Fig. 13.** Concordia diagram for the Thessaloniki diorite and representative CL images of zircons. The whitish circles represent individual spot analyses by SHRIMP. Spots THS 13.4.2 and THS 13.4.1 have resulted in identical ages.

As we have seen in Fig.1. The area were we have discovered the ophiolitic rocks was mapped by previous workers as an area occupied from the Chortiatis magmatic suite. Having this in mind we wanted to estimate the age of the Chortiatis magmatic suite and compare it to the age of the ophiolites. For that reason we moved in the area of the Chortiatis magmatic suite close to the ophiolite and we sampled the typical rock-type of this formation, a diorite from the Livadi area (sample L9). The sample preparation process was the same as for the ophiolite and the age of the zircons separated from the L9 sample was determined by SHRIMP in St.Petersburg, by T. Reischmann and D. Kostopoulos. We have chosen to date

this rock with the same method as in the case of the ophiolites in order to have comparable results.

The zircons separated are idiomorphic with very well developed oscillatory zoning suggesting igneous structure. The U/Th ratio is between 0.25 and 0.51 excluding, like in the case of the ohiolite, metamorphic origin. The analysed zircons yielded a concordia age of 159±4 Ma (MSWD=0.54), which is interpreted as the crystallisation age of the diorite (Fig. 14).

Comparing the age obtained from the ophiolite and the age of the Chortiatis magmatic suite as this was estimated on zircon from a diorite near the area of the ophiolte, we see that they have an age difference of 10Ma. The age difference lies outside the error of the two age determinations. This means that the formation of the ophiolite preceded the formation of the Chortiatis Magmatic Suite by 10 Ma.
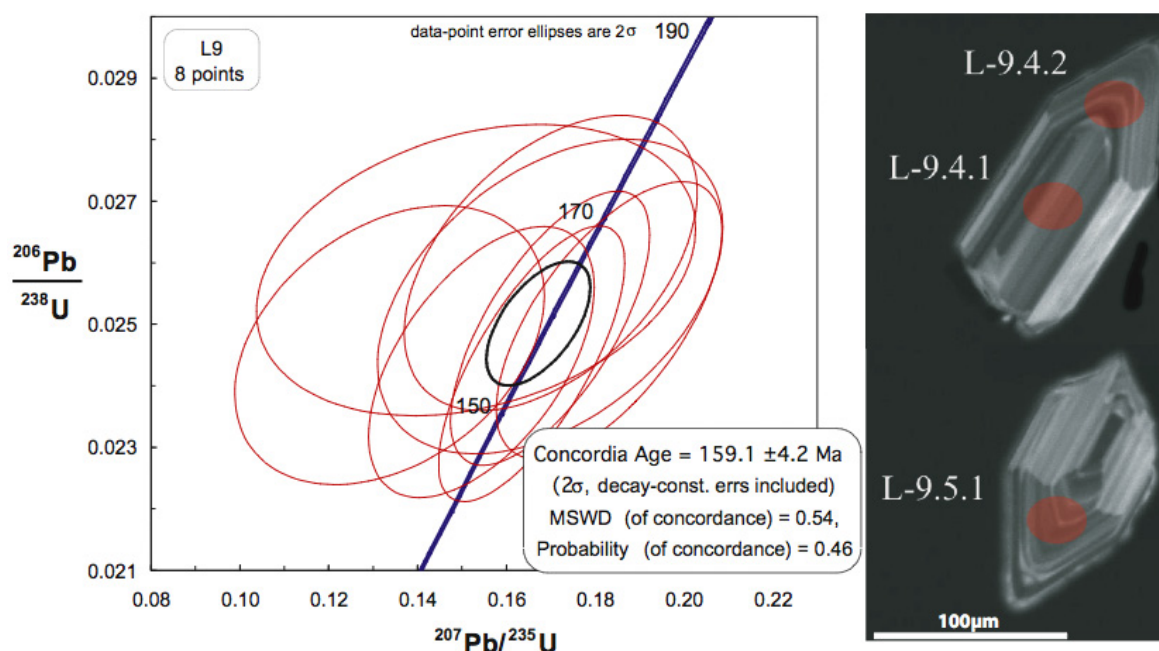


**Fig. 14.** Concordia diagram for the Chortiatis magmatic suite diorite. The reddish circles represent individual spot analyses by SHRIMP. Spots L-9.4.2 and L-9.4.1 have resulted in identical ages.

## 5.6 Summary and Conclusions

The new exposures as they have been revealed after the excavation activities around the city of Thessaloniki, form the extrusive part of a volcanic system that has previously not been investigated. This volcanic system is composed of lavas and both single and sheeted dykes, and it can be described in the frame of a dismembered ophiolite.

The rocks have been altered in the field of greenschist facies as it is evident from the breakdown of the primary mineralogical assemblage to typical greenschist facies assemblages including albite, chlorite, actinolite, epidote, titanite, and quartz.

Variation diagrams of major oxides and trace elements against Zr suggest that the major element concentration of the samples is disturbed while trace elements and rare earths e.g. Y, Nb, Ba, La, Sm, Yb, Hf, Ta, Th, appear to be undisturbed. Based on immobile during alteration elements the rocks are classified as subalkaline basalts to basaltic andesites and dacites.

The chemistry of the dykes and lavas from Thessaloniki have the typical characteristics of subduction zone magmatism. Normalized to N-MORB the samples have negative Nb anomaly, Th enrichment, and the majority of samples have a depletion trend of the HFSE from Yb to Nb. The samples THS 15 and THS16 have an enrichment trend of the HFSE. The majority of the samples have depleted LREE patterns except from THS 15 and 16 which are LREE enriched. Sample THS 37 and THS 42 have a slightly positive Eu anomaly suggesting plagioclase accumulation in the source, whereas the rest of the samples have negative Eu anomalies.

Nd and Sr isotopes show negative correlation. The calculated $\varepsilon_{Nd(167)}$ values are between 5.41 and -0,67 and the $^{87}Sr/^{86}Sr$ ratios between 0.711218 and 0.704944. The $\varepsilon_{Nd(167)}$ measured is lower that the $\varepsilon_{Nd,CHUR(167)}$. THS 16 deviates from the main trend of the rest of the samples towards much higher $^{87}Sr/^{86}Sr$. Petrogennetic modelling based on compatible vs incompatible element non-modal equilibrium melting modelling suggest 15 -25% of melting of a FSL source.

Tectonomagmatic discrimination based on trace elements classifies the samples as rocks formed in destructive plate margins.

Fingerprinting of the enriched component suggests that the both samples with LREE depleted and LREE enriched patterns have been affected by a component that carries Th, and its origin is the deep parts of a subduction zone. This component is also responsible for the negative correlation of the $^{143}Nd/^{144}Nd$ and $^{87}Sr/^{86}Sr$. Additionally the samples with LREE enriched patterns have seen a component that rises the concentration of the HFSE. This cannot be melt derived from the mafic fraction of the subduction zone, because of the low Sr/Y ratio of the samples. So it can be better explained by local enrichments of the mantle or continental crust or assimilation of continental crust.

Summing up all the observations made in this chapter on the geochemistry of the Thessaloniki ophiolite we can suggest that this is a suprasubduction zone ophiolite, probably formed in the stage of the evolution of island arc magmatism.

# Chapter 6. Geochemistry and petrology of the Kassandra and Sithonia ophiolites, N. Greece.

## 6.1 Geological setting

The Kassandra and Sithonia peninsulas are located in northern Greece and belong to the greater Chalkidiki peninsula (Fig. 1). To avoid using the term peninsula every time we want to refer to the study areas, the Kassandra peninsula will hereafter be referred to as simply Kassandra and the same will be applied for the Sithonia peninsula. Photos from the outcrops can be seen in Appendix G.
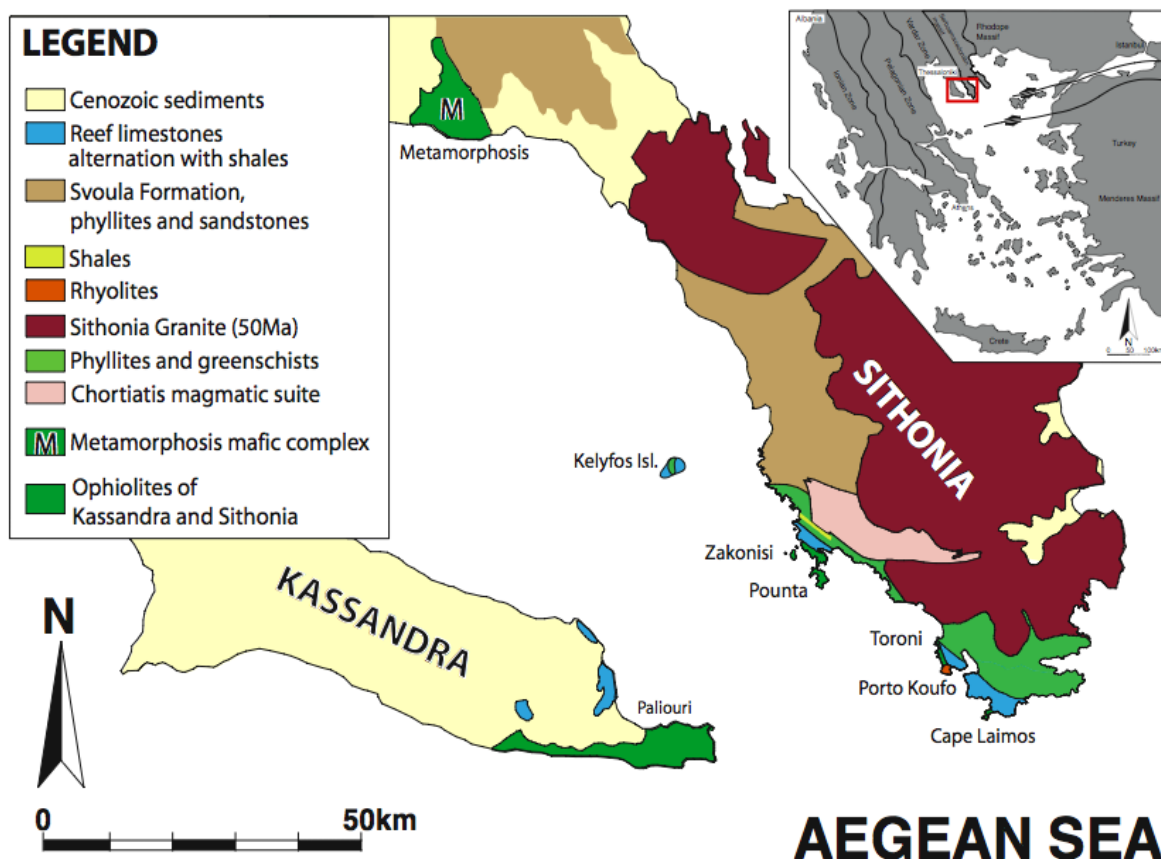


**Fig. 1.** Generalised geological map of the southern parts of the Chalkidiki peninsula. Ophiolitic outcrops are found at the southern tip of Kassandra peninsula and along the south-western coast of Sithonia peninsula (simplified and modified after Kockel (1977).

Kassandra is covered by a thick series of Late Cenozoic sedimentary rocks consisting of Neogene limestones, conglomerates, marls, psammites and sands. In the southern part of the peninsula there are some Cretaceous and Upper Jurassic limestones that outcrop among the sedimentary rocks. The southernmost part of Kassandra is dominated by the continuous outcrop of mafic extrusive rocks that have been described as ophiolite (Guy and Bornovas, 1965). The mafic outcrop on Kassandra is built up of massive lava flows and pillow lavas. The lavas are variably vesicular and have experienced seafloor alteration. Many of the vesicles have been filled by secondary minerals, such as zeolites. A usual alteration effect observed is epidotisation. The pillow

lavas have typical cooling features such as radial cracks that are observed throughout the lava outcrop. To the south, east and west the exposure is surrounded by the sea while to the north it borders the aforementioned Tertiary and Quaternary deposits, therefore the accurate positioning of Kassandra in the geotectonic zone framework of Greece is not straight forward.

In Sithonia the situation differs from that in Kassandra. The peninsula is dominated by the Eocene Sithonia Granite (Christofides et al 1990, 2001, de Wet at al 1989). In the north and central part of the peninsula the granite is in contact with the Triassic to Middle Jurassic Svoula flysch (Kaufmann et. al, 1976). Towards the south the Svoula flysch gives way to a series of mafic greenschists that are in contact with the Sithonia granite to their north-east. These greenschists are composed of epidote-chlorite, actinolite-epidote-chlorite and hornblende-epidote varieties with minor quantities of quartz. South of these greenschists we find a series of Upper Jurassic fossiliferous limestones. Southwest of these limestones, on Kelyfos Island, the areas of Zakonisi, Pounta, Toroni-Porto Koufo and the tip of Cape Laemos (see Fig. 1), there is a series of mafic magmatic rocks. On Kelyfos Island and at the coast of Toroni village (Byzantine Castle locality) typical pillow lava outcrops are extremely well preserved. In the Pounta area the mafic rocks consist of dykes and lavas flows. The dykes form a sheeted complex with screens of dioritic differentiates. A typical section of the upper part of a magma chamber outcrops further to the south, at the very tip of Sithonia (Cape Laemos). It consists of very coarse- to medium-grained (vari-textured) leucocratic Hbl-gabbros intruded by hornblendite veins; at the very top of the section the gabbroic rocks are in tectonic contact to mafic phyllites, and on top of the latter we see Upper Jurassic limestones. Examining closely these mafic phyllites we find pockets of less deformed material that from field observation can be assumed that they have masic composition. These phyllites were probably once part of the ophiolite that has been deformed due to the thrusting of the limestones.

In this chapter special emphasis will be placed on whole-rock major- and trace-element chemistry as well as on Rb-Sr and Sm-Nd isotopic data of the ophiolitic outcrops of the southern Chalkidiki peninsula described above. The geochronological data will be kneaded together with the geochemical data in order to estimate the geotectonic evolution of the ophiolite in relation with the surrounding rocks.

## 6.2 Mineralogy

The primary mineralogical assemblage observed in the lavas and dykes is plagioclase + clinopyroxene. From the primary mineralogical assamblage only relics of clinopyroxene mineral crystals has been partially preserved fresh; plagioclase and possibly olivine occur as pseudomorphs after secondary minerals. Altered plagioclase, clinopyroxene, orthopyroxene and hornblende are the only minerals observed in the cumulate rocks from Metamorphosis area. Secondary minerals are albite, actinolite, chlorite, epidote ± sphene, ± magnetite.
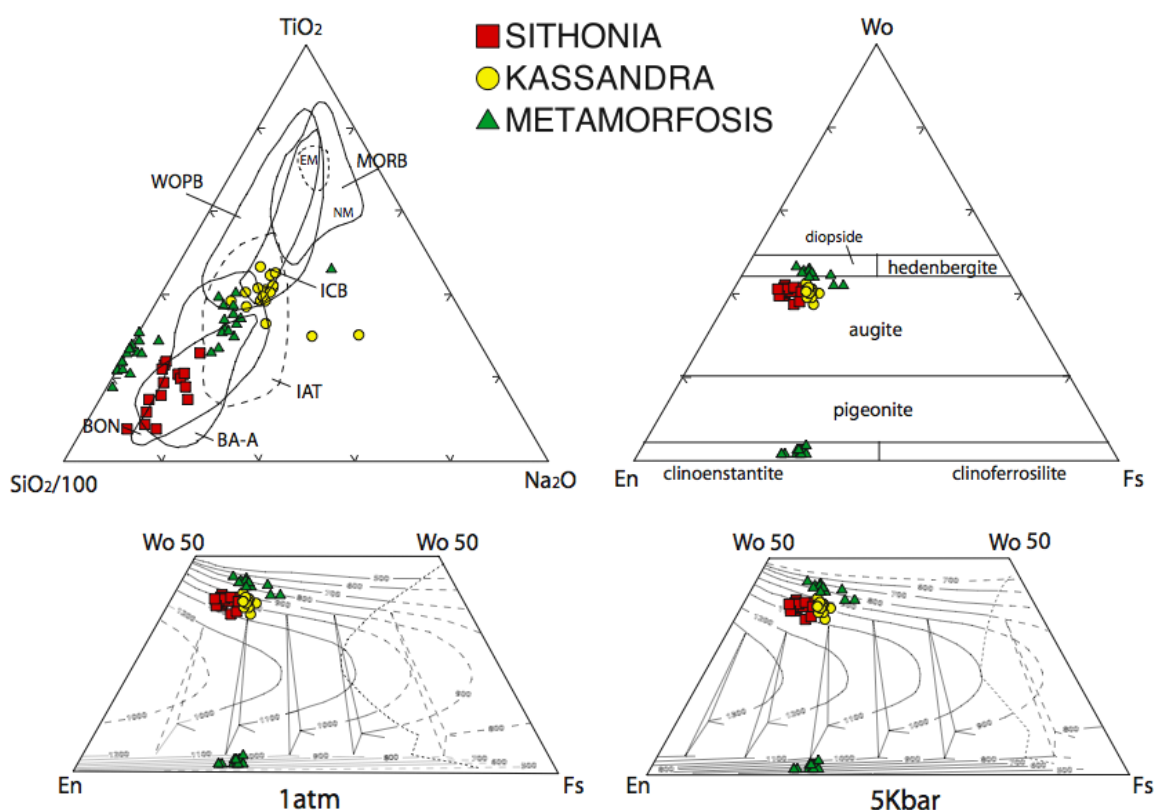
**Fig. 2.** Tectonic discrimination trianglular diagram for pyroxenes. ( fields after Beccaluva 1989). Classification triangle of pyroxenes (after Morimoto 1988) and a part of it with the isotherms proposed by Lindslay (1983). MORB: Mid-ocean rifdge basalts, WOPB: Within oceanic plate basalts, ICB: island-arc tholeiites, IAT: Island-arc tholeiites, BA-A: basaltic andesites and andesites, BON: boninites.

The clinopyroxenes (Cpx) have typical augite compositions (Fig. 2). The cpx from Sithonia have average composition $En_{49}Fs_{11.5}Wo_{39.5}$ whereas the cpx from Kassandra have $En_{44}Fs_{16}Wo_{40}$. The cpx from thecumulates from Metamorphosis are $En_{41}Fs_{16}Wo_{43}$. The orthoyroxenes (Opx) from Metamorphosis are $En_{66.5}Fs_{32.5}Wo_{1.5}$. The augites appear to have been altered to actinolite, chlorite and in some cases to calcite. The plagioclases have lost almost all of their Ca and have been altered to albite. Their average albite content is now $Ab_{96}$. The plagioclases also appear in some cases kaolinized and saussuritised.

Examining the position of the cpx plots relative to the isotherms as they have estimated from Lindslay (1983), we see that the cpx from Kassandra plot along higher T($^{o}$C) isotherms than the cpx from Sithonia. The pyroxenes from the Motamorphosis cumulate yield temperatures of around 800$^{o}$C.

Initial tectonomagmatic discrimination based on $TiO_2/SiO_2/Na_2O$ proposed scheme by Beccaluva (1989) classifiy the pyroxenes from Sithonia Kassandra and Metamorphosis as supra-subduction zone pyroxenes (Fig.2).

## 6.3 Geochemistry

### 6.3.1 Major and trace elements

The samples from both Sithonia and Kassandra have high LOI values that range from moderate (2 wt.wt%) to extremely high values (14 wt.wt%), suggesting that high amounts of hydrous minerals, like chlorite and actinolite, have been developed in the mineralogical assemblage of these rocks most probably during alteration. This implies that the major-element chemistry might have been distorted during this alteration event.
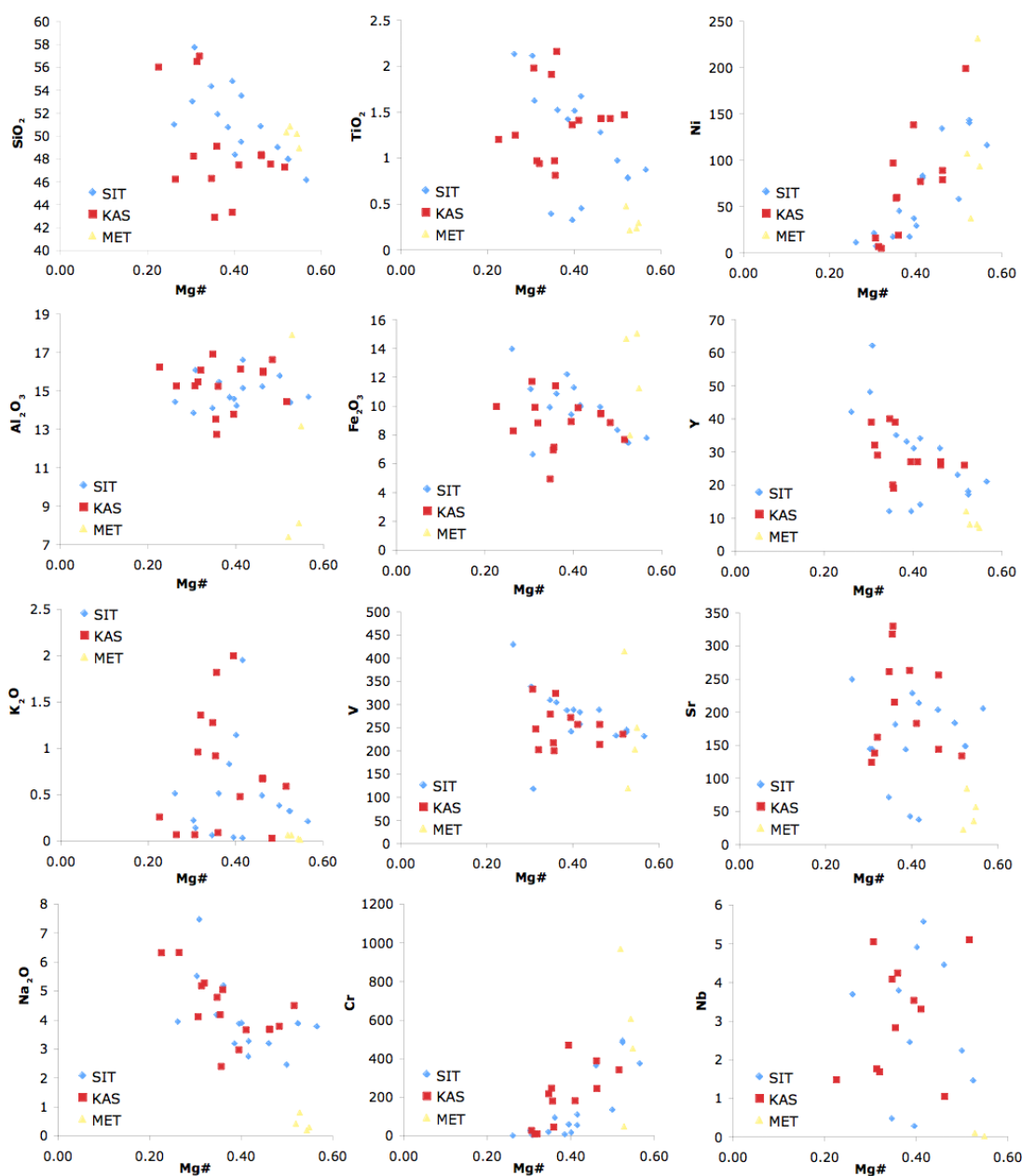


**Fig. 3.** Element versus Mg# for the mafic and acidic samples from the Sithonia and Kassandra ophiolite the nearby mafic cummualtes of the Metamorphosis area.

In Fig. 3 itis visible that the there is an irregular correlation of the mafor and trace elements towards Mg#. This can be interpreted as a result of the mobilization of elements due to alteration. For this reason we will try to examine the possible effects of the alteration using an alteration index such as Zr (Appendix F.). Examining the behaviour of the elements against the alteration index we see that the samples from Sithonia (SIT) are less affected by alteration than the samples from Kassandra (KAS). The major-element chemistry of both areas, however, appears to have been distorted with the exception of $TiO_2$, which seems to be relatively undisturbed. The concentration of the transitional metals seems to have been modified. Vanadium can be relied on but with precautions. Samples with low Zr have elevated V concentrations and do not follow the general trend. SIT samples show good correlations between trace elements and Zr. Ba, Sr and Rb are generally affected by alteration while the remainder of the elements seem to follow two different trends. As a final choice, the elements Zr, Y, REE, Hf, Ta and Th will be used for the petrogenetic investigations.

Examining the variation of the elements against Zr for Kassandra we see that they show two different trends. This is best seen in the Th vs. Zr variation diagram where two distinct and well-defined trends are formed. One trend follows the general trend shown by the Sithonia samples whereas the other corresponds to lower Th concentrations for the same Zr concentration. Closer examination of the diagrams of the other elements verifies this behaviour of the Kassandra samples. It is not clear at this point whether this reflects a primary feature of the magma or whether it is related to the alteration processes. This feature will be examined thoroughly in the following paragraphs.
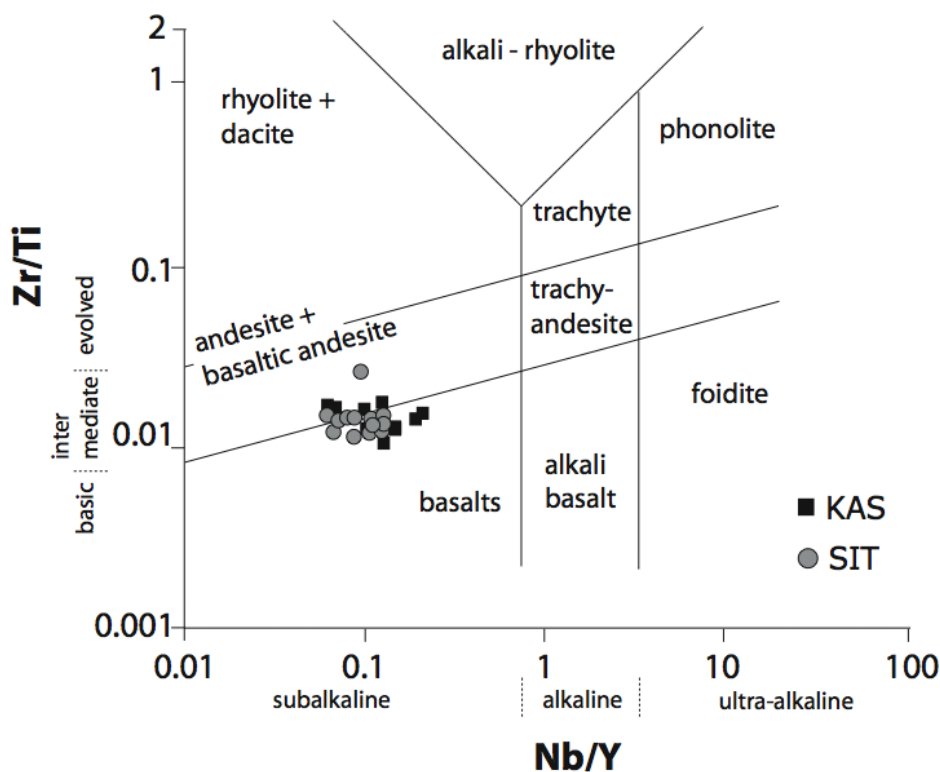


**Fig. 4.** Zr/Ti versus Nb/Y for the volcanic samples from the Kassandra and Sithonia ophiolites. (after Winchester and Floyd (1977) revised after Pearce et al 1996)

As discussed earlier, alteration played an important role in the redistribution of the major elements and in certain cases in that of the trace elements of the samples. Therefore only relatively immobile elements will be used to classify the samples. Using the Zr/Ti ratio plotted against the Nb/Y ratio (Fig. 4, after Winchester and Floyd 1977, revised after Pearce et al. 1996), the samples are classified as subalkalic basalts to basaltic andesites and andesites.
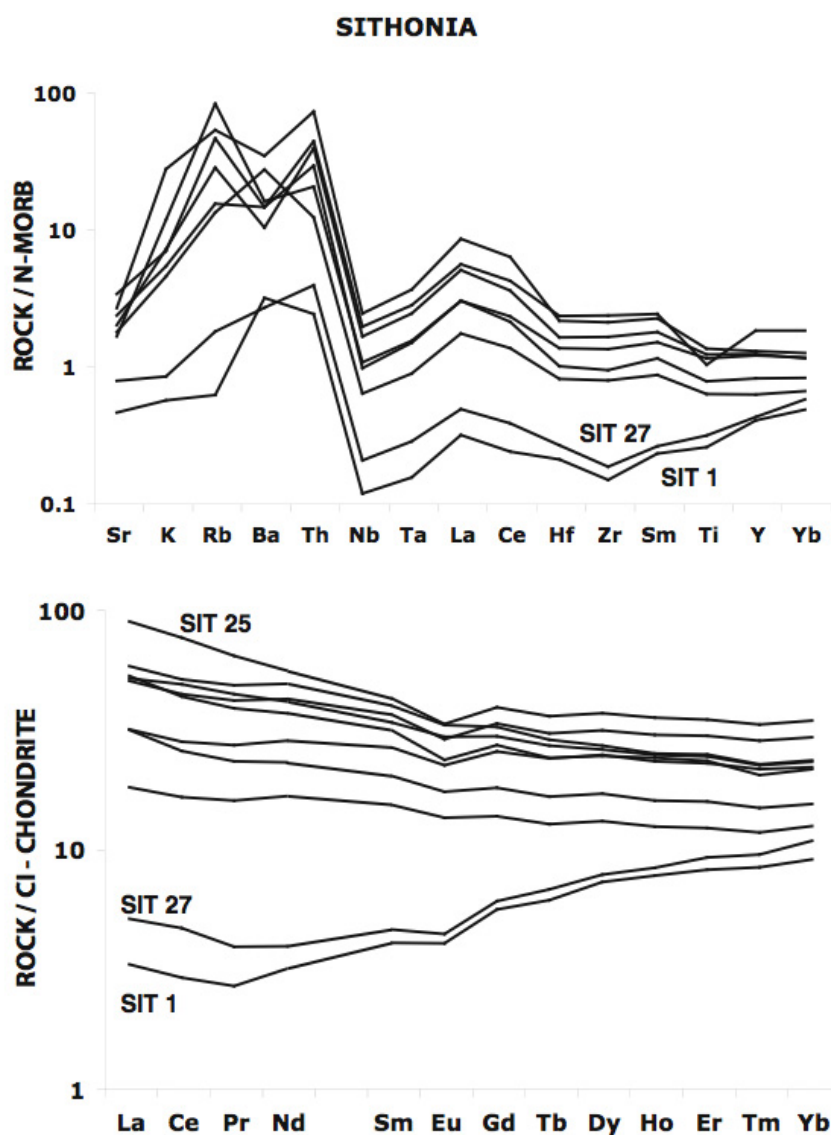


**Fig. 5. N**ormalised to C1 chondrite REE diagrams for the Sithonia samples. Normalised to N-MORB multielement "spiderdiagramms" for the same samples. Normalising values for N-MORB are from Pearce (1982, 1983) and C1 after and from McDonough and Sun (1995).

The Sithonia samples have $SiO_2$ contents between 46.12 and 57.72wt%, $TiO_2$ between 0.32 and 2.13wt%, MgO between 2.67 and 9.12wt% and total $Fe_2O_3$ between 6.63 and 13.94wt%. The Zr content of this group is between 10 and 170 ppm, Y values are between 11 and 50 ppm, V is between 117 and 429 ppm and Nb between 0.27 and 5.57 ppm. They are variably enriched in LILE as seen on N-MORB normalised multi-element diagrams (Fig. 5). The concentration of Th is especially high in all samples. The N-MORB normalised patterns display negative Nb anomalies and a characteristic hump in LILE, La and Ce. The normalised Nb/Yb ratio is equal to or higher than unity pointing towards a non-depleted source. Moreover, the negative anomaly in Nb and Ta in conjunction with the minor negative anomaly in Ti point towards equilibrium with residual rutile indicating the presence of a subduction-zone component (fluids and/or melts in equilibrium with eclogite-facies).
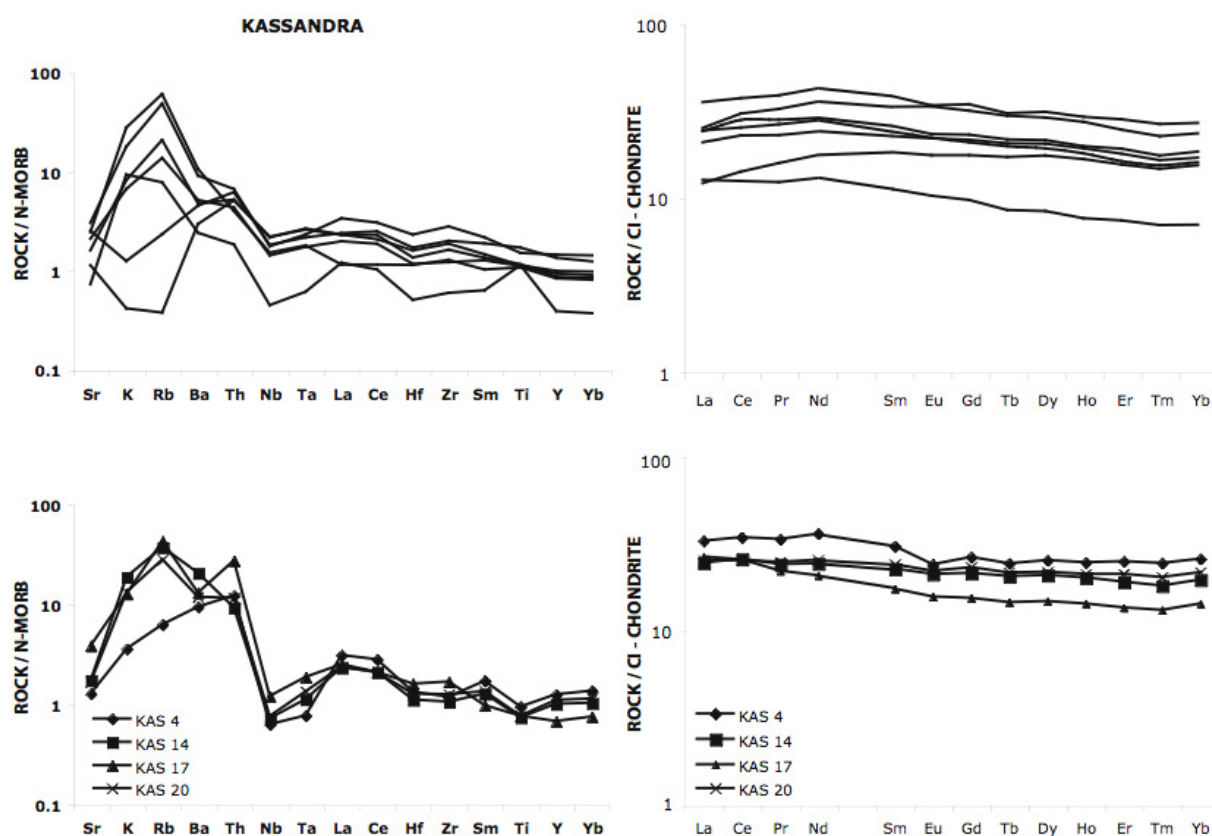


**Fig. 6.** **N**ormalised to C1 chondrite REE diagrams for the two groups of Kassandra samples. Normalised to N-MORB multielement "spiderdiagramms" for the same samples. Normalising values for N-MORB are from Pearce (1982 and 1983) and C1 after and from McDonough and Sun (1995).

Chondrite-normalised patterns for these rocks show enrichment in the LREE, negative Eu anomalies and moderately flat HREE patterns. The shape of the HREE patterns suggests that garnet was absent in the source region of the Sithonia basalts thus shallow melting, above the grt-lherzolite stability field is suggested. Sample SIT 25 (see Fig. 5) shows the strongest LREE enrichment and the most fractionated HREE patterns compared to the other Sithonia samples suggesting either that it was formed in deeper parts of the mantle from a more enriched source or that its source had experienced a larger modification from an enriched component. The normalised La/Yb ratio of this sample is 3.8, which is much higher than that of the other samples. This value is higher than the value for E-MORB (1.8; McDonough and Sun, 1995) but smaller than the value for OIB (11.64; McDonough and Sun, 1995) and the global subducted sediment (7.09; Plank and Langmuir, 1998). Two samples from Sithonia, namely SIT1 and SIT27 have very depleted patterns compared to N-MORB and the rest of the samples. The patterns of these samples are enriched in LILE, they have negative Nb anomalies followed by a positive anomaly in La and a negative one in Zr. Th is also enriched. There is a depletion trend of the HSFE from Yb to Nb suggesting that these samples have been derived from a quite depleted source. The chondrite-normalised REE patterns of these samples are characterised by LREE/HREE<1 and are much more depleted in all REE relative to the rest of the samples. The LREEs and MREEs form U-shaped patterns strongly resembling boninite patterns. There is also a negative Eu anomaly, suggesting either plagioclase fractionation or selective addition of LREE only.

The samples from Kassandra have $SiO_2$ contents between 38.3 and 56.99wt%, $TiO_2$ between 0.81 and 2.16wt%, MgO between 2.62 and 11.71wt% and total $Fe_2O_3$ between 4.94 and 11.71wt%. The Zr content of this group is between 44 and 207 ppm, Y values are between 10 and 40 ppm and V is between 200 and 333 ppm. The common characteristic of the KAS samples is the enrichment in LILE. The N-MORB normalized multi-element diagrams for the Kassandra samples can be separated into two groups based on the Th enrichment, Nb anomaly and the shape of the HSFE patterns (Fig. 6). The majority of the samples is only slightly enriched in Th and exhibits only a minor Nb anomaly.

The HSFE patterns are generally smooth and sub-parallel to the N-MORB line. Four samples form a second group that shows N-MORB normalised patterns similar to those of the Sithonia samples. In this group we discern the typical La-Ce hump of the Sithonia samples as well as the high enrichment in Th and the negative Nb anomaly. Contrary, however, to the uniform shape of the REE patterns of the Sithonia samples, the Kassandra rocks have variable shape of the REE patterns (Fig. 6). The normalised LREE are enriched relative to the HREE but the normalised La/Nd ratio is lower than 1 except for the samples that resemble Sithonia and have $(La/Nd)_n > 1$. Certain samples (e.g. KAS 9 and KAS10) show REE patterns typical of N-MORB. The HREE patterns are generally flat to slightly negatively fractionated. There is no evidence for garnet in the source region of these samples; the slight enrichment in the LREE and MREE over the HREE suggests a non-depleted magma source. The Kassandra samples have only minor to non existent Eu anomalies.

## 6.3.2 Sr and Nd isotopes

The Sr and Nd isotope data for the Sithonia and Kassandra ophiolites are presented in appendix E. The Nd initial ratios as well as the initial $\varepsilon_{Nd}$ values are calculated at 160 Ma as deduced from the geochronological investigation, which will be discussed along with the data from the other ophiolites in chapter 6. The chondritic values used for the calculation of the $\varepsilon_{Nd}$ are: $^{143}Nd/^{144}Nd=0.512638$ and $^{147}Sm/^{144}Nd=0.196700$.
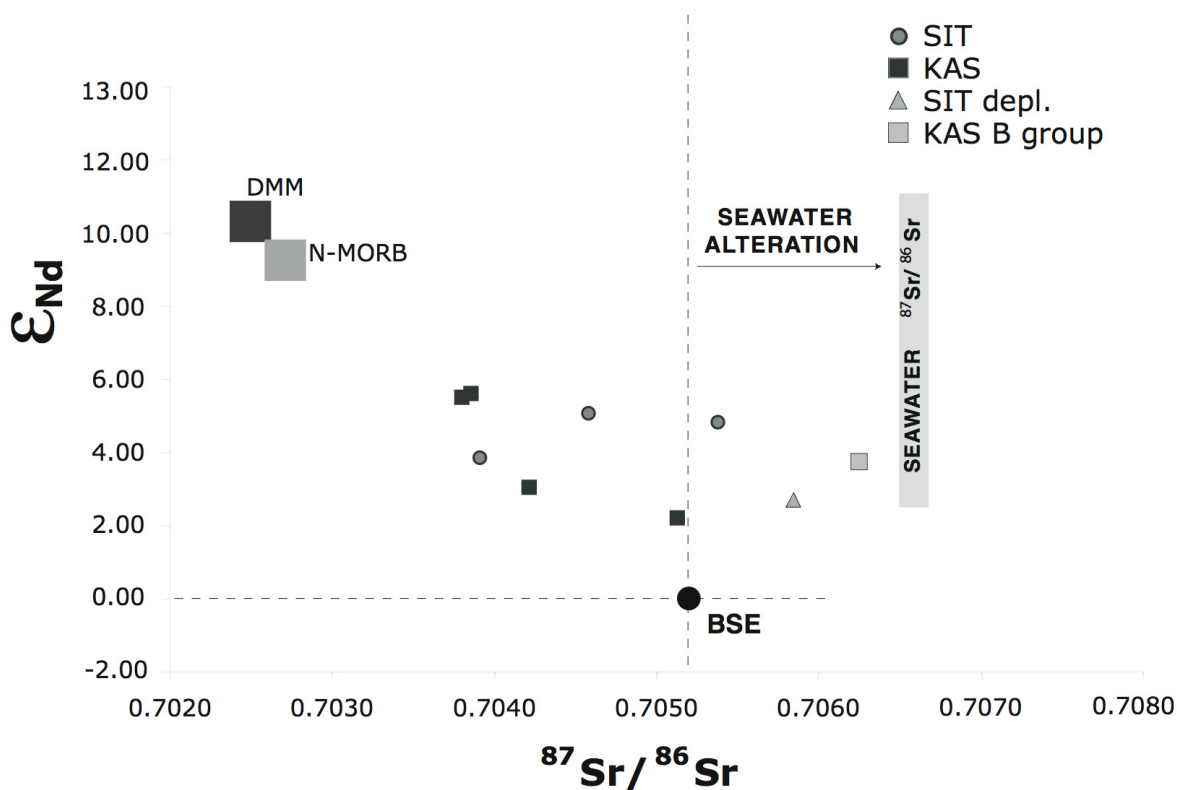


**Fig. 7.** $^{143}Nd/^{144}Nd$ versus $^{87}Sr/^{86}Sr$ plot for the Sthonia and Kassandra samples. Values for subducted sediment, DMM, and N-MORB as in Fig. 5, chapter 4. Seawater values are from Burke et. al (1982).

The samples from Kassandra have Nd concentrations between 1.66 and 5.66 ppm and Sm concentrations between 5.93 and 19.37 ppm respectively. The calculated $\varepsilon_{Nd(160)}$ values are higher than the $\varepsilon_{Nd\,(CHUR)}$ and range between 2.23 and 5.6 (Fig. 7). The samples from Kassandra have measured $^{87}Sr/^{86}Sr$ ratios between 0.704129 and 0.706727 (Fig. 7). The Sithonia samples have Nd concentrations between 1.43 and 22.09 ppm and Sm concentrations between 0.59 and 6.21 ppm respectively. The samples from Sithonia have measured $^{87}Sr/^{86}Sr$ ratios between 0.704231 and 0.707501. The calculated $\varepsilon_{Nd(160)}$ values for Sithonia values and range between 2.59 and 5.03. The

measured $^{87}Sr/^{86}Sr$ ratios for these samples are between 0.704231 and 0.707501. Sample SIT 1 which shows typically boninitic multi-element and REE patterns also shows the lowest calculated $\varepsilon_{Nd(160)}$ values.

The calculated $\varepsilon_{Nd(160)}$ values for all samples are positive suggesting that these rocks were derived from a mantle source. They are however much lower than the values for mid-ocean ridge basalts. This, in conjunction with the higher $^{87}Sr/^{86}Sr$ ratios of the samples compared to N-MORB implies that the source region of the Chalkidiki ophiolitic rocks has been modified by a component rich in radiogenic Sr and non-radiogenic Nd. The $^{87}Sr/^{86}Sr$ values measured for these samples are high with respect to the Nd isotopes. This can be explained by the effect of hydrothermal circulation of seawater.
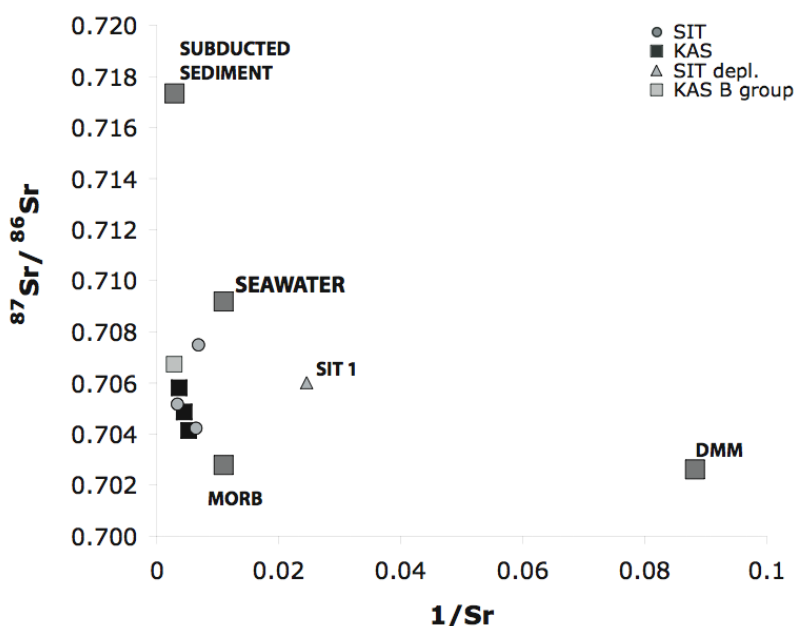


**Fig. 8.** $^{87}Sr/^{86}Sr$ vs 1/Sr plot for the Sthonia and Kassandra samples. Values for subducted sediment, DMM, and N-MORB as in Fig. 5, chapter 4. Seawater values are from Palmer and Edmond 1989.

In Fig. 7, the samples from Kassandra and most of the samples from Sithonia form a narrow trend towards higher $^{87}Sr/^{86}Sr$ for decreasing reciprocal Sr. Sample SIT 1 is displaced towards much higher 1/Sr values while its calculated $\varepsilon_{Nd(160)}$ value is the second lowest of all Chalkidiki samples interpreted as having a different evolution compared to its counterparts. The samples from both Sithonia and Kassandra have higher elemental and radiogenic Sr abundances than N-MORB forming a trendline towards subducted sediment and seawater, suggesting that these rocks were derived from a source modified by a subduction component and also have been affected by hydrothermal circulation of seawater.

### 6.3.3 Melting Model

For Sithonia and Kassandra the melting modelling will be also based on compatible vs incompatible element non-modal equilibrium modelling of Ti and Cr (Fig. 8) as described in the methods paragraph and used in the other ophiolites. As starting source we choose a fertile spinel lherzolite, since there is no evidence of melting in the garnet lherzolite field. Examining the behaviour of the samples on this diagram we can infer that the rocks from Kasandra require medium to low degrees of melting (10-5wt%) of a fertile spinel lherzolite. On the other hand the sample form Sithonia would require higher degrees of melting than the samples from Kassandra that would span between 10 and 20wt% of the a similar like in the Kassandra case source. Two of the samples from Sithonia namely SIT1 and SIT27 require a much more depleted source than the rest of the samples, which is in agreement with the C1 normalised REE patterns. A DSL that has melted around 10-15 % would explain the genesis of these two samples. A subset of three samples from Kassandra ophiolites plot within the rocks from Sithonia, suggesting similar source characteristics and similar melting properties.
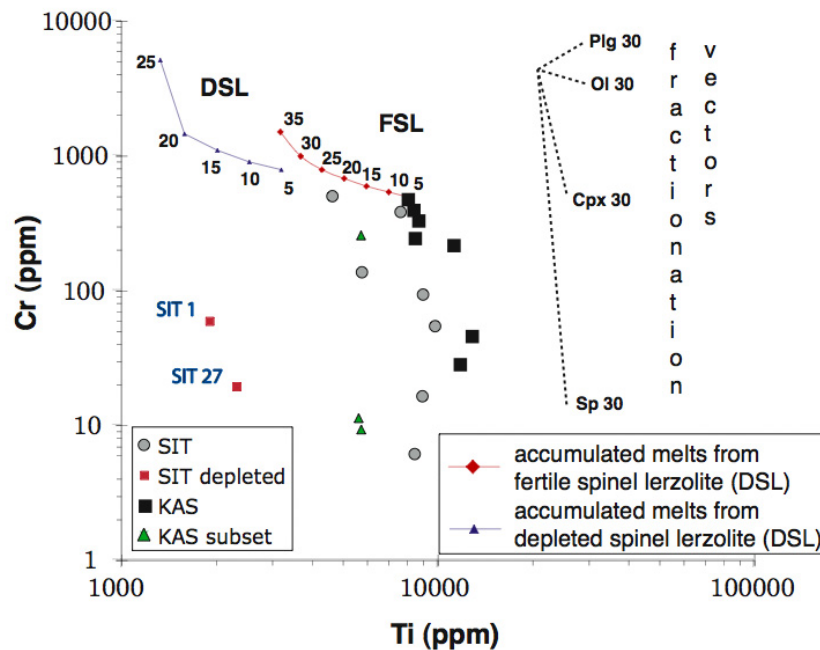


**Fig. 8.** Ti versus Cr diagram for the samples from Sithonia and Kassandra ophiolites. Disussion in text.

## 6.4 Tectonomagmatic discrimination

As discussed earlier in this chapter, the concentrations of many major and some important trace elements have been mobilized during alteration. To achieve effective tectonomagmatic

discrimination of the KAS and SIT samples we will make use of elements that remained as undisturbed as possible. These elements are: Ti, Y, V, Zr, Nb, Th, Hf and Ta, Sm, Yb

Pearce at al. (1979) used the ratios of Ti/Y and Nb/Y as a discriminating feature between within-plate magmatism and magmatism related to island arcs and mid-ocean ridges. None of the samples from Sithonia and Kassandra plot in the field of within-plate basalts; instead, they fall in the field of MORB and also in the field shared by both MORB and volcanic-arc basalts (Fig. 9). All Thessaloniki samples are tholeiitic and only a minor amount of them are slightly transitional to alkalic.
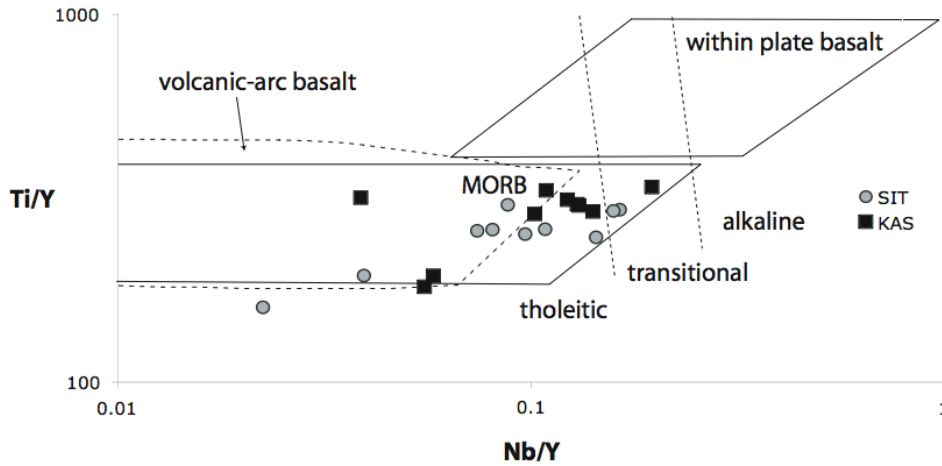


**Fig. 9.** Ti/Y versus Nb/Y plot for the samples from the Kassandra and Sithonia ophiolites (after Pearce et al, 1979)
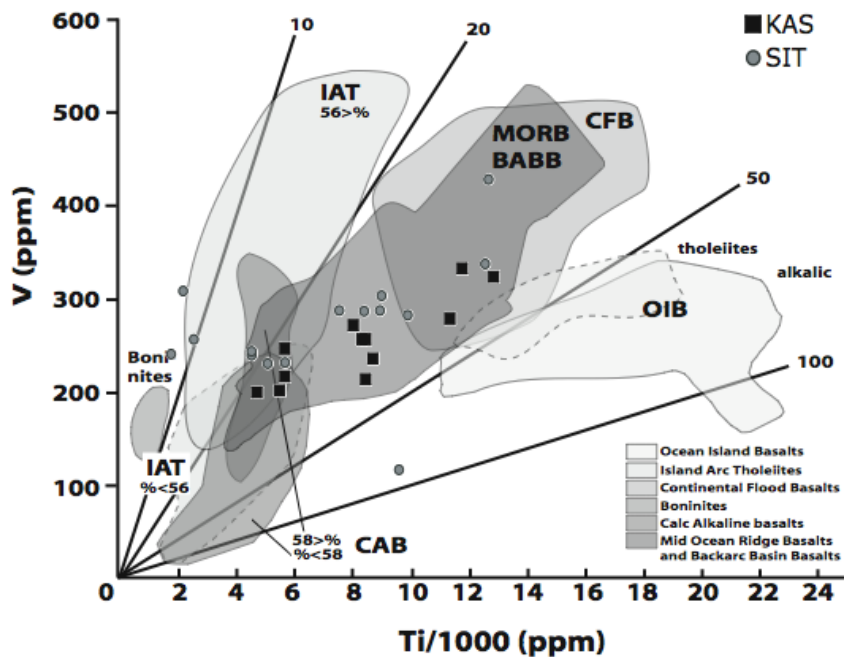


**Fig. 10.** Ti versus V diagram showing samples from the Sithonia and Kasandra ophiolite. (after Shervais 1981)

On the Ti vs. V discrimination diagram proposed by Shervais (1981), all samples from Kassandra plot in the field of mid-ocean ridge basalts (MORB) and back-arc basin basalts (BABB) (Fig. 10). The samples from Sithonia also plot in the same field with the exception of three samples that plot in the field of IAT. Among the latter, two samples are REE depleted, while the third has not been analysed for REE.

Meschede (1989) used the elements Zr, Y, and Nb to discriminate between WPB and other enriched basalts from N-MORB and IA volcanics. Nb can be used to investigate the mantle differentiation processes and the Zr/Nb ratio can be used as a proxy for enrichment or depletion processes in the mantle (Meschede, 1989 and references therein), while the Zr/Y ratio can be used to investigate long-term source heterogeneities thus distinguish between basalts erupted in within-plate settings and basalts erupted in mid-ocean ridges and volcanic arcs (Pearce and Cann, 1979 and references therein). Plotting the Sithonia samples on the Zr/4-Nb*2-Y diagram (Fig. 11) we observe that they fall within the field of N-MORB and volcanic-arc basalts, suggesting that there is no within-plate enriched mantle signature in the source of these rocks. The two samples that plot outside the discriminant fields are those with REE- depleted patters. The samples from Kassandra plot in the fields of volcanic-arc and N-MOR basalts.
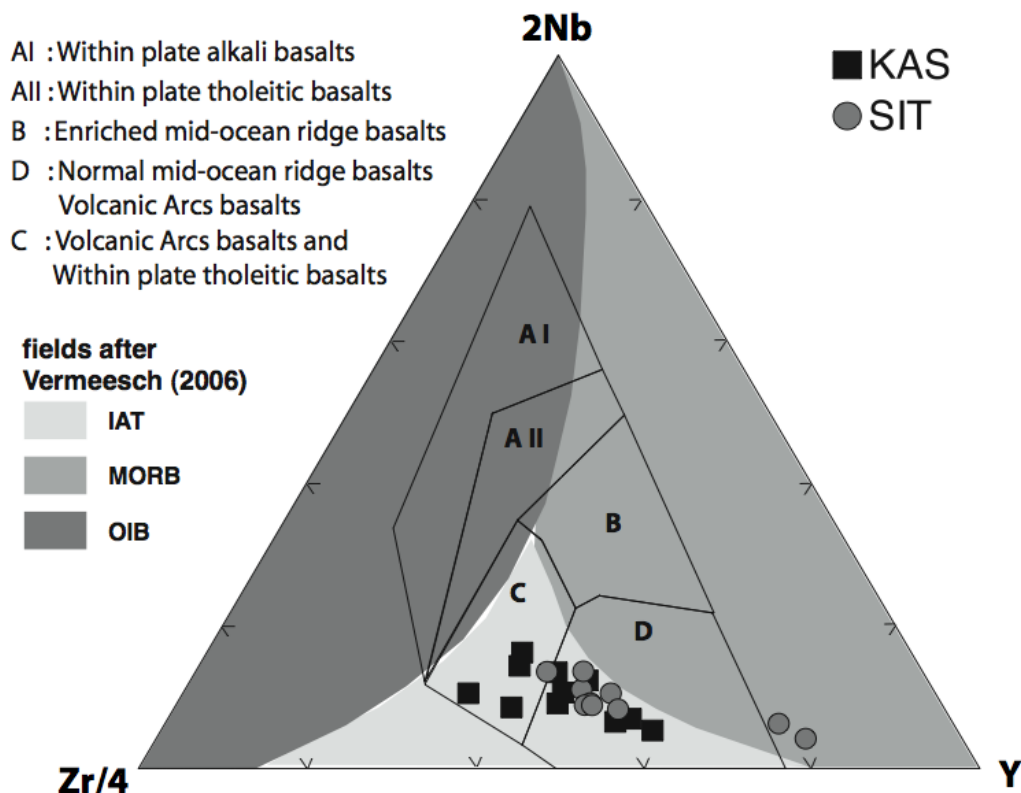


**Fig. 11.** Zr/4-Nb*2-Y diagram showing the classification of samples from the Sthonia and Kassandra ophiolites. (after Meschede 1986)

Based on the Hf/3-Th-Ta discrimination diagram proposed by Wood (1980), the samples from Sithonia plot in the field of rocks coming from destructive plate margins forming a trend towards higher Th concentrations (Fig. 12). The samples from Kassandra form two groups: one group exhibits the same behaviour as the Sithonia samples whereas the other straddles the boundary between the fields for N-MORB and destructive-plate margin basalts. The samples from the second group have distinctly higher Ta values implying that these rocks were derived from a source similar to or somewhat more depleted than that of N-MORB.
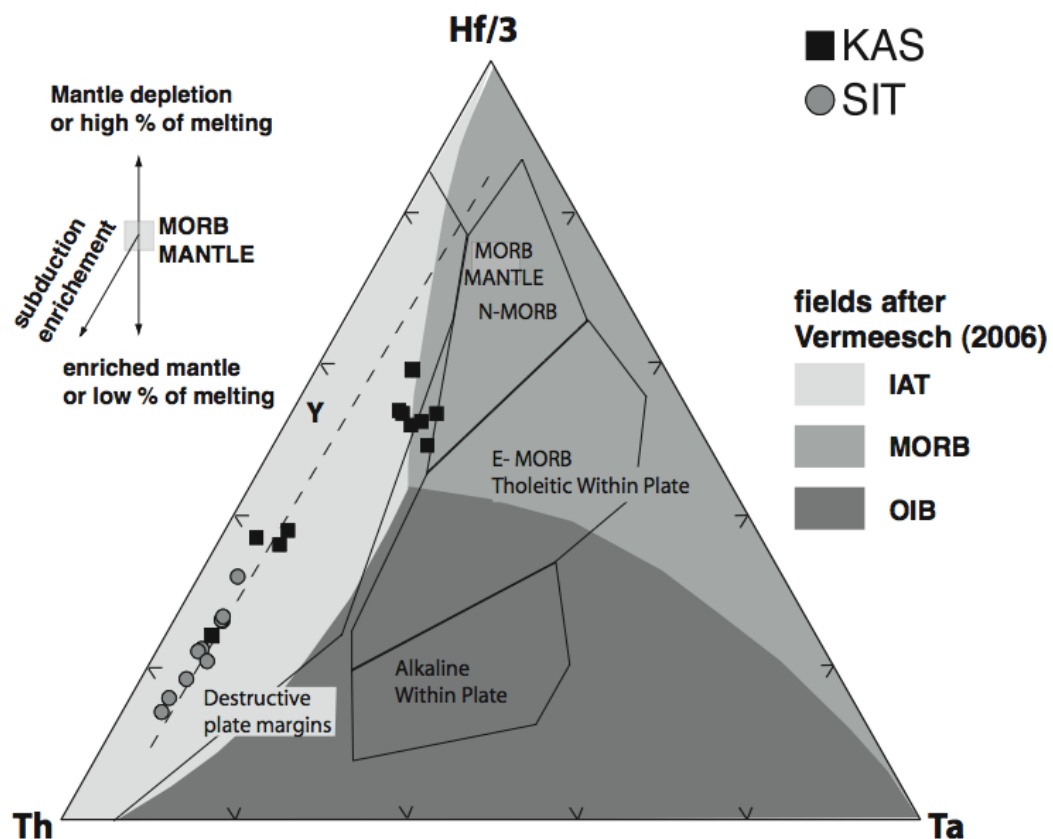


**Fig. 12.** Hf/3-Th-Ta diagram showing the distribution of samples from the Sthonia and Kassandra ophiolites. (after Wood 1980)

To summarize, there is no evidence of a within-plate or plume influence on the tectonic setting of the Sithonia and Kassandra ophiolitic volcanics. According to the Zr/4-Nb*2-Y and Ti-V discrimination diagrams, the samples from Sithonia show an N-MORB to BABB signature. But when we incorporate Th, a typical subduction-zone tracer, and Ta, a proxy of the source enrichment, the

samples plot in the field of basalts from destructive plate margins. The REE-depleted samples are displaced to lower $TiO_2$ contents and plot in the field of island-arc tholeiites. The samples from Kassandra display the same behaviour as the samples form Sithonia on the Zr/4-Nb*2-Y and Ti-V diagrams. However, they behave differently on the Hf/3-Th-Ta diagram. On this diagram the Kassandra samples are separated into two groups. One group plots in the field of basalts from destructive plate margins following the trend set by the Sithonia samples, while the other shows a transitional N-MORB - destructive-plate margin basalt character. A possible scenario that could incorporate the observed diversity of geochemical affinities in a single tectonic setting could be the evolution of a back-arc basin.

# 6.5 Identification of the subduction related enrichment processes

Examining the covariation between Th and Ta we see that the Sithonia samples as well as a small group of four samples from Kassandra are displaced from the mantle array towards higher Th/Yb values (see Fig. 13). Thorium addition has been interpreted by Pearce et. al. (1982) as the result of input from subduction-related processes. The remainder of the Kassandra samples show variable Ta/Yb ratios at nearly constant Th/Yb ratios. These samples plot slightly above the upper boundary of the MORB-OIB array in fig. 11, along a vector of Ta depletion towards the field of island-arc tholeiite and do not seem to have been affected by Th addition that has been observed for all other samples from this locality and Sithonia.
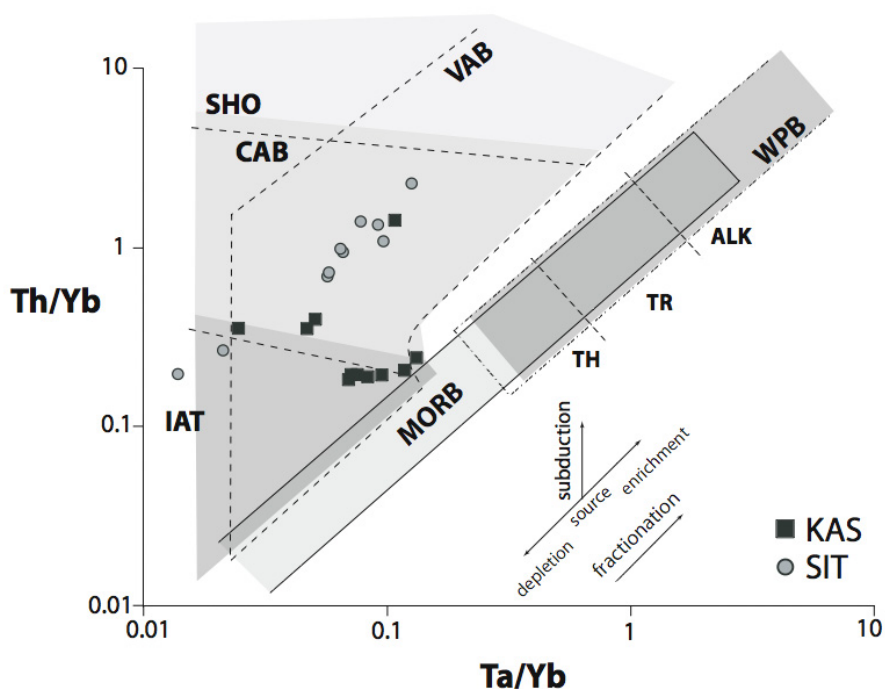


**Fig. 13.** Th/Yb versus Ta/Yb diagram for the samples from the Sthonia and Kassandra ophiolites. Fields after Pearce (1982)

Examining the covariation between Ba and Th we see that the samples from Kassandra form two groups of variable Ba/Yb values at nearly constant Th/Yb values (Fig. 14). This suggests that, in each group, enrichment in Ba has taken place without a concomitant enrichment in Th. The mobilization of Ba and other LILE can take place even at low temperatures in aqueous fluids while Th is mobilized at higher temperatures, thus greater depths, mainly in melts (Spandler at al. 2004 and references therein). The process of Ba enrichment has been interpreted by Pearce et al. (2005) as the effect of dehydration of the sedimentary cover of a subducting slab that takes place at shallow depths in a subduction zone. On the other hand, the samples from Sithonia have variable enrichment in Ba and Th and generally seem to follow a positive correlation vector between Ba/Yb and Th/Yb that can be ascribed to the addition of a component that was carrying both Th and Ba. This component is derived from melting sediments and has its origin at depths of 70-150 km where temperatures exceed 600°C as suggested by the addition of Th (Pearce et al. 2005, Spandler at al. 2004 and references therein).
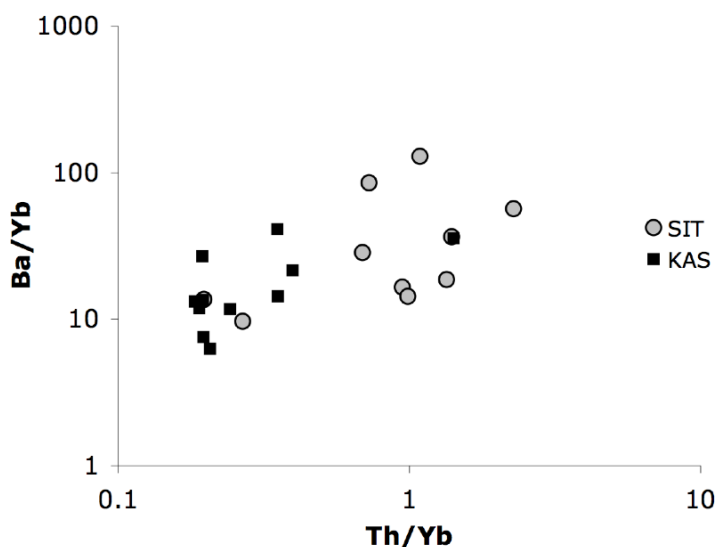


**Fig. 14.** Ba/Yb vs. Th/Yb plot for the samples from Sithonia and Kassandra.

The samples from Sithonia and the subset of four samples from Kassandra mentioned above show a positive correlation between Th/Yb and Nb/Yb ratios (Fig. 15) suggesting that the enrichment in Th and Nb is caused by the addition of silicate melts derived from the sedimentary cover of the subducted slab (Leat et al. 2005). The remainder of the Kassandra samples display variable Nb/Yb at nearly constant Th/Yb ratio values. If this increase in Nb is to be linked to enrichment processes

related to a subduction zone or the asthenosphere, there should be also an increase in Ba and Th. Since we can only notice an increase in Ba but not Th for these samples we can conclude that the reason for the increase in Nb is not related to subduction-zone enrichment processes and it must be sought in the source of these rocks. The Nb content of these samples is much less than that for OIB (~ 48 ppm) and E-MORB (~ 8.3 ppm) and approximates that for N-MORB (~2.33 ppm). We can therefore assume that this enrichment trend of Nb is caused by different degrees of melting of the source rather than enrichment from an Nb-enriched source.
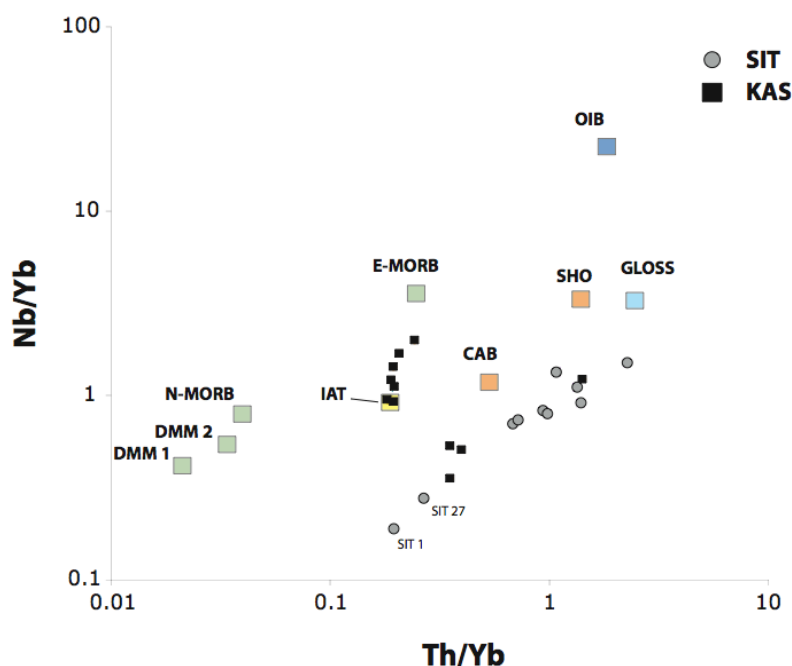


**Fig. 15.** Plot of Nb/Yb vs. Th/Yb for the samples from the Sithonia and Kassandra ophiolites.

# 6.6 Geochronology

Farther afield, to the southeast of Thessaloniki, we collected samples from the Metamorphosis area and the Sithonia peninsula, both belonging to the greater Chalkidiki peninsula. A very coarse-grained diorite (pegmatitic hornblende-gabbro) from the top part of the magma chamber and a medium-grained quartz-diorite (described as plagiogranite dyke by Gauthier, (1982)) from the high-level gabbroic section were sampled, respectively. The errors shown on the diagramms are at 1σ.

## 6.6.1 Metamorphosis area

Zircons separates from the Metamorphosis sample are idiomorphic to subidiomorphic with grain size ranging from 180 to 360µm. Some zircons have well-developed oscillatory zoning, whereas others not so well (Fig. 16). U/Th was measured between 0.19-0.47 excluding any metamorphic origin. Four zircons were initially dated using the $^{207}$Pb/$^{206}$Pb single-zircon evaporation (Kober 1986,1987) method and yielded an age of 159.8±3.8 Ma (personal communication with Felix Himmerkus).
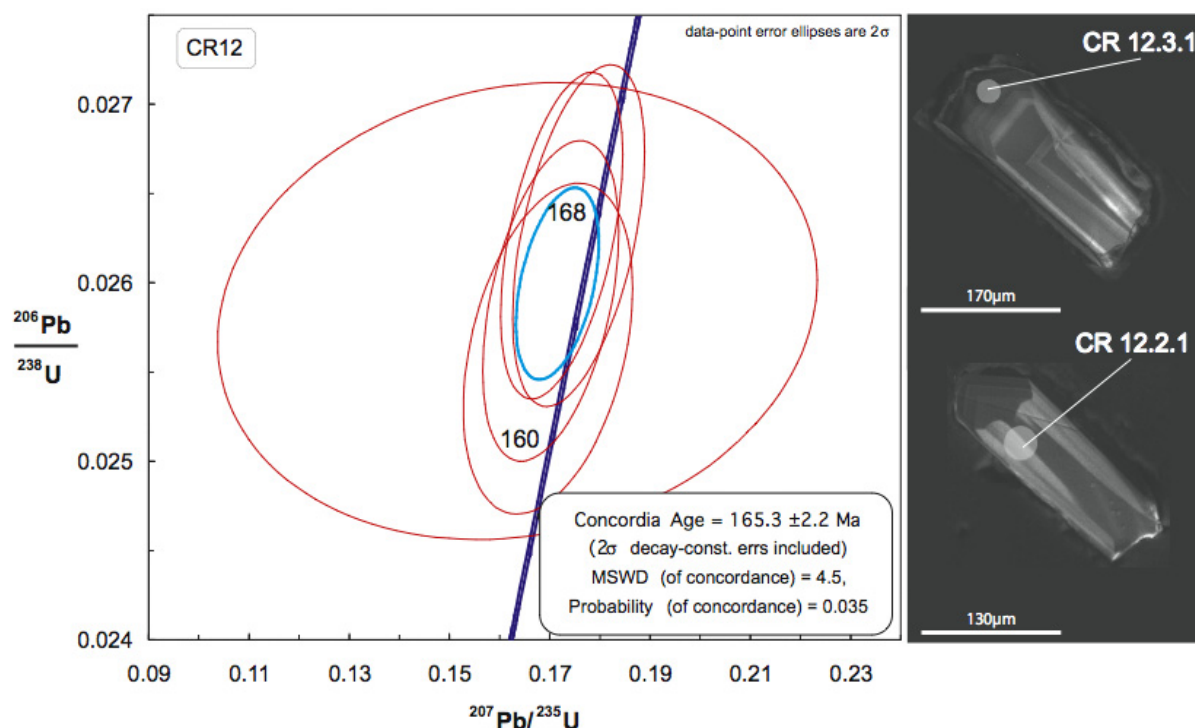


**Fig. 16.** Concordia diagram for the Metamorphosis pegmatitic hbl-gabbro and representative CL images of zircons. The whitish circles represent individual spot analyses by SHRIMP.

In order to verify this age we also measured some zircons by SHRIMP-II. Five spot on an equal number of zircons were analyzed. The zircons were concordant and yielded a concordia age of 165.3±2.2 Ma (MSWD=4.5; Fig. 16). There is a small difference in the ages obtained in the Metamorphosis and the age quoted by Mussalam and Jung (1986). The fact that do not anything aboutt he locality and the sample that is quoted by Mussalam an Jung cannot make the direct comparison possible.

## 6.6.2 Sithonia area

The zircons from the Sithonia diorite have mainly idiomorphic shape; only one crystal was found subidiomorphic with rounded corners. The grain size varies significantly between 65µm and 170 µm. Under cathodo-luminescence imaging the crystals reveal a restricted oscillatory zoning (Fig. 17). The crystals consist of a single domain and are dominated by homogeneous growth and only at the very rims it is possible to observe some zoning. The U/Th ratios for the zircons from sithonia are bwteen 0.67-1.01, typical of igneous zircnos.

A total of nine spot analyses on nine different zircon crystals were made. The measured zircons belong to a single age group and on a Terra-Wasserburg diagram conform to a non ancored line intersecting the concordia (Fig. 17) at a $^{238}$U/$^{206}$Pb average age of 160±1.2 Ma (MSWD=0.30). Both ages from the Chalkidiki bodies lie in the same geological period (Middle Jurrasic), but the diorite from Sithonia is slightly younger than the differenciate from Metamorphosis.
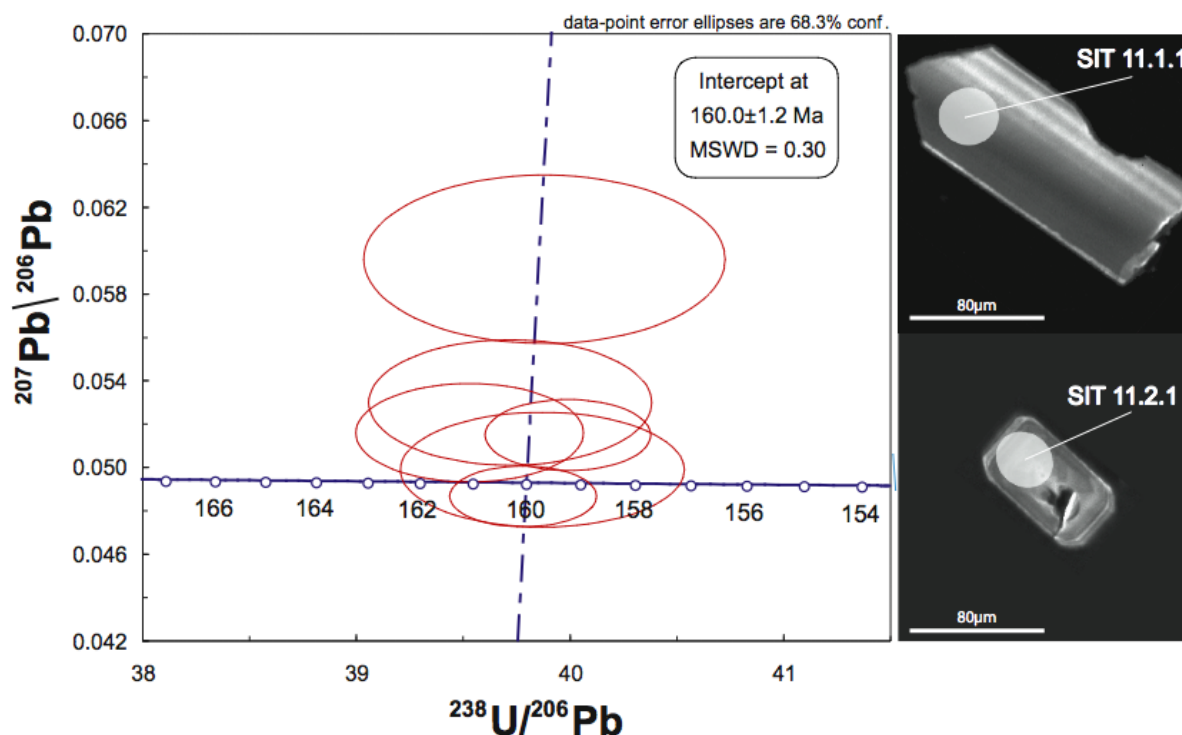


**Fig. 17.** Terra Wasserburg diagram for the Sithonia diorite and representative CL images of zircons. The whitish circles represent individual spot analyses by SHRIMP.

## 6.7 Summary and Conclusions

The mafic complexes that outcrop at the tips of the Kassandra and Sithonia Peninsulas, northern Greece, represent the extrusive, hypabyssal and upper magma chamber sections of an

ophiolite. Volcanic rocks and dykes area classified as basalts and basaltic andesites. The samples are altered to greenschist-facies metamorphic conditions. The primary mineralogical assemblage gave its position to chlorite, epidote, albite, titanite, actinolite and minor quartz. Only relics of clinopyroxene of augitic composition are preserved. In general Sithonia is less affected by alteration than Kassandra. The concentrations of the major elements, with the exception of $TiO_2$, are disturbed by alteration. Vanadium is generally undisturbed while the rest of the transitional metals are not. Rubidium and Sr seem to be in order for the Sithonia samples, whereas Ba shows signs of mobilization. Overall, elements such as Ti, Y, V, Zr, Nb, Th, Hf, Yb and Ta seem to be reliable and representative of the initial chemistry.

The samples from Sithonia have variably enriched LILE content in N-MORB normalised multielements diagrams. Thorium is enriched relative to the LILE and the rest of the HFSE, and there is a persistent negative Nb anomaly and a characteristic hump in La and Ce in all samples. The $(Nb/Yb)_N$ ratio is equal to or higher than one (except from two samples SIT1 and SIT27) pointing towards an enriched rather than a depleted source. Chondrite-normalised patterns show enrichment in LREE, a negative Eu anomaly and moderately flat HREE patterns suggesting that garnet was absent in the source thus shallow melting of the source above the garnet-lherzolite stability field. Two of the samples (SIT1 and SIT27) display much more depleted patterns than the rest of the Sithonia samples, testified by steep positive slopes from Yb to Nb and Nd to Yb in multi-element and REE profiles respectively. Their slightly U-shaped REE patterns strongly resemble those of boninites such as the ones erupted in the Arakapas Fault Belt of the Troodos ophiolite, Cyprus (Cameron, 1985).

The samples from Kassandra invariably show enrichment in LILE. On the basis of Th vs. Zr systematics they can be separated into two groups. One group (four samples) resembles Sithonia by having pronounced Th enrichment, negative Nb anomaly and similar HSFE patterns. The other group is only slightly enriched in Th and exhibits only a minor Nb anomaly. The HSFE patterns are generally smooth and subparallel to the N-MORB line. The samples have variable shape of the REE patterns. The LREE are enriched relative to the HREE but the La/Nd ratio is lower than 1 except for the samples of the group that resemble Sithonia that have La/Nd>1. Some of the samples show typical N-MORB shaped REE patterns. The HREE patterns are generally flat to slightly negatively sloping. There is no evidence of garnet in the source of these samples, and the slight enrichment in the LREE and MREE over the HREE suggests enrichment of the magma source. The Kassandra samples have only a minor to non-existent Eu anomaly.

The $\varepsilon_{Nd(160)}$ values of the samples from both ophiolites are positive and range from 2.2 to 5.6 suggesting that these rocks are mantle derived, while their source has been isotopically modified by an enriched component. The $^{87}Sr/^{86}Sr$ values are high (0.7041-0.7075) suggesting that these rocks have been affected by seawater alteration. Non modal equilibrium melting modelling of Ti and Cr suggests that Kasandra requires medium to low degrees of melting (10-5wt%) of a fertile spinel lherzolite while Sithonia would require higher degrees of melting between 10 and 20wt% of a FSL and

SIT1 and SIT27 require a much more depleted source than the rest namely a DSL that has melted around 10-15 %.

Tectonomagmatic discrimination classifies the Sithonia samples to MORB or BABB and as having been formed at destructive plate margins. Two samples from Sithonia are classified as IAT. On the Ti/V diagram (Shervais 1981) these two samples plot close to the boninite filed. A minor group of Kassandra samples share the same geochemical characteristics with Sithonia. The rest are classified as MORB or BABB and they are generally derived from more enriched sources. The best-fit scenario for the geotectonic setting of these samples is the evolution of back-arc basin magmatism. The Sithonia rocks seem to be more affected by subduction-zone derived contamination while the Kassandra samples show no to minor subduction-zone influence.

Fingerprinting the subduction component we see that the Sithonia samples and a minor population of the Kassandra samples have been affected by both silicate melts and aqueous fluids while the majority of the Kassandra samples have experienced only only Ba enrichment suggesting aqueous fluids.

It is evident from the geochemical data presented in this chapter that there are two geochemical signatures in the ophiolitic outcrops of Sithonia and Kassandra. The presence of geochemically similar rocks in both peninsulas implies that the evolution of both units should be tied in the same geotectonic scenario. In Sithonia, rocks were sampled from dykes intruding gabbros, from sheeted dyke exposures and from pillow lava and lava flow sections. The complete lack of MORB-like magmatism in these samples therefore suggests that Sithonia represents an early stage of back-arc basin development where the spreading centre is near the volcanic front (Fig. 17; see also Taylor & Martinez, 2003). In Kassandra, on the other hand, there is little evidence of arc-related material similar to that seen in Sithonia and the majority of samples show MORB-like chemistry with traces of subduction zone influence. It then follows that Kassandra magmatism ensued the formation of the arc-influenced back-arc magmatism of Sithonia.

There are two possible evolutionary scenarios for the evolution of both ophiolites based on the chemistry and the age constraints. Model A (Fig 18.) takes as fact that both Kassandra and Sitohnia ophiolites belong to same setting and can be fit to the evolutionary scenario of a supra-subduction zone setting that undergoes extension at 160 Ma where dynamically induced upwelling of asthenosphere that has been chemically modified by aqueous fluids and melts from the subducting slab leads to the formation of the Sithonia ophiolite, resulting in a geotectonic setting similar to that of the early stages of evolution of a back-arc basin due to the eastward subduction of the Vardar ocean beneath the Paikon arc. During a later stage, continuing mantle corner flow and convection caused further extension of the newly formed Sithonia crust thus nearly effectively decoupling the back-arc spreading centre from the volcanic front; fertile MORB-like magma flows into the back-arc region, from the asthenosphere, leading to the formation of the Kassandra ophiolite.

Model B (Fig. 19) takes as basis the fact that Sithonia and Kassandra ophiolites have formed in different settings and in different time. The catalyst in that scenario is the presence of boninite-like rocks in Sithonia (SIT1, SIT 27) and the similar age of this ophiolite to the Chortiatis Magmatic suite (sample L9, discussed in chapter 5). The evolution of these ophiolites would then be linked in an indirect way. In this case there is the opening of a back-arc basin as described in the previous paragraph at 167-165Ma as deduced by the age of the Metamorphosis diorite and the rest of the ophiolites. In that case the early stages of the opening are represented by the subset of the Kassandra samples that resemble the chemistry of the Sithonia ophiolite. Later stage of the evolution of this back-arc basin would result in the formation of the Kassandra  ophiolite similarly as described in the previous nodel. Then around 160Ma this back-arc basin would subduct eastwards contributing to the evolution of the Chortiatis magmatic suite and resulting in the formation of a fore-arc (implied by the presence of the boninites) mafic crust that leads to the genesis of the Sithonia ophiolite.

See next page
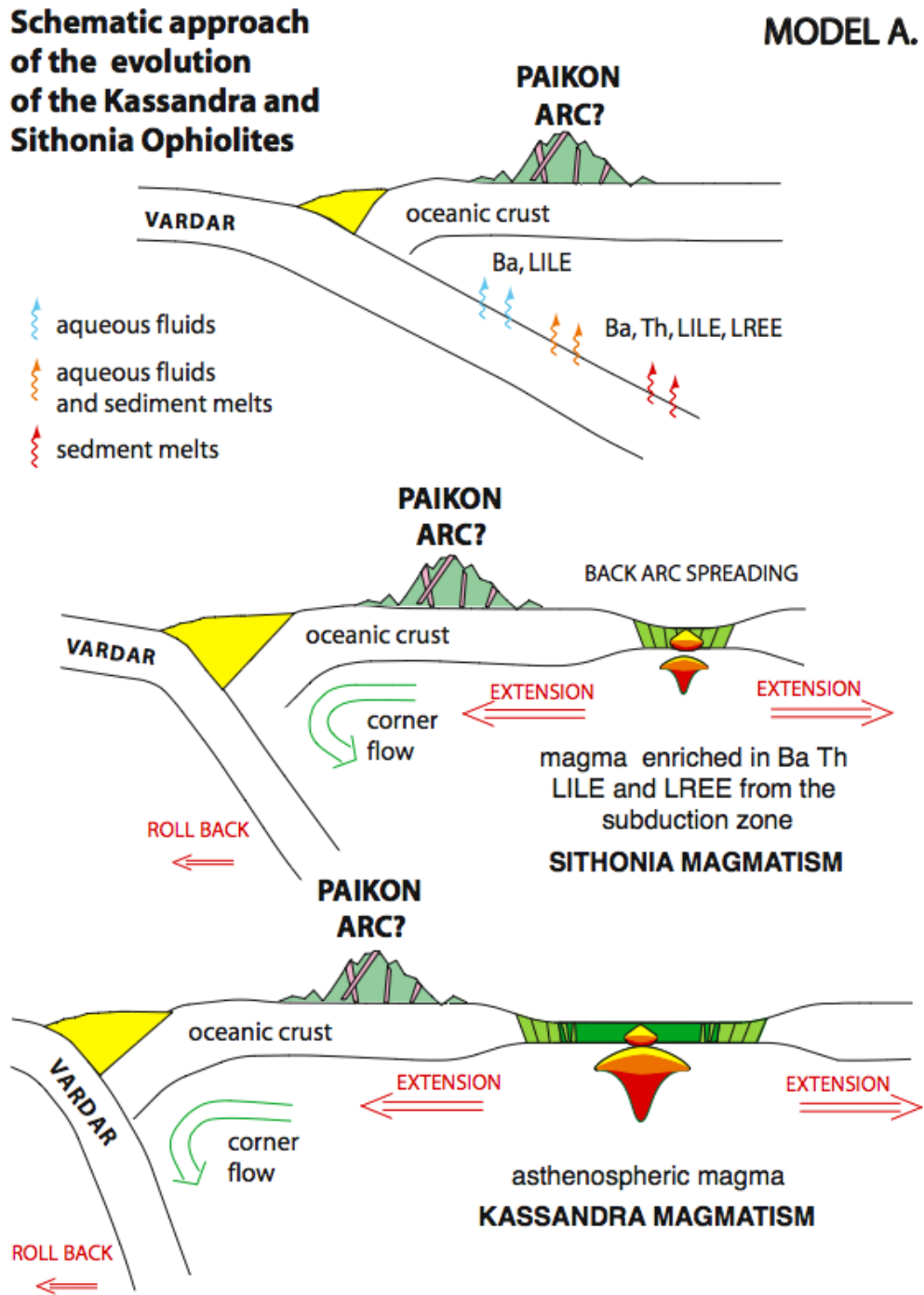
**Fig. 18**. Schematic approach of the evolution of the Kassandra-Sithonia ophiolite according to model A.
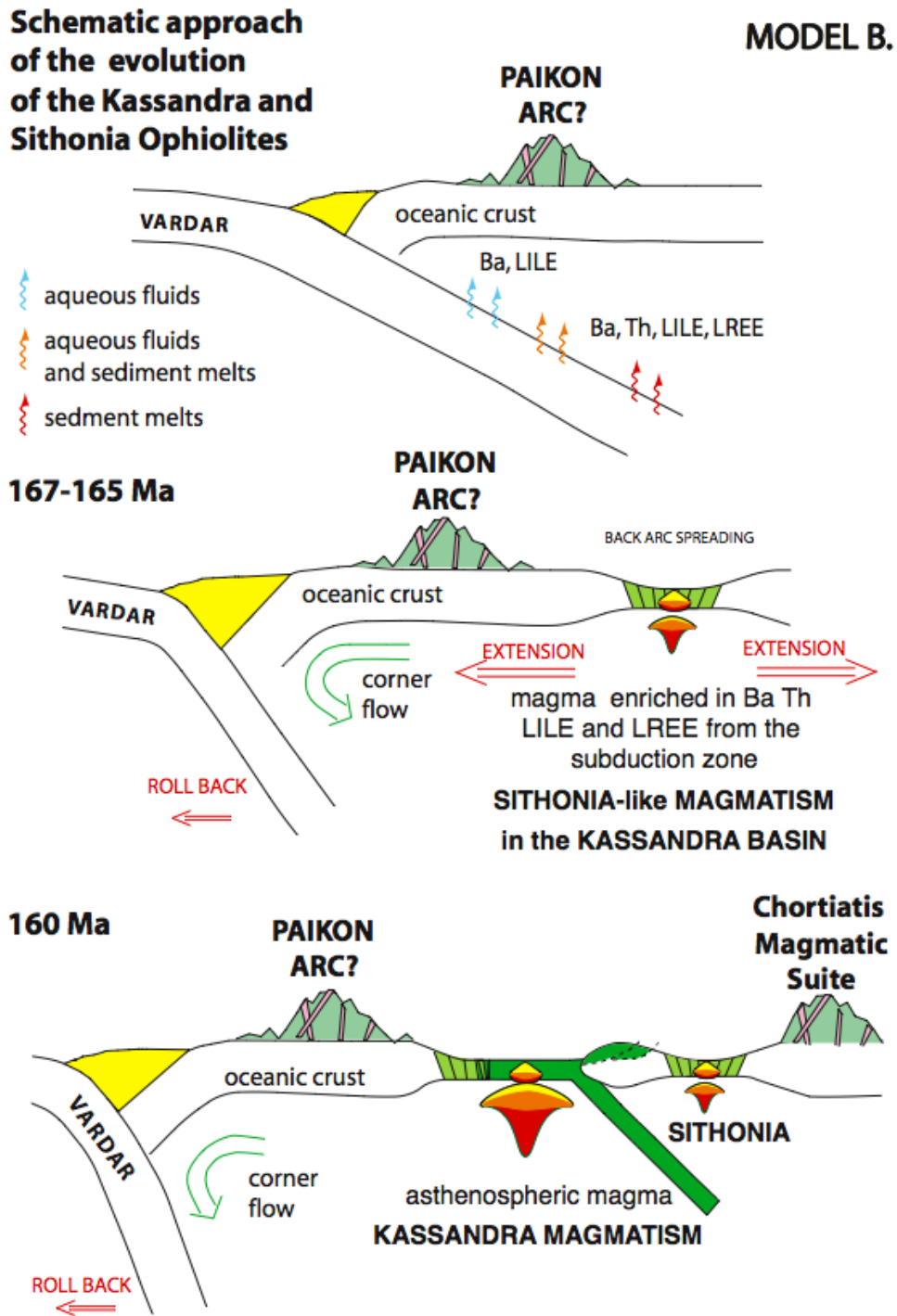
**Fig. 19**. Schematic approach of the evolution of the Kassandra-Sithonia ophiolite according to model B.

# Chapter 7. Synthesis and Conclusions

## 7.1 Introduction

As we have discussed before, the main problem that one was encountering in this area when it went to compare these ophiolites together was the lack or even absence of adequate geochemical data. Most of the comparisons made so far were based on major and a few trace element geochemical data coupled with lithological and stratigraphic criteria. There has not been an attempt so far to examine the isotopic characteristics of these ophiolites.  There are two main schools of thought concerning the occurrence of these ophiolites in this area. One considers these ophiolitc outcrops as olistholiths that have been transported to this position in eastward-westward direction from the Rhodope Massif (e.g. Ricou et al 1998, Michard et al. 1998). The second considers these bodies as in-situ or para-in-situ (e.g Haenel-Remy and Bebien 1985, Mussalam and Jung 1986, Jung and Mussalam 1985, Mussalam 1991, Tsikouras 1998) ophiolites that have evolved in ensialic marginal basins during the same time and due to broadly the same event.

In the following paragraphs we will try to examine the genetic relations of these ophiolites making a geochemical approach, try to understand their evolution and test if these ophiolites can be explained within the frame of the same geotectonic scheme. This we will be attempted by presenting a comparative study of these ophiolites examining the major, trace, isotopic as well as geochronological properties of these complexes

## 7.2 Geochemistry
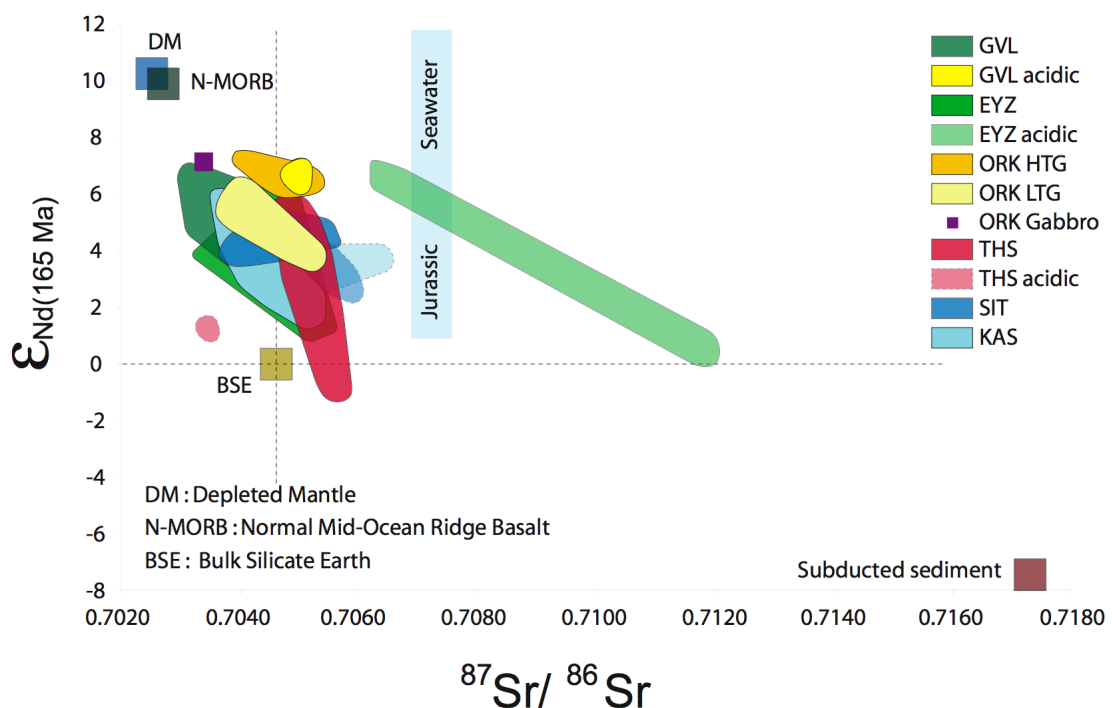


**Fig. 1**. $\varepsilon_{Nd}$ versus $^{87}Sr/^{86}Sr$ for the samples from all the ophiolitic complexes

As we have seen in the previous paragraphs the ophiolitic complexes are built of rocks that have formed in a supra-subduction zone setting. Examining the isotopic characteristics of these ophiolites we see that all of them consist of samples that have positive $\varepsilon_{Nd}$ values (Fig. 1). In the majority of the cases they are significantly lower than the values of DM and N-MORB. This observation suggests that all these rocks have derived from a mantle source that was modified by an enriched component. If we introduce the isotopic composition of the subducted sediment (Plank and Langmuir 1998) we can see that the isotopic composition of all the ophiolitic rocks could be the result of a mixing between this and a mantle source.

Another common feature of these ophiolites is the similar features they exhibit when examining Ce and Yb. In detail, Ce has a positive correlation to the Yb (Fig. 2). This, according to Hawkesworth et. al (1993), is rather a feature of the primitive island arcs in contrast to more mature arcs that have an increase of Ce for constant Yb.
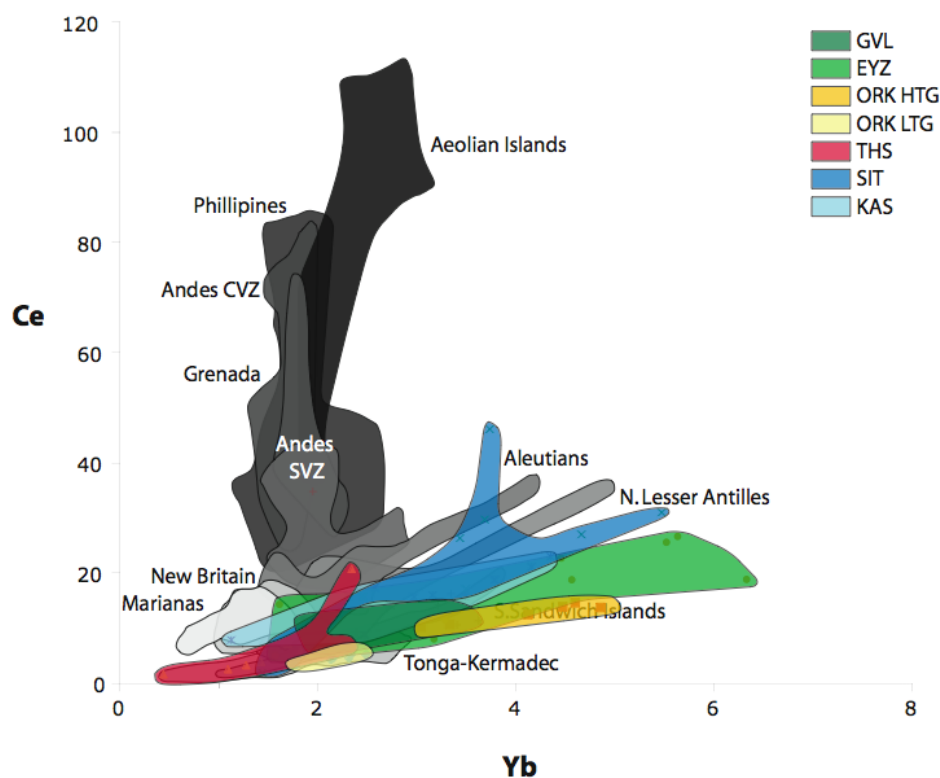


**Fig. 2**. Ce versus Yb for the samples from all the investigated ophiolitic complexes. Fields after Hawksworth (1993). Note that the ophiolites plot along with other complexes from intra-oceanic settings.

Examining the Hf/3-Th-Ta diagram (Fig. 3, Wood 1980) we see that EYZ and KAS samples plot between the destructive plate margins field and the field of N-MORB. The samples from the HTG from Oraeokastro plot also between the file of N-MORB and the arc field but for lower Ta and higher Hf concentrations than the previous. The HTG forms a trend

towards Th expanding into the field of the arc related rocks. The rest of the samples plot entirely in the field of the mafic rocks from destructive plate margins and form parallel trends of variable Th and Hf proportions at a fairly constant Ta that cluster and overlap together tightly.
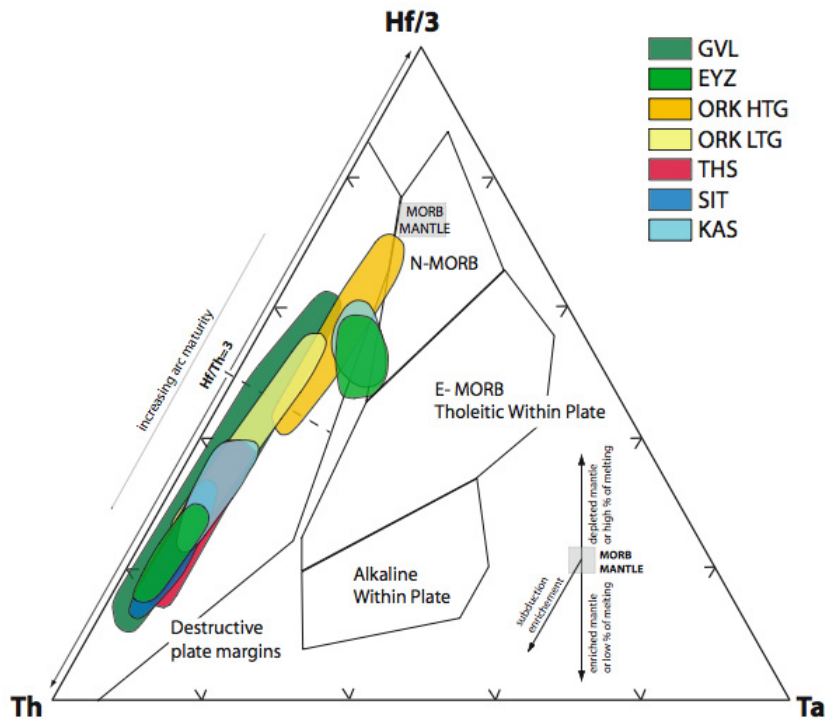
**Fig. 3.** Hf/3-Th-Ta diagram showing the samples from all the ophiolites. (after Wood 1980)
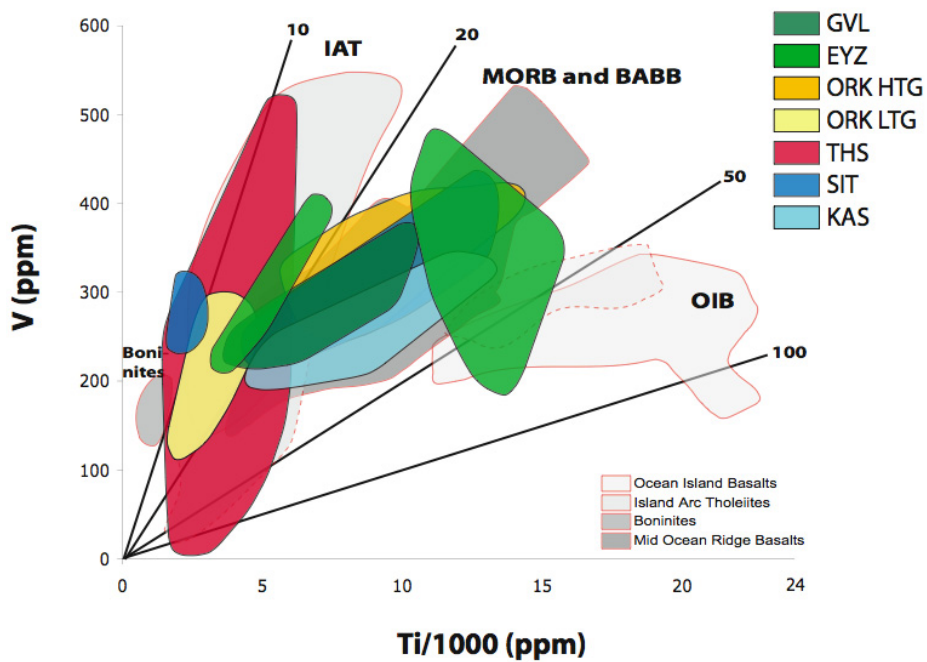
**Fig. 4.** Ti versus V diagram showing the mafic samples from the investigated ophiolitic complexes Fields after Shervais (1982).

THS, the LTG and a small fraction of the SIT and EYZ samples are classified as IAT in the Ti/V discrimination diagram proposed by (Fig. 4, Shervais 1982). The rest of the samples namely the HTG, GVL, KAS, and the majority of the SIT and EYZ form positive correlation trends of the V and the Ti. These are parallel to each other trends starting from the intersection area between the IAT and BABB field into the MORB and BABB field.

All the samples from the ophiolites that we have investigated are displaced in variable degrees from the mantle array towards higher Th/Yb values, as seen on the Th/Yb versus Ta/Yb diagram (Fig. 6, fields are from Pearce et al. (1982). This, according to the interpretation of Pearce et al. (1982) can be explained by the addition of Th from a subduction related component that Pearce et al. (2005) later termed as the Th-Ba component (Fig. 5). Pearce related that to a component released from the deeper parts of the subducted slab. According to Spandler et al. (2004) the depth at which Th can be released from the subducted slab through a aqueous fluid is between 70-150km were temperatures exceed 600°C. Johnson & Plank (1999) defined experimentally the sediment solidus to >750°C and suggested that Th can be mobilised for conditions above the solidus by a silicate melt. This means that all the sources of the samples have "seen contamination" from a silicate melt that was released in depths between 70-150 km and temperatures above 750°C.
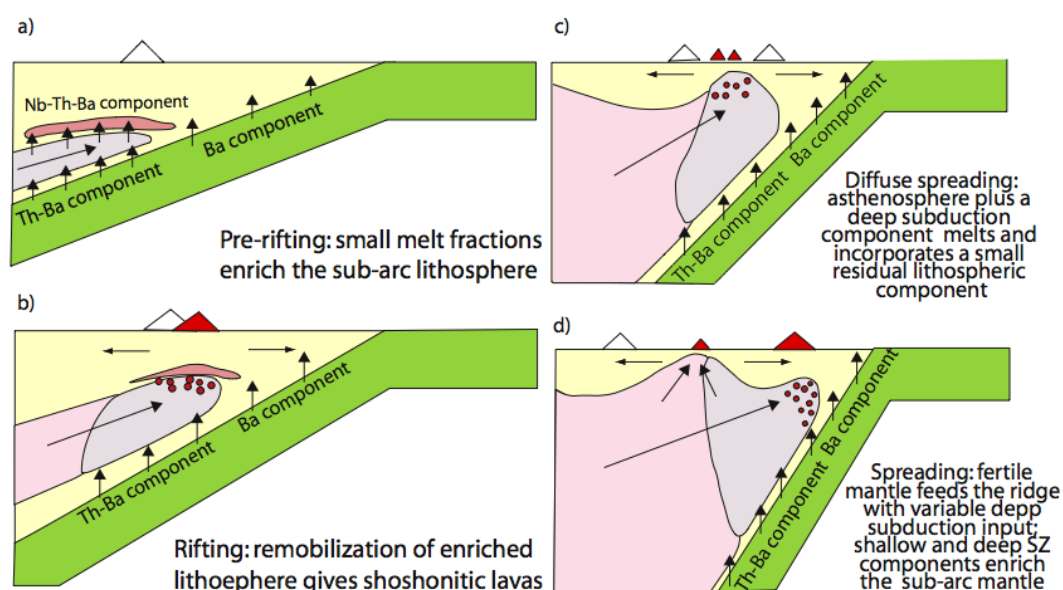


**Fig. 5.** Schematic approach of a subduction zone, the relative position of the subducted slab enriched components and the succession of the magmatic and geotectonic events. After Pearce (2005).

The LTG and the HTG form two vertical vectors of increasing Th/Yb in constant Ta/Yb. The majority of the samples from KAS and EYZ follow horizontal to the Ta/Yb vectors from the border of the mantle array into the IAT field, for almost constant Th/Yb. THS, SIT, as

well as a minor group of rocks from KAS and EYZ have similar positive correlation of the Th/Yb and the Ta/Yb ratios. These rocks form sub-parallel to the mantle array trends, which are very close and overlap each other.
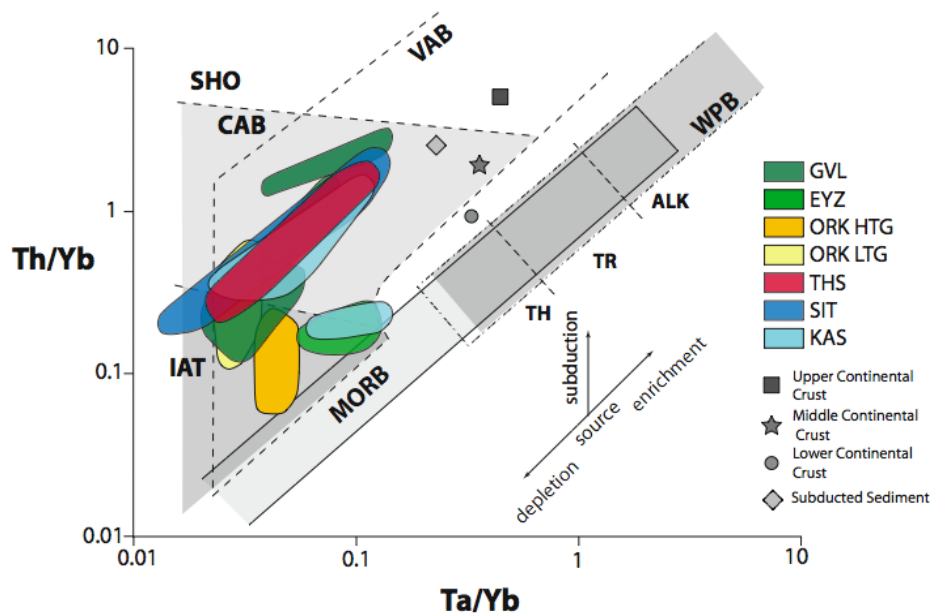


**Fig. 6.** Th/Yb versus Ta/Yb diagram for samples from all the ophiolites. (after Pearce 1982). CAB: continental arc basalts, VAB: volcanic arc basalts, IAT: island arc tholeiites, SHO: shoshonites. WPB:within plate basalts, MORB:mid-ocean ridge basalt.

## 7.2.1 Resumé of geochemistry

In the previous paragraph we presented a comparison of the geochemical and isotopic characteristics of the ophiolites. In this paragraph we will try to bind all the pieces of information together and propose a geotectonic evolution scenario for these ophiolites.
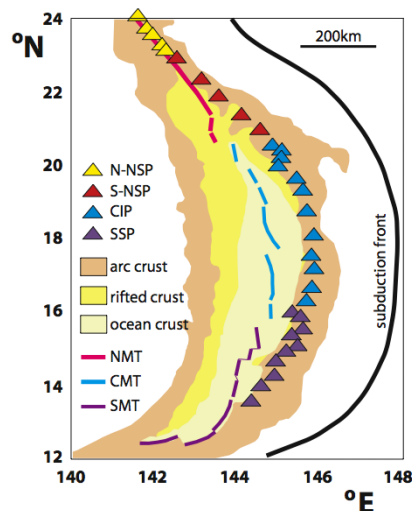


**Fig. 7.** Sketch of the Marianas arc-back-arc sytem and the positon of the arc, rifted and oceanic crust. The triangles represent the volcanic centers. The lines represent the spreading. After Pearce et al. (2005).

113

As we have seen the ophiolites are related together by the fact that their chemistry bears all the typical characteristics we meet in supra-subduction zone setting magmatism. Examining the chemistry of these ophiolites we see that they consist of rocks that have geochemical characteristics between transitional between MORB and an IAT. The similarities that they have in their isotopic characteristics as well as the similar grouped behaviour in discrimination diagrams and in the incompatible element ratios suggest that these complexes might have formed in the same mega-setting. The question now is to understand the mechanism or the setting where all these complexes have been formed and found together.
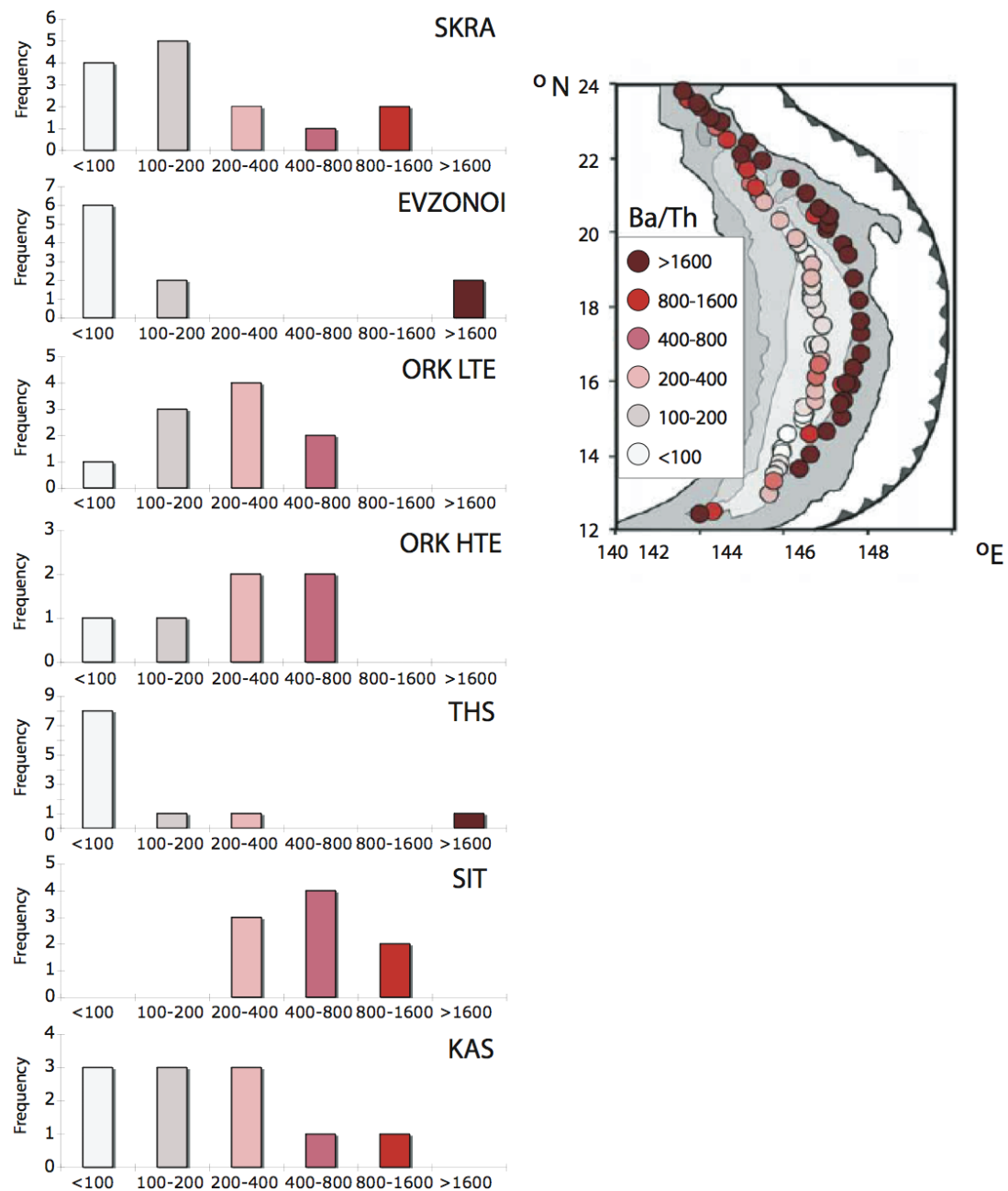


**Fig. 8**. Ba/Th distribution of the samples from all the ophiolites. The geochemical maps for Ba/Th and for the Marianas are from Pearce (2005).

The occurrence of all these different kinds of magmatism we found in the investigated ophiolites, as they have been examined during this study have been connected to the evolution of back-arc spreading of intra-oceanic crust. It would therefore be useful for our purpose to compare these ophiolites with the geochemistry of rocks from an acctualistic example of a arc- back-arc system. As such we have chosen maybe the most investigated arc-back-arc system, the case study of the Marianas (Fig. 7).
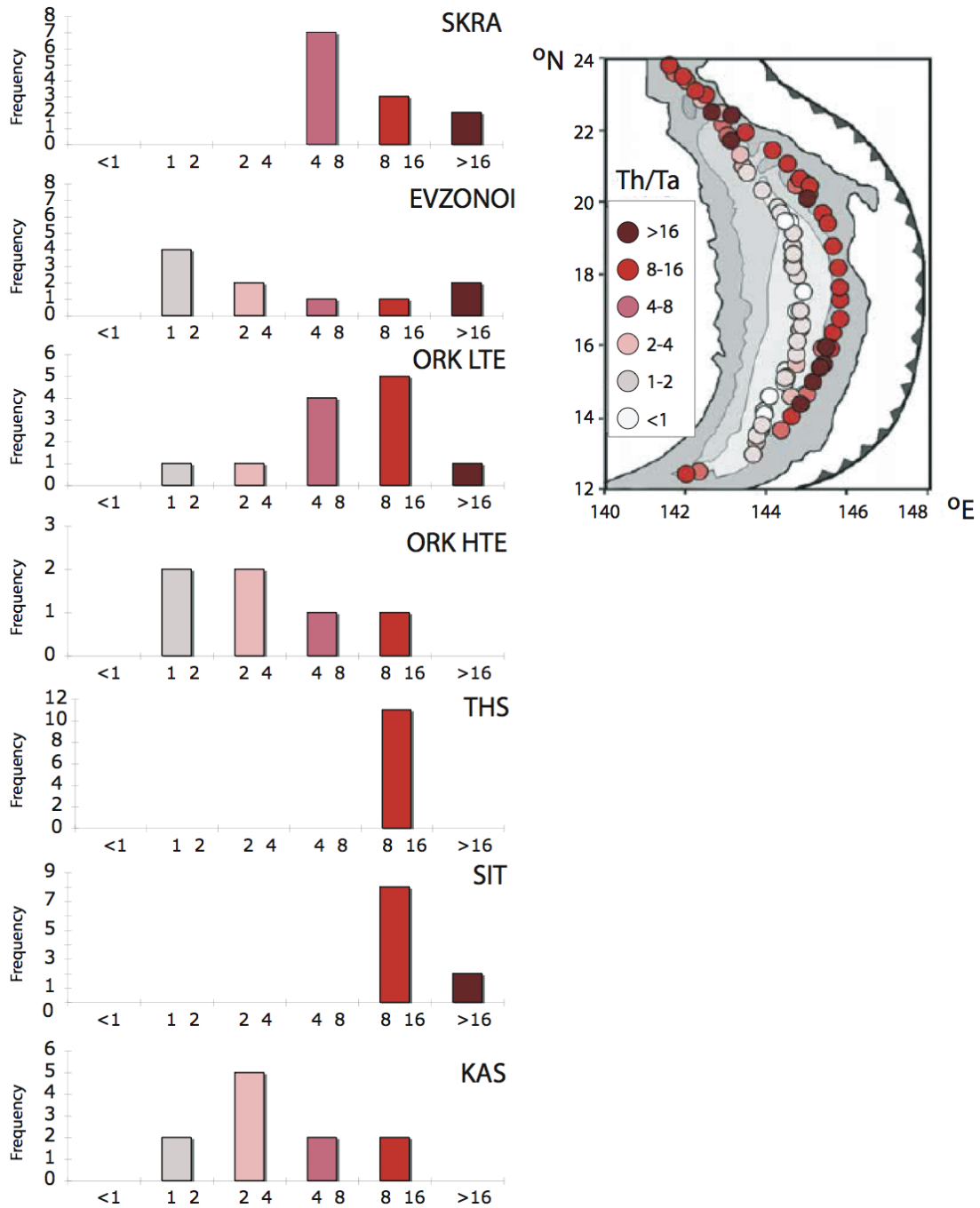


**Fig. 9**. Th/Ta distribution of the samples from all the ophiolites. The geochemical map for Th/Ta for the Marianas is from Pearce (2005).

Pearce et al. (2005) applied geochemical mapping of incompatible and subduction enriched elements to see the variation of those within the Marianas and to notice any possible systematic link between the abundance of these elements and the setting of the magmatism. In Fig. 8 and Fig. 9 we see two maps of the Ba/Th and Th/Ta. Pearce et al. (2005) noticed that the ratios had the highest values the closest to the front of the subduction and that they get lower with distance from the subduction front to the back-arc basin where ocean crust was formed. Looking at these maps we see that in the north where the back-arc meets the volcanic front rifting the ratios are getting higher.

Comparing these geochemical maps with the distribution of the Ba/Th and Th/Ta values for the samples from the ophiolites from the eastern Vardar, we see that the Ba/Th ratios are low and comparable to those of the rifted and ocean crust of the Marianas. Except from the case of the samples from THS that have Ba/Th values below 100, the crushing majority of the other ophiolites have samples with values higher that 100. Rare samples from THS, GVL, EYZ, that have LREE enriched C1-chondrite patterns and the lowest radiogenic Nd display very high values comparable to those close to the subduction front of the Marianas. The Th/Ta ratios on the other hand classify the samples in two groups, one with Th/Ta values higher than 4 which includes GVL, SIT, THS ORK-LTG and a minority of the ORK-HTG, and EYZ. The other group has lower that 4 ratios and includes the majority of the samples from EYZ, KAS, and the majority of the samples from ORK-HTG. The group with the low Th/Ta ratios, though, has values that are above or close to 2. Samples with Th/Ta less than 2 are located in the ocean crust far away from the volcanic front in the Marianas.

In conclusion, the samples from the ophiolites have Th/Ta and Ba/Th ratios higher than those from the ocean crust of the Marianas and excluding minor exceptions lower than those from the volcanic front. The values observed in the investigated ophiolites are closer to the values of the rifted crust from Marianas. The spread of the values of the ratios observed can be attributed to the process from the initial rift of the arc crust to slightly before the formation of the oceanic crust. This comes in correlation of the restricted size of the ophiolites, suggesting that they are the result of short-lived back-arc basin magmatic activity.

The only missing part to the scenario is the absence of typical arc magmatism. This unfortunately was not the subject of this thesis, but by combining information obtained from other authors we can lead to estimation on which magmatic complex that is located in the study area represents the volcanic arc that might be linked to the back-arc basin. In the area of the Eastern Vardar zone and the Serbomacedonian massif, there are acidic volcanics that outcrop abundantly. In the northern part (area of Guevguely), from east to west these are the acidic volcanics that outcrop in the Paikon subzone of the Vardar Zone, the low-K andesitic-dacitic volcanics found in the Skra complex, the later rhyolitic intrusions found in the Eyzonoi complex and the rhyolitic volcanism of the Mikro Dasos. Unfortunately the available chemical data are restricted to major and some trace element analyses. Some of them are also, according to our opinion, are not well documented. Collecting and evaluating the analyses

form Brown and Robertson (2004) and Anders et al. (2005) that we think are the most reliable and documented, we see that the andesites, dacites and rhyolite belong to the low-K series (Fig. 10).
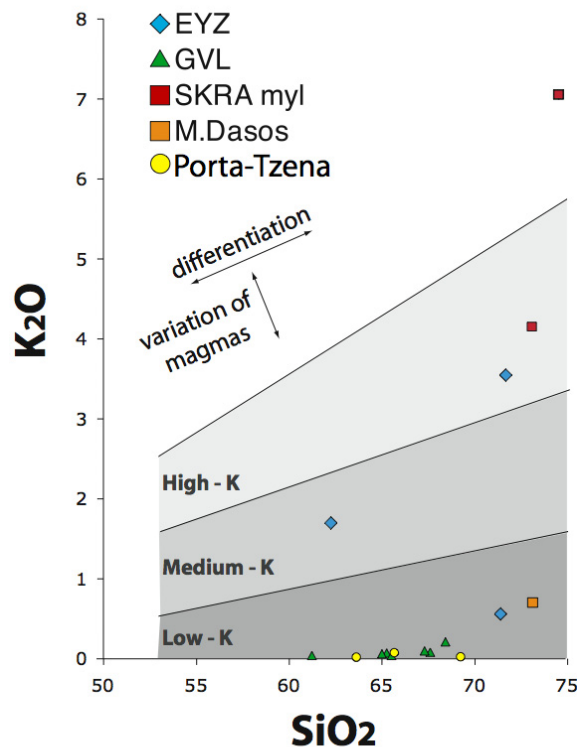


**Fig. 10.** SiO$_2$ versus K$_2$0 for the acidic rocks from the Paikon Massif(Porta-Tzena), the Guevguley complex and east from the Guevguly complex bordering the Serbomacedonian Massif. Fields after Peccerill and Taylor (1976).

To the south, as mentioned in Chapter 4, starting form the area of the city of Thessaloniki and going further south to Sithonia and Kassanda peninsulas, there is the continuous outcrop of the Chortiatis magmatic suite. Mussalam and Jung (1986) investigated these rocks (described as sills by Mussalam and Jung 1989) and as seen on Fig. 11 they also belong to the low-K$_2$O magmatic series. They suggested that they belong to an immature arc, that they placed onto attenuated continental crust. Unfortunately no numerical data were published from these rocks so no further comparison with the volcanics in the north could be made.

The low K$_2$O series of magma is considered to be typical of primitive arcs developed on oceanic crust (e.g. Tonga, Ewart et al. (1973), Kay and Hubbart (1978)). Miyashiro (1974) classified as Group-I volcanics with low-K$_2$O, LREE depletion, and included in this group samples from locations like Tonga, Kernadec, Marianas, South Sandwich, all of them being

known intra-oceanic settings. That is compatible with the results that we obtained from the ophiolites, which suggest formation in an intra-oceanic back-arc basin. Even if such estimation is not built on robust geochemical evidence and is restricted to the comparison of $K_2O$, because of the lack of available data, it should not be ruled out light-hearted. The fact that the chemistry of both the ophiolites and the acidic volcanics suggest that they have formed in samilar settings should enhance the probability that both are linked to the evolution of the same geotectonic setting.
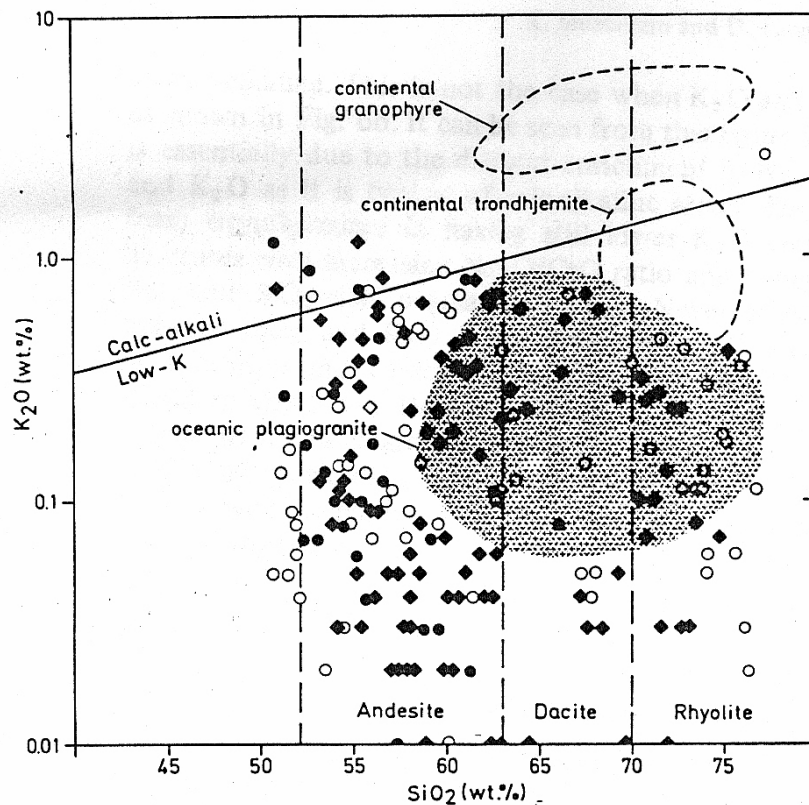


**Fig. 11.** Log $K_2O$ versus $SiO_2$ duagramm fro he Chortitis suite. The fields of continental granophyre and of oceanic plagiogranite afer Coleman (1977). Rock classification after Peccerillo and Taylor (1976). The presented diagram is a scan from Mussalam and Jung (1986).

Recent studies on the paleogeographic reconstruction of the Hellenides by van Hinsbergen et al. (2005) suggest an eastward intra-oceanic subduction in the Vardar Zone (Fig. 12). This comes in agreement with the observations we made from the geochemistry of the ophiolites and the acidic volcanics that occur in the easternmost border of the current configuration of the Vardar Zone.
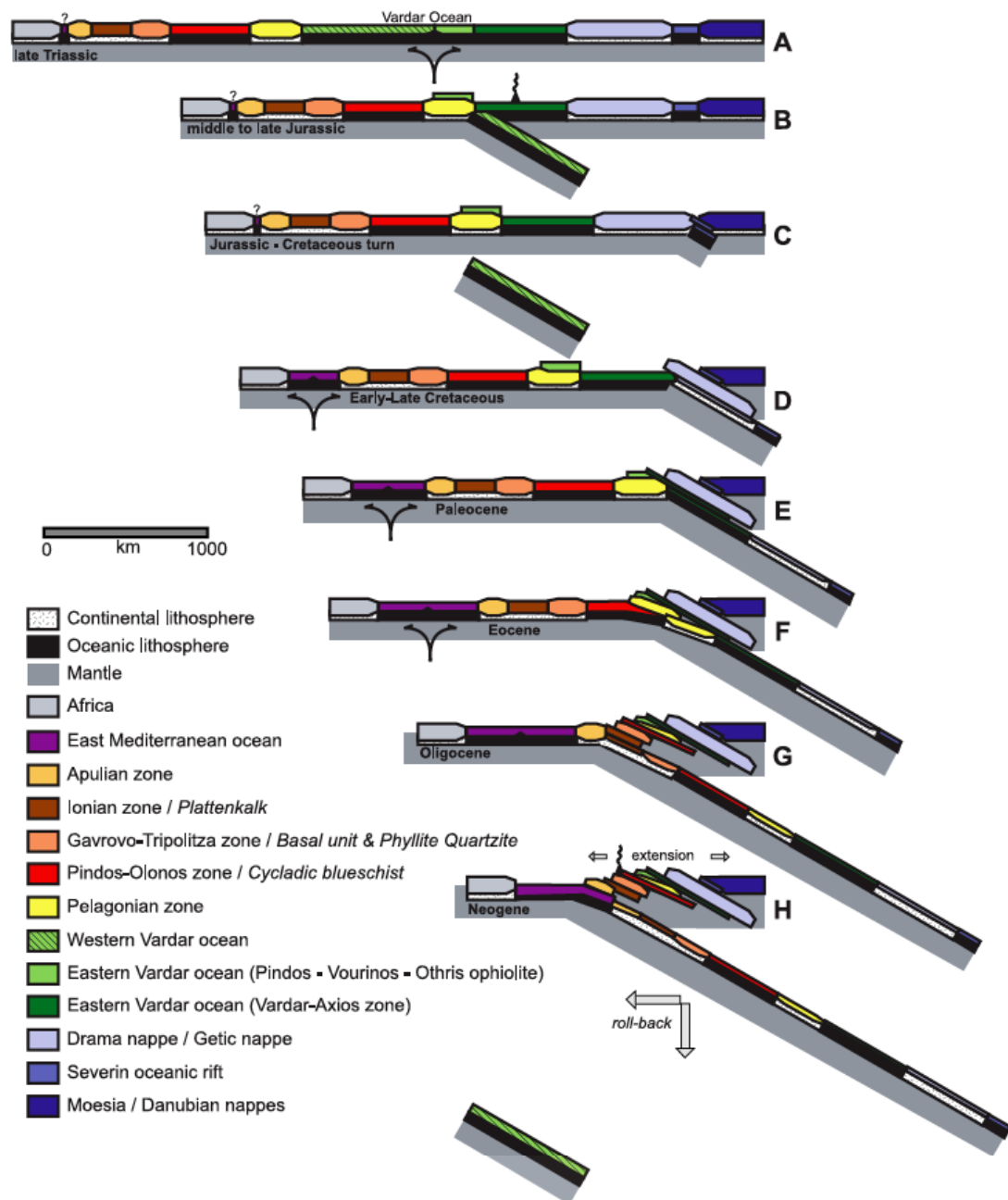
**Fig. 12.** Schematic overview of development of nappe stack and subduction during Alpine orogeny in Greece. (taken from van Hinsbergen et al. 2005). Note the intra-oceanic subduction that takes place within the Vardar zone proposed by the authors.

Brown and Robertson 2004, suggested a possible evolutionary scenario for the evolution of the Paikon arc and the adjacent ophiolites from their studies on the Voras mountains (N. Greec). According to their study during the Triassic a rifting evolved separating the Pelagonian from the Serbomacedonian Massif (Fig. 13). During Mid-Late Jurassic there was an eastward subduction of the Almopias Ocean below the continental margin which is

represented by the Serbomacedonian Massif (Fig. 13) that gave rise to the Paikon arc and the evolution of an ensialic back-arc basin (Guevguely ophiolite). Their model is constrained by strong field data as well as stratigrapic observations and correlations. Examining the chemical analyses they provide for magmatic rocks from the area we see that the andesites and dacites from Porta are low- $K_2O$ andesites that have depleted LREE C1-chondrite normalised patterns (Fig 19, Chapter 3).
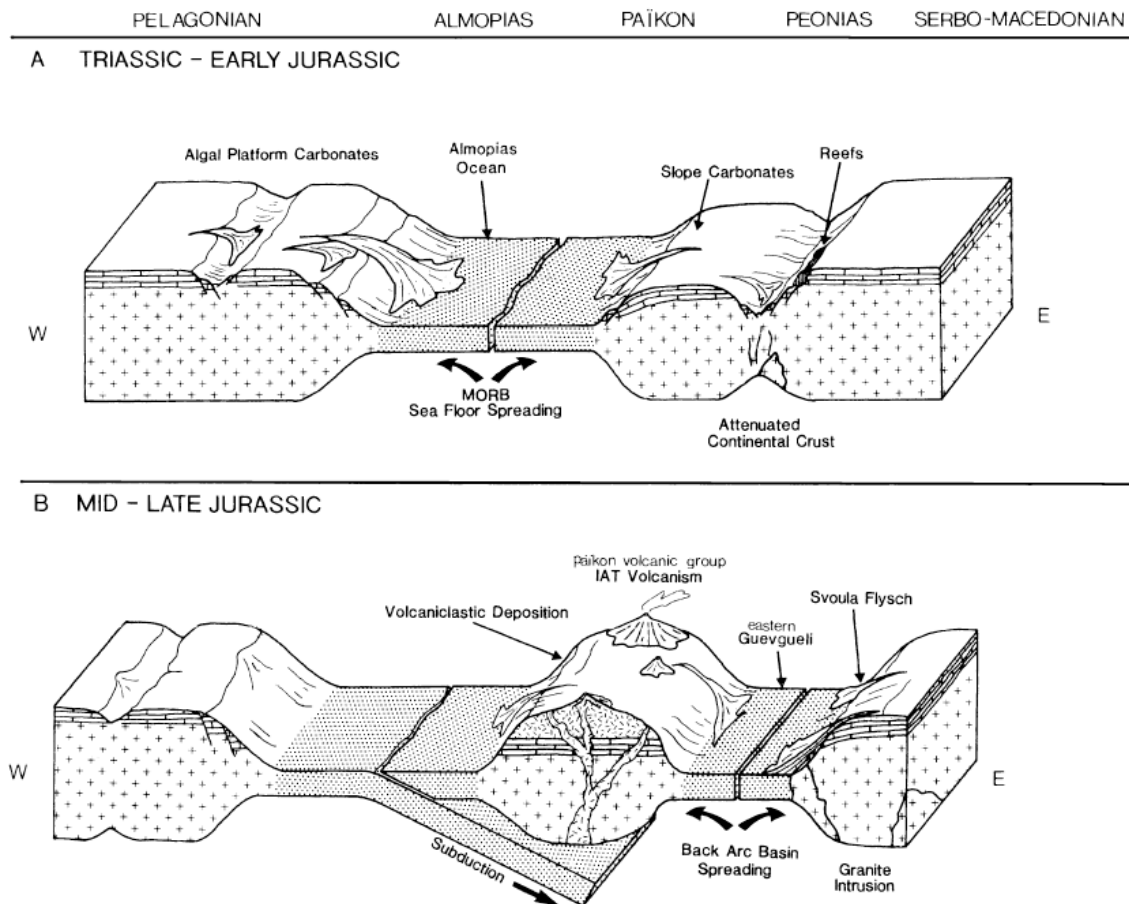


**Fig. 13**. Proposed tectonic model for the Vardar– Axios zone in the Voras Massif and adjacent areas. The model takes into account evidence from the Paikon Massif further south (Brown and Robertson, 1994, 2003) and the wider Vardar, Pelagonian and Serbo-Macedonian zone areas.
This figure is taken from Brown and Robertson 2004.

The difference between their model and the observations we made on the chemistry of the ophiolites is that they propose that the Paikon arc has been built on continental crust and therefore the ophiolites are related to ensialic rifting. This comes into contrast to the chemistry of the acidic samples from Paikon that belong to the low–$K_2O$ series and are LREE depleted, as deduced by the analyses provided in Brown and Robertson (2005) (Fig 19,

Chapter 3). On the other hand there is also acidic magmatism in the Painkon arc that belongs to the high-$K_2O$ and that it is 10Ma younger than the ohiolites(e.g. Griva, metvolcanics, 155 Ma, Anders et al. 2005), suggesting that it might be possible that the Paikon has evolved to a mature island arc like we see at present day configuration. I tend to believe that initially Paikon was built on thin crust, most probably oceanic and later as magmatism continued it the arc crust went thicker resulting to a more typical high-$K_2O$ arc volcanism.

# 7.3 Geochronology

The age of the investigated ophiolites, with exception of the Guevguely ophiolite, has not been determined so far with direct methods. In the previous chapters we have presented new geochronological data for all the complexes studied here in an attempt to provide accurate and precise determination on the timing of their formation. In this paragraph we will discuss the implications stemming from the ophiolite formation ages on the geotectonic evolution of the Vardar Zone and compare our data with similar data on ophiolites from the neighbouring zones.

Beginning from the north, the only radiometric age determinations existing for the Guevguely magmatic complex are those of Spray et al. (1984). These authors applied the $^{40}Ar/^{39}K$ method on biotite and kaersutite separates from gabbros and diorites of the complex and suggested a formation age between 149±3 and 163±3 Ma. Danielian et al. (1996) extracted radiolarians from the deep-sea sedimentary cover directly overlying the ophiolitic extrusives in the Evzoni complex and determined an Oxfordian age (161.2-155.7 Ma); they suggested an early Late Jurassic age for the formation of both the Guevguely and Evzoni complexes. In the south there is a noticeable paucity of data. Mussalam and Jung (1986) have reported (as personal communication with Kreuzer) a K-Ar age of 174±4.8 Ma for a hornblende gabbro from the "Thessaloniki Ophiolite". However, details on sample locality and measured isotope ratios were not reported. This age is in good agreement (within error) with the age determination we made for the same ophiolite.

Previous geochronological investigations were mostly restricted to K/Ar dating of hornblende separates from gabbros and diorites. This method, although it is suitable for dating such kind of rocks, can be quite sensitive during metamorphism and especially in the presence of fluids. Taking under consideration all the above we decided to choose a more stable isotopic system for the given conditions such as the U-Th-Pb in the mineral zircon, because zircon is a uranium-bearing mineral that is widely used for isotopic dating. Its resistance to metamorphism and its high closure temperature for the U/Th/Pb system make it highly reliable for age determinations.

## 7.3.1 Resumé of geochronology

As deduced from chapters 3-6, the Guevguely, Oraeokastron, Thessaloniki and Chalkidiki ophiolites represent relics of oceanic crust that was formed during different evolutionary stages of back-arc rifting in a supra-subduction zone setting in Middle Jurassic. The age of the Guevguely ophiolite has been precisely determined as 167±1.2 Ma, the Thessaloniki ophiolite as 169±1.4 Ma, the Kassandra ophiolite as 167±2.2 Ma  and the Sithonia ophiolite as 160±1.2 Ma.. This crust is now found emplaced on an intricately structured continental margin as this is represented by the western border of the Serbo-Macedonian Massif. Evidently, ophiolite obduction took place during the upper Middle Jurassic between 169-160 Ma (Bathonian-Callovian). Another example of Jurassic magmatism in this area is the Chortiatis magmatic suite. Kockel (1971) used this term to define a series of acidic to intermediate volcanics that outcrop in the Circum-Rhodope Belt forming a northwest-southeast trending zone parallel to the ophiolites. Schunemann (1985) and Kassoli et al (1990) proposed a volcanic-arc setting for these rocks. Chemistry excluding, the striking difference between the rocks of the Chortiatis magmatic suite and the ophiolites is that the former are tectonised and isoclinically folded. Jung and Mussalam (1986) suggested that the Chortiatis magmatic suite is tectonically emplaced on top of the ophiolites. The age Chortiatis magmatic suite has been also investigated in this study and was determined as 159±4.2 Ma.

It has recently been proposed that exhumation of the Rhodope Metamorphic Core Complex was achieved through a clockwise rotation of the Chalkidiki block by approximately 30° (Brun and Sokoutis, 2007). Interestingly, restoration of this block to its original position before rotation brings in line the complexes studied here with the Samothraki marginal-basin ophiolite further southeast, for which available radiometric K/Ar data on hornblende separates from a high-level diorite suggest a mean formation age of 155±7 Ma (Tsikouras and Hatzipanagiotou, 1990). In a more recent study, Koglin at al. (2007) proposed a 160± 5 Ma age for the formation of the Samothraki ophiolite based on zircon dating by SHRIMP-II. The age obtained by Koglin et al. (2007) for Samothraki is identical to the age of Sithonia obtained in this study. These ages are in the same range of ages measured for the ophiolitic complexes of Guevguely, and Thessaloniki. However, there is an apparent decrease of ages from northwest to southeast.

A compilation of the available radiometric ages for the ophiolitic occurrences in the Dinarides and the Hellenides and the Vardar Zone is shown in Fig. 14. It is evident that ophiolitic magmatism in the Balkan area took place during the Middle Jurassic between 170 and 160 Ma, with only exception the ophiolite on the Lesvos island. It is intresting to notice that the two ophiolite belts, namely the Hellenide-Dinaride and the Vardar Zone that run from

the Pannonian Basin to the island of Crete in the Mediterranean Sea, have been formed during the same period.
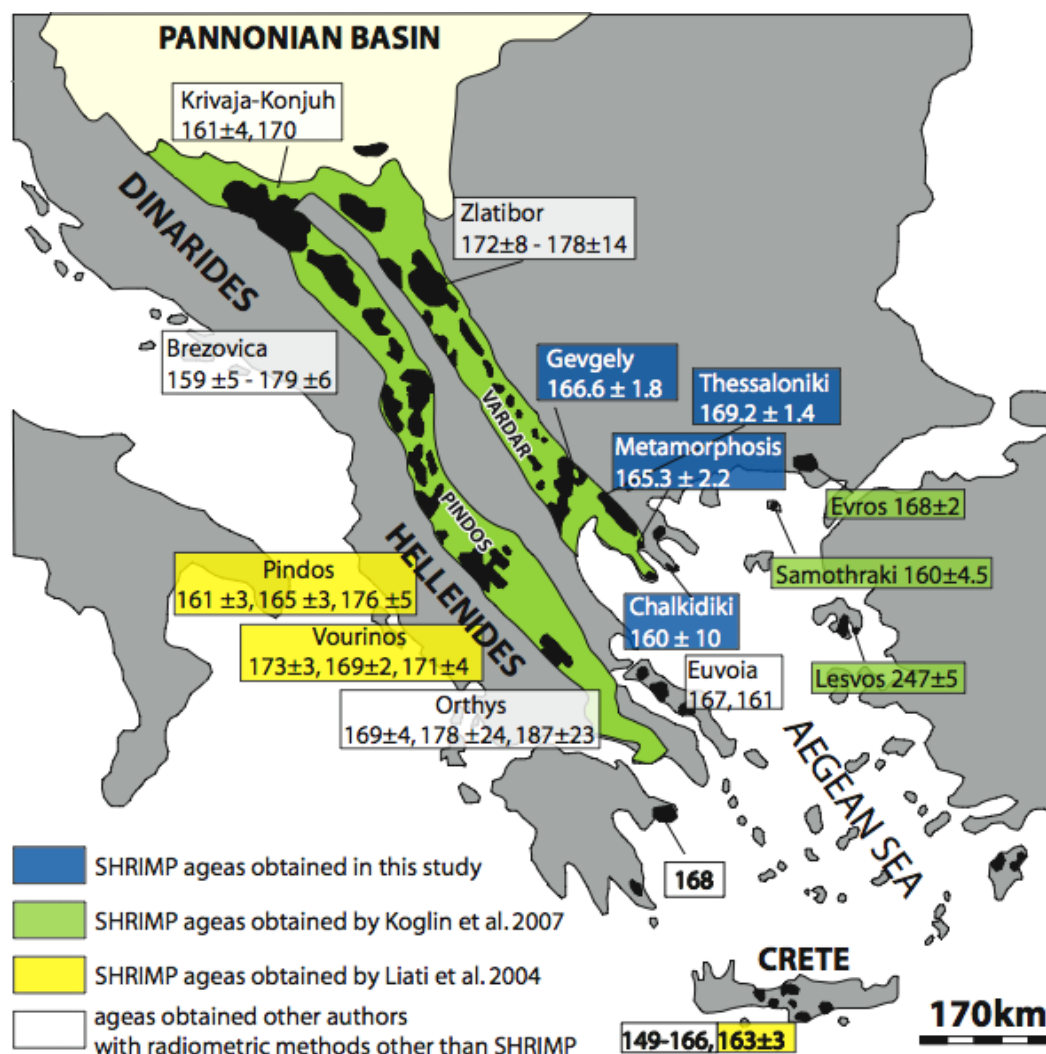


**Fig. 14.** Compilation of radiometric ages of ophiolites from the Dinarides-Hellenides. (Modified from Spray 1984 and Liati 2004). Krivaja – Konjuh and Zlatibor: Lanphère et al. (1975). Brezovica: Okrusch et al. (1978), Karamata and Lovric (1978). Pindos: Roddick et al. (1979), Thuizat et al. (1981), Spray et al. (1984), Liati et al. (2004). Vourinos: Spray and Roddick (1980); Spray et al. (1984), Liati et al. (2004). Orthrys: Ferrière (1982). Crete: Koepke et al. (1985, 2002), Liati et al. (2004). Evvia: Spray et al. (1984).

On Lesvos Island, about 150 km SSE of Samothraki, remnants of a dismembered ophiolite are exposed, resting tectonically on Permo-Carboniferous crystalline basement. They are composed of a sub-ophiolitic mélange unit overlain by a mantle tectonite unit with local occurrences of amphibolite sole rocks in between the two units. The sub-ophiolitic mélange unit contains basalts of WPB and MORB affinity conformably overlain by cherts and pelagic limestones carrying Triassic conodonts (Papanikolaou, 1999). Koglin et al. (2007)

123

confirmed the Triassic age of the Lesvos ophiolite by dating zircons from a gabbro sample belonging to the mélange unit. Published K/Ar ages on hornblende separates from the amphibolite sole (Hatzipanagiotou and Pe-Piper, 1995) suggest an ophiolite obduction at 155±5 Ma. The data imply the existence of a Triassic ocean basin that was destructed in Late Jurassic. In the western Vardar zone, the presence of tectonically dismembered upper parts of ophiolites composed of MORB-type lavas and their pelagic sedimentary cover of Late Triassic to Late Jurassic age has been clearly documented by Stais (1993) and Brown and Robertson (2004). Taken collectively, the data presented herein suggest the presence of a Mesozoic Vardar-Lesvos Ocean that was subducting to the east underneath a Permo-Carboniferous continental margin during the Middle-Late Jurassic. This process was responsible for triggering the subduction-related magmatism as exposed in Guevguely, Oraeokstro, Thessaloniki, Chalkidiki and most probably Samothraki and Evros.
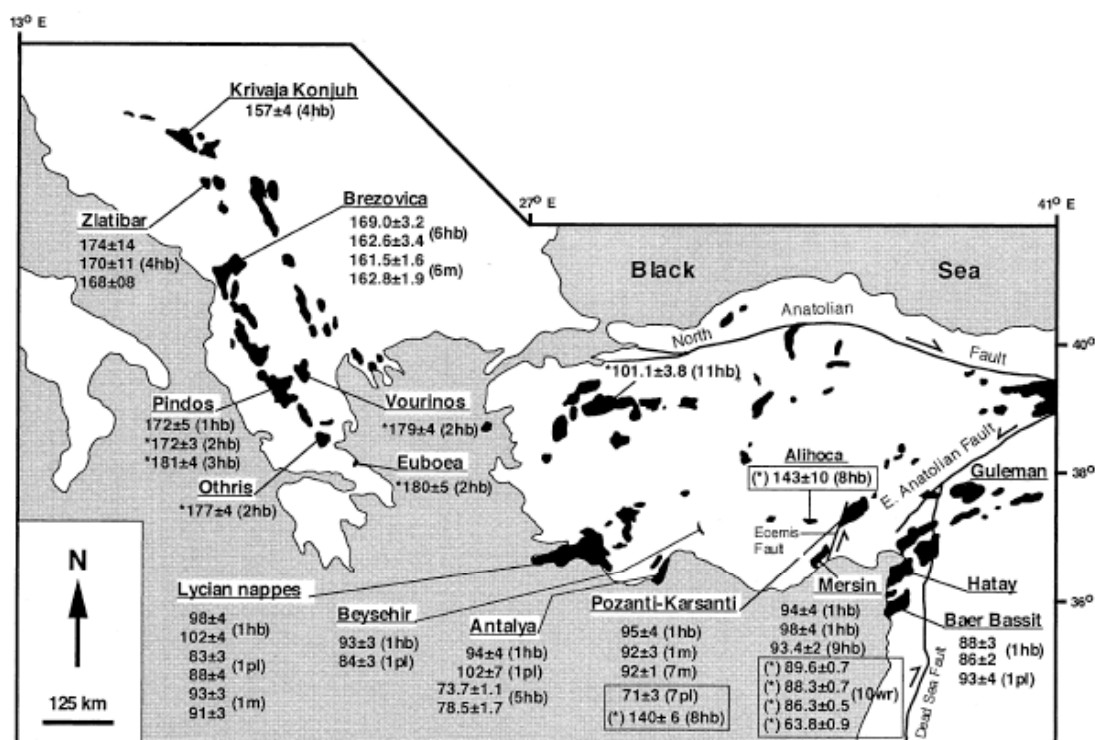


**Fig. 15.** Regional map of the eastern Mediterranean summarizing K–Ar and $^{40}$Ar/$^{39}$Ar. Geochronologic data for the metamorphic soles of ophiolites. hb: hornblende; pl: plagioclase; m: mica; wr: whole rock. Boxes indicate post-tectonic dike injection in the Pozanti–Karsanti, Alihoca and Mersin ophiolites. Numbers in parentheses indicate references as follows: 1: Thuizat et al. (1981); 2: Spray and Roddick (1980); 3: Roddick et al. (1979); 4: Lanphere et al. (1975); 5: Yilmaz and Maxwell (1982); 6: Okrusch et al. (1978); 7: Thuizat et al. (1978); 8: Dilek and Thy (1992); 9: Parlak et al. (1995); 10: Parlak and Delaloye (1996); 11: Harris et al. (1994). The map is taken from Parlak and Delaoye (1999).

Liati et al. (2004) analysed zircons (SHRIMP-II) from a gabbro and a trondhjemite from the Pindos and Vourinos ophiolites respectively. They obtained formation ages between

172.9 and 168.5 Ma for the Vourinos ophiolite, and an age around 171.3 Ma for the Pindos ophiolite. These ophiolites have been interpreted to have-been formed above an eastward-dipping subduction zone, in a fore-arc setting by spreading during the initial stages of intra-oceanic subduction (e.g. Kostopoulos, 1988; Jones and Robertson, 1991, Moores 1969, Jackson et al. 1975, Rassios and Smith 2000) The supra-subduction zone (SSZ) setting deduced for these ophiolites is mainly based on petrological-geochemical criteria, such as the presence of island-arc tholeiites and boninites in the extrusive sequence, the presence of pyroxene-dominated ultramafic cumulates in the plutonic sequence, and the harzburgitic nature of the mantle sequence. In the case of the Pindos ophiolite, however, there are rocks that carry distinct mid-ocean ridge and supra-subduction zone characteristics (e.g. Kostopoulos, 1988). The similarity in the chemistry of the ophiolites in both sides of the Pelagonian Zone can leave a question on whether all these ophiolites are fragments of the same ocean that was located in the area of the Vardar Zone. It is not a target of this thesis to examine the hypothesis whether these ophiolites have come from the same root zone or not. However it is important to point out the apparent similarity of the geochemical and, after the results of this thesis, the geochronological characteristics of these ophiolites.

Parlak and Delaoye (1999) presented a compilation of Ar/Ar and K-Ar radiometric ages of ophiolites from the eastern Mediterranean region (Fig. 15). It becomes immediately obvious from their age map that the ophiolitic and sub-ophiolitic rocks in Turkey and the Middle East have much younger ages than the ophiolites in Greece and the central Balkans by about 70 Ma. This marked age difference can be either ascribed to a significant widening of the wedge-shaped Neotethys Ocean towards the southeast that brought about delayed ridge destruction via intra-oceanic subduction and subsequent obduction of the SSZ ophiolitic complexes onto the nearest continental margin or to the simplified scenario that Balkan ophiolites belong to a different branch of the Tethyan system that evolved much earlier than the neo-tethyan one that resulted to the formation of the Turkish and Middle East ophiolites.

## 7.4. Summary and Conclusions

Northern Greece is a geologically complex area where continental blocks of different provenance and age came together. These continental blocks, or terranes, are separated by zones of low-grade to amphibolite facies rock associations of both sedimentary and igneous origin. From east to west the metamorphic continental block of the Rhodope Massif comes into contact with that of the Serbo-Macedonian Massif along the Athos-Volvi-Thermes suture zone. In turn, the Serbo-Macedonian Massif is bordered to the west by the Peonias subzone of the Vardar Zone. Their interface is a narrow belt of rocks consisting of limestones, metasedimentary and volcanosedimentary rocks, as well as granitic rocks and ophiolites, which has been termed the Circum-Rhodope Belt.

In the frame of the present thesis the geochemistry, petrology and geochronology of the ophiolites that are located between the eastern part of the Peonias subzone of the Vardar Zone and the Serbo-Macedonian Massif along the Circum-Rhodope Belt were studied in order to gain insights on the processes that lead to their genesis and evolution. From north to south the studied ophiolites are the Guevguely, Oraeokastro, Thessaloniki, and Chalkidiki ophiolites. The importance of these ophiolites is that they mark a subduction zone in the easternmost border of the Vardar Ocean, suggesting that there was an active margin along the southernmost border of the Serbo-Macedonian and Rhodope massif. A detailed study would allow us to understand the processes that took place at the active margin where the suture of this system took place.

The aim of this thesis was accomplished through detailed studies on the mineral as well on the whole rock geochemistry using high-precision analytical equipment. To constrain the results obtained from the chemistry the isotopic systems of Sm and Nd as well as of Sr were investigated. In order to precisely place the evolution of these ophiolites in time U-Pb geochronology on zircons was conducted using a SHRIMP-II.

The Guevguley ophiolite can be divided in two complexes based on the petrological and geochemical characteristics, namely the Skra and the Evzonoi complexes. The Skra complex occupies the western part of the Guevguely ophiolite while the Evzonoi complex occupies the eastern part as it is divided by the Fanos granite. The Skra complex is characterised by bimodal magmatism. Two rock suites were recognised: one is dominated by mafic rocks with $SiO_2$ content ranging up to 52 wt%, the other is composed of acidic rocks having $SiO_2$ content between 61 and 66wt%. The acidic samples are low-K, LILE and LREE-depleted. The depletion in LILE can be attributed to hydrothermal circulation that took place after the formation of these rocks and resulted in leaching the samples from the LILE. The depletion in REE is clearly a magmatic phenomenon; the samples closely resemble the andesites and dacites that erupt in the Tonga - Kermadec arc (Ewart 1973). Th is enriched in all samples. Nb and Ta form negative anomalies in the multielement profiles. The mafic samples have mainly LREE-depleted patterns. Slightly LREE-enriched samples are also present. HREE patterns are all flat suggesting melting in the spinel lerzolite field.

The Evzonoi complex is built up from mafic rocks. Scarce rhyolitic dykes cross cut all the mafic dykes and can be was assigned to a later event of magatism. Some rare andesites are found to cross cut the mafic dykes. The samples from Evzonoi have a variable LILE content. Th is slightly enriched while in some samples it very difficult to distinguish this enrichment. Nb and Ta form slight negative anomalies. The HFSE form patterns subparralel to the N-MORB line. The LREE are depleted and the HREE have flat patyterns resembling the patterns of the Skra samples. The rhyolite have fractionated REE patterns. LREE are highly enriched relative to the HREE and the HREE patterns are flat.

The isotopic systematics of the samples, are characterized by positive $\epsilon_{Nd(165Ma)}$ values that are lower than the DMM or N-MORB values, suggesting that these samples have

derived from a mantle source that has been isotopically modified by an enriched component. This enriched component as deduced by the co-variation between Nd isotopes with $SiO_2$ or Nb/Th is most probably a subduction-derived hydrous fluid and/or melt; rather than AFC processes. The samples from both complexes have been derived from a mantle source that has previously experienced melt extraction and that has been modified by the addition of fluids and melts derived from the sedimentary cover of the subducted slab. Evzonoi show lower enrichment from the subducted slab component than the Skra complex.

The chemistry of the samples from the Guevguely ophiolite have typical charcterstics of subduction-zone magmatism. Tectonomagmatic discrimination based on Ti/V and Zr/4-Y-2Nb systematics classifies the samples from Skra and Evzonoi as MORB and VAB or IAT whereas tectonomagmatic discrimination based on Th-Hf/3-Ta systematics classifies the samples as having derived from destructive plate margins while on the same diagram the samples from Evzonoi plot between the fields of N-MORB and basalts from destructive plate margins. Compatible vs incompatible element non-modal equilibrium melting modelling suggest that the sanples from Skra complex could be explained by 15-10% of melting of a FSL while the Evzonoi complex could explained by less than 5% of melting of similar source

Oraiokastro ophiolite is built up of extrusive rocks and gabbros. The extrusive rocks of the ophiolite are classified as basalts and basaltic andesites. On the basis of their major element chemistry and especially their $TiO_2$ content two groups of mafic extrusive samples that can be distinguished. A high $TiO_2$ (HTE) and a low $TiO_2$ group (LTE). Both groups have LREE depleted and flat HREE C1-chondrite normalised patterns, but the high-$TiO_2$ has higher total REE ($\Sigma$REE) content.  Thorium is enriched in both groups, being more enriched in the low $TiO_2$ group. Th follows distinct enrichment vectors for each groups towards higher Th/Yb ratios suggesting that the influence of the subduction component is different for the two groups. Multi-element diagrams show that both groups have been affected by contamination of the magma source, probably due to subduction zone fluids. REE systematics suggests that the low- $TiO_2$ group is derived from a depleted, relative to the N-MORB source, whereas the high- $TiO_2$ group is derived from a similar to the N-MORB source. The two groups can also be distinguished on the basis of their isotopic characteristics. Samples from both groups plot outside the mantle array suggesting that the Sr isotopic system was modified by seawater alteration.

Tectonic setting discrimination diagrams indicate a subduction zone environment for the LTE and a middle ocean ridge or back-arc basin environment for the HTE. Th/Yb versus Ta/Yb diagram reveals that both groups have a subduction component addition. The gabbros have a complex behaviour, plotting around the line that discriminates between low and high-Ti gabbros. Acidic samples plot in the volcanic-arc field, except for an intrusive diorite rock which was classified as ocean-ridge granite.

Petrogenetic modelling suggests that the rocks from the HTE require very low degrees of melting (~5wt%) of a fertile spinel lherzolite, while those of the LTE require higher

degrees of melting (~25wt%) of the same source. The LTE can be alternatively explained by <5wt% melting of a depleted spinel lherzolite. Cr-spinels from serpentinised harzburgites yield degrees of melting between 15.3 and 18.5 wt%, while the later generation of Al-spinels from the same rocks yield degrees of melting less than 5wt%.

The chemistry of the dykes and lavas from the Thessaloniki ophiolite have the typical characteristics of subduction zone magmatism. Normalized to N-MORB the samples have negative Nb anomaly, Th enrichment, and the majority of samples have a depletion trend of the HFSE from Yb to Nb. Rare samples and have an enrichment trend of the HFSE. The majority of the samples have depleted LREE patterns except from some which are LREE enriched. There are samples that have a slightly positive Eu anomaly suggesting plagioclase accumulation in the source, whereas the rest of the samples have negative Eu anomalies.

Nd and Sr isotopes show negative correlation. The calculated $\varepsilon_{Nd(167)}$ values are between 5.41 and -0,67 and the $^{87}Sr/^{86}Sr$ ratios between 0.711218 and 0.704944. The $\varepsilon_{Nd(167)}$ measured is lower that the $\varepsilon_{Nd,CHUR(167).}$. Petrogennetic modelling based on compatible vs incompatible element non-modal equilibrium melting modelling suggest 15 -25% of melting of a FSL source. Tectonomagmatic discrimination based on trace elements classifies the samples as samples formed in destructive plate margins.

Fingerprinting of the enriched component suggests that the both samples with LREE depleted and LREE enriched patterns have been affected by a component that carries Th, and its origin is the deep parts of a subduction zone. This component is also responsible for the negative correlation of the$^{143}Nd/^{144}Nd$ and $^{87}Sr/^{86}Sr$. Additionally the samples with LREE enriched patterns have seen a component that rises the concentration of the HFSE. This cannot be melt derived from the mafic fraction of the subduction zone, because of the low Sr/Y ratio of the samples. So it can be better explained by local enrichments of the mantle or continental crust or assimilation of continental crust.

The southernmost ophiolite are the Sithonia and Kassandra ophiolites. The samples from Sithonia have variably enriched LILE content in N-MORB normalised multielements diagrams. Thorium is enriched relative to the LILE and the rest of the HFSE, and there is a persistent negative Nb anomaly and a characteristic hump in La and Ce in all samples. The $(Nb/Yb)_N$ ratio is equal to or higher than one (except from two samples SIT1 and SIT27) pointing towards an enriched rather than a depleted source. Chondrite-normalised patterns show enrichment in LREE, a negative Eu anomaly and moderately flat HREE patterns suggesting that garnet was absent in the source thus shallow melting of the source above the garnet-lherzolite stability field. Two of the samples display much depleted patterns, testified by steep positive slopes from Yb to Nb and Nd to Yb in multi-element and REE profiles respectively. Their slightly U-shaped REE patterns strongly resemble those of boninites such as the ones erupted in the Arakapas Fault Belt of the Troodos ophiolite, Cyprus (Cameron, 1985).

The samples from Kassandra invariably show enrichment in LILE. On the basis of Th vs. Zr systematics they can be separated into two groups. One group (four samples) resembles Sithonia by having pronounced Th enrichment, negative Nb anomaly and similar HSFE patterns. The other group is only slightly enriched in Th and exhibits only a minor Nb anomaly. The HSFE patterns are generally smooth and subparallel to the N-MORB line. The samples have variable shape of the REE patterns. The LREE are enriched relative to the HREE but the La/Nd ratio is lower than 1 except for the samples of the group that resemble Sithonia that have La/Nd>1. Some of the samples show typical N-MORB shaped REE patterns. The HREE patterns are generally flat to slightly negatively sloping. There is no evidence of garnet in the source of these samples, and the slight enrichment in the LREE and MREE over the HREE suggests enrichment of the magma source. The Kassandra samples have only a minor to non-existent Eu anomaly.

The $\varepsilon_{Nd(160)}$ values of the samples from both ophiolites are positive and range from 2.2 to 5.6 suggesting that these rocks are mantle derived, while their source has been isotopically modified by an enriched component. The $^{87}Sr/^{86}Sr$ values are high (0.7041-0.7075) suggesting that these rocks have been affected by seawater alteration. Non modal equilibrium melting modelling of Ti and Cr suggests that Kasandra requires medium to low degrees of melting (10-5wt%) of a fertile spinel lherzolite while Sithonia would require higher degrees of melting between 10 and 20wt% of a FSL and  SIT1 and SIT27 require a much more depleted source than the rest namely a DSL that has melted around 10-15 %.

Tectonomagmatic discrimination classifies the Sithonia samples to MORB or BABB and as having been formed at destructive plate margins. Two samples from Sithonia are classified as IAT. A minor group of Kassandra samples share the same geochemical characteristics with Sithonia. The rest are classified as MORB or BABB and they are generally derived from more enriched sources. The best-fit scenario for the geotectonic setting of these samples is the evolution of back-arc basin magmatism. The Sithonia rocks seem to be more affected by subduction-zone derived contamination while the Kassandra samples show no to minor subduction-zone influence.

Trying to investigate the nature of the subduction component we see that the Sithonia samples and a minor population of the Kassandra samples have been affected by both silicate melts and aqueous fluids while the majority of the Kassandra samples have experienced only only Ba enrichment suggesting aqueous fluids.

Melting modelling of the samples from both ophiolitic outcrops suggests that Kasandra could be explained by 10-5wt% melting of Sp-Lherzolite while Sithonia could be better explained by higher degrees of melting of similar source.

Summing up the results obtained by the geochemical characteristics of these ophiolites we conclude that these ophiolites represent relics of supra-subduction zone ophiolites that have formed as a result of back-arc spreading. Each ophiolite has distinct but altogether similar to the rest chemical characteristics. Comparing the chemistry of these

ophiolites to an actual case study of arc-rifting and back arc opening like the Mariannas we see that these ophiolites are the pieces of a puzzle portraying the evolution of a similar setting during the Middle Jurrasic.

A possible evolutionary scenario for these ophiolites would include an eastward subduction of the Vardar Ocean in an intra-oceanic setting during the Middle Jurassic. In the first stages of supra-subduction zone development (170-165 Ma), formation of low-$K_2O$ acidic magmatism (Paikon andesites, Mikro Dassos rhyolites and parts of the Chortiatis Magmatic Suite) took place. Generation of mafic magmatism occurred contemporaneously, as we find it in the western part of the Guevguely ophiolite (Skra complex), Thessaloniki, Oraeokastro (represented by a low-$TiO_2$ group of mafic extrusives) and, to a lesser extend, in Kassandra. As subduction continued the arc was rifted further as a result of subduction rollback and asthenosphere upwelling, and formation of the eastern part of the Guevguely ophiolite (Evzoni complex), Oraeokastro (represented by a high-$TiO_2$ group of mafic extrusives) and Kassandra ophiolites (161-155 Ma) took place in a setting similar to the back arc region of the Marianas. Initiation of eastward subduction below the Chortiatis–Mikro Dassos arc occurred synchronously with these events and resulted in the closure of the back-arc basin and the evolution of the Sithonia ophiolite in the fore-arc region.

In conclusion, the formation of these ophiolites took place between 170-155Ma during the evolution of a marginal sea, which we term as the Paionias Sea, in the back-arc region of an intra-oceanic subduction that too place in the eastern border of the Vardar Ocean.

### a) Triassic?

initiation of intra-oceanic sub-duction in the Vardar Ocean

### b) Mid-Jurassic

Initial stages of imature intra-oceanic arc builting.
Eruption of low-$K_2O$ acidic magmatism and the beginning of the Paikon Arc (Porta-Tzena).

### c) ~167 Ma

Eruption of magma with typical subduction zone characteristics. In this stage we have the formation of the Skra, the LTE-Oraeokastro, the Thessaloniki and initiation of Kassandra ophiolites .

### d) 160-155 Ma

Eruption of magma with with more astheospheric-like characteristics. In this stage we have the formation of the Evzonoi, HTE-Oraeokastro and Kassandra ophiolites. Contemporaneously we have the initiation of a subduction to eastern side of this back-arc basin and the formation of the Sithonia ophiolite in the forearc region of the Chortiatis arc.



**Fig. 16**. Schematic map cross-section of the evolution of the ophiolites.

# Literature

Anders, B., Reischmann, T., Poller, U. 2002. Geochemistry and Geochronology of Basement Rocks from the Pelagonian Zone, Greece. Geochimica et Cosmochimica Acta, 66, A19. Aubouin J., 1965. Geosynclines Developments in Geotectonics. Vol O. Elsevier ed., Amsterdam, 335p.

Anders, B., Reischmann, T., Poller, U. & Kostopoulos, D. 2003. First zircon ages from South Pilion and Skiathos Island, Greece. Berichte der Deutschen Mineralogischen Gesellschaft, Beiheft zum European Journal of Mineralogy, 15(1), 5.

Anders, B., Reischmann, T, Poller, U. & Kostopoulos, D. 2005. Age and origin of granitic rocks of the eastern Vardar Zone Greece: new constrains on the evolution of the Internal Hellenides. J. Geol. Soc. London. Vol. 162, 857-870

Anonymous, 1972. Penrose field conference on ophiolites. Geotimes 17, 24– 25.

Aubouin J., 1965. Geosynclines. Development in geotectonics 1. Elsevier, 335 p

Baroz, F., Bebie´n, J. & Ikenne, M. 1987. An example of high-pressure lowtemperature metamorphic rocks from an island arc: the Paikon Series (Innermost Hellenides, Greece). Journal of Metamorphic Petrology, 5, 509–527.

Barry T.L., Pearce J.A., Leat P.T., Millar I.L., le Roex A.P., 2006. Hf isotope evidence for selective mobility of high-field-strength elements in a subduction setting: South Sandwich Islands Earth and Planetary Science Letters 252 223–244

Beard, J. S., 1986. Characteristic mineralogy of arc-related cumulate gabbros: Implications for the tectonic setting of gabbroic plutons and for andesite genesis, Geology, 14(10), 848-851,

Bébien, J., Dubois, R., Gauthier, A., 1986. Example of ensialicophiolites emplaced in a wrench zone: innermost Hellenicophiolite belt (Greek Macedonia). Geology 14, 1016–1019.

Bébien, J., Baroz, J., Caperdi, S., Venturelli, G., 1987. Magmatisme basique associe´es a` l'ouverture d'un basin marginal dans les He´llenides internes au Jurassic. Ofioliti 12, 53–70.

Bébien, J. 1982. L'association igne´e de Gue´vgue´li (Mace´doine grecque). Expressiond'un magmatisme ophiolitique dans une de´chirure continentale. DSc thesis, Universite´ de Nancy I.

Bébien, J., Platevoet, B. & Mercier, J. 1994. Geodynamic significance of the Paikon Massif in the Hellenides: contribution of the volcanic rock studies. Bulletin of the Geological Society of Greece, XXX(1), 63–67.

Beccaluva, L., Maccciotta, G., Piccardo, G.B., and Zeda, O., 1989. Clinopyroxene composition of ophiolite basalts as petrogenetic indicator. Chem. Geol., 77, 165-182.

Beintema, K.A, Mason, P.R.D, Nelson, D.R, White, S.H. & Wijbrans, J.R. 2003. New constraints on the timing of tectonic events in the Archaean Central Pilbara Craton, Western Australia. Journal of the Virtual Explorer 13. (http://www.virtualexplorer.com.au/2003/13/1/html/)

Bertrand, P. & Mercier, J.-C., 1985. The mutual solubility of coexisting ortho- and clinopyroxene: toward an absolute geothermometer for the natural system? Earth and Planetary Science Letters 76, 109–122.

Black, L. P., Kamo, S. L., Allen, C. M., Davis, D. W., Aleinikoff, J. N., Valley, J. W., Mundil, R., Campbell, I. H., Korsch, R. J., Williams, I. S., Foudoulis, C., 2004, Improved $^{206}Pb/^{238}U$ microprobe geochronology by the monitoring of a trace-element-related matrix effect;

SHRIMP, ID–TIMS, ELA–ICP–MS and oxygen isotope documentation for a series of zircon standards. Chemical Geology, 205, 115–140.

Black, L. P., Kamo, S. L., Allen, C. M., Aleinikoff, J. N., Davis, D. W., Valley, J. W., Korsch, R. J., Foudoulis, C. 2003: TEMORA 1: a new zircon standard for Phanerozoic U-Pb geochronology. Chemical Geology, 200, 155-170.

Boudier , F., and Nicolas A., 1985. Harzburgite and Lerzholite subtypes in ophiolitic and oceanic environments. Earth and Planetary Science Letters, 76, 84-92.

Boynton, W.V., 1984. Cosmochemistry of the rare earth elements: meteorite studies. In: Henderson, P. (Ed.), Rare Earth Element Geochemistry. Elsevier, Amsterdam, pp. 63–114.

Brogniart, A., 1827. Classification et caracteres mineralogique des roches homogenes et heterogenes. F.G. Levrault, Paris

Brown, S.A.M. & Robertson, A.H.F. 1994. New structural evidence from the Mesozoic–Early Tertiary Paikon Unit, Northern Greece. Bulletin of the Geological Society of Greece, XXX(1), 159–170.

Brown, S.A.M. & Robertson, A.H.F. 2003. Sedimentary geology as a key to understanding the tectonic evolution of the Mesozoic–Early Tertiary Paikon Massif, Vardar suture zone, N Greece. Sedimentary Geology, 160, 179–212.

Brown, S.A.M. & Robertson, A.H.F. 2004. Evidence for Neotethys rooted within the Vardar suture zone from the Voras Massif, northernmost Greece. Tectonophysics, 381, 143–173.

Brun, J-P., Sokoutis D., 2007. Kinematics of the Southern Rhodope Core Complex. Int J. Earth. Sci (Geol Rundsch), published online first.

Burg, J.P., Ricou, L.E., Ivanov, Z., Godfriaux, I., Dimov, D., Klain, L., 1996. Syn-metamorphic nappe complex in the Rhodope Massif: structure and kinematics. Terra Nova 8, 6 –15.

Burke, W.H., Denison, R.E., Hetherington, E.A., Koepnick, R.B., Nelson, H.F. & Otto, J.B. 1982. Variation of seawater $^{87}Sr/^{86}Sr$ throughout Phanerozoic time. *Geology* **10**, 516-519.

Cameron, W. E., E. G. Nisbet, and V. J. 1980. Dietrich Petrographic dissimilarities between ophiolitic and ocean floor basalts, in Ophiolites: Proceedings of the International Ophiolite Symposium, edited by A. Panayiotou, pp. 182-192, Geol. Surv. Dep., Nicosia, Cyprus.

Cameron, W. E., 1985. Petrology and origin of primitive lavas from the Troodos ophiolite, Cyprus, Contrib. Mineral. Petrol., 89 (2-3), 239-255.

Claoue-Long, J. S., Compston, W, Roberts, J., Fanning, C. M., 1995. Two Carboniferous ages: a comparison of SHRIMP zircon dating with conventional zircon ages and 40Ar/39Ar analysis. In: Bergen W. A., Kent D. V., Aubrey M. P., Hardenbol J., (Eds.), Geochronology Time Scales and Global Stratigraphic Correlation. SEPM (Society for Sedimentary Geology), Special Publication, v. 54, pp 2-3-21.

Cohen, R. S., and R. K. O'Nions, 1982. The lead, neodymium and strontium isotopic structure of ocean ridge basalts, J. Petrol., 23(3), 299-324.

Coleman, R. G., 1977. Ophiolites. Berlin-Heidelberg: Springer-Verlag.

Coleman, R. G., 1981, Tectonic setting for ophiolite obduction in Oman: Journal of Geophysical Research, v. 86, no. B4, p. 2497-2508.

Compston, W., 1999.  Geological age by instrumental analysis: the 29th Hallimond Lecture.

Mineralogical Magazine, 63, 297-311.

Compston, W., Williams, I. S. and Meyer, C. 1984: U-Pb geochronology of zircons from lunar breccia 73217 using a sensitive high mass-resolution ion microprobe. Journal of Geophysical Research, 89 supplement, B525- B534.

Crawford, A.J., Beccaluva, L. & Serri, G. 1981. Tectono-magmatic evolution of the West Philippine-Mariana region and the origin of boninites. Earth and Planetary Science Letters, 54, 346–356.

Crawford, A. J., Falloon, T. J., and Green, D. H., 1989.Classification, petrogenesis, and tectonic setting of boninites, in Boninites and Related Rocks, edited by A. J. Crawford, pp. 2-49, Unwin Hyman, Boston, Mass.

Christofides, G., Soldatos, T., Koroneos, A., 1990. Geochemistry and evolution of the Fanos granite, N. Greece. Mineralogy and Petrology 43: 49-63.

Christofides, G., Koroneos, A., Soldatos, T., Eleftheriadis, G. and Kilias, A., 2001. Eocene magmatism (Sithonia and Elatia plutons) in the Internal Hellenides and implications for Eocene–Miocene geological evolution of the Rhodope massif (Northern Greece). In: H. Downes and V. Orlando, Editors, Tertiary Magmatism in the Dinarides, Acta Vulcanologica vol. 13, pp. 73–89.

Dana, E. S., 1949. A textbook of mineralogy. 4th edn., New York: John Wiley & Sons.

Danelian, T., Robertson, A. H. F. & Dimitriadis, S. 1996: Age and significance of radiolarian sediments within basic extrusives of the marginal basin Guevgueli Ophiolite (northern Greece). Geological Magazine, 133, 127-136.

Defant, M.J., & Drummond, M.S., 1990. Derivation of some modern arc magmas by melting of young subducted lithosphere. Nature 347, 662-665.

De Wet, A.P. et al., 1989. Geology and geochronology of the Arnea, Sithonia and Ouranoupolis intrusions, Chalkidiki peninsula, Northern Greece. Tectonophysics, 161: 65–79.

Dick, H. J. B., 1989. Abyssal peridotites, very slow spreading ridges and ocean ridge magmatism, in Magmatism in the Ocean Basins, Geol. Soc. Spec. Publ., 142, 71- .

Dick, H. J. B., and Bullen, T., 1984. Chromian spinel as a petrogenetic indicator in abyssal and alpine-type peridotites and spatially associated lavas, Contrib. Mineral. Petrol., 86(1), 54-76.

Dilek Y. & Flower, M.F.J. 2003. Arc-trench rollback and forearc accretion: 2. A model template for ophiolites in Albania, Cyprus, and Oman. In: D‹LEK, Y. & ROB›NSON, P.T. (eds), Ophiolites in Earth History. Geological Society, London, Special Publications 218, 43–68.

Dilek, Y., Thy, P., 1992. Structure, petrology, and geochronology of mafic dike intrusions in the Tauride belt (S. Turkey) and implications for the Neotethyan paleogeography. American Geophysical Union Meeting, 7–11 December, San Francisco, CA, p. 546.

Dimitriadis, S., 1980. Discussion of 'The Thessaloniki Gabbros' by E. Sapountzis  J. Petrology 21: 437-440.

Dimitrijevic, M.D., 1957. The structure of the crystalline region between Slisane and Presovo.- 2. Kongres Geologa FNRJ, Sarajevo, p. 629-634.

Dixon, J.E. & Dimitriadis, S., 1984. Metamorphosed ophiolitic rocks from the Serbo-Macedonian Massif, near lake Volvi, North-east Greece. – In: Dixon, J.E. & Robertson, A.H.F.,

editors (1984): The Geological Evolution of the eastern Mediterranean. Geol. Soc. London, Spec. Publ., 17: 603–618.

Drury M.R. and van Roermund  H.L.M., 1988: Metasomatic origin for Fe-Ti-rich multiphase inclusions in olivine from kimberlite xenoliths. Geology, 16, 1035-1038.

Ernewein, M., Pflumio, C., and Whitechurch, H., 1988. The death of an accretion zone as evidenced by the magmatic history of the Sumail Ophiolite (Oman), in The Ophiolites of Oman, edited by F. Boudier and A. Nicolas, Tectonophysics, 151, 247-274.

Ewart, A., Bryan, W.B., Gill, J.B., 1973. Mineralogy and geochemistry of the younger volcanic islands of Tonga, S.W. Pacific. J. Petrol. 14, 429–465.

Ewart A., and Hawkesworth C.J., 1987. The Pleistocene–Recent Tonga–Kermadec arc lavas: interpretation of new isotopic and rare earth data in terms of a depleted mantle source model, Journal of Petrology, 28, pp. 495–530.

Ferrière, J., 1982. Paléogéographie et tectonique superposéoes dans les Hellenides internes: les massifs de l'Othrys et du Pélion (Grèce septentrionale). Sociétéde la Géologie du Nord 8, 1 – 970.

Ferrière. J., Bonneau, M., Caridroit. M., Bellier, J.-P., Gorican, S. & Kollmann. H. 2001. Les nappes tertiaires du Paikon (zone du Vardar, Macédoine, Grèce): arguments stratigraphiques pour une nouvelle interprétation structurale. Comptes Rendus de l'Académie des Sciences, Earth and Planetary Sciences, 332, 695-702.

Flower, M.F.J. & Dilek, Y. 2003. Arc-trench rollback and forearc accretion: I. A collision-induced mantle flow model for Tethyan ophiolites. In: DILEK, Y. & ROBINSON, P.T. (eds) Ophiolites in Earth History. Geological Society, London, Special Publications, 218, 21-41.

Gass, I.G., Neary, C.R., Plant, J., Robertson, A.H.F., Simonian,K.O., Swewing, J.D.., Spooner, E.T.C., Wilson, R.A.M., 1975.Comments on "The Troodos ophiolitic complex was probably formed in an island arc" by A. Miyashiro. Earth and Planetary Science Letters 25, 236–238.

Gauthier, A., 1984. La ceinture ophiolitique de Chalcidique (Grèce du Nord) : Etude d'un cas de variations longitudinales, pétrologiques et structurales. Thèse 3$^e$ cycle, Université de Nancy 1, 290p.

Godfriaux, I., Ricou, L.E., 1991. Le Paikon, une feneˆtre dans les He´llenides internes (Macedoine, Gre`ce). C.R. Acad. Sci., Paris 313 (II), 1479– 1484.

Goldstein S.L, O'Nions R.K., and Hamilton P.J., 1984. A Sm-Nd study of atmospheric dusts and particulates from major river systems. Earth and Planetary Science Letters, 70, 221-236.

Gurenko, A.A. & Chaussidon, M., 1995. Enriched and depleted primitive melts included in olivine from Icelandic tholeiites: origin by continuous melting of a single mantle column. Geochim. Cosmochim. Acta 59, 2905-2917.

Gumann, S., Lahaye, Y. & Brey, G. P. 2003: Iridium-Strip – Rhyolite enthüllen ihre Details. Berichte der Deutschen Mineralogischen Gesellschaft, Beiheft zum European Journal of Mineralogy, 15, 72.

Haenel-Remy S., & Bébien J., 1985. The Oreokastro ophiolite (Greek Macedonia): an important component of the innermost Hellenic ophiolite belt. Ofioliti, 10 ,2/3, 279.

Hamelin, B., Dupre, B., and Allegre, C. J., 1984.The lead isotope systematics of ophiolite complexes, Earth Planet. Sci. Lett., 67(3), 351-366.

Hanan, B. B., and Schilling, J.-G., 1989. Easter microplate evolution: Pb isotope evidence, J. Geophys. Res., 94, 7432-7448.

Hart, S.R., & Dunn, T., 1993. Experimental cpx/melt partitioning of 24 trace elements. Contrib. Mineral. Petrol. 113, 1-8.

Harris, N.B.W., Kelley, S., Okay, A.I., 1994. Post-collision magmatism and tectonics in northwest Anatolia. Contrib. Mineral. Petrol. 117, 241–252.

Hawkesworth, C.J., Norry, M. J., Roddick, J.C., Baker, P.E., Francis, P.W., Thorpe, R.S. 1979. $^{143}Nd/^{144}Nd$, $^{87}Sr/^{86}Sr$ and incompatible element variations in calc-alkaline andesites and plateau lavas from South America. Earth Planet Sci Lett 42:45-57.

Hawkesworth, C.J., Powell, M., 1980. Magma genesis in the Lesser Antilles island arc. Earth Planet Sci Lett 51:297-308.

Hawkesworth, C.J., Gallagher, K., Hergt, J.M., & McDermott, F., (993. Mantle slab contributions in arc magmas. Annu. Rev. Earth Planet. Sci. 21, 175-204.

Hebert, R., and Laurent, R., 1990.Mineral chemistry of the plutonic section of the Troodos Ophiolite: New constraints for genesis of arc-related ophiolites, in Ophiolites: Oceanic Crustal Analogues: Proceedings of the Symposium ``Troodos 1987'', edited by J. Malpas, E.M. Moores, A. Panayiotou, and C. Xenophontos, pp. 149-163, Geol. Surv. Dep., Nicosia, Cyprus.

Hellebrand, E., Snow, J. E., Mühe, R., 2002. Mantle melting beneath Gakkel Ridge Arctic Ocean: abyssal peridotite spinel compositions Chemical Geology 182, 227–235.

Himmerkus, F., Reischmann T. & Kostopoulos D., 2002. First evidence for Silurian Magmatism in the Serbo-Macedonian Massif, northern Greece, Geochimica et Cosmochimica Acta , 66, A330. Goldschmidt Conference Abstract Volume.

Himmerkus F., Reischmann T. & Kostopoulos D., 2003. The Serbo-Macedonian Massif, the oldest crustal segment of the internal Hellenides, identified by zircon ages. Geophysical Research Abstracts, 5: 05671.

Himmerkus F., Reischmann T. & Kostopoulos D., 2004b. Triassic rifting recorded in Gondwana derived Tethyan terranes, Serbo-Macedonian Massif, northern Greece. Berichte der Deutschen Mineralogischen Gesellschaft, Beihefte zum European Journal of Mineralogy, Vol. 16: 57.

Himmerkus F., Reischmann T. & Kostopoulos D., 2006: Late Proterozoic and Sillurian basement units within the Sebo-Macedonian Massif, northern Greece: the significance of therrane accretion in the Hellenides. In Roberston, A. H. F. & Mountrakis, D. (eds). Tectonic Development of the Eastern Mediterranean Region. Geological Society, London, Special Publications, 260, 35–50.

Himmerkus F., Zachariadis, P., Reischmann T. & Kostopoulos D. 2005: The mafic complexes of the Athos-Volvi- Zone – a suture zone between the Serbo-Macedonian Massif and the Rhodope Massif? Geophysical Research Abstracts, 7, 10240.

IGME 1983: Geological Map of Greece, scale 1:500 000, Institute of Geology and Mineral Exploration, Athens.

Ito, E., White, W. M., and Goepel, C., 1987. The O, Sr, Nd and Pb isotope geochemistry of MORB, Chem. Geol., 62(3-4), 157-176.

Jacobshagen, V. (Editor.), 1986. Geologie von Griechenland. Gebrüder Borntraeger, Berlin, Stuttgart, 363 p.

Jackson, E.D., Green, H.W., Moores, E.M., 1975. The Vourinos ophiolite, Greece: cyclic units of lineated cumulates overlying harzburgite tectonite. Geol. Soc. Amer. Bull. 86, 390– 398.

Jacobsen, S. B., and Wasserburg, G. J., 1979. Nd and Sr isotopic study of the Bay of Islands ophiolite complex and the evolution of the source of midocean ridge basalts, J. Geophys. Res., 84, 7429-7445.

Jochum, K. P., Dingwell, D. B., Rocholl, A., Stoll, B., Hofmann, A. W., Becker, S., et al. 2000. The preparation and preliminary characterisation of eight geological MPI-DING reference glasses for in-situ microanalysis. Geostandards Newsletter 24, 87–133.

Johnson, K.T.M., Dick, H.J.B., & Shimizu, N., 1990. Melting in the oceanic upper mantle, an ion microprobe study of diopsides in abyssal peridotites. J. Geophys. Res. 95, 2661-2678.

Johnson M.C. & Plank T., 1999. Dehydration and Melting Experiments Constrain the Fate of Subducted Sediments. Geochemstry Geophysics Geosystems. 1, 1999GC000014.

Jones, G., Robertson, A.H.F., 1991. Tectono-stratigraphy and evolution of the Pindos ophiolite and associated units. J. Geol. Soc. 148, 267– 288.

Jones, J.H., 1995. Experimental trace element partition. In Rock Physics and Phase Relations, a Handbook of Physical Constants. American Geophysical Union, Washington, D.C. (73-104).

Jung, G., Mussallam, K., Burgath, K., Kockel, F., Mohr, M., Raschka, H., 1980. Ultramafic and related rocks of Chalkidiki. Proc. Int. Symp. Metals Mafic Ultramafic Complexes, vol. 3, pp. 24–42.

Jung, G., Mussallam, K., 1985. The Sithonia ophiolite: a fossil oceanic crust. Ofioliti 10, 329– 342.

Juteau, T., Beurrier, M., Dahl, R., and Nehlig, P., 1988. Segmentation at a fossil spreading axis: The plutonic sequence of the Wadi Haymiliyah area (Haylayn Block, Sumail Nappe, Oman), in The Ophiolites of Oman, edited by F. Boudier and A. Nicolas, Tectonophysics, 151, 167- 197.

Juteau, T., M. Ernewein, I. Reuber, H. Whitechurch, and R. Dahl, 1988. Duality of magmatism in the plutonic sequence of the Sumail Nappe, Oman. Tectonophysics, 15, 107-135.

Kamenetsky, V., Crawford, A.J. and Meffre, S, 2001. Factors controlling chemistry of magmatic spinel: an empirical study of associated olivine, Cr-Spinel and melt inclusions from primitive rocks. Journal Of Petrology. 42, 4, 655-671.

Karamata, S., Lovric, A., 1978. The age of metamorphic rocks of Brezovica and its importance for the explanation of ophiolite emplacement. Bull. Acad. Serb. Sci. Arts, Cl. Natur. Math. Sci. Natur. 17, 1 –9.

Kassoli-Fournaraki, A., 1990. Metabasite dikes in the southeastern part of the Chortiatis series (Northern Greece): petrology and P-T conditions of metamorphism. Schweizerische Mineralogische und Petrographische Mitteilungen, 70, 437-447.

Kauffmann, G., Kockel, F., and Mollat, H., 1976. Notes on the stratigraphic and paleogeographic position of the Svoula Formation in the Innermost Zone of thhe Hellenides (Northern Greece). Bull. Soc. Geol. France, 18, 225-230.

Kay, R.W., Hubbard, N.J., 1978. Trace elements in ocean ridge basalts. Earth Planet Sci Lett 38:95–116.

Keppler, H., 1996. Constraints from partitioning experiments on the composition of subduction-zone fluids, Nature, 380, 237-240.

Klein, E.M., 2004. Geochemistry of the Igneous Oceanic Crust. In: Treatise on Geochemistry. Holland, H.D. and Turekian, K.K. (Editors), Elsevier, Amsterdam. 3: 433-463.

Kober, B., 1986. Whole grain evaporation for $^{207}Pb/^{206}Pb$ age investigations on single zircons using a double filament thermal ion source. Contributions to Mineralogy and Petrology 93, 482–90.

Koepke, J., Kreuzer, H., Seidel, E., 1985. Ophiolites in the Southern Aegean arc (Crete, Karpathos, Rhodes)—linking the ophiolite belts of the Hellenides and the Taurides. Ofioliti 10, 343–354.

Koepke, J., Seidel, E., Kreuzer, H., 2002. Ophiolites on the Southern Aegean islands Crete, Karpathos and Rhodes: composition, geochronology and position within the ophiolite belts of the Eastern Mediterranean. Lithos 65, 183– 203.

Koglin N., Reischmann T., Kostopoulos D., Matukov D., Sergeev S., 2007. Zircon SHRIMP ages and the origin of ophiolitic rocks from the NE Aegean region, Greece. Geophysical Research Abstracts, Vol. 9, EGU2007-A-06848

Kostopoulos, D., 1988. Geochemistry, Petrogenesis and Tectonic Setting of the Pindos ophiolite, NW Greece. PhD Thesis. Univ. of Newcastle upon Tyne. 528 pp.

Kostopoulos, D. K., & Murton, B. J., 1992. Origin and distribution of components in boninite genesis: significance of the OIB component. In: Murton, L. M. & Browning, P. (eds) Ophiolites and Their Modern Oceanic Analogues. Geological Society, London, Special Publication 60, 133-154.

Kostopoulos, D. K., Reischmann, T., & Sklavounos, S. A., 2001. Palaeozoic and Early Mesozoic magmatism and metamorphism in the Serbo-Macedonian Massif, central Macedonia, northern Greece. EUG XI, Symposium LS03, p.318.

Kelemen, P.B., Hanghoj, K., and Greene, A.R., 2004. One View of the Geochemistry of Subduction-related Magmatic Arcs, with an Emphasis on Primitive Andesite and Lower Crust. In: Treatise on Geochemistry. Holland, H.D. and Turekian, K.K. (Editors), Elsevier, Amsterdam. 3: 593-659.

Kober, B., 1987. Single-zircon evaporation combined Pb + emitter-bedding for $^{207}Pb/^{206}Pb$ age investigations using thermal ionmass spectrometry, and applications to zirconology. Contributions to Mineralogy and Petrology 96, 63–71.

Kockel, F., & Mollat, H., 1977. Erläuterungen zur geologischen Karte der Chalkidiki und angrenzender Gebiete 1:100000 (Nord-Griechenland). Bundesanstalt für Geowissenschaften und Rohstoffe, Hannover 119 p.

Lanphre, M.A., Coleman, R.G., Karamata, S., Pamic, J., 1975. Age of amphibolites associated with Alpine peridotites in the Dinaride ophiolite zone, Yugoslavia. Earth Planet. Sci. Lett. 26, 271–276.

Larionov, A. N., Andreichev, V. A. & Gee D. G., 2004. The Vendian alkaline igneous suite of northern Timan: ion microprobe U–Pb zircon ages of gabbros and syenite. In: GEE, D. G. &

Liati, A., Gebauer, D., Fanning, C. M., 2004. The age of ophiolitic rocks of the Hellenides

(Vourinos, Pindos, Crete): first U–Pb ion microprobe (SHRIMP) zircon ages. Chemical Geology, 207, 171– 188.

Lindsley, D.H., 1983. Pyroxene thermometry. Am Mineral 68: 477–493

Ludwig, K. R., 2005a. SQUID 1.12 A User's Manual. A Geochronological Toolkit for Microsoft Excel. Berkeley Geochronology Center Special Publication. 22 p. http://www.bgc.org/klprogrammenu.html

Ludwig, K. R., 2005b. User's Manual for ISOPLOT/Ex 3.22. A Geochronological Toolkit for Microsoft Excel. Berkeley Geochronology Center Special Publication. 71 p.

Magganas, A., 2002. Constraints on the petrogenesis of Evros ophiolite extrusives, NE Greece. Lithos 65: 165–182

Malpas, J., Moores E. M., 1990. In A. Panayiotou, and C. Xenophontos (Eds.), Ophiolites: Oceanic Crustal Analogues: Proceedings of the Symposium ``Troodos 1987'', 733 pp., Geol. Surv. Dep., Nicosia, Cyprus.

McCulloch, M.T. and Gamble, J.A., 1991. Geochemical and geodynamical constraints on subduction zone magmatism. Earth Planet. Sci. Lett., 102, 358–374.

McCulloch, M. T., and Cameron, W. E., 1983. Nd-Sr isotopic study of primitive lavas from the Troodos ophiolite, Cyprus: Evidence for a subduction-related setting, Geology, 11(12), 727-731.

McCulloch, M. T., R. T. Gregory, G. J. Wasserburg, and H. P. Taylor Jr., 1980. A neodymium, strontium, and oxygen isotopic study of the Cretaceous Samail Ophiolite and implications for the petrogenesis and seawater-hydrothermal alteration of oceanic crust. Earth Planet. Sci. Lett., 46(2), 201-211.

McDonough, W.F., and S.-s. Sun, The composition of the Earth, Chem. Geol., 120, 1995, 223-253.

Mercier, J. 1966. Mouvements orogéniques et magmatisme d'age Jurassique Supérieur–É ocrétacé dans les Zones Internes des Hellénides (Macédoine, Grèce). Revue de Géographie Physique et de Géologie Dynamique (2), VIII(4), 265–278.

Mercier, J. & Vergély, P. 1994. Is the Paikon Massif a tectonic window in the Axios–Vardar Zone? (Internal Hellenides, Macedonia, Greece). Bulletin of the Geological Society of Greece, XXX(1), 115–120.

Mercier, J., Vergély, P. & Bébien, J. 1975. Les ophiolites helléniques «obductées» au Jurassique supérieur sont-elles les vestiges d'un Océan téthysien ou d'une mer marginale péri-européene? Comptes Rendes Sommaires de la Société Géologique de France, 17, 108–111.

Meshede M. 1986. A method of discriminating between different types of Mid-Ocean ridge basalts and continental tholeiites with the Nb-Zr-Y diagram. Chem Geol 56 (3/4): 207-218.

Michard, A., Feinberg, H., Montigny, R., 1998. Supra-ophiolite formations from the Thessaloniki nappes (Greece) and associated magmatism; an intra-oceanic subduction predating the Vardar obduction. C.R. Acad. Sci., Paris 327, 437–499.

Michard, A., Goffé, B., Liati, A. & Mountrakis, D. 1994. Blueschist-facies assemblages in the peri-Rhodopian zone, and hints for an eohellenic HP–LT belt in northern Greece. Bulletin of the Geological Society of Greece, XXX(1), 185–192.

Miyashiro, A., 1973. The Troodos ophiolite complex was probably formed in an island arc complex. Earth and Planetary Science Letters 19, 218– 224.

Moore, J.G., 1975, Mechanism of formation of pillow lava: American Scientist, v. 63, p. 269-277.

Moores, E.M., 1969. Petrology and structure of the Vourinos ophiolitic complex of northern Greece. Special Paper-Geological Society of America 118.

Moores, E.M., Vine, F.J., 1971. The Troodos Massif, Cyprus and other ophiolites as oceanic crust: evaluations and implications. Philosophical Transactions of the Royal Society of London. A 268, 433– 466.

Morimoto, N., 1989. Nomenclature of pyroxenes, Can. Mineral. 27, pp. 143–156.

Mountrakis, D., 1984. Γεωλογία της Ελλάδας (engl. transl. Geology of Greece). University Press.

Mountrakis, D., 1984. Structural evolution of the Pelagonian Zone in Northwestern Macedonia, Greece. In: Dixon JE, Robertson AHF (eds) The geological evolution of the Eastern Mediterranean. Geol Soc Lond Spec Publ 17:581-590.

Mountrakis, D., 1986. The Pelagonian Zone in Greece: a polyphase-deformed fragment of the Cimmeran Continent and its role in the geotectonic evolution of the eastern Mediterranean. Journal of Geology, 94, 335–347.

Münker, C., Wörner, G., Yogodzinskic, G., Churikova, T., 2004. Behaviour of high field strength elements in subduction zones: constraints from Kamchatka–Aleutian arc lavas Earth and Planetary Science Letters 224, 275– 293.

Mussallam, K., 1991. Geology, geochemistry and the evolution of an oceanic lithosphere rift at Sithonia, NE Greece. In: Peters, T., Nicholas, A., Coleman, R.G. (Eds.), Ophiolite Genesis and Evolution of Oceanic Lithosphere. Kluwer Academic Publishing, Dordrecht, pp. 685–704.

Mussallam, K. & Jung D. 1986. Petrology and geotectonic significance of salic rocks preceding ophiolites in the eastern Vardar Zone, Greece. TMPM Tschermaks Mineralogische und Petrographische Mitteilungen 35, 217–42.

Neumann, P., & Zacher, W., 2004. The Cretaceous sedimentary history of the Pindos Basin (Greece). Int J Earth Sci (Geol Rundsch) 93:119–131

Nicolas, A., 1989. Structures of ophiolites and dynamics of oceanic lithosphere. Series in Petrology and Structural Geology, vol. 4. Kluwer Academic Publishing, Dordrecht. 367 pp.

Nicolas, A., and Boudier, F., 2003. Where ophiolites come from and what do they tell us. Geol. Soc. Am. (Spec. Paper), 373, 137–152.

Nimis, P., 1995. A clinopyroxene geobaromete for basaltic systems based on crystal-structure modeling. Contribut. Mineral. Petrol., 121, 115-125.

Nimis, P., 1999. Clinopyroxene geobarometry of magmatic rocks. Part 2. Structural geobarometers for basic to acid, tholeiitic and mildly alkaline magmatic systems. Contributions to Mineralogy and Petrology 135, 62–74.

Okrusch, M., Seidel, E., Kreuzer, H., Harre, W., 1978. Jurassic age of metamorphism at the base of the Brecovica peridotite (Yugoslavia). Earth Planet. Sci. Lett. 39, 291–297.

Ozawa, K., & Shimizu, N., 1995. Open-system melting in the upper mantle: constraints from the Hayachine–Miyamori ophiolite, northeastern Japan. J. Geophys. Res. 100, 22,315-22,335.

Palmer, M.R., and Edmond, J.M., 1989. The Strontium Isotope Budget of the Modern Ocean. Earth and Planetary Science Letters 92(1): 11-26. doi: 10.1016/0012-821X(89)90017-4.

Papanikolaou., D., 1986. Γεωλογία της Ελλάδας (engl. transl. Geology of Greece). University of Athens, lecture notes. 253p.

Parlak, O., Delaloye, M., 1996. Geochemistry and timing of post-metamorphic dike emplacement in the Mersin ophiolite (southern Turkey): new age constraints from 40Ar=39Ar geochronology. Terra Nova 8, 585–592.

Parlak, O. & Delaloye, M. 1999. Precise $^{40}Ar\sim^{39}Ar$ ages from the metamorphic sole of the Mersin ophiolite (southern Turkey). Tectonophysics, 301, 145-158.

Parlak, O., Delaloye, M., Bingol, E., 1995. Origin of subophiolitic metamorphic rocks beneath the Mersin ophiolite, southern Turkey. Ofioliti 20, 97–110.

Pearce, J.A., 1982. Trace element characteristics of lavas from destructive plate boundaries. In Andesites: Orogenic Andesites and Related Rocks (R.S. Thorpe, ed.). John Wiley & Sons, Chichester, U.K. (525-548).

Pearce J.A., 1983. Role of the sub-continenetal lithosphere in magma genesis at active continental margin. In: C.J. Hawkesworth and M.J. Norry (Eds.), Continental basalts and mantle xenoliths. Shiva Publ. Co., Nantwich, p. 230-249.

Pearce, J.A., 1996. A user's guide to basalt discrimination diagrams. In: Trace element geochemistry of volcanic rocks; applications for massive sulphide exploration. Short Course Notes, Geol. Ass. Can. 12, 79-113.

Pearce, J.A., Baker, P.E., Harvey, P.K., & Luff, I.W., 1995. Geochemical evidence for subduction fluxes, mantle melting and fractional crystallization beneath the South Sandwich Island arc. J. Petrol. 36, 1073-1109.

Pearce, J.A., Cann, J.R., 1973. Tectonic setting of basic volcanic rocks determined using trace element analysis. Earth and Planetary Science Letters 19, 290– 300.

Pearce, J.A., Harris, N.B.W., & Tindle, A.G., 1984. Trace element discrimination diagrams for the tectonic interpretation of granitic rocks. Journal of Petrology, 25, 956–983.

Pearce, J.A., Lippard, S.J., Roberts, S., 1984. Characteristics and tectonic significance of supra-subduction zone ophiolites. In: Kokelaar, B.P., Howells, M.F. (Eds.), Marginal Basin Geology. Special Publication-Geological Society of London, vol. 6, pp. 77– 89.

Pearce, J.A., and Norry, M.J., 1979. Petrogenetic Implications of Ti, Zr, Y, and Nb Variations in Volcanic Rocks. Contributions to Mineralogy and Petrology, 69: 33-47.

Pearce, J.A., & Peate, D.W., 1995. Tectonic implications of the composition of volcanic arc magmas. Annu. Rev. Earth Planet. Sci. 23, 251-285.

Pearce J., Stern J., Bloomer S. and Fryer P., 2005. Geochemical mapping of the Mariana arc-basin system: Implications for the nature and distribution of subduction components. Geochemstry Geophysics Geosystems. 6, doi:10.1029/2004GC000895.

Peccerillo, A., and Taylor, S.R., 1976. Geochemistry of Eocene calc-alkaline volcanic rocks from the Kastamonu area, northern Turkey. Contributions to Mineralogy and Petrology, 58, pp. 63–81.

Peucat, J.J., Vidal, P., Bernard-Griffiths, J., and Condie, K.C., 1988. Sr, Nd and Pb isotopic systematics in the Archean low to high-grde transition zone of southern India: syn accretion vs. post accretion granultes. Journal of Geology, 97, 537-550.

Plank, T., and Langmuir, C.H., 1998. The geochemical composition of subducting sediment and its consequences for the crust and mantle. Chemical Geology 145: 325-394

Rassios, A., Smith, A.G., 2000. Constraints on the formation and emplacement age of western Greek ophiolites (Vourinos, Pindos, Othrys) inferred from deformation structures in peridotites. Geol. Soc. Am., Spec. Pap. 349, 473–483.

Rehkamper, M., and Hofmann, A.W., 1997. Recycled ocean crust and sediment in Indian Ocean MORB. Earth and Planetary Science Letters 147(1-4): 93-106.

Reisberg, L., & Zindler, A., 1986. Extreme isotopic variation in the upper mantle: evidence from Ronda. Earth and Planetary Science Letters 81, 29–45

Ricou, L.-E., Burg, J.-P., Godfriaux, I., Ivanov, Z. 1998. Rhodope and Vardar: the metamorphic and the olistostromic paired belts related to the Cretaceous subduction under Europe. Geodynamica Acta (Paris), 11, (6): 285-309.

Ricou, L.E., Godfriaux, I., 1991. Une coupe a` travers les ophiolites et gneiss allochthones entre le massif Pelagonien et la feneˆtre du Paikon (Gre`ce du Nord). C.R. Acad. Sci., Paris 313 (II), 1595– 1601.

Ricou, L.E., Godfriaux, I., 1995. Mise au point sur la feneˆtre multiple du Paikon et la structure du Vardar en Gre`ce. C.R. Acad. Sci., Paris, Seˆrie IIa 321, 601– 608.

Robinson, P. T., and Malpas, J., 1990. The Troodos ophiolite: New perspective on its origin and emplacement, in Ophiolites: Oceanic Crustal Analogues: Proceedings of the Symposium ``Troodos 1987'', edited by J. Malpas, E. M. Moores, A. Panayiotou, and C. Xenophontos, pp. 13-26, Geol. Surv. Dep., Nicosia, Cyprus,

Roddick, J.C., Cameron, W.A., Smith, A.G., 1979. Permo-Triassic and Jurassic 40Ar/39Ar ages from Greek ophiolites and associated rocks. Nature 279, 788– 790.

Rudnick, R.L., and Gao, S., 2004. Composition of the Continental Crust. In: Treatise on Geochemistry. Holland, H.D. and Turekian, K.K. (Editors), Elsevier, Amsterdam. 3: 1-64.

Sharp, I. & Robertson, A. 1994. Late Jurassic–Lower Cretaceous oceanic crust and sediments of the eastern Almopias Zone, NW Macedonia (Greece); implications for the evolution of the eastern 'Internal' Hellenides. Bulletin of the Geological Society of Greece, XXX(1), 47–61.

Saunders, A.D., Tarney, J., Weaver, S.D., 1980. Transverse geochemical variations across the Antarctic Peninsula: implications for the genesis of calc-alkaline magmas. Earth Planet Sci Lett 46:344- 360

Sapountzis, E., 1979. The Thessaloniki gabbros. /. Petrology, 20, 37-70.

Schunemann, M., 1985. Contributions of the geology, geochemistry and tectonics of the Chortiatis Series metamorphic calc-alkaline suite, Chalkidiki, northern Greece, PhD Thesis, Univ. Hamburg, 165.

Serri, G., 1981. The petrochemistry of ophiolite gabbroic complexes: a key for the classification of ophiolites into low-Ti and high-Ti types. Earth Planet. Sci. Lett. 52, 203–212.

Shaw, M.D., .2000. Continous (Dynamic) melting theory revised. The Canadian Mineralogist, vol.38,1041-1063.

Shervais, J.W., 1982. Ti-V plots and the petrogenesis of modern and ophiolitic lavas. Earth Planet Sci Lett 59:101–118.

Shervais, J.W., 2001. Birth, death, and resurrection: The life cycle of suprasubduction zone ophiolites. G3 - Geochemistry, geophysics geosystems. An electronic journal of the earth sciences, 2, available from the address: http://g-cubed.org.

Soldatos, T., Koroneos, A., Christofides, G., 1993. Origin and evolution of the Fanos granite (Macedonia, Northern Greece): trace and REE modelling constraints. In Panagos's Honorary Volume. Technical University Publications B: Athens; 330-349.

Spandler, C., Hermann, J., Arculus, R., and Mavrogenes, J., 2004. Geochemical heterogeneity and elemental mobility in deeply subducted oceanic crust; insights from high-pressure mafic rocks from New Caledonia, Chem. Geol. 206 (2004), pp. 21–42.

Spray, J. G., Bébien, J., Rex, D. C., Rodick, J. C., 1984. Age constraints on the igneous and metamorphic evolution of the Hellenic-Dinaric ophiolites. In: Dixon, J. E., & Robertson, A. H. F. (Eds.), The Geological Evolution of the Eastern Mediterranean. Geol. Soc. London, Sp. Publ., 17, 619– 627.

Spray J.G. and Roddick J.C., 1980. Petrology and  40Ar/39Ar Geochronology of some Hellenic Sub-Ophiolite Metamorphic rocks. Contributions to mineralogy and petrology, 72, 43-55.

Stacey, J. S. & Kramers, J. D. 1975: Approximation of terrestrial lead isotope evolution by a two-stage model. Earth and Planetary Science Letters, 26, 207-221.

Stais A., 1993, Evolution geodynamique des basins msozoiques vardariens: domains de Peonias et d ' Almopias. These de Dostorat de l ' Universite des Sciences et Technologies de Lile.

Steidger, R. H. & Jäger, E. 1977. Subcommission on geochronology: convention on the use of decay constants in geo- and cosmochronology. Earth and Planetary Science Letters, 36, 359–362.

Steinmann, G., 1927. Die ophiolitischen Zonen in den mediterranen Kettengebirgen. C. R. XVIme Congr. Geol. Int., 1926, Fasc. II, 637–667.

Stern, R.J., Bloomer, S.H., 1992. Subduction zone infancy: examples from the Eocene Izu – Bonin–Mariana and Jurassic California arcs. Geological Society of America Bulletin 104, 1621–1636.

Suess, E., 1893. Are great ocean depths permanent? Natural Sciences 2: 180 –187.

Suess, E., 1909. Das Antlitz der Erde. (Bd 31) Tempsky, Vien Freytag Leipzig.

Sun, S.-s., and McDonough, W.F., 1989. Chemical and isotopic systematics of oceanic basalts: Implications for mantle composition and processe.  In Magmatism in ocean basins eds A.D. Saunders and M.J. Norry. Geological Society Special Publication Classics. 313-345.

Suzuki, K., 1987. Grain-boundary enrichment of incompatible elements in some mantle peridotites. Chemical Geology, 63, 319-334.

Tatsumi, Y., Eggins, S., 1995. Subduction Zone Magmatism. Blackwell, London, 211 pp.

Taylor, B., and F. Martinez, Back-arc basin basalt systematics, Earth Planet. Sci. Lett., 210, 481-497.

Tera, F., Wasserburg. G.J., 1972. U–Th–Pb systematics in three Apollo 14 basalts and the problem of initial Pb in lunar rocks. Earth Planet Sci Lett 14:281–304.

Theye T., Seidel E., & Vidal O., 1992. Carpholite, sudoite, and chloritoid in low-grade high-pressure metapelites from Crete and the Peloponnese, Greece. Eur. J. Mineral., 4, 487-507.

Thuizat, R., Whitechurch, H., Montigny, R., Juteau, T., 1981. K– Ar dating of some infra-ophiolitic metamorphic soles from the Eastern Mediterranean: new evidence for oceanic thrustings before obduction. Earth Planet. Sci. Lett. 52, 302– 310.

Tsikouras, B., 1992. "Οι Οφιόλιθοι της Νήσου Σαμοθράκης. Διερεύνηση των γεωλογικών, πετρολογικών και γεωχημικών χαρακτηριστικών των οφιόλιθων και γειτονικών τους εμφανίσεων." ("The ophiolites of Samothraki Island. Investigations of the geological, petrological and geochemical characteristics of the ophiolites and of the associated adjacent formations") PhD Thesis, University of Patras, Greece.

Tsikouras, B., Pe-Piper, G., & Hatzipanagiotou, K., 1990. A new date for an ophiolite of the northeastern margin of the Vardar Zone, Samothraki, Greece. N. Jb. Miner. Mh., H. 11, 521-527.

Tsikouras, B., Hatzipanagiotou, K., 1998. Petrogenetic evolution of an ophiolite fragment in an ensialic marginal basin, northern Aegean (Samothraki Island, Greece). European Journal of Mineralogy 10, 551– 567.

Turpaud P., 2006. Characterization of igneous terranes by zircon dating: implications for the UHP relics occurrences and suture identification in the Central Rhodope Greece. Phd Thesis, Johannes Gutenberg University of Mainz, Germnany, 107p.

Umino, S., Yanai, S., Jaman, A. R., Nakamura, Y., and Iiyama, J. T., 1990.The transition from spreading to subduction: Evidence from the Semail Ophiolite, northern Oman Mountains, in Ophiolites: Oceanic Crustal Analogues: Proceedings of the Symposium ``Troodos 1987'', edited by J. Malpas, E.M. Moores, A. Panayiotou, and C. Xenophontos, pp. 149-163, Geol. Surv. Dep., Nicosia, Cyprus.

van Hinsbergen, D.J.J. , Hafkenscheid, E., Spakman, W., Meulenkamp, J.E., Wortel, W., 2005. Nappe stacking from subduction of oceanic and continental lithosphere below Greece. Geology, v.33, 325-328.

Vermeesch P., 2006b: Tectonic discrimination diagrams reivised. Geochemistry Geophysics Geosystems, 7, Nr.6.

White, W. M. & Patchett, J. 1984: Hf-Nd-Sr isotopes and incompatible element abundances in island arcs: implications for magma origins and crust mantle evolution. Earth and Planetary Science Letters, 67, 167-185.

Williams I.S. 1998. U-Th-Pb Geochronology by ion microprobe. In: Applications in microanalytical techniques to understanding mineralizing processes. Revievs in Economic Geology., v7, p.1-35.

Wiedenbeck, M., Alle′, P., Corfu, F., Griffin, W. L., Meier, M., Oberli, F., von Quadt, A., Roddick, J. C. & Spiegel, W. 1995: Three natural zircon standards for U-Th-Pb, Lu-Hf, trace

element and REE analyses. Geostandards Newsletter, 19, 1-23.

Winchester, J.A., Floyd, P.A., 1977. Geochemical discrimination of different magma series and their differentiation products using immobile elements. Chem Geol 20: 325–343.

Witt, G. and Seck, H.A., 1989. Origin of amphibole in recrystalised and porphyroblastic mantle xenoliths from Rhenish Massif: implications for the nature of mantle metasomatism. Earth and Planetary Science Letters, 91, 327-340.

Wood, D.A., 1980. The application of a Th–Hf–Ta diagram to problems of tectonomagmatic classification, and to establishing the nature of crustal contamination of basaltic lavas of the British Tertiary volcanic province. Earth Planet. Sci. Lett. 50, 11-30.

Workman, R.K., and Hart, S.R., 2005. Major and trace element composition of the depleted MORB mantle (DMM). Earth and Planetary Science Letters 231: 5.

Yilmaz, P.O., Maxwell, J.C., 1982. K–Ar investigations from the Antalya complex ophiolites, SW Turkey. Ofioliti 2, 527–538.

Yang, Huai-Jen, Sen, G., & Shimizu, N., 1998. Mid-ocean ridge melting: constraints from lithospheric xenoliths at Oahu, Hawaii. J. Petrol. 39, 277-295.

Zachariadis P., 2002. Petrology and geochemistry of the Oraeokastron Ophiolite, northern Greece. M.Sc. Thesis, Aristotle University of Thessaloniki, Greece (in Greek, with English Summary).

Zack, T., Foley, S.F., & Jenner, G.A., 1997. A consistent partition coefficient set for clinopyroxene, amphibole and garnet from laser ablation microprobe analysis of garnet pyroxenites from Kakanui, New Zealand. Neues Jahrb. Mineral., Abh. 172, 23-41.

Zindler, A., and Jagoutz, E., 1988. Mantle cryptology. Geochemica and Csmochemica Acta. 52, 319-333.

# APPENDICES

# APPENDIX A

---

## Sample localities

In this appendix we present the GPS coordinates of the sample localities as well as their field description.

## APPENDIX A-Ia : SKRA SAMPLES

| sample name | | description | comments | GPS | |
|---|---|---|---|---|---|
| GVL | 1 | dyke | vesicular | n.a. | n.a. |
| GVL | 2 | dyke | | n.a. | n.a. |
| GVL | 3 | dyke | | n.a. | n.a. |
| GVL | 4 | dyke | | n.a. | n.a. |
| GVL | 5 | flow | vesicular | n.a. | n.a. |
| GVL | 6 | cummulate | Px-phyric | 41.05.39 | 22.23.24 |
| GVL | 7 | cummulate | | 41.05.39 | 22.23.43 |
| GVL | 8 | dyke | mafic intrudind GVL 7 | 41.05.45 | 22.24.53 |
| GVL | 9 | dyke | | 40.05.42 | 22.25.01 |
| GVL | 10 | dyke | fine grained | // | // |
| GVL | 11 | dyke | doleritic | // | // |
| GVL | 12 | dyke | | // | // |
| GVL | 13 | dyke | | 41.05.42 | 22.25.13 |
| GVL | 14 | dyke | intruding gabbro | 41.05.40 | 22.25.19 |
| GVL | 15 | dyke | Plg phyric | 41.05.42 | 22.26.14 |
| GVL | 16 | dyke | intruding gabbro | // | // |
| GVL | 17 | mullonite | felsic, Plg-granite posible protolith, Griva | 40.57.06 | 22.25.12 |
| GVL | 18 | dyke | intruding gabbro | 40.57.09 | 22.25.17 |
| GVL | 19 | dyke | | 40.57.10 | 22.25.17 |

### GOUMENISSSA TO KARPI

| sample name | | description | comments | GPS | |
|---|---|---|---|---|---|
| GVL | 20 | lava | hyaloclastite | 40.57.59 | 22.26.15 |
| GVL | 21 | lava | enclaves with zeolites | // | // |
| GVL | 22 | lava | enclaves | // | // |
| GVL | 23 | lava | fresh | // | // |

## APPENDIX A- Ib : EYZONOI SAMPLES

| sample name | | description | comments | GPS | |
|---|---|---|---|---|---|
| EYZ | 1 | dyke | intrudung in EYZ 2 | 41.07.04 | 22.33.14 |
| EYZ | 2 | dyke | | // | // |
| EYZ | 3 | dyke | chilled margin possibly of EYZ2 | // | // |
| EYZ | 4 | dyke | Px-phyric | // | // |
| EYZ | 5 | dyke | | 41.07.02 | 22.33.15 |
| EYZ | 6 | dyke | | // | // |
| EYZ | 7 | dyke | cross cuts the EYZ 6 | // | // |

### EYZONOI CUSTOMS AREA

| sample name | | description | comments | GPS | |
|---|---|---|---|---|---|
| EYZ | 8 | dyke | felsic, dacite?, mafic xenoliths | 41.06.20 | 22.33.45 |
| EYZ | 9 | dyke | vesicular | // | // |
| EYZ | 10 | dyke | | // | // |
| EYZ | 11 | dyke | | // | // |
| EYZ | 12 | dyke | | // | // |

the dacite is the last dyke that intrudes in the sequence.

| sample name | | description | comments | GPS | |
|---|---|---|---|---|---|
| EYZ | 13 | dyke | | n.a. | n.a. |
| EYZ | 14 | dyke | acidic | n.a. | n.a. |
| EYZ | 15 | lava | pillow | 41.05.11 | 22.35.01 |
| EYZ | 16 | dyke | mafic, Peukodasos locality | 41.02.17 | 22.35.07 |

## APPENDIX A-II : ORAIOKASTRO SAMPLES

| sample name | | description | comments | GPS | |
|---|---|---|---|---|---|
| ORK | 71 | gabbro | medium grained | 40.44.41 | 22.53.33 |
| ORK | 72 | gabbro | medium grained | 40.44.41 | 22.53.37 |
| ORK | 73 | gabbro | coarse grained | 40.44.40 | 22.53.38 |
| ORK | 74 | gabbro | coarse grained | na | na |
| ORK | 75 | gabbro | medium grained | na | na |
| ORK | 76 | gabbro | dark coloured gabbro | na | na |
| ORK | 77 | gabbro | leucogabbro | na | na |
| ORK | 78 | gabbro | very coarse grained dark coloured | na | na |

*the rest of the samples that are presenetd in this study have been sampled during the Msc studies of Mr. Panagiotis Zachariadis. The gps coordinates can be found in his Msc Thesis that has been planed in the Aristotle University odf Thessaloniki.*

# APPENDIX A-III : THESSALONIKI SAMPLES

| sample name | | description | comments | GPS | |
|---|---|---|---|---|---|
| | | | **KAUTANTZOGLEIO** | | |
| THS | 1 | gabbro | thin section | 40.37.40 | 22.58.38 |
| THS | 2 | dyke | contact between two dykes, thin section | | |
| THS | 3 | dyke | contact between two dykes, thin section | | |
| | | | **CENTRAL CHALKIDIKI** | | |
| THS | 4 | dunite | fresh close to Vavdos | 40.23.22 | 23.19.50 |
| THS | 5 | cummulate | Px | 40.23.31 | 23.19.53 |
| THS | 6 | cummulate | PX+Plg+Ol | | |
| THS | 7 | cummulate | PX+Plg+Ol, coarse grained | 39.55.50 | 23.43.49 |
| THS | 8 | cummulate | Px | | |
| | | | **TRIADI - LANARI** | | |
| THS | 9 | gabbro | coarse grained | 40.33.22 | 23.04.03 |
| THS | 10 | Px-ite | | 40.33.25 | 23.04.06 |
| THS | 11 | dunite | outscirts of tTriadi village | 40.32.47 | 23.03.31 |
| | | | **THESSALONIKI CITY** | | |
| THS | 12 | dunite | serpentinised, close to Phillipeion Hotel | 40.38.54 | 22.58.59 |
| THS | 13 | gabbro | medium grained | 40.38.34 | 22.58.14 |
| THS | 14 | dyke | leucocratic, Agios Pavlos | 40.38.06 | 22.58.21 |
| THS | 15 | dyke | fine grained, Agios Pavlos | // | // |
| THS | 16 | dyke | doleritic, Agios Pavlos | // | // |
| THS | 17 | dyke | fine grained | 40.37.29 | 22.58.53 |
| THS | 18 | dyke | contact of THS 17 nad THS 19 | // | // |
| THS | 19 | dyke | doleritic | // | // |
| THS | 20 | dyke | felsic | // | // |
| THS | 21 | dyke | fine grained | // | // |
| THS | 22 | dyke | includes contact of THS 21 and THS 22 | // | // |
| THS | 23 | trondjemite | pond, two bodies | 40.37.25 | 22.58.55 |
| THS | 24 | dyke | fine grained, includes chilled margin | // | // |
| | | | **AGIA ANASTASIA MONASTERY** | | |
| THS | 30 | dyke | doleritic | 40.28.18 | 23.12.19 |
| THS | 31 | dyke | intruding gabbro | 40.28.18 | 23.12.19 |
| THS | 32 | gabbro | coarse grained | 40.28.17 | 23.12.14 |
| | | | **THESSALONIKI CITY** | | |
| THS | 33 | lava | vesicular, Municipality of Agios Pavlos | 40.38.23 | 22.57.43 |
| THS | 34 | dyke | medium grained, Euagelistria subburb | 40.38.03 | 22.58.05 |
| THS | 35 | dyke | fine grained, Euagelistria subburb | // | // |
| THS | 36 | dyke | fine grained, Euagelistria subburb | // | // |
| THS | 37 | dyke | Kautantzogleio section | 40.37.40 | 22.58.38 |
| THS | 38 | dyke | Kautantzogleio section | // | // |
| THS | 39 | dyke | Kautantzogleio section | // | // |
| THS | 40 | dyke | Kautantzogleio section | // | // |
| THS | 41 | dyke | Kautantzogleio section | // | // |
| THS | 42 | dyke | Kautantzogleio section | // | // |

## APPENDIX A-IVa : METAMORPHOSIS SAMPLES

| sample name | | description | comments | GPS | |
|---|---|---|---|---|---|
| MET | 1 | Px-ite | red coloured | 40.14.06 | 23.33.66 |
| MET | 2 | gabbro | massive | * | * |
| MET | 3 | gabbro | vesicular | * | * |
| MET | 4 | Plag-granite | | * | * |
| MET | 5 | gabbro | highly sheared , thin section | * | * |
| MET | 6 | Hornblendite | pillow | * | * |
| MET | 7 | gabbro | pillow | * | * |
| MET | 8 | Hornblendite | | * | * |
| MET | 9 | lava | pillow | 40.14.02 | 23.33.51 |
| MET | 10 | gabbro | Psakoudia | 40.15.39 | 23.29.07 |

*all samples between MET 1 and MET 9 whre sampled accros the metamorphosis beach, the GPS coordinate of MET1 and MET 9 define the beginning annd end of the section*

## APPENDIX A-IVb :  KASSANDRA SAMPLES

| sample name | | description | comments | GPS | |
|---|---|---|---|---|---|
| | | | *PALIOURI* | | |
| KAS | 1 | lava | red coloured | 39.55.70 | 23.44.33 |
| KAS | 2 | flow | massive | 39.55.96 | 23.544.68 |
| KAS | 3 | lava | vesicular | | |
| KAS | 4 | flow | | 39.55.56 | 23.44.34 |
| KAS | 5 | lava | pillow, red coloured | | |
| KAS | 6 | lava | pillow | | |
| KAS | 7 | lava | pillow | 39.55.50 | 23.43.49 |
| KAS | 8 | lava | pilow, vesicular, radila cracks | 39.55.26 | |
| KAS | 9 | lava | pillow | 23.42.18 | |
| KAS | 10 | lava | pillow | | |
| KAS | 11 | lava | pillow | 39.54.46 | 23.42.13 |
| KAS | 12 | lava | pillow | 39.54.53 | 23.42.11 |
| KAS | 13 | lava | flow, fine grained | | |
| KAS | 14 | lava | flow, fine grained | 39.55.07 | 23.41.01 |
| KAS | 15 | lava | flow, fine grained | 39.55.06 | 23.40.52 |
| KAS | 16 | lava | flow, fine grained | 39.55.01 | 23.41.34 |
| KAS | 17 | lava | flw, Qz-veins and vesicles | 39.54.57 | 23.41.36 |
| KAS | 18 | lava | hyaloclastite | 39.55.18 | 23.41.48 |
| KAS | 19 | lava | vesicular | 39.55.00 | 23.43.19 |
| KAS | 20 | lava | pillow | 39.55.22 | 23.44.06 |
| KAS | 21 | lava | pillow like shaped | 39.55.30 | 23.44.43 |
| KAS | 22 | lava | pillow like shaped | 39.55.47 | 23.44.25 |

# APPENDIX A-V : SITHONIA SAMPLES

| sample name | | description | comments | GPS | |
|---|---|---|---|---|---|
| | | | **WEST COAST OF SITHONIA** | | |
| | | | | | |
| *SIT* | *1* | dyke | doleritic, cape Kamenos | 40.03.18 | 23.48.11 |
| *SIT* | *2* | flow | massive, doleritic | 40.02.55 | 23.48.34 |
| *SIT* | *3* | dyke | | 40.01.40 | 23.49.14 |
| *SIT* | *4* | flow | | 40.01.02 | 23.49.07 |
| | | | | | |
| | | | ***POUNTA PENINSULA*** | 40.01.03 | 23.49.12 |
| | | | | | |
| *SIT* | *5* | dyke | dolerite | | |
| *SIT* | *6* | dyke | chilled margin of SIT5 | | |
| *SIT* | *7* | dyke | Plg-phyric | | |
| *SIT* | *8* | dyke | chilled margin os SIT9 | | |
| *SIT* | *9* | dyke | doleritic | | |
| *SIT* | *10* | dyke | Plg-phyric | | |
| *SIT* | *11* | dyke | diorite, in varied-texture gabbro | | |
| | | | | | |
| *SIT* | *12* | felsic | thin section only | | |
| *SIT* | *13* | granite | the Sithonia Granite | | |
| | | | | | |
| | | | ***TORONI CASTLE*** | 39.58.37 | 23.54.01 |
| | | | | | |
| *SIT* | *14* | lava | pillow | | |
| *SIT* | *15* | lava | pillow | | |
| | | | | | |
| | | | **EAST COAST OF SITHONIA** | | |
| | | | | | |
| *SIT* | *16* | Hbl- Bi gneiss | | 40.10.28 | 23.50.24 |
| *SIT* | *17* | mullonite | | 40.10.20 | 23.51.01 |
| *SIT* | *18* | amphibolite | Plg+ Amph | 40.03.57 | 23.59.20 |
| *SIT* | *19* | amphibolite | fine grained, leucocratic layers | | |
| *SIT* | *20* | Msc - Bi gneiss | | 40.03.24 | 23.59.20 |
| *SIT* | *21* | amphibolite | fine graind, epidote veins | | |
| *SIT* | *22* | amphibolite | medium grained | 39.59.61 | 23.57.30 |
| *SIT* | *23* | ampibolite | gabbroic texture | | |
| *SIT* | *24* | ampibolite | Plg+Amph | | |
| | | | | | |
| | | | ***CAPE LAIMOS*** | 40.01.32 | 23.51.13 |
| | | | | | |
| *SIT* | *25* | lava | pillow | | |
| *SIT* | *26* | lava | pillow | | |
| *SIT* | *27* | lava | highly sheared, pillow lava | | |

# APPENDIX B  SHRIMP ANALYSES

| Sample Name | U ppm | Th ppm | $^{232}$Th /$^{238}$U | $^{206}$Pb ppm | $^{238}$U /$^{206}$Pb uncorrected | % err | $^{207}$Pb/$^{206}$Pb uncorrected | % err | $^{206}$Pb /$^{238}$U (Ma) $^{204}$Pbcorr Age | 1s err ± |
|---|---|---|---|---|---|---|---|---|---|---|
| **Gevgely** | | | | | | | | | | |
| GV1.1.1 | 84 | 68 | 0.84 | 2 | 38.2450 | 1.9391 | 0.0547 | 6.5566 | 172.2 | 3.3 |
| GV1.2.1 | 31 | 21 | 0.72 | 1 | 38.0018 | 3.6364 | 0.0795 | 8.7497 | 167.4 | 7.2 |
| GV1.3.1 | 94 | 67 | 0.73 | 2 | 35.6214 | 1.3848 | 0.0587 | 4.1970 | 178.4 | 3.0 |
| GV1.2.2 | 33 | 23 | 0.71 | 1 | 37.9561 | 2.2295 | 0.0647 | 6.6016 | 172.8 | 5.7 |
| GV1.4.1 | 288 | 148 | 0.53 | 7 | 37.9073 | 0.8162 | 0.0559 | 2.5667 | 166.3 | 1.8 |
| GV1.5.1 | 31 | 22 | 0.75 | 1 | 37.3972 | 2.2377 | 0.0604 | 6.6800 | 185.8 | 9.1 |
| GV1.6.1 | 134 | 100 | 0.77 | 3 | 37.9861 | 1.1084 | 0.0581 | 3.4166 | 167.5 | 2.1 |
| GV1.7.1 | 64 | 49 | 0.79 | 1 | 37.2297 | 1.5202 | 0.0552 | 4.6993 | 165.0 | 7.7 |
| **Thessaloniki** | | | | | | | | | | |
| SAT-13.1.1 | 500 | 190 | 0.39 | 12 | 37.2033 | 0.7678 | 0.0656 | 2.2341 | 167.7 | 1.6 |
| SAT-13.2.1 | 508 | 137 | 0.28 | 12 | 36.8455 | 0.7624 | 0.0615 | 3.7713 | 170.4 | 1.5 |
| SAT-13.3.1 | 411 | 158 | 0.40 | 9 | 37.9300 | 0.8698 | 0.0610 | 3.7405 | 165.6 | 2.1 |
| SAT-13.4.1 | 83 | 33 | 0.41 | 2 | 35.7470 | 1.8284 | 0.1036 | 4.2747 | 162.7 | 7.2 |
| SAT-13.4.2 | 871 | 157 | 0.19 | 20 | 37.1914 | 0.5912 | 0.0566 | 1.8238 | 169.4 | 1.2 |
| SAT-13.5.1 | 620 | 248 | 0.41 | 14 | 37.2104 | 0.7356 | 0.0553 | 2.2715 | 169.5 | 1.4 |
| SAT-13.6.1 | 267 | 109 | 0.42 | 6 | 37.1945 | 1.0529 | 0.0704 | 3.6026 | 164.6 | 2.5 |
| SAT-13.7.1 | 948 | 126 | 0.14 | 22 | 36.6055 | 0.6618 | 0.0547 | 1.7767 | 172.9 | 1.2 |
| SAT-13.8.1 | 482 | 177 | 0.38 | 11 | 37.9388 | 0.7878 | 0.0576 | 2.4404 | 165.3 | 1.7 |
| **Chortiatis Magmatic Suite** | | | | | | | | | | |
| L-9.1.1 | 407 | 202 | 0.51 | 9.13 | 38.3000 | 3.8000 | 0.0504 | 3.8000 | 165.4 | 6.2 |
| L-9.2.1 | 605 | 265 | 0.45 | 13 | 40.0000 | 3.7000 | 0.0511 | 4.1000 | 159.6 | 5.8 |
| L-9.3.1 | 479 | 114 | 0.25 | 10.8 | 38.2000 | 3.7000 | 0.0513 | 3.0000 | 164.7 | 6.1 |
| L-9.4.1 | 489 | 185 | 0.39 | 10.2 | 41.0000 | 3.8000 | 0.0499 | 3.4000 | 155.1 | 5.8 |
| L-9.4.2 | 538 | 144 | 0.28 | 11.5 | 40.1000 | 3.7000 | 0.0487 | 3.1000 | 157 | 5.8 |
| L-9.5.1 | 550 | 231 | 0.43 | 11.6 | 40.7000 | 3.7000 | 0.0513 | 3.1000 | 155.3 | 5.7 |
| L-9.6.1 | 828 | 243 | 0.30 | 17.8 | 40.0000 | 3.6000 | 0.0508 | 2.7000 | 158.8 | 5.7 |
| L-9.6.2 | 697 | 237 | 0.35 | 15.3 | 39.1000 | 4.1000 | 0.0521 | 3.3000 | 162 | 6.6 |
| **etramorphosis** | | | | | | | | | | |
| CR12.1.1 | 129 | 24 | 0.19 | 3 | 38.1050 | 1.8586 | 0.0580 | 4.2078 | 164.5 | 3.3 |
| CR12.2.1 | 411 | 152 | 0.38 | 9 | 38.0176 | 1.4864 | 0.0497 | 2.1250 | 167.1 | 2.5 |
| CR12.3.1 | 1042 | 321 | 0.32 | 23 | 38.4562 | 1.4067 | 0.0509 | 1.3334 | 164.8 | 2.3 |
| CR12.4.1 | 1021 | 466 | 0.47 | 23 | 38.0072 | 1.4165 | 0.0490 | 1.3358 | 167.1 | 2.3 |
| CR12.5.1 | 579 | 220 | 0.39 | 13 | 38.8262 | 1.4644 | 0.0518 | 1.7610 | 163.1 | 2.4 |
| **Sithonia** | | | | | | | | | | |
| SIT11.1.1 | 216 | 162 | 0.78 | 4 | 41.7345 | 1.2807 | 0.0517 | 4.3011 | 152.6 | 1.9 |
| SIT11.2.1 | 177 | 115 | 0.67 | 4 | 39.8832 | 1.3604 | 0.0596 | 4.2839 | 161.0 | 2.4 |
| SIT11.3.1 | 342 | 240 | 0.73 | 8 | 39.0951 | 0.9971 | 0.0479 | 3.4363 | 161.6 | 1.8 |
| SIT11.4.1 | 268 | 209 | 0.80 | 6 | 39.7169 | 1.1104 | 0.0530 | 3.6159 | 156.3 | 2.2 |
| SIT11.5.1 | 329 | 320 | 1.01 | 8 | 37.0872 | 0.9691 | 0.0482 | 3.3294 | 172.8 | 2.3 |
| SIT11.6.1 | 294 | 253 | 0.89 | 6 | 39.8664 | 1.0510 | 0.0499 | 3.5372 | 160.4 | 1.7 |
| SIT11.8.1 | 1026 | 818 | 0.82 | 22 | 39.7787 | 0.5735 | 0.0487 | 1.8946 | 159.9 | 0.9 |
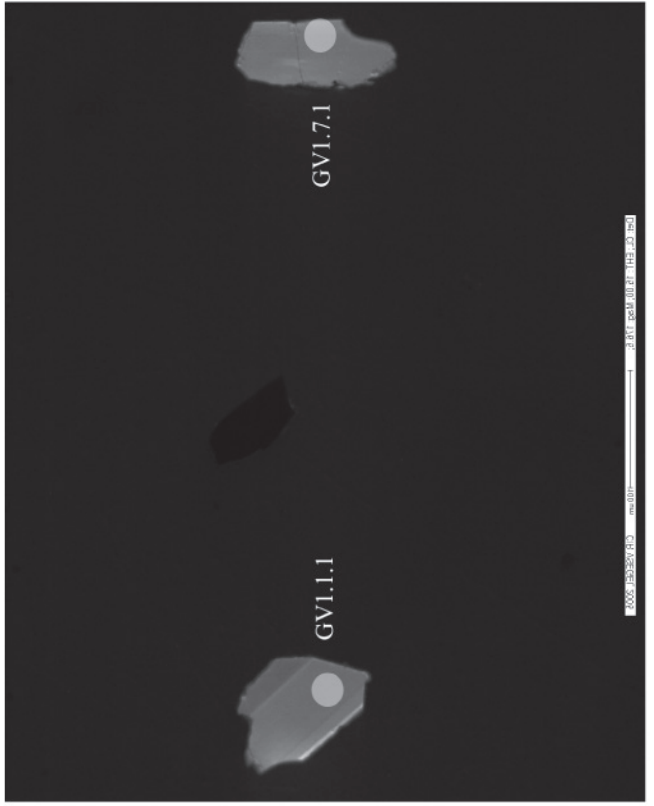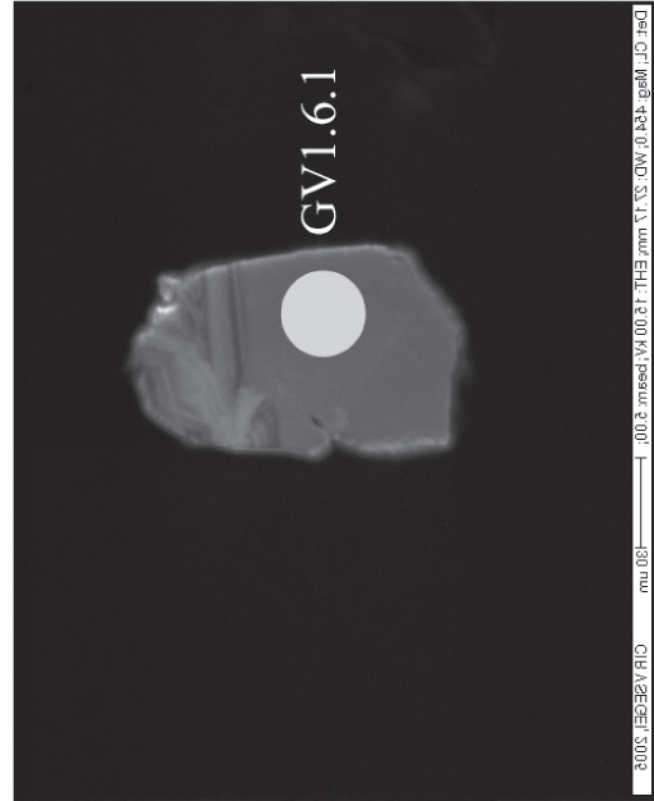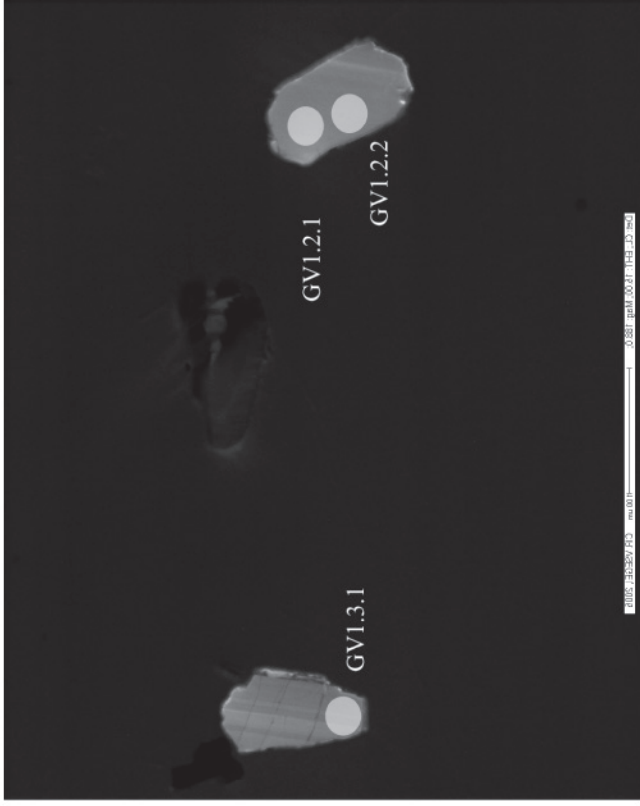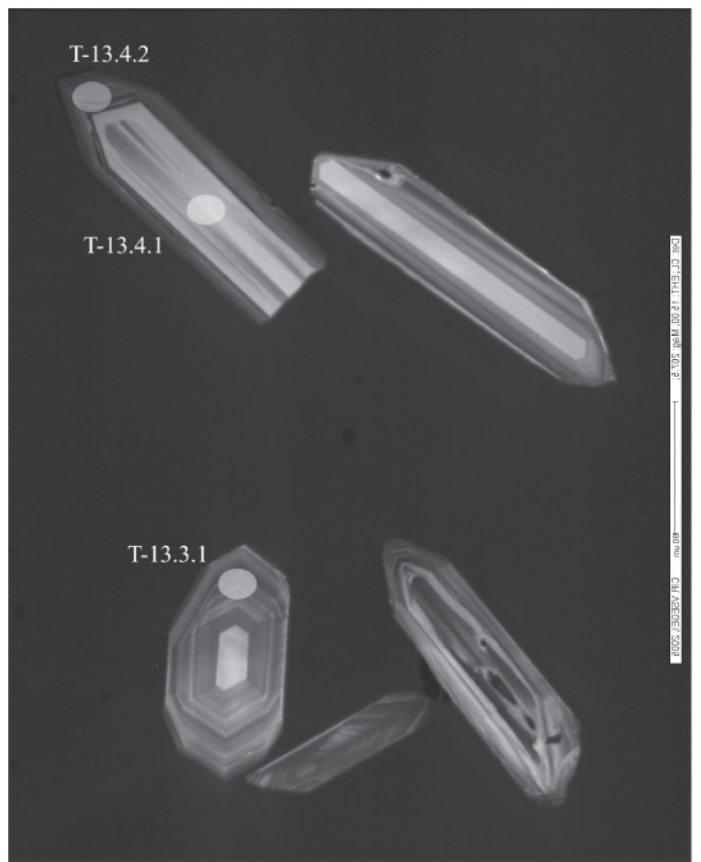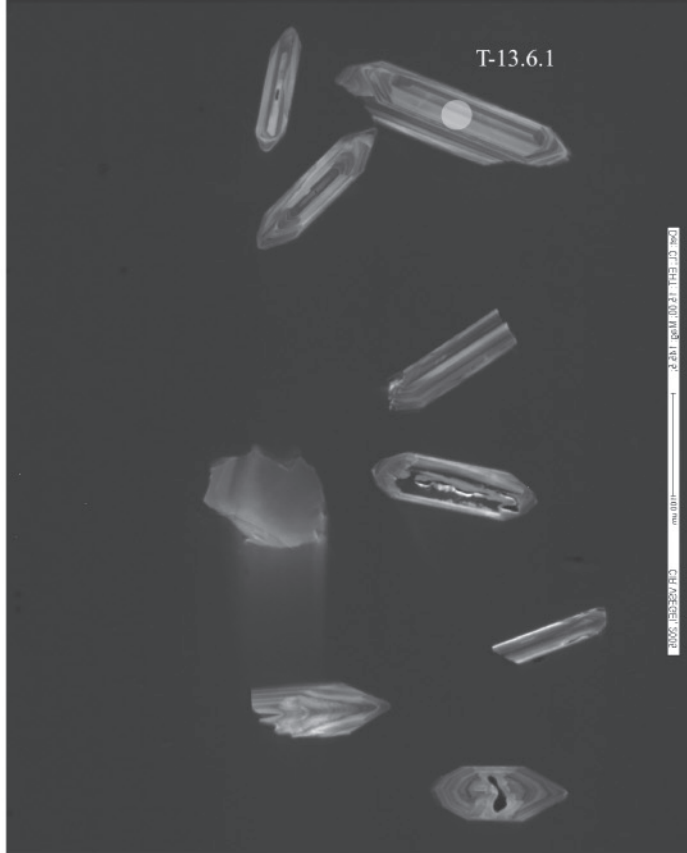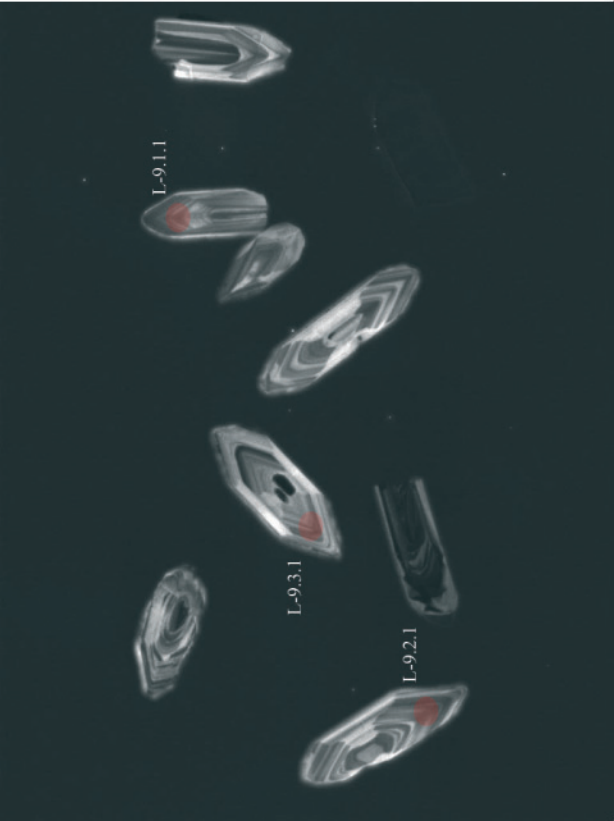
GV1.2.1
GV1.2.2
GV1.3.1
GV1.7.1
GV1.1.1
GV1.4.1
GV1.5.1
GV1.6.1

L-9.4.2
L-9.4.1
L-9.5.1

L-9.6.1 L-9.7.1

L-9.1.1
L-9.3.1
L-9.2.1
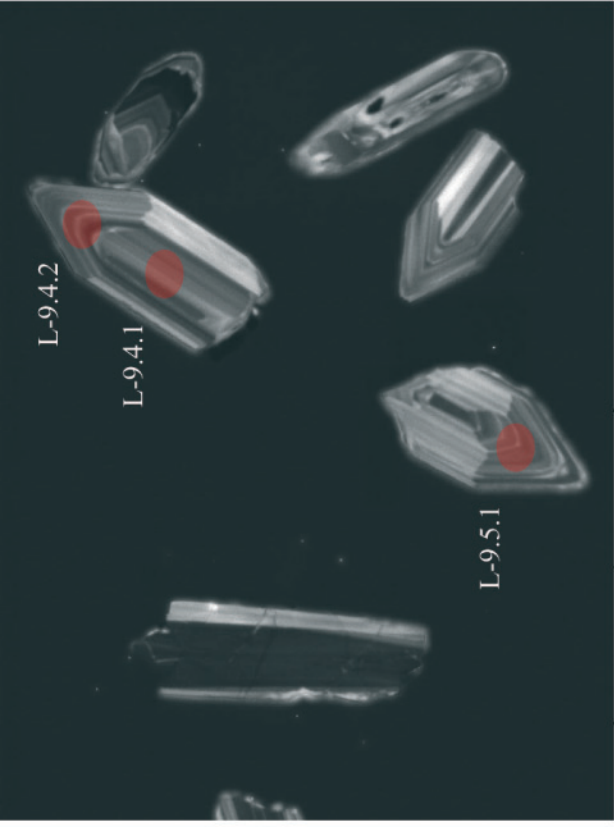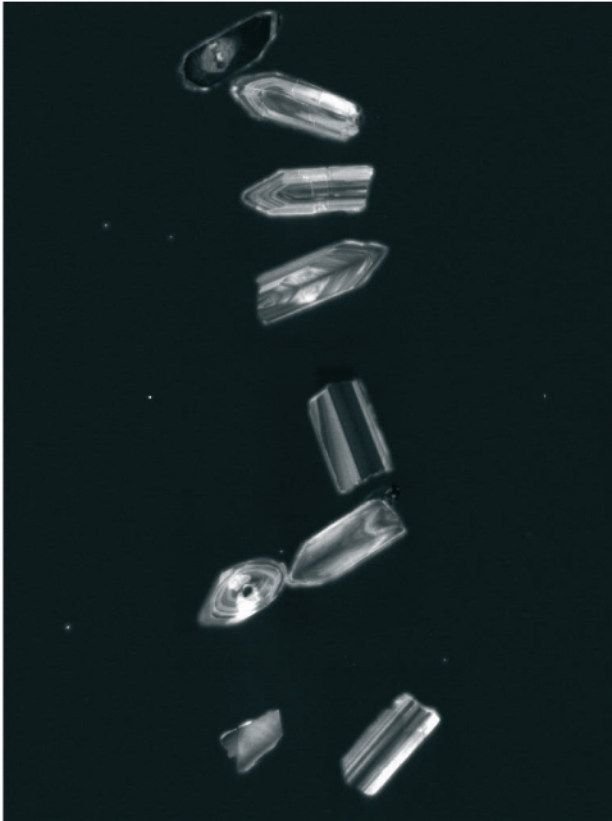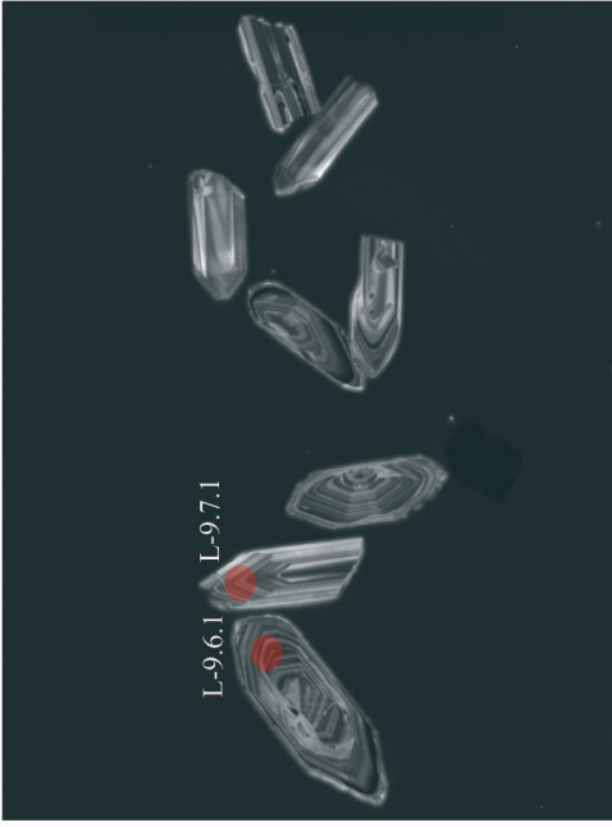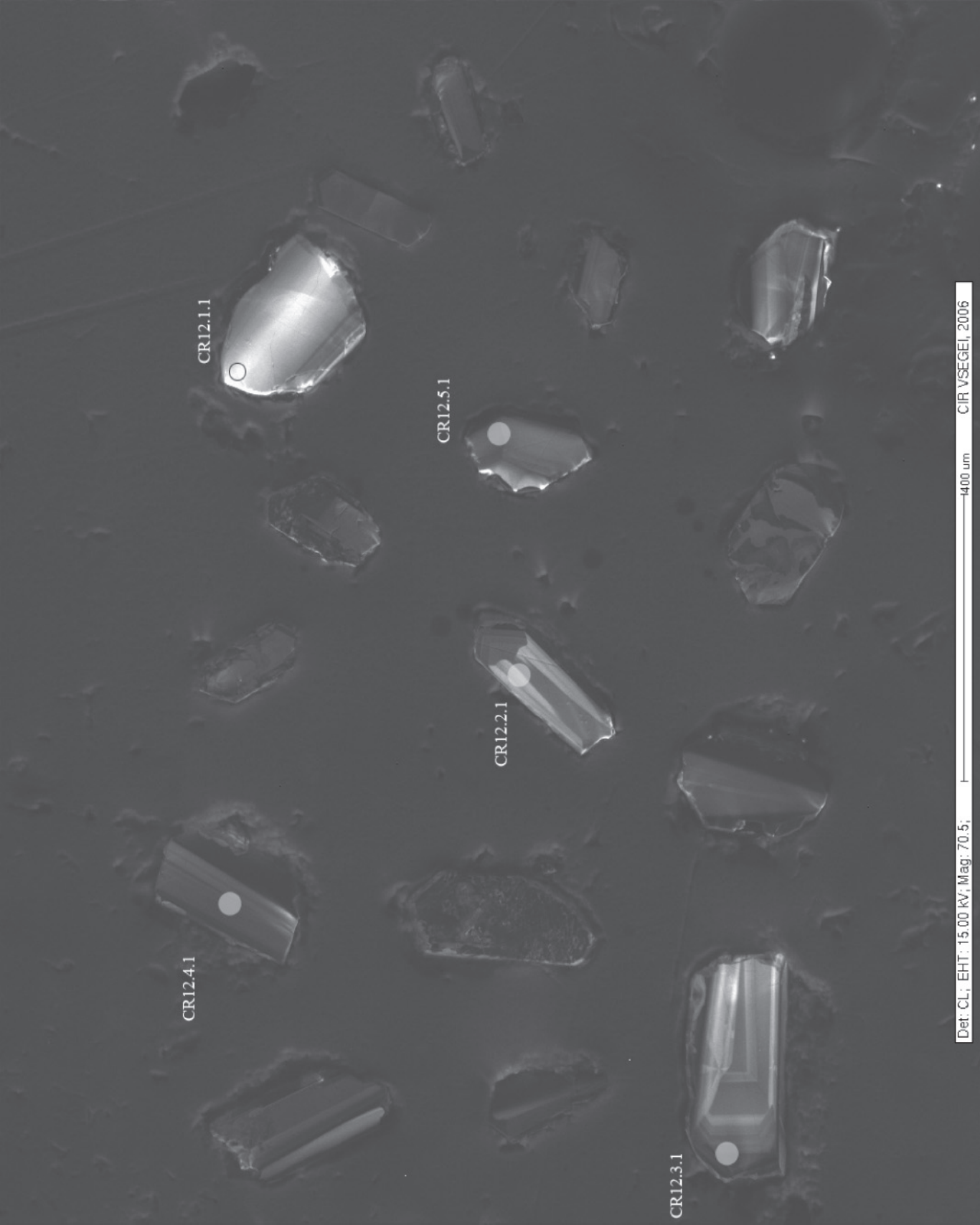
CR12.1.1

CR12.5.1

CR12.2.1

CR12.4.1

CR12.3.1

Det: CL; EHT: 15.00 kV; Mag: 70.5; 400 um CIR VSEGEI, 2006
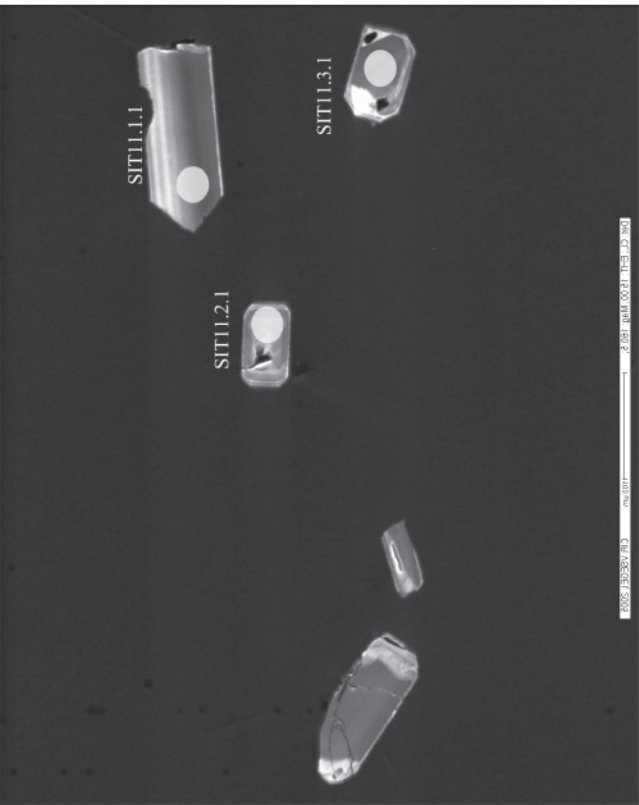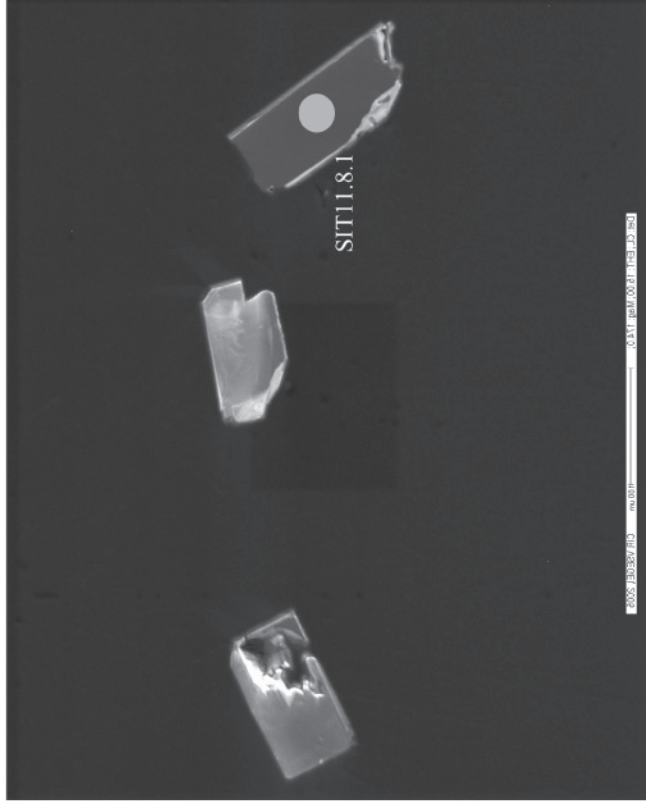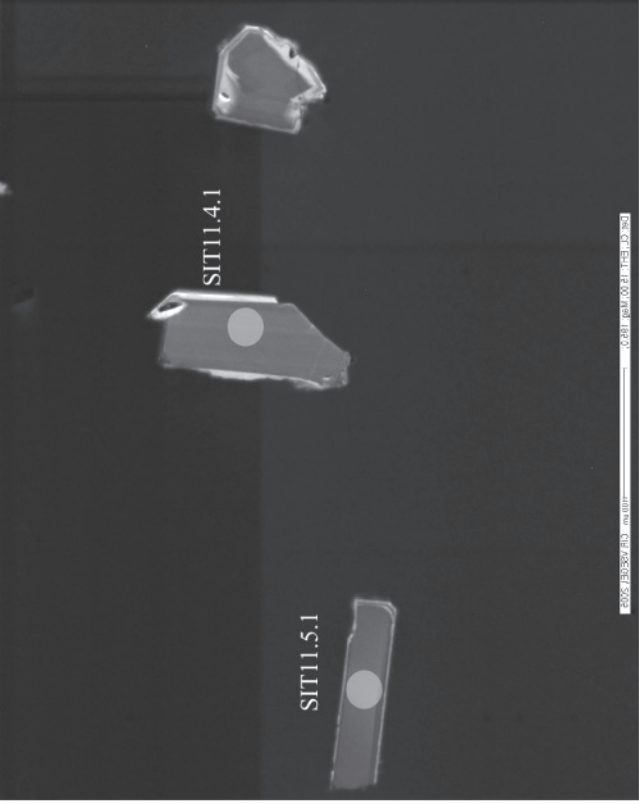
**Table 1 a. Chemical compositions of major and trace elements for the Skra and Fanos samples**

| | | Skra | | | | | | | | | | | | | | | | Fanos |
|---|---|---|---|---|---|---|---|---|---|---|---|---|---|---|---|---|---|---|
| name | | GLV1 | GLV2 | GLV3 | GVL4 | GVL 23 | GVL 22 | GVL 21 | GVL08 | GVL10 | GVL11 | GVL12 | GVL13 | GVL14 | GVL15 | GVL16 | GVL18 | FA 02 |
| description | | dyke | dyke | dyke | dyke | lava | lava | lava | dyke | dyke | dyke | dyke | dyke | dyke | dyke | dyke | dyke | dyke |
| **major elements** | | | | | | | | | | | | | | | | | | |
| $SiO_2$ | % | 68.41 | 67.60 | 67.28 | 65.25 | 65 | 61.22 | 65.5 | 51.01 | 49.96 | 52.09 | 50.29 | 51.50 | 50.02 | 52.71 | 50.47 | 49.31 | 53.24 |
| $TiO_2$ | % | 0.60 | 0.58 | 0.65 | 1.24 | 1.14 | 1 | 0.72 | 1.38 | 1.11 | 1.10 | 1.57 | 1.69 | 1.06 | 0.68 | 0.74 | 0.82 | 0.54 |
| $Al_2O_3$ | % | 13.51 | 13.56 | 13.70 | 13.16 | 13.6 | 14.68 | 13.67 | 16.07 | 15.78 | 16.54 | 14.67 | 15.28 | 15.12 | 15.63 | 16.03 | 14.61 | 16.26 |
| $Fe_2O_3$ | % | 6.82 | 7.96 | 7.51 | 6.03 | 7.28 | 9.11 | 8.23 | 8.76 | 10.33 | 8.49 | 10.93 | 11.53 | 8.77 | 8.02 | 8.71 | 8.61 | 6.22 |
| MnO | % | 0.11 | 0.04 | 0.05 | 0.06 | 0.14 | 0.16 | 0.11 | 0.13 | 0.14 | 0.12 | 0.13 | 0.13 | 0.15 | 0.13 | 0.17 | 0.14 | 0.29 |
| MgO | % | 1.79 | 1.11 | 1.13 | 2.61 | 2.52 | 4.22 | 2.94 | 6.23 | 7.00 | 5.09 | 5.53 | 4.77 | 9.59 | 6.95 | 8.01 | 9.65 | 6.98 |
| CaO | % | 0.71 | 1.20 | 1.58 | 3.10 | 1.44 | 0.63 | 0.37 | 13.33 | 11.98 | 13.16 | 10.16 | 10.09 | 9.94 | 8.49 | 11.10 | 11.53 | 7.25 |
| $Na_2O$ | % | 6.28 | 6.70 | 7.02 | 6.69 | 5.77 | 5.16 | 5 | 1.39 | 2.18 | 1.49 | 2.31 | 3.02 | 2.44 | 3.90 | 2.58 | 2.02 | 3.34 |
| $K_2O$ | % | 0.21 | 0.08 | 0.10 | 0.07 | 0.06 | 0.04 | 0.04 | 0.05 | 0.06 | 0.05 | 0.06 | 0.10 | 0.11 | 0.80 | 0.42 | 0.05 | 2.86 |
| $P_2O_5$ | % | 0.15 | 0.15 | 0.18 | 0.41 | 0.4 | 0.36 | 0.21 | 0.12 | 0.08 | 0.09 | 0.18 | 0.13 | 0.12 | 0.13 | 0.07 | 0.07 | 0.23 |
| $Cr_2O_3$ | % | | | | | | | | 0.0136 | 0.0149 | 0.0166 | 0.0083 | 0.0097 | 0.0762 | 0.0381 | 0.0292 | 0.0707 | 0.0414 |
| NiO | % | | | | | | | | 0.0055 | 0.0067 | 0.0053 | 0.0028 | 0.0035 | 0.0288 | 0.0156 | 0.0092 | 0.0223 | 0.0147 |
| L.O.I. | % | 1.93 | 1.22 | 1.02 | 1.45 | 3.01 | 3.6 | 2.54 | 1.21 | 1.25 | 1.53 | 1.24 | 0.75 | 2.43 | 2.1 | 1.58 | 1.66 | 2.76 |
| SUM | % | 100.52 | 100.20 | 100.22 | 100.06 | 100.37 | 100.169 | 99.32 | 99.686 | 99.891 | 99.772 | 97.077 | 98.995 | 99.845 | 99.596 | 99.935 | 98.563 | |
| **trace elements** | | | | | | | | | | | | | | | | | | |
| Sc | ppm | 11 | 8 | 11 | 18 | 14 | 14 | 12 | 44 | 37 | 32 | 34 | 33 | 34 | 31 | 40 | na | 27 |
| V | ppm | 3 | 6 | 7 | 34 | 41 | 22 | 13 | 308 | 295 | 268 | 295 | 365 | 240 | 233 | 245 | na | 186 |
| Cr | ppm | 6 | 4 | 4 | 2 | - | - | 1 | 83 | 99 | 113 | 47 | 55 | 580 | 260 | 204 | na | 321 |
| Co | ppm | 6 | 9 | 1 | 11 | 6 | 8 | 7 | 31 | 38 | 31 | 33 | 37 | 42 | 26 | 30 | na | 22 |
| Ni | ppm | 3 | 4 | 0 | 2 | 2 | 2 | - | 47 | 59 | 43 | 33 | 37 | 219 | 115 | 78 | na | 120 |
| Cu | ppm | 1 | 3 | 2 | 2 | 4 | 8 | 62 | 7 | 19 | 9 | 13 | 7 | 70 | 3 | 38 | na | 2 |
| Zn | ppm | 108 | 16 | 107 | 14 | 131 | 76 | 45 | 28 | 30 | 24 | 30 | 28 | 62 | 49 | 79 | na | 67 |
| Ga | ppm | 20 | 23 | 21 | 15 | 17 | 20 | 20 | 15 | 15 | 16 | 17 | 20 | 16 | 16 | 14 | na | 17 |
| Rb | ppm | 4 | 4 | 5 | 3 | 3 | 3 | 3 | 3 | 3 | 2 | 4 | 4 | 5 | 26 | 12 | na | 243 |
| Sr | ppm | 59 | 77 | 60 | 50 | 34 | 22 | 21 | 205 | 183 | 251 | 169 | 214 | 170 | 360 | 278 | na | 592 |
| Y | ppm | 79 | 79 | 79 | 62 | 64 | 51 | 51 | 31 | 25 | 24 | 33 | 33 | 25 | 20 | 21 | na | 14 |
| Zr | ppm | 334 | 334 | 335 | 200 | 221 | 278 | 305 | 86 | 66 | 67 | 92 | 99 | 85 | 85 | 55 | na | 116 |
| Nb | ppm | 8 | 8 | 7 | 4 | 5 | 6 | 8 | 2 | 2 | 1 | 2 | 3 | 2 | 3 | 2 | na | 7 |
| Ba | ppm | 28 | 10 | 35 | 3 | -6 | -18 | 4 | - | 0 | - | - | - | 10 | 133 | 100 | na | 707 |

X

**Table 1 b. Chemical compositions of major and trace elements for the Eyzonoi**

Eyzonoi

| | | EYZ1 | EYZ3 | EYZ4 | EYZ5 | EYZ6 | EYZ7 | EYZ9 | EYZ10 | EYZ11 | EYZ11 | EYZ12 | EYZ16 | EYZ 15 | EYZ 13 | EYZ8 | EYZ2 |
|---|---|---|---|---|---|---|---|---|---|---|---|---|---|---|---|---|---|
| description | | dyke | dyke | dyke | dyke | dyke | dyke | dyke | dyke | dyke | dyke | dyke | dyke | lava pillow | dyke | dyke | dyke |
| **major elements** | | | | | | | | | | | | | | | | | |
| $SiO_2$ | % | 49.36 | 50.18 | 54.33 | 52.59 | 51.16 | 51.83 | 48.13 | 51.90 | 56.68 | 56.34 | 47.61 | 52.45 | 50.08 | 73.12 | 71.65 | 62.26 |
| $TiO_2$ | % | 1.34 | 2.54 | 1.83 | 2.27 | 2.60 | 2.37 | 0.74 | 2.05 | 1.18 | 1.18 | 1.93 | 1.90 | 0.59 | 0.27 | 0.31 | 1.03 |
| $Al_2O_3$ | % | 14.31 | 13.52 | 13.39 | 13.65 | 13.55 | 13.26 | 15.57 | 14.03 | 15.23 | 15.20 | 15.54 | 13.90 | 11.92 | 13.23 | 12.89 | 14.76 |
| $Fe_2O_3$ | % | 12.66 | 15.32 | 12.38 | 13.82 | 15.08 | 15.04 | 9.71 | 12.48 | 9.68 | 9.72 | 13.37 | 12.74 | 6.52 | 2.14 | 2.24 | 7.22 |
| MnO | % | 0.19 | 0.19 | 0.29 | 0.20 | 0.32 | 0.24 | 0.26 | 0.20 | 0.10 | 0.10 | 0.21 | 0.23 | 0.1 | 0.02 | 0.03 | 0.08 |
| MgO | % | 7.22 | 5.40 | 4.83 | 4.56 | 4.66 | 4.72 | 7.81 | 6.51 | 3.97 | 3.94 | 4.71 | 4.94 | 4.06 | 0.64 | 0.71 | 2.58 |
| CaO | % | 4.97 | 4.38 | 5.05 | 4.81 | 4.23 | 5.10 | 8.23 | 3.11 | 2.36 | 2.36 | 6.72 | 5.13 | 16.02 | 0.96 | 1.14 | 2.79 |
| $Na_2O$ | % | 4.83 | 4.72 | 5.55 | 6.00 | 4.94 | 5.40 | 2.80 | 4.51 | 4.90 | 4.88 | 5.33 | 5.14 | 4.06 | 6.5 | 4.60 | 5.28 |
| $K_2O$ | % | 0.09 | 0.05 | 0.08 | 0.08 | 0.21 | 0.10 | 1.95 | 0.30 | 2.02 | 2.01 | 0.09 | 0.36 | 0.09 | 0.7 | 3.55 | 1.70 |
| $P_2O_5$ | % | 0.15 | 0.32 | 0.35 | 0.27 | 0.41 | 0.23 | 0.06 | 0.26 | 0.22 | 0.22 | 0.22 | 0.31 | 0.1 | 0.03 | 0.06 | 0.15 |
| $Cr_2O_3$ | % | 0.009 | 0.0032 | 0.0026 | 0.0042 | 0.0041 | 0.0056 | 0.0105 | 0.0031 | 0.0003 | 0.0004 | 0.0035 | 0.0062 | 0.06 | | | |
| NiO | % | 0.0058 | 0.0014 | 0.0019 | 0.001 | 0.0013 | 0.0012 | 0.0058 | 0.0018 | | | 0.0008 | 0.0019 | 0.0165 | | | |
| L.O.I. | % | 1.59 | 2.51 | 1.93 | 1.68 | 2.36 | 1.75 | 4.89 | 4.58 | 3.45 | 1.96 | 4.15 | 1.89 | 1.3 | 7.4 | 1.62 | 2.14 |
| SUM | % | 96.716 | 99.136 | 100.02 | 99.935 | 99.527 | 100.06 | 100.17 | 99.928 | 99.788 | 97.919 | 99.888 | 99.013 | 94.897 | 105.028 | 98.799 | 99.982 |
| **trace elements** | | | | | | | | | | | | | | | | | |
| Sc | ppm | n.a. | 32 | 36 | 43 | 32 | 31 | 23 | 43 | 35 | n.a. | 32 | 35 | 35 | 4 | 21 | 34 |
| V | ppm | n.a. | 364 | 406 | 199 | 363 | 236 | 261 | 286 | 404 | n.a. | 406 | 470 | 231 | 22 | 257 | 233 |
| Cr | ppm | n.a. | 12 | - | 117 | 23 | 16 | - | 77 | 4 | n.a. | 6 | 20 | 440 | 5 | 5 | 43 |
| Co | ppm | n.a. | 42 | 36 | 33 | 31 | 28 | 26 | 43 | 29 | n.a. | 32 | 42 | 29 | 5 | 18 | 32 |
| Ni | ppm | n.a. | 21 | 18 | 32 | 16 | 23 | 5 | 52 | 12 | n.a. | 19 | 22 | 129 | 3 | 9 | 24 |
| Cu | ppm | n.a. | 29 | 6 | 85 | 5 | 21 | 4 | 121 | 65 | n.a. | 9 | 8 | 29 | 1 | 22 | 67 |
| Zn | ppm | n.a. | 42 | 81 | 42 | 64 | 70 | 28 | 48 | 48 | n.a. | 47 | 78 | 39 | 10 | 58 | 78 |
| Ga | ppm | n.a. | 19 | 20 | 14 | 22 | 18 | 19 | 15 | 23 | n.a. | 19 | 18 | 11 | 12 | 12 | 19 |
| Rb | ppm | n.a. | 12 | 3 | 3 | 8 | 4 | 78 | 75 | 5 | n.a. | 3 | 5 | 4 | 30 | 23 | 13 |
| Sr | ppm | n.a. | 69 | 55 | 134 | 85 | 69 | 158 | 281 | 142 | n.a. | 66 | 75 | 98 | 121 | 203 | 121 |
| Y | ppm | n.a. | 42 | 57 | 13 | 58 | 62 | 24 | 19 | 41 | n.a. | 49 | 50 | 14 | 28 | 26 | 59 |
| Zr | ppm | n.a. | 155 | 195 | 31 | 198 | 190 | 122 | 52 | 127 | n.a. | 170 | 148 | 56 | 231 | 112 | 178 |
| Nb | ppm | n.a. | 8 | 9 | 2 | 8 | 7 | 7 | 3 | 3 | n.a. | 9 | 6 | 2 | 8 | 4 | 6 |
| Ba | ppm | n.a. | - | - | 11 | - | - | 288 | 294 | - | n.a. | - | - | 20 | 125 | 560 | 13 |

**Table 3 a. Chemical compositions of major and trace elements for the Oraiokastro and Monolofos samples aquired by X.R.F.**

| name | | MLF01 | MLF02 | MLF04 | MLF03 | ORK09 | ORK10 | ORK71 | ORK72 | ORK73 | ORK74 | ORK75 | ORK76 | ORK77 | ORK78 |
|---|---|---|---|---|---|---|---|---|---|---|---|---|---|---|---|
| | | **Monolofos area** | | | | **gabbro** | | | | | | | | | |
| description | | unknown in Harz * | dyke in MLF03 * | dyke in MLF 03 * | Harz-burgite * | dyke * | dyke * | gabbro | gabbro | gabbro | gabbro | gabbro | gabbro | gabbro | gabbro |
| **major elements** | | | | | | | | | | | | | | | |
| $SiO_2$ | % | 37.19 | 33.91 | 44.24 | 40.34 | 48.42 | 49.78 | 47.71 | 46.71 | 47.70 | 47.30 | 47.66 | 47.10 | 49.12 | 49.32 |
| $TiO_2$ | % | 1.66 | 1.59 | 1.35 | 0.06 | 0.32 | 0.32 | 0.31 | 0.25 | 0.33 | 0.16 | 0.28 | 0.28 | 0.24 | 0.40 |
| $Al_2O_3$ | % | 19.68 | 20.27 | 15.43 | 2.14 | 18.70 | 15.72 | 15.84 | 19.48 | 16.78 | 21.46 | 19.20 | 16.00 | 20.49 | 16.71 |
| $Fe_2O_3$ | % | 10.61 | 7.19 | 11.57 | 8.3 | 4.98 | 5.93 | 6.41 | 5.54 | 6.11 | 5.16 | 5.13 | 6.93 | 4.30 | 5.55 |
| MnO | % | 0.14 | 0.17 | 0.18 | 0.08 | 0.09 | 0.11 | 0.11 | 0.09 | 0.11 | 0.08 | 0.10 | 0.12 | 0.08 | 0.11 |
| MgO | % | 6.36 | 7.74 | 4.88 | 36.67 | 7.60 | 10.21 | 10.40 | 8.22 | 9.56 | 7.35 | 8.28 | 11.66 | 6.38 | 7.88 |
| CaO | % | 16.52 | 23.5 | 17.97 | 0.67 | 12.17 | 12.12 | 15.14 | 14.04 | 14.95 | 13.49 | 14.68 | 13.01 | 14.33 | 13.82 |
| $Na_2O$ | % | 0.1 | 0 | 0.25 | 0 | 3.36 | 2.77 | 1.39 | 1.91 | 1.62 | 1.98 | 2.34 | 1.80 | 2.52 | 2.92 |
| $K_2O$ | % | 0.02 | 0 | 0.43 | 0.01 | 0.16 | 0.06 | 0.11 | 0.10 | 0.06 | 0.10 | 0.11 | 0.17 | 0.08 | 0.18 |
| $P_2O_5$ | % | 0.02 | 0 | 0.10 | 0 | 0.02 | 0.01 | 0.00 | 0.00 | 0.00 | 0.00 | 0.00 | 0.00 | 0.00 | 0.04 |
| $Cr_2O_3$ | % | 0.0407 | 0.0438 | 0.0382 | 0.3757 | 0.08 | 0.07 | 0.1575 | 0.0623 | 0.1657 | 0.0677 | 0.1102 | 0.1399 | 0.0171 | 0.0148 |
| NiO | % | 0.0182 | 0.0221 | 0.0111 | 0.2677 | 0.02 | 0.02 | 0.0244 | 0.0177 | 0.0258 | 0.0291 | 0.0195 | 0.0265 | 0.0084 | 0.0093 |
| L.O.I. | % | 6.72 | 5.17 | 3.06 | 11.47 | 3.67 | 2.70 | 2.64 | 3.28 | 2.65 | 3.94 | 2.82 | 3.80 | 2.61 | 1.94 |
| SUM | % | 99.08 | 99.56 | 99.51 | 100.38 | 99.59 | 99.83 | 100.24 | 99.71 | 100.04 | 101.13 | 100.73 | 101.01 | 100.16 | 98.91 |
| **trace elements** | | | | | | | | | | | | | | | |
| Sc | ppm | 50 | 30 | 54 | 1 | 38 | 43 | 53 | 40 | 55 | 25 | 44 | n.a | n.a | 53 |
| V | ppm | 375 | 346 | 313 | 60 | 131 | 140 | 168 | 128 | 177 | 76 | 156 | n.a | n.a | 198 |
| Cr | ppm | 329 | 320 | 291 | 2,735 | 655 | 568 | 1,288 | 548 | 1,458 | 596 | 951 | n.a | n.a | 130 |
| Co | ppm | 47 | 33 | 45 | 116 | 27 | 43 | 40 | 38 | 38 | 35 | 28 | n.a | n.a | 31 |
| Ni | ppm | 161 | 182 | 90 | 2,010 | 126 | 168 | 199 | 142 | 213 | 233 | 157 | n.a | n.a | 80 |
| Cu | ppm | 6 | 110 | 74 | 9 | 80 | 52 | 82 | 32 | 67 | 102 | 63 | n.a | n.a | 87 |
| Zn | ppm | 69 | 87 | 88 | 43 | 30 | 34 | 36 | 33 | 33 | 31 | 29 | n.a | n.a | 34 |
| Ga | ppm | 28 | 17 | 16 | 4 | 12 | 13 | 12 | 13 | 12 | 14 | 15 | n.a | n.a | 13 |
| Rb | ppm | 2 | 2 | 15 | 1 | 3 | 2 | 5 | 4 | 3 | 2 | 4 | n.a | n.a | 4 |
| Sr | ppm | 30 | 17 | 159 | 8 | 194 | 128 | 163 | 190 | 169 | 201 | 206 | n.a | n.a | 174 |
| Y | ppm | 12 | 6 | 26 | 2 | 9 | 10 | 10 | 7 | 11 | 5 | 9 | n.a | n.a | 13 |
| Zr | ppm | 233 | 105 | 24 | 1 | 13 | 16 | 24 | 22 | 26 | 21 | 25 | n.a | n.a | 34 |
| Nb | ppm | 15 | 16 | 3 | 1 | 2 | 2 | 0 | 1 | 1 | 1 | 0 | n.a | n.a | 1 |
| Ba | ppm | n.a | n.a | 104 | 14 | 11 | 24 | 18 | 8 | 11 | 12 | 5 | n.a | n.a | 13 |

Samples with * are taken from: Zachariadis P., 2002. Petrology and geochemistry of the Oraeokastron Ophiolite, northern Greece. M.Sc. Thesis, Aristotle University of Thessaloniki, Greece (in Greek, with English Summary).

**Table 3 b. Chemical compositions of major and trace elements for the low TiO2 Oraiokastro samples aquired by X.R.F.**

**Low TiO2 basalts**

| | | ORK 31 | ORK07 | ORK05 | ORK11 | ORK08 | ORK06 | ORK14 | ORK15 | ORK 37 | ORK 32 | ORK 38 | ORK 56 | ORK 39 | ORK 52 |
|---|---|---|---|---|---|---|---|---|---|---|---|---|---|---|---|
| description | | tonalite | dyke | dyke | dyke | dyke | dyke | lava | lava | dyke | dyke | dyke | dyke | ch m 38 | flow |
| | | * | * | * | * | * | * | * | * | * | * | * | * | * | * |
| **major elements** | | | | | | | | | | | | | | | |
| $SiO_2$ | % | 48.61 | 51.95 | 52.15 | 52.62 | 52.82 | 53.20 | 55.58 | 55.73 | 52.42 | 52.82 | 53.03 | 53.38 | 53.85 | 55.94 |
| $TiO_2$ | % | 0.11 | 0.62 | 0.48 | 0.70 | 0.68 | 0.48 | 0.80 | 0.76 | 0.62 | 0.70 | 0.69 | 0.53 | 0.69 | 0.98 |
| $Al_2O_3$ | % | 27.07 | 15.21 | 15.84 | 15.97 | 15.43 | 15.35 | 13.51 | 12.55 | 15.42 | 14.67 | 15.19 | 13.89 | 15.38 | 14.18 |
| $Fe_2O_3$ | % | 1.44 | 8.28 | 8.25 | 8.87 | 8.38 | 8.11 | 8.53 | 7.49 | 8.43 | 9.03 | 8.45 | 9.27 | 8.40 | 12.01 |
| MnO | % | 0.03 | 0.13 | 0.13 | 0.14 | 0.14 | 0.14 | 0.17 | 0.17 | 0.12 | 0.14 | 0.14 | 0.13 | 0.14 | 0.16 |
| MgO | % | 2.38 | 7.53 | 7.57 | 5.78 | 7.17 | 6.98 | 7.20 | 6.51 | 7.83 | 8.35 | 7.27 | 7.89 | 7.01 | 5.13 |
| CaO | % | 9.82 | 9.44 | 7.31 | 7.77 | 8.34 | 8.63 | 4.74 | 6.33 | 7.27 | 5.61 | 7.16 | 8.19 | 8.32 | 3.13 |
| $Na_2O$ | % | 4.35 | 2.91 | 4.59 | 4.97 | 4.31 | 3.94 | 5.03 | 4.69 | 4.44 | 5.09 | 4.43 | 2.71 | 4.04 | 4.80 |
| $K_2O$ | % | 1.23 | 0.04 | 0.40 | 0.20 | 0.20 | 0.42 | 1.46 | 1.86 | 0.25 | 0.12 | 0.46 | 0.03 | 0.30 | 0.12 |
| $P_2O_5$ | % | 0.00 | 0.05 | 0.03 | 0.06 | 0.06 | 0.03 | 0.07 | 0.07 | 0.05 | 0.06 | 0.06 | 0.04 | 0.06 | 0.07 |
| $Cr_2O_3$ | % | 0.0196 | 0.04 | 0.03 | 0.00 | 0.03 | 0.02 | 0.02 | 0.02 | 0.0410 | 0.0361 | 0.0328 | 0.0354 | 0.0319 | 0.0044 |
| NiO | % | 0.0034 | 0.01 | 0.01 | 0.01 | 0.01 | 0.01 | 0.01 | 0.01 | 0.0133 | 0.0125 | 0.0111 | 0.0118 | 0.0112 | 0.0035 |
| L.O.I. | % | 5.08 | 3.36 | 2.71 | 2.71 | 2.56 | 1.95 | 3.55 | 3.32 | 3.62 | 3.53 | 3.59 | 4.31 | 1.19 | 3.85 |
| SUM | % | 100.12 | 99.57 | 99.50 | 99.80 | 100.15 | 99.26 | 100.66 | 99.50 | 100.54 | 100.16 | 100.51 | 100.42 | 99.42 | 100.39 |
| **trace elements** | | | | | | | | | | | | | | | |
| Sc | ppm | 14 | 36 | 35 | 33 | 37 | 38 | 26 | 31 | 34 | 35 | 35 | 37 | 34 | 29 |
| V | ppm | 39 | 257 | 241 | 282 | 258 | 245 | n.a | 256 | 248 | 248 | 259 | 285 | 255 | 322 |
| Cr | ppm | 175 | 287 | 194 | 19 | 278 | 190 | n.a | 123 | 324 | 286 | 258 | 268 | 256 | 22 |
| Co | ppm | 8 | 33 | 38 | 34 | 32 | 33 | n.a | 28 | 39 | 32 | 34 | 34 | 33 | 34 |
| Ni | ppm | 33 | 104 | 70 | 43 | 97 | 66 | n.a | 58 | 107 | 101 | 92 | 92 | 90 | 29 |
| Cu | ppm | 39 | 55 | 109 | n.a | 58 | 24 | n.a | 9 | 79 | 97 | 67 | 56 | 42 | n.a |
| Zn | ppm | 10 | 66 | 60 | 58 | 67 | 62 | n.a | 53 | 64 | 72 | 66 | 62 | 66 | 45 |
| Ga | ppm | 13 | 15 | 14 | 14 | 15 | 14 | n.a | 11 | 13 | 11 | 13 | 12 | 15 | 15 |
| Rb | ppm | 9 | 2 | 6 | 4 | 3 | 8 | n.a | 11 | 2 | n.a | 2 | n.a | 1 | n.a |
| Sr | ppm | 328 | 73 | 128 | 123 | 102 | 112 | n.a | 107 | 105 | 87 | 102 | 66 | 96 | 44 |
| Y | ppm | 3 | 18 | 15 | 19 | 20 | 15 | n.a | 21 | 19 | 20 | 21 | 16 | 21 | 25 |
| Zr | ppm | n.a | 34 | 23 | 40 | 42 | 24 | n.a | 49 | 35 | 40 | 41 | 27 | 41 | 52 |
| Nb | ppm | 1 | 2 | 1 | 2 | 3 | 2 | n.a | 2 | 2 | 2 | 2 | 2 | 2 | 2 |
| Ba | ppm | 19 | 2 | 28 | 16 | 22 | 25 | n.a | 42 | 15 | 2 | 12 | 3 | 14 | n.a |

**Table 3 c. Chemical compositions of major and trace elements for the high TiO2 Oraiokastro samples aquired by X.R.F.**

**High TiO2 basalts**

| name | | ORK 53 | ORK21 | ORK 57 | ORK 50 | ORK17 | ORK 54 | ORK 58 | ORK 58B | ORK 55 | ORK13 | ORK 34 | ORK 65 | ORK12 | ORK 67 |
|---|---|---|---|---|---|---|---|---|---|---|---|---|---|---|---|
| description | | thick flow | epidosite | dyke | lava | lava | dyke epd | dyke | ch m 58 | dyke | lava | lava pillow | dyke | lava | dyke |
| | | * | * | * | * | * | * | * | * | * | * | * | * | * | * |
| $SiO_2$ | % | 42.62 | 46.11 | 47.63 | 47.66 | 48.93 | 49.09 | 49.17 | 49.78 | 50.31 | 51.02 | 53.25 | 55.05 | 55.74 | 56.61 |
| $TiO_2$ | % | 2.32 | 1.34 | 1.81 | 1.39 | 1.72 | 1.74 | 1.71 | 1.86 | 1.62 | 1.74 | 1.81 | 1.53 | 1.58 | 1.29 |
| $Al_2O_3$ | % | 16.05 | 14.9 | 15.46 | 16.80 | 12.51 | 14.83 | 14.00 | 14.22 | 12.63 | 14.04 | 14.91 | 14.44 | 14.15 | 13.95 |
| $Fe_2O_3$ | % | 12.82 | 12.02 | 12.77 | 11.80 | 11.56 | 12.40 | 11.82 | 12.42 | 11.32 | 10.01 | 11.10 | 10.92 | 8.61 | 9.63 |
| MnO | % | 0.16 | 0.13 | 0.22 | 0.10 | 0.18 | 0.22 | 0.20 | 0.21 | 0.15 | 0.11 | 0.13 | 0.16 | 0.06 | 0.13 |
| MgO | % | 3.49 | 3.33 | 6.44 | 3.29 | 6.66 | 6.70 | 6.39 | 6.41 | 7.75 | 7.74 | 4.41 | 4.59 | 5.85 | 4.60 |
| CaO | % | 12.20 | 19.03 | 8.93 | 7.28 | 5.46 | 10.11 | 9.42 | 9.11 | 10.84 | 4.94 | 5.98 | 4.60 | 2.58 | 4.79 |
| $Na_2O$ | % | 3.88 | | 3.58 | 5.59 | 5.1 | 2.77 | 3.48 | 3.51 | 2.75 | 4.53 | 4.61 | 5.35 | 4.68 | 5.60 |
| $K_2O$ | % | 0.20 | | 0.16 | 0.53 | 0.13 | 0.26 | 0.16 | 0.29 | 0.04 | 0.8 | 1.13 | 1.32 | 1.2 | 1.62 |
| $P_2O_5$ | % | 0.25 | | 0.18 | 0.49 | 0.17 | 0.05 | 0.16 | 0.15 | 0.00 | 0.15 | 0.19 | 0.14 | 0.13 | 0.19 |
| $Cr_2O_3$ | % | 0.0187 | 0.0109 | 0.0094 | -0.0006 | 0.0188 | 0.0168 | 0.0288 | 0.0217 | 0.0120 | 0.0292 | 0.0040 | 0.0016 | 0.029 | 0.0030 |
| NiO | % | 0.0064 | 0.006 | 0.0051 | 0.0019 | 0.0071 | 0.0051 | 0.0078 | 0.0068 | 0.0106 | 0.0081 | 0.0017 | 0.0017 | 0.0089 | 0.0021 |
| L.O.I. | % | 6.19 | 2.06 | 2.53 | 5.63 | 3.89 | 1.80 | 7.28 | 2.03 | 2.43 | 4.09 | 2.34 | 1.98 | 4.71 | 1.52 |
| SUM | % | 100.2 | 98.94 | 99.72 | 100.57 | 96.34 | 99.99 | 103.82 | 100.02 | 99.89 | 99.19 | 99.87 | 100.08 | 99.33 | 99.92 |
| **trace elements** | | | | | | | | | | | | | | | |
| Sc | ppm | 46 | 42 | 43 | 28 | 34 | 45 | 44 | 42 | 40 | 34 | 37 | 32 | 31 | 26 |
| V | ppm | 408 | 122 | 375 | 40 | 379 | 359 | 344 | 366 | 397 | 370 | 328 | 340 | 330 | 259 |
| Cr | ppm | 132 | 22 | 62 | n.a | 151 | 116 | 224 | 164 | 77 | 226 | 14 | 3 | 229 | 21 |
| Co | ppm | 37 | 33 | 40 | 22 | 39 | 36 | 40 | 39 | 56 | 30 | 34 | 33 | 36 | 26 |
| Ni | ppm | 61 | 58 | 45 | 15 | 57 | 47 | 66 | 61 | 84 | 64 | 18 | 17 | 69 | 20 |
| Cu | ppm | 2 | n.a | n.a | n.a | 37 | n.a | 124 | 59 | 29 | 43 | n.a | n.a | 43 | n.a |
| Zn | ppm | 106 | 32 | 92 | 54 | 92 | 524 | 91 | 94 | 84 | 82 | 31 | 40 | 71 | 20 |
| Ga | ppm | 22 | 27 | 17 | 25 | 16 | 18 | 16 | 17 | 13 | 15 | 19 | 16 | 16 | 15 |
| Rb | ppm | 1 | 2 | 2 | 4 | 2 | n.a | 1 | 5 | n.a | 7 | 12 | 7 | 9 | 6 |
| Sr | ppm | 52 | 1,755 | 286 | 225 | 56 | 132 | 158 | 193 | 44 | 83 | 113 | 94 | 77 | 62 |
| Y | ppm | 26 | 6 | 45 | 19 | 43 | 24 | 39 | 38 | 8 | 34 | 42 | 36 | 29 | 40 |
| Zr | ppm | 37 | 5 | 89 | 7 | 109 | 18 | 113 | 111 | 3 | 104 | 118 | 89 | 94 | 112 |
| Nb | ppm | 4 | 1 | 4 | 1 | 4 | 2 | 4 | 4 | 2 | 4 | 4 | 3 | 3 | 4 |
| Ba | ppm | n.a | n.a | n.a | n.a | n.a | n.a | n.a | 15 | n.a | n.a | 38 | 12 | 13 | 6 |

| name | | ORK16 | ORK 35 | ORK 36 | ORK 66 |
|---|---|---|---|---|---|
| | | | | *felsic rocks* | |
| description | | lava | hyaloclast | lava | felsic |
| | | * | * | * | * |
| SiO$_2$ | % | 63.14 | 65.81 | 66.13 | 70.66 |
| TiO$_2$ | % | 0.89 | 0.35 | 0.30 | 0.36 |
| Al$_2$O$_3$ | % | 13.42 | 12.77 | 4.57 | 13.76 |
| Fe$_2$O$_3$ | % | 6.44 | 6.04 | 1.54 | 3.88 |
| MnO | % | 0.09 | 0.03 | 0.07 | 0.03 |
| MgO | % | 2.82 | 0.47 | 0.67 | 0.56 |
| CaO | % | 3.77 | 11.72 | 14.21 | 3.73 |
| Na$_2$O | % | 5.44 | 0.44 | 0.83 | 4.68 |
| K$_2$O | % | 1.20 | 0.02 | 0.78 | 1.07 |
| P$_2$O$_5$ | % | 0.31 | 0.05 | 0.05 | 0.08 |
| Cr$_2$O$_3$ | % | | 0.0006 | 0.0040 | |
| NiO | % | | 0.0004 | 0.0006 | |
| L.O.I. | % | 1.78 | 2.27 | 12.27 | 1.26 |
| SUM | % | 99.31 | 99.97 | 101.42 | 100.07 |

trace elements

| | | | | | |
|---|---|---|---|---|---|
| Sc | ppm | 15 | 16 | 12 | 7 |
| V | ppm | 58 | 52 | 36 | 44 |
| Cr | ppm | 1 | 10 | 36 | |
| Co | ppm | 17 | 5 | 2 | 10 |
| Ni | ppm | 5 | 8 | 8 | 4 |
| Cu | ppm | | 2 | 8 | 2 |
| Zn | ppm | 18 | 12 | 18 | 12 |
| Ga | ppm | 15 | 35 | 6 | 18 |
| Rb | ppm | 8 | n.a | 26 | 2 |
| Sr | ppm | 117 | 892 | 216 | 234 |
| Y | ppm | 45 | 53 | 12 | 60 |
| Zr | ppm | 162 | 220 | 194 | 283 |
| Nb | ppm | 5 | 7 | 8 | 4 |
| Ba | ppm | 41 | 12 | 105 | 13 |

**Table 4 a. Chemical compositions of major and trace elements for the Thessaloniki and Central Chalkidiki samples**

| | | Central Chalkidiki | | | | Lanari | | Thessaloniki | | | | | | | |
|---|---|---|---|---|---|---|---|---|---|---|---|---|---|---|---|
| name | | THS-5 | THS-6 | THS-7 | THS-8 | THS-9 | THS-11 | THS-13 | THS-15 | THS-16 | THS-17 | THS-19 | THS-20 | THS-21 | THS-23 |
| description | | cummulat | cummulate | cummulate | cummulate | gabbro | dunite | diorite | dyke | dyke | dyke | dyke | dyke | dyke | trondjemite |
| | | Px-ite | PX+Plg+Ol | PX+Plg+Ol | Px-ite | | serpentinised | | | | | doleritic | | | |
| **major elements** | | | | | | | | | | | | | | | |
| $SiO_2$ | % | 40.47 | 46.41 | 52.24 | 50.64 | 47.69 | 34.74 | 71.58 | 58.60 | 62.89 | 53.00 | 55.46 | 70.79 | 59.22 | 70.90 |
| $TiO_2$ | % | 0.02 | 0.08 | 0.15 | 0.11 | 0.10 | 0.02 | 0.26 | 0.65 | 0.53 | 0.95 | 0.76 | 0.35 | 0.71 | 0.46 |
| $Al_2O_3$ | % | 0.64 | 11.99 | 2.34 | 1.67 | 17.58 | 0.35 | 13.87 | 15.85 | 15.59 | 15.66 | 15.57 | 12.55 | 14.61 | 13.85 |
| $Fe_2O_3$ | % | 8.27 | 4.22 | 4.36 | 5.53 | 4.95 | 6.82 | 2.37 | 7.14 | 8.51 | 12.30 | 10.59 | 4.59 | 10.27 | 2.37 |
| MnO | % | 0.11 | 0.08 | 0.14 | 0.12 | 0.10 | 0.09 | 0.03 | 0.09 | 0.14 | 0.18 | 0.16 | 0.05 | 0.13 | 0.03 |
| MgO | % | 42.61 | 16.18 | 18.73 | 21.56 | 10.72 | 37.41 | 0.63 | 4.13 | 12.90 | 5.39 | 4.51 | 0.44 | 3.31 | 1.07 |
| CaO | % | 0.64 | 16.91 | 20.67 | 18.34 | 14.58 | 3.14 | 2.21 | 7.13 | 7.09 | 6.36 | 7.72 | 6.79 | 5.78 | 4.99 |
| $Na_2O$ | % | -0.04 | 0.08 | 0.09 | 0.02 | 0.57 | -0.05 | 4.57 | 3.43 | 3.44 | 1.76 | 1.49 | 2.93 | 2.42 | 3.66 |
| $K_2O$ | % | 0.00 | 0.01 | -0.03 | 0.00 | 0.04 | 0.00 | 1.51 | 0.03 | 2.06 | 0.01 | 0.01 | 0.04 | 0.01 | 0.58 |
| $P_2O_5$ | % | -0.01 | -0.01 | | -0.01 | -0.01 | 0 | 0.11 | 0.07 | 0.05 | 0.04 | 0.05 | 0.08 | 0.05 | 0.1 |
| $Cr_2O_3$ | % | 0.3799 | 0.2136 | | 0.5095 | 0.026 | 0.3999 | | 0.0097 | | 0.0044 | 0.0011 | | 0.0005 | |
| NiO | % | 0.2923 | 0.0349 | | 0.0432 | 0.0103 | 0.2861 | | 0.0029 | | 0.0012 | 0.0005 | | 0.0001 | |
| L.O.I. | % | 7.16 | 3.37 | 1.5 | 2.06 | 3.09 | 17.75 | 2.83 | 2.64 | 2.86 | 3.98 | 3.4 | 1.32 | 3.12 | 1.41 |
| SUM | % | 100.544 | 99.564 | 100.193 | 100.585 | 99.439 | 100.959 | 99.964 | 99.776 | 116.08 | 99.627 | 99.723 | 99.933 | 99.636 | 99.4 |
| **trace elements** | | | | | | | | | | | | | | | |
| Sc | ppm | 10 | 42 | 83 | 65 | 44 | 7 | 9 | 24 | 20 | 29 | 28 | 15 | 25 | 14 |
| V | ppm | 40 | 117 | 247 | 179 | 128 | 16 | 19 | 143 | 134 | 503 | 308 | 15 | 290 | 17 |
| Cr | ppm | 2197 | 1422 | 2924 | 3431 | 213 | 2189 | 14 | 84 | 789 | 15 | 14 | 1 | 5 | 1 |
| Co | ppm | 118 | 49 | 34 | 49 | 38 | 114 | 2 | 25 | 42 | 44 | 36 | 1 | 30 | 9 |
| Ni | ppm | 2118 | 286 | 213 | 334 | 86 | 2155 | 6 | 24 | 306 | 17 | 9 | 0 | 4 | 5 |
| Cu | ppm | -36 | 81 | 6 | 42 | 74 | -42 | 2 | 3 | -3 | 45 | 7 | 101 | 263 | 7 |
| Zn | ppm | 36 | 20 | 20 | 25 | 28 | 15 | 18 | 26 | 41 | 74 | 65 | 14 | 53 | 12 |
| Ga | ppm | 2 | 7 | 4 | 5 | 10 | 3 | 16 | 15 | 14 | 16 | 17 | 14 | 17 | 14 |
| Rb | ppm | 2 | 2 | 2 | 2 | 2 | 2 | 54 | 3 | 27 | 2 | 2 | 2 | 3 | 11 |
| Sr | ppm | 4 | 50 | 7 | 5 | 75 | 48 | 97 | 153 | 23 | 139 | 156 | 179 | 110 | 150 |
| Y | ppm | 2 | 5 | 6 | 6 | 4 | 2 | 29 | 22 | 16 | 18 | 18 | 31 | 19 | 26 |
| Zr | ppm | 16 | 18 | 18 | 18 | 17 | 16 | 120 | 90 | 72 | 50 | 50 | 88 | 58 | 102 |
| Nb | ppm | 2 | 3 | 1 | 1 | 2 | 1 | 9 | 4 | 3 | 1 | 1 | 2 | 3 | 4 |
| Ba | ppm | 15 | 12 | 27 | 21 | 15 | 11 | 381 | 17 | 389 | 1 | 1 | 5 | 5 | 63 |

**Table 4 b. Chemical compositions of major and trace elements for the Thessaloniki and samples**

| name | | THS-24 | THS 33 | THS-34 | THS-35 | THS 36 | THS 37 | THS 39 | THS 41 | THS 42 | THS 43 |
|---|---|---|---|---|---|---|---|---|---|---|---|
| description | | dyke | lava vesicular | dyke | dyke | dyke | dyke | dyke | dyke | dyke | dyke |

**major elements**

| | | | | | | | | | | | |
|---|---|---|---|---|---|---|---|---|---|---|---|
| $SiO_2$ | % | 55.49 | 63.92 | 58.71 | 52.57 | 61.85 | 52.49 | 60.86 | 55.6 | 53.43 | 58.26 |
| $TiO_2$ | % | 0.41 | 0.77 | 0.82 | 0.53 | 0.84 | 0.39 | 0.68 | 0.39 | 0.33 | 0.91 |
| $Al_2O_3$ | % | 14.09 | 15.43 | 15.43 | 16.35 | 15.04 | 15.2 | 15.21 | 16 | 15.68 | 14.62 |
| $Fe_2O_3$ | % | 7.45 | 7.44 | 7.90 | 8.40 | 6.81 | 7.94 | 7.65 | 7.52 | 8.03 | 8.06 |
| MnO | % | 0.12 | 0.08 | 0.09 | 0.11 | 0.09 | 0.14 | 0.09 | 0.13 | 0.14 | 0.13 |
| MgO | % | 7.19 | 2.56 | 2.69 | 6.78 | 2.14 | 7.18 | 2.69 | 5.85 | 5.34 | 3.18 |
| CaO | % | 10.72 | 1.56 | 5.39 | 5.82 | 3.58 | 13.49 | 7.67 | 9.4 | 14.5 | 6.82 |
| $Na_2O$ | % | 1.12 | 5.72 | 4.47 | 2.96 | 4.84 | 0.52 | 2.41 | 2.02 | 0.14 | 2.28 |
| $K_2O$ | % | 0.02 | 0.09 | 0.10 | 0.15 | 0.59 | 0.03 | 0.01 | 0.01 | 0.01 | 0.01 |
| $P_2O_5$ | % | 0.02 | 0.09 | 0.07 | 0.03 | 0.08 | 0.01 | 0.06 | 0.03 | 0.01 | 0.05 |
| $Cr_2O_3$ | % | 0.0347 | 0.0004 | 0.001 | 0.0029 | 0.0003 | 0.0362 | -0.0003 | 0.0181 | 0.0144 | 0.0014 |
| NiO | % | 0.0081 | 0 | -0.0007 | 0.0024 | -0.0004 | 0.0098 | -0.001 | 0.0056 | 0.0031 | -0.0008 |
| L.O.I. | % | 2.72 | 2.22 | 3 | 5.12 | 3.6 | 2.45 | 2.29 | 3.12 | 2.53 | -0.3 |
| SUM | % | 99.377 | 99.878 | 98.658 | 98.829 | 99.452 | 99.893 | 99.625 | 100.097 | 100.157 | 94.02 |

**trace elements**

| | | | | | | | | | | | |
|---|---|---|---|---|---|---|---|---|---|---|---|
| Sc | | 35 | 18 | na | na | 19 | 36 | 21 | 32 | 27 | 41 |
| V | ppm | 199 | 95 | na | na | 140 | 190 | 148 | 165 | 261 | 193 |
| Cr | ppm | 255 | 18 | na | na | 12 | 281 | 11 | 144 | 10 | 118 |
| Co | ppm | 29 | 14 | na | na | 11 | 27 | 14 | 27 | 26 | 29 |
| Ni | ppm | 64 | 7 | na | na | 7 | 89 | 1 | 48 | 10 | 31 |
| Cu | ppm | 7 | 3 | na | na | 7 | 2 | 120 | 4 | 6 | 85 |
| Zn | ppm | 39 | 32 | na | na | 29 | 27 | 24 | 47 | 38 | 43 |
| Ga | ppm | 13 | 17 | na | na | 17 | 13 | 17 | 14 | 15 | 15 |
| Rb | ppm | 2 | 4 | na | na | 16 | 4 | 3 | 3 | 3 | 3 |
| Sr | ppm | 146 | 94 | na | na | 98 | 74 | 157 | 113 | 139 | 132 |
| Y | ppm | 14 | 28 | na | na | 25 | 12 | 22 | 15 | 22 | 11 |
| Zr | ppm | 39 | 107 | na | na | 104 | 35 | 68 | 44 | 61 | 31 |
| Nb | ppm | 2 | 5 | na | na | 5 | 2 | 3 | 2 | 2 | 1 |
| Ba | ppm | 8 | 63 | na | na | 243 | 24 | 5 | 9 | -11 | 14 |

**Table 4 a. Chemical compositions of major and trace elements for the Sithonia samples**

| name | | Skra | | | | | | | | | | | | | | |
|---|---|---|---|---|---|---|---|---|---|---|---|---|---|---|---|---|
| | | SIT1 | SIT2 | SIT3 | SIT4 | SIT5 | SIT6 | SIT7 | SIT8 | SIT9 | SIT14 | SIT14 | SIT15 | SIT 25 | SIT 26 | SIT 27 |
| description | | dyke | flow | dyke | flow | dyke | dyke | dyke | dyke | dyke | lava | lava | lava | lava | lava | lava |
| | | doleritic | | | | doleritic | | | | doleritic | pillow | pillow | pillow | pillow | pillow | pillow |
| **major elements** | | | | | | | | | | | | | | | | |
| $SiO_2$ | % | 54.76 | 53.48 | 49.00 | 50.73 | 51.88 | 52.99 | 50.82 | 57.72 | 50.99 | 47.95 | 47.95 | 46.12 | 49.46 | 48.35 | 54.32 |
| $TiO_2$ | % | 0.32 | 0.45 | 0.97 | 1.42 | 1.52 | 2.11 | 1.28 | 1.62 | 2.13 | 0.78 | 0.78 | 0.87 | 1.67 | 1.51 | 0.39 |
| $Al_2O_3$ | % | 14.57 | 15.13 | 15.78 | 14.66 | 15.45 | 13.84 | 15.21 | 16.07 | 14.41 | 14.38 | 14.38 | 14.68 | 16.6 | 14.21 | 14.1 |
| $Fe_2O_3$ | % | 9.40 | 9.94 | 8.31 | 12.18 | 10.84 | 11.16 | 9.92 | 6.63 | 13.94 | 7.43 | 7.43 | 7.76 | 10.03 | 11.26 | 9.89 |
| MnO | % | 0.15 | 0.16 | 0.14 | 0.19 | 0.17 | 0.16 | 0.16 | 0.08 | 0.13 | 0.12 | 0.12 | 0.17 | 0.16 | 0.17 | 0.22 |
| MgO | % | 5.56 | 6.40 | 7.50 | 6.91 | 5.55 | 4.39 | 7.65 | 2.67 | 4.46 | 7.39 | 7.39 | 9.12 | 6.45 | 6.82 | 4.74 |
| CaO | % | 6.77 | 8.33 | 10.22 | 7.02 | 6.39 | 6.65 | 8.97 | 5.47 | 6.54 | 8.86 | 8.86 | 7.13 | 6.66 | 6.02 | 5.35 |
| $Na_2O$ | % | 3.86 | 3.26 | 2.45 | 3.18 | 5.18 | 5.51 | 3.18 | 7.46 | 3.93 | 3.87 | 3.87 | 3.77 | 2.73 | 3.89 | 4.16 |
| $K_2O$ | % | 0.04 | 0.03 | 0.38 | 0.83 | 0.51 | 0.22 | 0.49 | 0.14 | 0.51 | 0.32 | 0.32 | 0.21 | 1.95 | 1.14 | 0.06 |
| $P_2O_5$ | % | 0.01 | 0.01 | 0.09 | 0.12 | 0.19 | 0.25 | 0.13 | 0.41 | 0.19 | 0.08 | 0.08 | 0.09 | 0.24 | 0.17 | 0.01 |
| L.O.I. | % | 4.23 | 3.35 | 5.00 | 3.12 | 2.67 | 10.90 | 2.48 | 2.09 | 2.47 | 8.91 | 8.91 | 14.28 | 4.28 | 5.96 | 9.03 |
| SUM | % | 99.67 | 100.56 | 99.87 | 100.36 | 100.36 | 108.19 | 100.38 | 100.34 | 99.70 | 100.18 | 100.18 | 104.27 | 100.254 | 99.501 | 102.259 |
| **trace elements** | | | | | | | | | | | | | | | | |
| Sc | ppm | 48 | 38 | 38 | 39 | 29 | 32 | 34 | 22 | 34 | 37 | 36 | 38 | 28 | 37 | 33 |
| V | ppm | 241 | 257 | 232 | 287 | 304 | 338 | 288 | 117 | 429 | 240 | 244 | 231 | 283 | 288 | 309 |
| Cr | ppm | 58 | 109 | 134 | 6 | 93 | 25 | 363 | 3 | 0 | 482 | 491 | 374 | 55 | 16 | 19 |
| Co | ppm | 33 | 43 | 38 | 50 | 35 | 33 | 40 | 20 | 36 | 34 | 42 | 42 | 48 | 43 | 34 |
| Ni | ppm | 37 | 83 | 58 | 17 | 45 | 21 | 134 | 7 | 11 | 143 | 140 | 116 | 81 | 29 | 17 |
| Cu | ppm | 86 | 144 | 58 | 49 | 30 | 109 | 6 | 7 | 9 | 43 | 241 | 46 | 11 | 18 | 63 |
| Zn | ppm | 74 | 84 | 70 | 95 | 80 | 54 | 41 | 32 | 45 | 65 | 165 | 89 | 116 | 83 | 123 |
| Ga | ppm | 14 | 14 | 16 | 19 | 17 | 17 | 16 | 19 | 20 | 13 | 13 | 12 | 21 | 18 | 13 |
| Rb | ppm | 3 | 2 | 10 | 47 | 18 | 9 | 24 | 5 | 24 | 10 | 10 | 8 | 30 | 36 | 4 |
| Sr | ppm | 42 | 37 | 183 | 143 | 181 | 144 | 203 | 144 | 249 | 148 | 148 | 205 | 213 | 228 | 71 |
| Y | ppm | 12 | 14 | 23 | 33 | 35 | 48 | 31 | 62 | 42 | 18 | 17 | 21 | 34 | 31 | 12 |
| Zr | ppm | 28 | 32 | 76 | 100 | 133 | 174 | 104 | 244 | 141 | 66 | 66 | 72 | 140 | 114 | 28 |
| Nb | ppm | 1 | 2 | 4 | 3 | 6 | 7 | 3 | 8 | 5 | 2 | 2 | 3 | 5 | 5 | 2 |
| Ba | ppm | 26 | 12 | 83 | 99 | 51 | - | 83 | - | 43 | 168 | 168 | 320 | 175 | 410 | 30 |

*SIT 14 was analysed two times.                                                                                          XVIII

**Table 4 b. Chemical compositions of major and trace elements for the Kassandra samples**

| name | | Fanos | | | Eyzonoi | | | | | | | | | | | |
|---|---|---|---|---|---|---|---|---|---|---|---|---|---|---|---|---|
| name | | KAS3 | KAS4 | KAS7 | KAS7 | KAS6 | KAS 8 | KAS 9 | KAS 10 | KAS 14 | KAS 16 | KAS 17 | KAS 19 | KAS20 | KAS 21 | KAS21 |
| description | | lava | lava | lava | lava | lava pillow | lava | lava pillow | lava pillow | lava pillow | lava | lava | lava | lava pillow | lava pillow | lava pillow |
| **major elements** | | | | | | | | | | | | | | | | |
| SiO$_2$ | % | 46.29 | 56.01 | 48.27 | 48.37 | 46.23 | 47.28 | 43.34 | 49.1 | 56.99 | 38.35 | 42.89 | 47.48 | 56.52 | 48.23 | 47.53 |
| TiO$_2$ | % | 1.91 | 1.20 | 1.43 | 1.43 | 1.25 | 1.47 | 1.36 | 2.16 | 0.94 | 0.81 | 0.97 | 1.41 | 0.97 | 1.98 | 1.43 |
| Al$_2$O$_3$ | % | 16.92 | 16.24 | 15.96 | 16.03 | 15.25 | 14.44 | 13.79 | 15.24 | 16.08 | 12.74 | 13.54 | 16.14 | 15.46 | 15.27 | 16.63 |
| Fe$_2$O$_3$ | % | 4.94 | 9.97 | 9.45 | 9.48 | 8.28 | 7.67 | 8.91 | 11.4 | 8.83 | 7.14 | 6.94 | 9.88 | 9.91 | 11.71 | 8.84 |
| MnO | % | 0.15 | 0.16 | 0.14 | 0.15 | 0.09 | 0.15 | 0.18 | 0.18 | 0.16 | 0.11 | 0.1 | 0.14 | 0.16 | 0.18 | 0.13 |
| MgO | % | 2.37 | 2.62 | 7.31 | 7.34 | 2.68 | 7.36 | 5.24 | 5.77 | 3.74 | 3.56 | 3.43 | 6.2 | 4.08 | 4.66 | 7.45 |
| CaO | % | 13.65 | 4.53 | 9.57 | 9.59 | 11.81 | 9.81 | 14.2 | 7.05 | 3.2 | 17.89 | 13.97 | 9.78 | 2.78 | 9.63 | 8.99 |
| Na$_2$O | % | 4.78 | 6.32 | 3.67 | 3.69 | 6.33 | 4.5 | 2.97 | 5.05 | 5.28 | 2.4 | 4.18 | 3.66 | 5.18 | 4.11 | 3.78 |
| K$_2$O | % | 1.28 | 0.26 | 0.68 | 0.67 | 0.07 | 0.59 | 2 | 0.09 | 1.36 | 1.82 | 0.92 | 0.48 | 0.96 | 0.07 | 0.03 |
| P$_2$O$_5$ | % | 0.21 | 0.17 | 0.17 | 0.17 | 0.15 | 0.18 | 0.16 | 0.27 | 0.11 | 0.1 | 0.07 | 0.16 | 0.11 | 0.24 | 0.20 |
| L.O.I. | % | 8.21 | 3.07 | 3.64 | 3.64 | 8.37 | 5.82 | 8.4 | 3.19 | 3.38 | 15.68 | 13.34 | 4.39 | 3.39 | 4.55 | 4.65 |
| SUM | % | 100.74 | 100.53 | 100.33 | 100.61 | 100.57 | 99.344 | 100.643 | 99.513 | 100.076 | 100.642 | 100.382 | 99.741 | 99.51 | 100.625 | 99.71 |
| **trace elements** | | | | | | | | | | | | | | | | |
| Sc | ppm | 43 | na | 38 | 30 | na | 31 | 35 | 28 | 26 | 35 | 32 | 33 | 28 | 36 | na |
| V | ppm | 279 | na | 214 | 257 | na | 236 | 272 | 324 | 202 | 200 | 217 | 257 | 247 | 333 | na |
| Cr | ppm | 217 | na | 388 | 245 | na | 342 | 470 | 45 | 11 | 180 | 246 | 181 | 9 | 28 | na |
| Co | ppm | 40 | na | 24 | 37 | na | 49 | 37 | 32 | 17 | 31 | 24 | 36 | 24 | 32 | na |
| Ni | ppm | 97 | na | 79 | 89 | na | 199 | 138 | 19 | 5 | 60 | 59 | 77 | 7 | 16 | na |
| Cu | ppm | 54 | na | 38 | 47 | na | 52 | 50 | 32 | 35 | 25 | 24 | 45 | 47 | 34 | na |
| Zn | ppm | 89 | na | 64 | 72 | na | 82 | 81 | 94 | 85 | 75 | 76 | 76 | 89 | 100 | na |
| Ga | ppm | 18 | na | 14 | 18 | na | 13 | 16 | 15 | 18 | 13 | 13 | 17 | 18 | 20 | na |
| Rb | ppm | 32 | na | 4 | 15 | na | 13 | 40 | 4 | 26 | 40 | 25 | 11 | 17 | 4 | na |
| Sr | ppm | 261 | na | 256 | 144 | na | 134 | 263 | 215 | 162 | 330 | 318 | 183 | 138 | 124 | na |
| Y | ppm | 40 | na | 27 | 26 | na | 26 | 27 | 39 | 29 | 19 | 20 | 27 | 32 | 39 | na |
| Zr | ppm | 197 | na | 105 | 116 | na | 123 | 103 | 134 | 91 | 73 | 92 | 105 | 97 | 147 | na |
| Nb | ppm | 5 | na | 4 | 3 | na | 5 | 4 | 5 | 2 | 4 | 2 | 4 | 2 | 4 | na |
| Ba | ppm | 34 | na | 2 | 29 | na | 7 | 69 | -20 | 129 | 117 | 75 | 14 | 63 | - | na |

**The sample KAS 21 was used as duplicate to check the reproducibility of the analytical equipment from the major elements analyses**

**EYZONOI SAMPLES**

| Sample | | EYZ 1 | EYZ 2 | EYZ 3 | EYZ 4 | EYZ 6 | EYZ 8 | EYZ 9 | EYZ 10 | EYZ 12 | EYZ 15 | EYZ 16 |
|---|---|---|---|---|---|---|---|---|---|---|---|---|
| Rb | ppm | 0.35 | 1.37 | 5.93 | 0.38 | 6.15 | 35.43 | 11.51 | 88.77 | 1.27 | 1.41 | 1.13 |
| Sr | ppm | 15.46 | 151.04 | 71.68 | 52.52 | 88.38 | 351.63 | 70.11 | 332.85 | 88.49 | 117.47 | 83.18 |
| Y | ppm | 13.98 | 41.19 | 30.86 | 57.11 | 51.44 | 39.66 | 40.29 | 19.26 | 28.20 | 14.64 | 50.89 |
| Zr | ppm | 44.69 | 128.43 | 101.57 | 202.86 | 173.83 | 181.39 | 155.54 | 48.13 | 98.63 | 48.56 | 183.56 |
| Nb | ppm | 1.66 | 3.64 | 2.77 | 9.49 | 8.35 | 5.26 | 7.00 | 1.16 | 3.82 | 1.30 | 7.08 |
| Ba | ppm | 2.17 | 13.15 | 24.07 | 11.47 | 19.60 | 895.35 | 36.75 | 341.75 | 15.97 | 18.34 | 11.21 |
| | | | | | | | | | | | | |
| La | ppm | 1.86 | 9.42 | 4.14 | 6.44 | 8.93 | 24.34 | 7.17 | 4.63 | 2.94 | 5.81 | 10.22 |
| Ce | ppm | 5.01 | 22.71 | 11.51 | 18.88 | 25.58 | 49.00 | 18.79 | 10.57 | 8.05 | 14.27 | 26.64 |
| Pr | ppm | 0.81 | 3.35 | 1.89 | 3.20 | 3.84 | 6.20 | 2.95 | 1.51 | 1.36 | 1.98 | 4.10 |
| Nd | ppm | 4.33 | 16.70 | 10.35 | 17.59 | 19.67 | 26.89 | 15.40 | 7.85 | 7.45 | 9.15 | 20.77 |
| Sm | ppm | 1.43 | 4.88 | 3.33 | 5.98 | 6.01 | 6.29 | 4.77 | 2.16 | 2.69 | 2.37 | 6.27 |
| Eu | ppm | 0.38 | 1.63 | 0.98 | 1.44 | 1.80 | 1.49 | 1.31 | 0.78 | 0.76 | 0.73 | 2.00 |
| Gd | ppm | 1.96 | 6.31 | 4.49 | 8.29 | 7.81 | 6.70 | 6.33 | 2.81 | 3.89 | 2.59 | 8.21 |
| Tb | ppm | 0.35 | 1.08 | 0.76 | 1.47 | 1.34 | 1.04 | 1.08 | 0.51 | 0.69 | 0.41 | 1.40 |
| Dy | ppm | 2.43 | 7.35 | 5.27 | 10.06 | 9.10 | 6.81 | 7.38 | 3.41 | 4.99 | 2.66 | 9.27 |
| Ho | ppm | 0.53 | 1.55 | 1.13 | 2.18 | 1.91 | 1.44 | 1.55 | 0.71 | 1.10 | 0.55 | 1.97 |
| Er | ppm | 1.56 | 4.52 | 3.39 | 6.48 | 5.58 | 4.29 | 4.62 | 2.12 | 3.30 | 1.65 | 5.92 |
| Tm | ppm | 0.23 | 0.65 | 0.49 | 0.93 | 0.81 | 0.62 | 0.67 | 0.30 | 0.47 | 0.23 | 0.84 |
| Yb | ppm | 1.56 | 4.44 | 3.28 | 6.31 | 5.50 | 4.12 | 4.55 | 2.03 | 3.16 | 1.61 | 5.62 |
| | | | | | | | | | | | | |
| Lu | ppm | 0.23 | 0.68 | 0.51 | 0.96 | 0.82 | 0.65 | 0.70 | 0.31 | 0.48 | 0.24 | 0.86 |
| Hf | ppm | 1.24 | 3.62 | 2.73 | 5.56 | 4.50 | 4.84 | 4.41 | 1.35 | 2.67 | 1.46 | 4.95 |
| Ta | ppm | 0.11 | 0.26 | 0.19 | 0.70 | 0.53 | 0.42 | 0.51 | 0.09 | 0.28 | 0.12 | 0.49 |
| Pb | ppm | 0.89 | 2.34 | 1.62 | 1.63 | 1.51 | 10.79 | 2.01 | 1.52 | 2.63 | 6.84 | 1.39 |
| Th | ppm | 0.23 | 1.66 | 0.54 | 1.21 | 0.91 | 10.32 | 1.17 | 1.12 | 0.59 | 2.31 | 1.26 |
| U | ppm | 0.07 | 0.49 | 0.14 | 0.35 | 0.33 | 3.05 | 0.40 | 0.32 | 0.17 | 0.92 | 0.31 |

**SKRA SAMPLES**

| Sample | | GVL 8 | GVL 10 | GVL 11 | GVL 12 | GVL 13 | GVL 14 | GVL 15 | GVL 16 | GVL 18 | GVL 21 | GVL 22 | GVL 23 | GVL 23 |
|---|---|---|---|---|---|---|---|---|---|---|---|---|---|---|
| Rb | ppm | 0.48 | 0.22 | 0.38 | 0.15 | 0.44 | 3.70 | 26.13 | 12.35 | 0.53 | 0.39 | 0.28 | 0.49 | 0.63 |
| Sr | ppm | 205.99 | 208.44 | 266.99 | 166.95 | 223.46 | 166.33 | 387.62 | 322.52 | 163.92 | 17.51 | 20.68 | 33.33 | 33.09 |
| Y | ppm | 32.11 | 22.57 | 22.96 | 32.58 | 30.85 | 31.55 | 18.52 | 18.16 | 18.55 | 43.47 | 49.20 | 63.74 | 68.03 |
| Zr | ppm | 151.08 | 51.37 | 48.80 | 67.56 | 81.47 | 101.85 | 77.69 | 37.31 | 50.14 | 278.12 | 261.01 | 220.12 | 239.28 |
| Nb | ppm | 1.47 | 1.07 | 0.60 | 1.12 | 1.55 | 2.26 | 3.10 | 1.03 | 0.88 | 5.70 | 6.19 | 5.15 | 5.20 |
| Ba | ppm | 6.06 | 11.99 | 6.97 | 9.72 | 16.47 | 26.18 | 146.20 | 108.94 | 17.62 | 8.06 | 7.25 | 12.69 | 14.61 |
| | | | | | | | | | | | | | | |
| La | ppm | 4.13 | 2.29 | 3.36 | 3.44 | 5.48 | 6.43 | 15.25 | 5.63 | 1.87 | 10.15 | 8.81 | 9.74 | 10.05 |
| Ce | ppm | 11.22 | 6.55 | 9.08 | 10.42 | 14.14 | 16.13 | 34.67 | 11.66 | 5.72 | 27.16 | 23.52 | 27.10 | 28.13 |
| Pr | ppm | 1.86 | 1.13 | 1.50 | 1.81 | 2.30 | 2.47 | 4.37 | 1.67 | 1.03 | 4.18 | 4.02 | 4.58 | 4.74 |
| Nd | ppm | 10.15 | 6.45 | 8.37 | 10.18 | 12.10 | 12.87 | 18.13 | 7.96 | 5.94 | 20.02 | 20.42 | 24.11 | 25.07 |
| Sm | ppm | 3.42 | 2.26 | 2.67 | 3.45 | 3.70 | 3.88 | 4.02 | 2.24 | 2.05 | 5.29 | 6.01 | 7.68 | 7.99 |
| Eu | ppm | 0.97 | 0.86 | 1.05 | 1.05 | 1.40 | 1.42 | 1.23 | 0.82 | 0.74 | 1.15 | 1.68 | 2.29 | 2.26 |
| Gd | ppm | 4.60 | 3.14 | 3.60 | 4.81 | 4.83 | 4.99 | 3.71 | 2.94 | 2.83 | 6.14 | 7.33 | 9.88 | 10.33 |
| Tb | ppm | 0.80 | 0.57 | 0.62 | 0.85 | 0.82 | 0.83 | 0.55 | 0.49 | 0.49 | 1.05 | 1.25 | 1.68 | 1.76 |
| Dy | ppm | 5.56 | 4.00 | 4.18 | 5.82 | 5.60 | 5.54 | 3.40 | 3.20 | 3.34 | 7.30 | 8.41 | 11.23 | 11.88 |
| Ho | ppm | 1.19 | 0.84 | 0.87 | 1.24 | 1.16 | 1.18 | 0.68 | 0.66 | 0.71 | 1.65 | 1.82 | 2.38 | 2.52 |
| Er | ppm | 3.65 | 2.51 | 2.56 | 3.63 | 3.42 | 3.46 | 1.94 | 1.95 | 2.05 | 5.73 | 6.13 | 7.35 | 7.85 |
| Tm | ppm | 0.52 | 0.35 | 0.36 | 0.51 | 0.48 | 0.49 | 0.28 | 0.27 | 0.29 | 0.90 | 0.92 | 1.06 | 1.13 |
| Yb | ppm | 3.62 | 2.33 | 2.39 | 3.40 | 3.21 | 3.34 | 1.95 | 1.85 | 1.97 | 6.61 | 6.72 | 7.19 | 7.70 |
| | | | | | | | | | | | | | | |
| Lu | ppm | 0.58 | 0.34 | 0.35 | 0.50 | 0.48 | 0.51 | 0.29 | 0.29 | 0.29 | 1.10 | 1.12 | 1.08 | 1.16 |
| Hf | ppm | 3.60 | 1.52 | 1.65 | 2.17 | 2.39 | 2.53 | 2.19 | 1.25 | 1.45 | 7.54 | 7.18 | 6.05 | 6.54 |
| Ta | ppm | 0.10 | 0.08 | 0.05 | 0.10 | 0.11 | 0.17 | 0.27 | 0.08 | 0.06 | 0.41 | 0.45 | 0.37 | 0.38 |
| Pb | ppm | 0.09 | 0.15 | 0.16 | 0.15 | 0.18 | 0.33 | 4.50 | 7.20 | 0.32 | 0.80 | 0.97 | 1.33 | 1.50 |
| Th | ppm | 1.19 | 0.37 | 0.51 | 0.52 | 0.92 | 1.31 | 5.65 | 2.54 | 0.27 | 2.13 | 2.01 | 1.73 | 1.86 |
| U | ppm | 0.33 | 0.07 | 0.09 | 0.06 | 0.13 | 0.34 | 1.18 | 0.56 | 0.08 | 0.98 | 1.10 | 1.28 | 1.35 |

**ORAIOKASTRO SAMPLES**

| Sample | | ORK13 | ORK32 | ORK37 | ORK38 | ORK39 | ORK57 | ORK5 | ORK6 | ORK7 | ORK8 | ORK11 | ORK12 | ORK14 | ORK15 | ORK17 | ORK34 | ORK38 |
|--------|------|-------|-------|-------|-------|-------|-------|------|------|------|------|-------|-------|-------|-------|-------|-------|-------|
| | | ppm | ppm | ppm | ppm | ppm | ppm | ppm | ppm | ppm | ppm | ppm | ppm | ppm | ppm | ppm | ppm | ppm |
| Rb | ppm | 5.06 | 1.06 | 3.45 | 3.77 | 2.41 | 2.92 | 5.46 | 7.07 | 0.46 | 2.49 | 3.33 | 7.05 | 8.28 | 10.89 | 0.75 | 11.27 | 4.12 |
| Sr | ppm | 83.42 | 84.47 | 105.48 | 104.09 | 94.09 | 290.16 | 129.17 | 114.92 | 69.71 | 102.60 | 130.86 | 74.18 | 55.09 | 113.64 | 53.73 | 113.34 | 153.65 |
| Y | ppm | 36.49 | 18.65 | 18.23 | 20.40 | 18.55 | 43.09 | 14.50 | 14.70 | 18.00 | 20.81 | 19.50 | 28.77 | 20.06 | 21.55 | 44.25 | 40.71 | 29.84 |
| Zr | ppm | 103.71 | 39.97 | 34.36 | 42.50 | 38.11 | 73.78 | 24.41 | 22.63 | 33.09 | 41.27 | 35.26 | 89.41 | 46.83 | 48.33 | 105.29 | 106.39 | 93.84 |
| Nb | ppm | 2.27 | 0.80 | 0.67 | 0.82 | 0.82 | 2.84 | 0.49 | 0.41 | 0.68 | 0.84 | 0.99 | 1.95 | 0.99 | 1.02 | 2.24 | 3.07 | 2.21 |
| Ba | ppm | 22.95 | 9.36 | 13.93 | 17.35 | 19.35 | 14.94 | 24.99 | 22.82 | 9.07 | 20.65 | 18.34 | 34.78 | 41.83 | 54.76 | 7.89 | 54.64 | 28.97 |
| | | | | | | | | | | | | | | | | | | |
| La | ppm | 4.10 | 1.53 | 1.59 | 1.89 | 1.83 | 4.18 | 1.15 | 1.16 | 1.49 | 1.87 | 2.04 | 3.12 | 2.48 | 2.29 | 5.01 | 5.14 | 3.67 |
| Ce | ppm | 12.47 | 4.32 | 4.37 | 5.19 | 5.21 | 13.69 | 3.15 | 3.12 | 4.07 | 5.04 | 5.29 | 10.17 | 6.47 | 6.26 | 13.84 | 14.59 | 10.60 |
| Pr | ppm | 2.09 | 0.72 | 0.71 | 0.84 | 0.83 | 2.38 | 0.50 | 0.50 | 0.67 | 0.83 | 0.83 | 1.76 | 1.02 | 1.01 | 2.26 | 2.37 | 1.73 |
| Nd | ppm | 11.69 | 4.20 | 4.07 | 4.69 | 4.61 | 13.47 | 2.83 | 2.81 | 3.86 | 4.66 | 4.44 | 9.67 | 5.58 | 5.59 | 12.47 | 12.85 | 9.45 |
| Sm | ppm | 3.91 | 1.56 | 1.51 | 1.72 | 1.70 | 4.58 | 1.11 | 1.11 | 1.47 | 1.76 | 1.62 | 3.30 | 1.91 | 2.02 | 4.29 | 4.35 | 3.20 |
| Eu | ppm | 1.35 | 0.52 | 0.57 | 0.59 | 0.62 | 1.50 | 0.41 | 0.44 | 0.55 | 0.61 | 0.58 | 1.16 | 0.73 | 0.72 | 1.48 | 1.29 | 1.11 |
| Gd | ppm | 5.29 | 2.42 | 2.30 | 2.63 | 2.43 | 6.29 | 1.72 | 1.76 | 2.27 | 2.60 | 2.37 | 4.39 | 2.69 | 2.86 | 5.90 | 5.81 | 4.37 |
| Tb | ppm | 0.94 | 0.46 | 0.42 | 0.49 | 0.45 | 1.10 | 0.32 | 0.33 | 0.42 | 0.48 | 0.44 | 0.77 | 0.49 | 0.51 | 1.03 | 1.04 | 0.76 |
| Dy | ppm | 6.66 | 3.38 | 3.16 | 3.61 | 3.30 | 7.84 | 2.45 | 2.47 | 3.16 | 3.58 | 3.31 | 5.38 | 3.51 | 3.67 | 7.31 | 7.38 | 5.37 |
| Ho | ppm | 1.41 | 0.74 | 0.70 | 0.79 | 0.73 | 1.68 | 0.55 | 0.55 | 0.69 | 0.79 | 0.73 | 1.13 | 0.76 | 0.80 | 1.59 | 1.59 | 1.16 |
| Er | ppm | 4.11 | 2.23 | 2.09 | 2.35 | 2.17 | 4.86 | 1.66 | 1.66 | 2.07 | 2.32 | 2.18 | 3.16 | 2.23 | 2.28 | 4.58 | 4.54 | 3.33 |
| Tm | ppm | 0.61 | 0.34 | 0.31 | 0.36 | 0.32 | 0.72 | 0.26 | 0.25 | 0.31 | 0.35 | 0.33 | 0.46 | 0.34 | 0.34 | 0.67 | 0.68 | 0.49 |
| | | | | | | | | | | | | | | | | | | |
| Yb | ppm | 4.11 | 2.31 | 2.15 | 2.49 | 2.34 | 4.84 | 1.78 | 1.75 | 2.13 | 2.48 | 2.31 | 3.04 | 2.34 | 2.30 | 4.46 | 4.59 | 3.32 |
| Lu | ppm | 0.62 | 0.36 | 0.33 | 0.38 | 0.35 | 0.72 | 0.28 | 0.27 | 0.33 | 0.37 | 0.36 | 0.44 | 0.36 | 0.36 | 0.68 | 0.68 | 0.50 |
| Hf | ppm | 3.04 | 1.38 | 1.18 | 1.45 | 1.31 | 2.52 | 0.85 | 0.79 | 1.12 | 1.34 | 1.19 | 2.57 | 1.40 | 1.41 | 2.85 | 3.02 | 2.52 |
| Ta | ppm | 0.18 | 0.07 | 0.06 | 0.09 | 0.07 | 0.20 | 0.06 | 0.03 | 0.06 | 0.06 | 0.08 | 0.15 | 0.07 | 0.08 | 0.17 | 0.23 | 0.17 |
| Pb | ppm | 0.82 | 0.33 | 0.49 | 0.40 | 0.71 | 0.45 | 0.53 | 0.84 | 0.26 | 0.68 | 0.59 | 0.63 | 0.18 | 0.64 | 1.22 | 0.36 | 0.50 |
| Th | ppm | 0.48 | 0.88 | 0.58 | 0.47 | 0.35 | 0.93 | 0.66 | 5.13 | 0.27 | 0.94 | 0.67 | 0.27 | 0.38 | 1.24 | 0.30 | 0.77 | 0.43 |
| U | ppm | 0.13 | 0.14 | 0.14 | 0.14 | 0.15 | 0.04 | 0.10 | 0.13 | 0.09 | 0.15 | 0.11 | 0.44 | 0.11 | 0.10 | 0.16 | 0.24 | 0.10 |

**ORAIOKASTRO GABBROS**

| Sample | | ORK10 | ORK9 | ORK71 | ORK72 | ORK73 | ORK76 | ORK77 |
|--------|-----|-------|------|-------|-------|-------|-------|-------|
| | | ppm | ppm | ppm | ppm | ppm | ppm | ppm |
| Rb | ppm | 0.95 | 1.95 | 1.44 | 1.25 | 0.59 | 1.84 | 0.86 |
| Sr | ppm | 135.35 | 214.92 | 177.48 | 207.63 | 180.93 | 126.25 | 210.50 |
| Y | ppm | 10.57 | 8.90 | 8.78 | 6.30 | 9.47 | 7.89 | 6.58 |
| Zr | ppm | 16.82 | 13.23 | 6.86 | 6.56 | 9.12 | 6.46 | 4.38 |
| Nb | ppm | 0.37 | 0.31 | 0.05 | 0.08 | 0.12 | 0.05 | 0.03 |
| Ba | ppm | 17.78 | 9.92 | 5.69 | 7.59 | 4.33 | 8.80 | 4.18 |
| | | | | | | | | |
| La | ppm | 0.86 | 0.68 | 0.40 | 0.51 | 0.60 | 0.38 | 0.41 |
| Ce | ppm | 2.38 | 1.99 | 1.34 | 1.47 | 1.75 | 1.28 | 1.20 |
| Pr | ppm | 0.40 | 0.35 | 0.27 | 0.26 | 0.32 | 0.25 | 0.22 |
| Nd | ppm | 2.34 | 2.06 | 1.77 | 1.54 | 1.99 | 1.67 | 1.43 |
| Sm | ppm | 0.93 | 0.81 | 0.79 | 0.59 | 0.86 | 0.71 | 0.59 |
| Eu | ppm | 0.42 | 0.44 | 0.44 | 0.43 | 0.47 | 0.41 | 0.45 |
| Gd | ppm | 1.42 | 1.25 | 1.27 | 0.93 | 1.34 | 1.14 | 0.95 |
| Tb | ppm | 0.27 | 0.23 | 0.23 | 0.17 | 0.25 | 0.21 | 0.18 |
| Dy | ppm | 1.96 | 1.65 | 1.70 | 1.21 | 1.80 | 1.52 | 1.27 |
| Ho | ppm | 0.42 | 0.35 | 0.36 | 0.26 | 0.38 | 0.32 | 0.27 |
| Er | ppm | 1.21 | 0.98 | 1.02 | 0.72 | 1.07 | 0.91 | 0.76 |
| Tm | ppm | 0.18 | 0.14 | 0.15 | 0.10 | 0.16 | 0.13 | 0.11 |
| | | | | | | | | |
| Yb | ppm | 1.13 | 0.95 | 0.95 | 0.67 | 1.04 | 0.87 | 0.69 |
| Lu | ppm | 0.17 | 0.14 | 0.14 | 0.10 | 0.15 | 0.13 | 0.10 |
| Hf | ppm | 0.60 | 0.44 | 0.31 | 0.27 | 0.39 | 0.28 | 0.20 |
| Ta | ppm | 0.03 | 0.03 | 0.01 | 0.01 | 0.01 | 0.01 | 0.00 |
| Pb | ppm | 0.47 | 0.21 | 0.11 | 0.15 | 0.42 | 0.10 | 0.32 |
| Th | ppm | 0.28 | 0.14 | 0.05 | 0.02 | 0.28 | 2.64 | 0.31 |
| U | ppm | 0.05 | 0.02 | 0.00 | 0.00 | 0.02 | 0.00 | 0.00 |

# THESSALONIKI SAMPLES

|      |     | THS 15 | THS 15 | THS 16 | THS 17 | THS 19 | THS 21 | THS 24 | THS 33 | THS 37 | THS 39 | THS 41 | THS 42 |
|------|-----|--------|--------|--------|--------|--------|--------|--------|--------|--------|--------|--------|--------|
| Rb   | ppm | 0.24   | 0.20   | 26.21  | 0.04   | 0.02   | 0.05   | 0.14   | 0.45   | 0.38   | 0.06   | 0.03   | 0.04   |
| Sr   | ppm | 159.23 | 161.95 | 23.00  | 149.89 | 162.57 | 111.63 | 148.57 | 31.63  | 82.77  | 167.81 | 124.69 | 149.05 |
| Y    | ppm | 20.55  | 22.99  | 18.78  | 17.78  | 15.38  | 17.13  | 11.92  | 3.66   | 10.28  | 20.08  | 14.23  | 8.92   |
| Zr   | ppm | 84.54  | 80.97  | 73.46  | 40.79  | 32.29  | 51.13  | 25.87  | 9.10   | 18.99  | 60.65  | 34.81  | 15.94  |
| Nb   | ppm | 3.17   | 4.65   | 2.04   | 0.99   | 0.82   | 1.07   | 0.64   | 0.21   | 0.41   | 1.27   | 0.76   | 0.37   |
| Ba   | ppm | 11.74  | 11.60  | 362.04 | 3.24   | 2.59   | 3.23   | 3.33   | 3.14   | 7.93   | 4.73   | 3.47   | 2.76   |
|      |     |        |        |        |        |        |        |        |        |        |        |        |        |
| La   | ppm | 10.11  | 9.67   | 5.70   | 2.76   | 2.28   | 3.23   | 1.50   | 0.57   | 1.16   | 2.83   | 3.99   | 0.98   |
| Ce   | ppm | 20.67  | 21.13  | 12.19  | 6.05   | 5.85   | 6.98   | 3.65   | 1.44   | 3.18   | 7.26   | 7.10   | 2.38   |
| Pr   | ppm | 2.51   | 2.68   | 1.55   | 0.85   | 0.84   | 0.96   | 0.55   | 0.20   | 0.46   | 1.04   | 0.83   | 0.34   |
| Nd   | ppm | 11.17  | 11.91  | 7.29   | 4.42   | 4.29   | 4.93   | 2.91   | 1.00   | 2.40   | 5.25   | 3.85   | 1.83   |
| Sm   | ppm | 2.90   | 3.18   | 2.06   | 1.52   | 1.49   | 1.63   | 1.08   | 0.33   | 0.86   | 1.78   | 1.25   | 0.71   |
| Eu   | ppm | 0.71   | 0.77   | 0.56   | 0.57   | 0.56   | 0.56   | 0.39   | 0.11   | 0.37   | 0.63   | 0.43   | 0.31   |
| Gd   | ppm | 3.27   | 3.79   | 2.66   | 2.29   | 2.09   | 2.26   | 1.54   | 0.48   | 1.30   | 2.61   | 1.78   | 1.10   |
| Tb   | ppm | 0.54   | 0.63   | 0.45   | 0.42   | 0.37   | 0.41   | 0.28   | 0.09   | 0.24   | 0.48   | 0.33   | 0.21   |
| Dy   | ppm | 3.78   | 4.19   | 3.28   | 3.09   | 2.63   | 3.01   | 2.11   | 0.64   | 1.72   | 3.44   | 2.37   | 1.51   |
| Ho   | ppm | 0.79   | 0.87   | 0.70   | 0.67 z |        | 0.67   | 0.46   | 0.14   | 0.39   | 0.76   | 0.52   | 0.34   |
| Er   | ppm | 2.31   | 2.53   | 2.04   | 2.03   | 1.71   | 2.01   | 1.35   | 0.42   | 1.18   | 2.09   | 1.59   | 1.01   |
| Tm   | ppm | 0.34   | 0.36   | 0.30   | 0.31   | 0.26   | 0.30   | 0.21   | 0.06   | 0.17   | 0.31   | 0.24   | 0.15   |
| Yb   | ppm | 2.34   | 2.48   | 2.08   | 2.14   | 1.82   | 2.13   | 1.43   | 0.44   | 1.28   | 2.24   | 1.70   | 1.10   |
|      |     |        |        |        |        |        |        |        |        |        |        |        |        |
| Lu   | ppm | 0.35   | 0.38   | 0.32   | 0.33   | 0.27   | 0.33   | 0.22   | 0.07   | 0.19   | 0.34   | 0.26   | 0.16   |
| Hf   | ppm | 2.54   | 2.58   | 2.18   | 1.42   | 1.07   | 1.62   | 0.91   | 0.29   | 0.64   | 1.90   | 1.10   | 0.56   |
| Ta   | ppm | 0.26   | 0.34   | 0.17   | 0.08   | 0.06   | 0.10   | 0.05   | 0.02   | 0.03   | 0.10   | 0.06   | 0.03   |
| Pb   | ppm | 1.14   | 1.32   | 0.18   | 0.83   | 1.27   | 0.95   | 0.65   | 0.12   | 0.40   | 0.83   | 0.71   | 1.08   |
| Th   | ppm | 3.86   | 3.97   | 2.40   | 0.84   | 0.56   | 1.00   | 0.61   | 0.19   | 0.35   | 1.13   | 0.65   | 0.29   |
| U    | ppm | 0.79   | 0.67   | 0.46   | 0.32   | 0.25   | 0.37   | 0.22   | 0.06   | 0.13   | 0.44   | 0.27   | 0.15   |

*The sample THS 15 was analysed two times , each in diffenet analalising batces to test the reproducibility of the*
*analytical equipment*                                                                                    XXV

## SITHONIA SAMPLES

| | | SIT 1 | SIT 3 | SIT 4 | SIT 5 | SIT 7 | SIT 9 | SIT 14 | SIT 25 | SIT 26 | SIT 27 |
|---|---|---|---|---|---|---|---|---|---|---|---|
| **Rb** | ppm | 0.34 | 8.46 | 45.36 | 15.48 | 25.36 | 20.93 | 7.25 | 29.00 | 34.76 | 0.99 |
| **Sr** | ppm | 40.61 | 207.46 | 145.84 | 176.08 | 297.62 | 254.25 | 156.63 | 235.26 | 250.27 | 69.46 |
| **Y** | ppm | 11.09 | 22.46 | 32.90 | 33.68 | 50.19 | 42.56 | 17.09 | 35.59 | 34.43 | 11.77 |
| **Zr** | ppm | 10.76 | 68.19 | 96.76 | 119.39 | 170.23 | 148.79 | 57.53 | 151.96 | 120.45 | 13.47 |
| **Nb** | ppm | 0.27 | 2.23 | 2.44 | 3.79 | 4.45 | 3.69 | 1.45 | 5.57 | 4.91 | 0.47 |
| **Ba** | ppm | 19.55 | 89.30 | 98.74 | 63.76 | 89.68 | 66.17 | 168.04 | 211.08 | 476.00 | 16.62 |
| | | | | | | | | | | | |
| **La** | ppm | 0.77 | 7.36 | 7.38 | 12.38 | 13.61 | 11.81 | 4.25 | 20.85 | 12.09 | 1.20 |
| **Ce** | ppm | 1.76 | 15.58 | 16.98 | 26.22 | 30.91 | 26.87 | 9.97 | 46.09 | 29.59 | 2.84 |
| **Pr** | ppm | 0.25 | 2.13 | 2.49 | 3.56 | 4.42 | 3.82 | 1.46 | 5.86 | 4.06 | 0.36 |
| **Nd** | ppm | 1.43 | 10.40 | 12.80 | 16.68 | 22.09 | 19.10 | 7.51 | 25.11 | 18.65 | 1.78 |
| **Sm** | ppm | 0.59 | 2.96 | 3.88 | 4.59 | 6.21 | 5.33 | 2.23 | 5.79 | 4.94 | 0.68 |
| **Eu** | ppm | 0.22 | 0.96 | 1.24 | 1.31 | 1.85 | 1.60 | 0.75 | 1.83 | 1.64 | 0.25 |
| **Gd** | ppm | 1.10 | 3.55 | 5.02 | 5.33 | 7.67 | 6.56 | 2.70 | 6.35 | 5.81 | 1.19 |
| **Tb** | ppm | 0.22 | 0.59 | 0.85 | 0.86 | 1.28 | 1.09 | 0.45 | 1.02 | 0.97 | 0.24 |
| **Dy** | ppm | 1.77 | 4.14 | 6.01 | 5.95 | 8.96 | 7.62 | 3.18 | 6.58 | 6.33 | 1.90 |
| **Ho** | ppm | 0.42 | 0.86 | 1.25 | 1.29 | 1.91 | 1.62 | 0.67 | 1.35 | 1.34 | 0.45 |
| **Er** | ppm | 1.30 | 2.49 | 3.61 | 3.70 | 5.49 | 4.70 | 1.94 | 3.93 | 3.85 | 1.46 |
| **Tm** | ppm | 0.21 | 0.36 | 0.53 | 0.50 | 0.81 | 0.69 | 0.29 | 0.55 | 0.55 | 0.23 |
| **Yb** | ppm | 1.44 | 2.46 | 3.49 | 3.43 | 5.46 | 4.65 | 1.98 | 3.73 | 3.68 | 1.72 |
| | | | | | | | | | | | |
| **Lu** | ppm | 0.24 | 0.36 | 0.51 | 0.54 | 0.83 | 0.71 | 0.30 | 0.55 | 0.55 | 0.28 |
| **Hf** | ppm | 0.42 | 2.01 | 2.72 | 3.27 | 4.70 | 4.09 | 1.63 | 4.31 | 3.37 | 0.53 |
| **Ta** | ppm | 0.02 | 0.19 | 0.20 | 0.32 | 0.36 | 0.30 | 0.11 | 0.47 | 0.36 | 0.04 |
| **Pb** | ppm | 0.89 | 4.38 | 5.27 | 1.43 | 1.08 | 0.99 | 5.15 | 12.15 | 4.05 | 4.47 |
| **Th** | ppm | 0.28 | 3.43 | 2.41 | 4.61 | 5.16 | 4.59 | 1.44 | 8.51 | 4.00 | 0.46 |
| **U** | ppm | 0.12 | 1.13 | 0.76 | 1.19 | 1.46 | 1.36 | 0.49 | 2.61 | 1.06 | 0.23 |

# KASSANDRA SAMPLES

|      |     | KAS 3  | KAS 4  | KAS 7 | KAS 8  | KAS 9  | KAS 10 | KAS 14 | KAS 17 | KAS 19 | KAS 20 | KAS 21 |
|------|-----|--------|--------|-------|--------|--------|--------|--------|--------|--------|--------|--------|
| Rb   | ppm | 26.98  | 3.50   | 4.33  | 11.59  | 33.80  | 1.31   | 20.80  | 23.96  | 7.63   | 15.70  | 0.21   |
| Sr   | ppm | 271.18 | 115.51 | 65.16 | 143.54 | 219.38 | 226.43 | 156.30 | 347.68 | 188.78 | 150.83 | 101.99 |
| Y    | ppm | 40.42  | 35.31  | 10.93 | 24.30  | 23.35  | 37.67  | 28.41  | 19.06  | 26.30  | 30.99  | 27.70  |
| Zr   | ppm | 206.92 | 87.68  | 44.02 | 119.70 | 94.59  | 147.49 | 78.52  | 124.26 | 90.14  | 93.00  | 137.89 |
| Nb   | ppm | 4.09   | 1.48   | 1.05  | 5.10   | 3.53   | 4.24   | 1.68   | 2.82   | 3.31   | 1.77   | 5.05   |
| Ba   | ppm | 56.99  | 59.12  | 15.17 | 29.94  | 66.59  | 28.36  | 129.84 | 81.89  | 32.39  | 74.57  | 18.53  |
|      |     |        |        |       |        |        |        |        |        |        |        |        |
| La   | ppm | 8.40   | 7.78   | 3.01  | 5.72   | 2.87   | 5.97   | 5.82   | 6.30   | 4.94   | 5.98   | 5.78   |
| Ce   | ppm | 22.85  | 21.02  | 7.67  | 17.17  | 8.65   | 18.67  | 15.82  | 15.68  | 14.01  | 15.58  | 15.50  |
| Pr   | ppm | 3.60   | 3.11   | 1.14  | 2.61   | 1.47   | 3.00   | 2.23   | 2.04   | 2.13   | 2.30   | 2.45   |
| Nd   | ppm | 19.37  | 16.42  | 5.93  | 13.14  | 8.03   | 16.25  | 11.09  | 9.48   | 10.98  | 11.66  | 12.72  |
| Sm   | ppm | 5.66   | 4.52   | 1.66  | 3.54   | 2.71   | 4.93   | 3.36   | 2.57   | 3.34   | 3.55   | 3.82   |
| Eu   | ppm | 1.91   | 1.35   | 0.58  | 1.25   | 0.99   | 1.89   | 1.19   | 0.89   | 1.24   | 1.24   | 1.31   |
| Gd   | ppm | 6.84   | 5.27   | 1.94  | 4.15   | 3.50   | 6.28   | 4.27   | 3.07   | 4.29   | 4.59   | 4.58   |
| Tb   | ppm | 1.11   | 0.88   | 0.31  | 0.71   | 0.62   | 1.07   | 0.74   | 0.53   | 0.74   | 0.78   | 0.78   |
| Dy   | ppm | 7.66   | 6.23   | 2.07  | 4.73   | 4.30   | 7.11   | 5.13   | 3.63   | 5.03   | 5.35   | 5.27   |
| Ho   | ppm | 1.59   | 1.34   | 0.42  | 0.98   | 0.91   | 1.49   | 1.10   | 0.78   | 1.05   | 1.15   | 1.08   |
| Er   | ppm | 4.51   | 4.00   | 1.19  | 2.59   | 2.49   | 3.94   | 3.05   | 2.17   | 2.86   | 3.39   | 3.06   |
| Tm   | ppm | 0.65   | 0.60   | 0.17  | 0.38   | 0.36   | 0.56   | 0.45   | 0.32   | 0.41   | 0.50   | 0.43   |
| Yb   | ppm | 4.34   | 4.15   | 1.13  | 2.57   | 2.47   | 3.78   | 3.15   | 2.30   | 2.73   | 3.48   | 2.97   |
|      |     |        |        |       |        |        |        |        |        |        |        |        |
| Lu   | ppm | 0.66   | 0.64   | 0.17  | 0.39   | 0.38   | 0.57   | 0.48   | 0.35   | 0.41   | 0.53   | 0.44   |
| Hf   | ppm | 4.73   | 2.74   | 1.04  | 2.78   | 2.34   | 3.49   | 2.29   | 3.30   | 2.39   | 2.62   | 3.27   |
| Ta   | ppm | 0.30   | 0.10   | 0.08  | 0.34   | 0.24   | 0.29   | 0.15   | 0.25   | 0.23   | 0.18   | 0.35   |
| Pb   | ppm | 0.42   | 1.15   | 0.30  | 0.86   | 2.89   | 2.33   | 10.57  | 5.86   | 1.21   | 14.59  | 1.38   |
| Th   | ppm | 0.80   | 1.47   | 0.22  | 0.62   | 0.48   | 0.74   | 1.11   | 3.27   | 0.52   | 1.38   | 0.61   |
| U    | ppm | 0.42   | 0.41   | 0.06  | 0.34   | 0.16   | 0.21   | 0.75   | 1.72   | 0.20   | 0.87   | 0.23   |

| Sample | Rock type | Sr (ppm) | Rb (ppm) | $^{86}Sr/^{87}Sr$ measured | err 2σ | Sm (ppm) | Nd (ppm) | $^{147}Sm/^{144}Nd$ measured | $^{143}Nd/^{144}Nd$ measured | err 2σ | $\varepsilon_{Nd}$ |
|---|---|---|---|---|---|---|---|---|---|---|---|
| **ORAIOKASTRO** | | | | | | | | | | | |
| **ORK-6** | **Basalt** | 114.92 | 7.07 | 0.704242 | 0.8 | 1.10 | 2.81 | 0.2364 | 0.512949 | 11 | 5.2 |
| **ORK-8** | **Basalt** | 102.6 | 2.49 | 0.704209 | 1.0 | 1.66 | 4.44 | 0.2253 | 0.512983 | 11 | 6.1 |
| **ORK 37** | **Basalt** | 105.48 | 3.45 | 0.705446 | 1.3 | 1.70 | 4.10 | 0.2488 | 0.512898 | 8 | 4.0 |
| **ORK-58** | **Basalt** | 193 | 4.12 | 0.704748 | 1.2 | 4.13 | 12.48 | 0.2002 | 0.512985 | 8 | 6.7 |
| **ORK 57** | **Basalt** | 290.16 | 2.92 | 0.704207 | 1.0 | 4.60 | 13.50 | 0.2044 | 0.513008 | 39 | 7.1 |
| **ORK-13** | **Basalt** | 83.42 | 5.06 | 0.705586 | 1.0 | 3.80 | 11.34 | 0.2026 | 0.512977 | 10 | 6.5 |
| **ORK 34** | **Basalt** | 113.34 | 11.27 | 0.705320 | 1.2 | 4.40 | 12.90 | 0.2047 | 0.512973 | 20 | 6.4 |
| **ORK 73** | **Gabbro** | 180.93 | 0.59 | 0.703419 | 1.0 | 0.90 | 2.00 | 0.2700 | 0.513083 | 12 | 7.1 |
| **ORK 12** | **Basalt** | 74.18 | 7.05 | 0.706687 | 1.0 | | | | | | 0.0 |
| **ORK-16** | **Basalt** | 117 | | | | 5.03 | 15.98 | 0.1902 | 0.512957 | 11 | 6.4 |
| **THESSALONIKI** | | | | | | | | | | | |
| **THS-15** | **Andesite** | 159.23 | 0.24 | 0.705652 | 1.5 | 2.75 | 10.41 | 0.1597 | 0.512563 | 11 | -0.7 |
| **THS-16** | **Andesite** | 23 | 26.21 | 0.711218 | 0.9 | 1.79 | 6.20 | 0.1743 | 0.512673 | 14 | 1.2 |
| **THS-17** | **Basalt** | 149.89 | 0.04 | 0.70528 | 1.1 | 1.52 | 4.45 | 0.2063 | 0.512851 | 11 | 4.0 |
| **THS 19** | **Basalt** | 162.57 | 0.02 | 0.705171 | 1.2 | 1.49 | 4.29 | *0.2084* | 0.512871 | 5 | 4.3 |
| **THS-21** | **Basalt** | 111.63 | 0.05 | 0.705126 | 1.1 | 1.69 | 5.18 | 0.1972 | 0.512846 | 8 | 4.0 |
| **THS-24** | **Basalt** | 148.57 | 0.14 | 0.705001 | 1.2 | 1.13 | 3.10 | 0.2197 | 0.512823 | 9 | 3.1 |
| **THS 37** | **Basalt** | 82.77 | 0.38 | 0.704944 | 1.1 | 0.86 | 2.40 | *0.2150* | 0.512935 | 10 | 5.4 |
| **GUEVGUELY** | | | | | | | | | | | |
| **GVL 8** | **Basalt** | 205.99 | 0.48 | 0.704025 | 1.1 | 3.42 | 10.15 | *0.2020* | 0.512950 | 6 | 6.0 |
| **GVL-13** | **Basalt** | 223.46 | 0.44 | 0.703527 | 1.5 | 3.87 | 12.43 | 0.1883 | 0.512940 | 13 | 6.1 |
| **GVL-14** | **Basalt** | 166.33 | 3.7 | 0.703429 | 0.6 | 3.07 | 10.41 | 0.1782 | 0.512864 | 9 | 4.8 |
| **GVL-16** | **Basalt** | 322.52 | 12.35 | 0.70533 | 1.2 | 2.48 | 8.60 | 0.1744 | 0.512736 | 8 | 2.4 |
| **GVL 18** | **Basalt** | 163.92 | 0.53 | 0.703206 | 0.9 | 2.05 | 5.94 | *0.2069* | 0.512982 | 5 | 6.5 |
| **GVL 22** | **Basalt** | 20.68 | 0.28 | 0.705193 | 1.0 | 6.01 | 20.42 | *0.1767* | 0.512966 | 9 | 6.8 |
| **GVL 23** | **Basalt** | 33.1 | 0.63 | 0.705057 | 1.2 | 7.69 | 24.11 | *0.1912* | 0.512964 | | 6.5 |
| **EYZ-2** | **Basalt** | 151.04 | 1.368 | 0.706522 | 1.3 | 6.84 | 21.55 | 0.1918 | 0.512966 | 11 | 6.5 |
| **EYZ 8** | **Basalt** | 351.63 | 35.43 | 0.712489 | 1.2 | 6.29 | 26.89 | *0.1404* | 0.512608 | | 0.6 |
| **EYZ-9** | **Basalt** | 70.11 | 11.51 | 0.704665 | 1.1 | 2.18 | 7.54 | 0.1751 | 0.512819 | 8 | 4.0 |
| **EYZ-12** | **Basalt** | 88.49 | 1.27 | 0.704665 | 1.3 | 4.94 | 16.92 | 0.1766 | 0.512898 | 8 | 5.5 |
| **EYZ 1** | **Basalt** | 15.46 | 0.35 | 0.704692 | 1.2 | 1.43 | 4.33 | *0.1980* | 0.512920 | 12 | 5.5 |
| **EYZ 15** | **Basalt** | 117.48 | 1.41 | 0.70533 | 1.0 | 2.37 | 9.15 | *0.1552* | 0.512663 | 11 | 1.4 |
| **EYZ 6** | **Basalt** | 88.38 | 6.15 | 0.7052 | 1.4 | 6.01 | 19.67 | *0.1833* | 0.512937 | | 6.1 |
| **SITHONIA KASSANDRA** | | | | | | | | | | | |
| **SIT 1** | **Basalt** | 40.61 | 0.34 | 0.705910 | 1.3 | 0.59 | 1.43 | *0.2476* | 0.512826 | 16 | 2.6 |
| **SIT 7** | **Basalt** | 297.62 | 25.36 | 0.705169 | 1.2 | 6.21 | 22.09 | *0.1687* | 0.512866 | 12 | 5.0 |
| **SIT 14** | **Basalt** | 156.63 | 7.25 | 0.704231 | 1.4 | 2.23 | 7.51 | *0.1782* | 0.512815 | | 3.8 |
| **SIT 4** | **Basalt** | 145.84 | 45.36 | 0.707501 | 1.3 | 3.88 | 12.80 | *0.1819* | 0.512868 | 8 | 4.8 |
| **KAS 3** | **Basalt** | 271.18 | 26.98 | 0.705810 | 1.5 | 5.66 | 19.37 | *0.1753* | 0.512729 | | 2.2 |
| **KAS 9** | **Basalt** | 219.38 | 33.8 | 0.704851 | 1.0 | 2.71 | 8.03 | *0.2025* | 0.512928 | | 5.5 |
| **KAS 7** | **Basalt** | 65.16 | 4.33 | 0.704666 | 1.0 | 1.66 | 5.93 | *0.1680* | 0.512764 | 8 | 3.1 |
| **KAS 19** | **Basalt** | 188.78 | 7.63 | 0.704129 | 1.0 | 3.34 | 10.98 | *0.1825* | 0.512910 | 12 | 5.6 |
| **KAS 17** | **Basalt** | 347.68 | 23.96 | 0.706727 | 1.2 | 2.57 | 9.48 | *0.1627* | 0.512793 | 12 | 3.7 |

# APPENDIX F ELEMENT vs Zr PLOTS

XXX

# Guevguely Complex

## X.R.F.

**LA-ICPMS**

XXXII
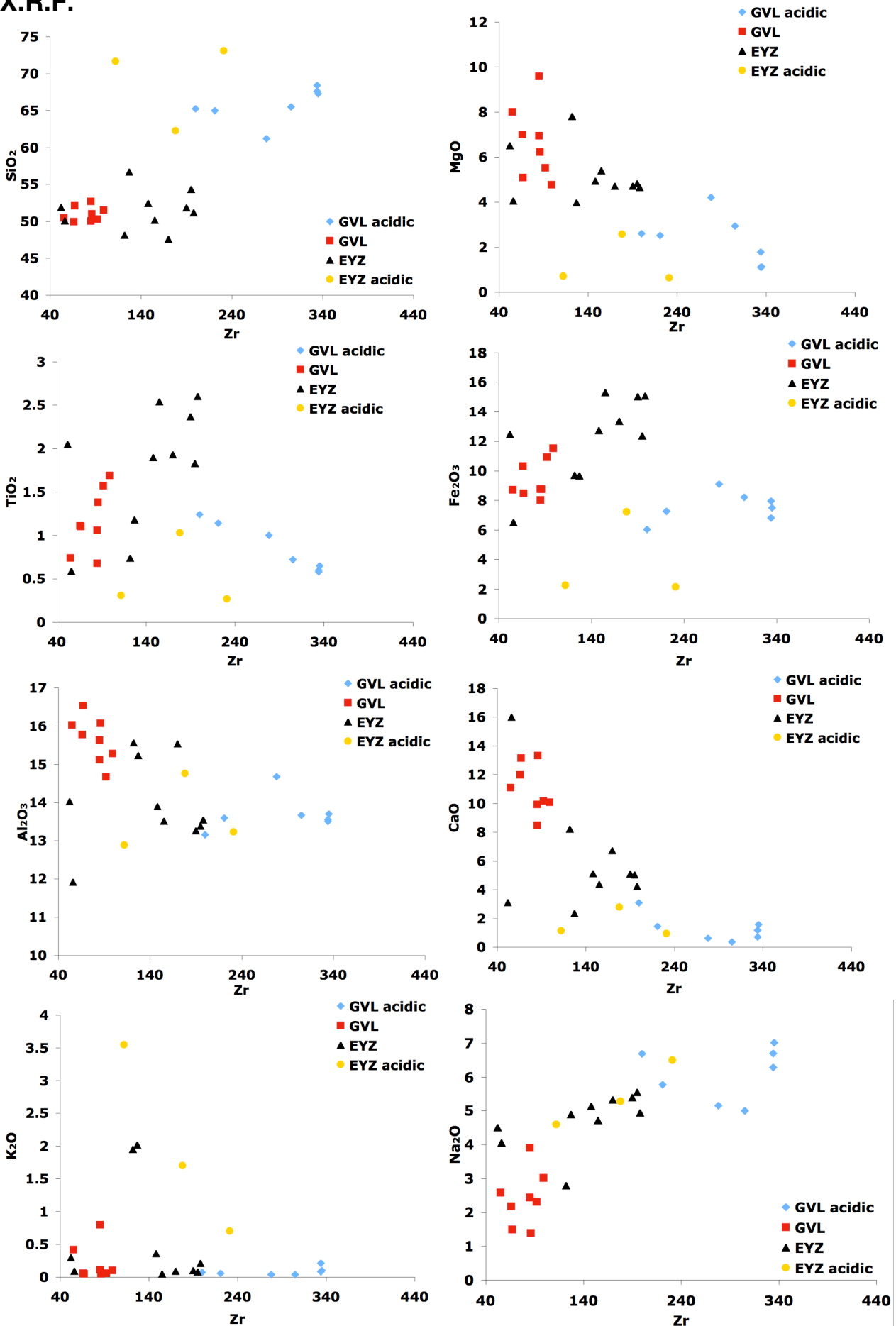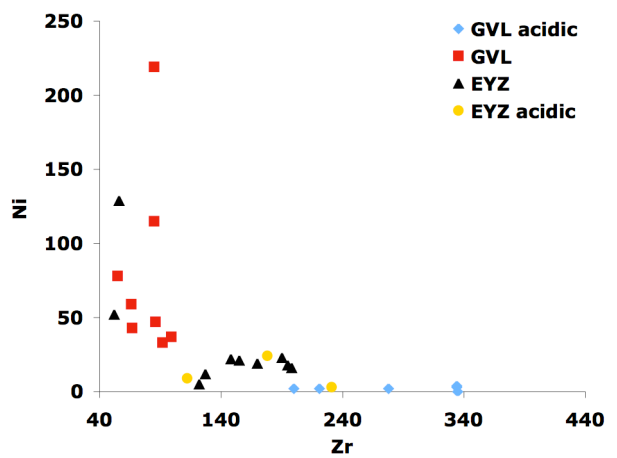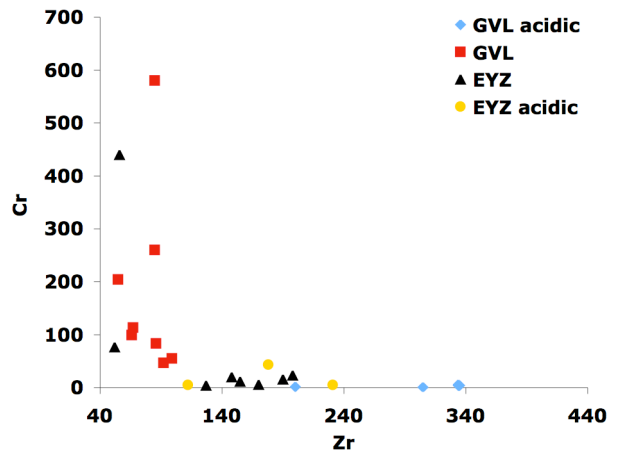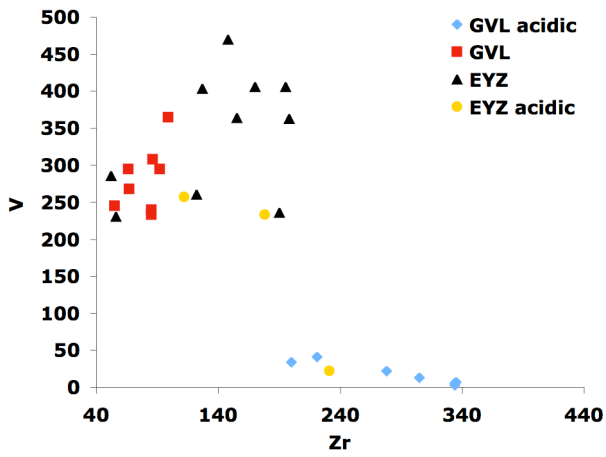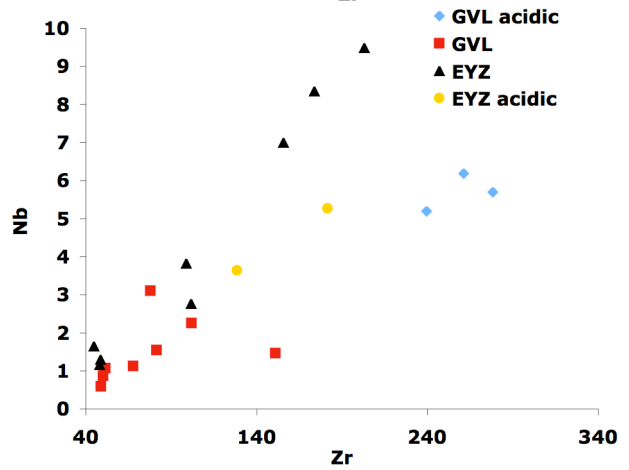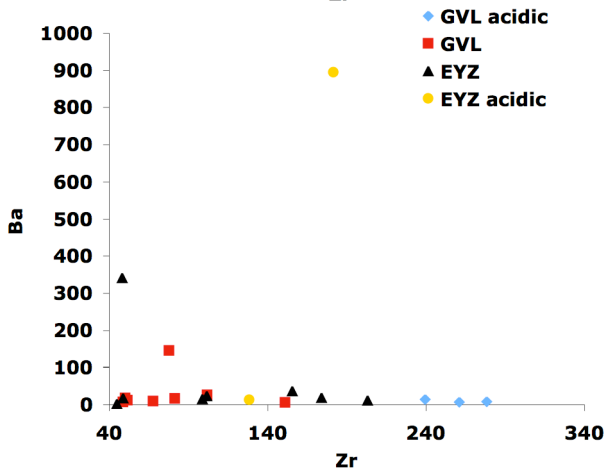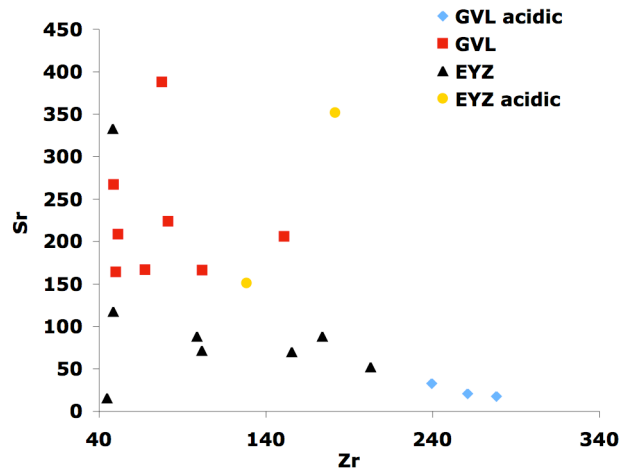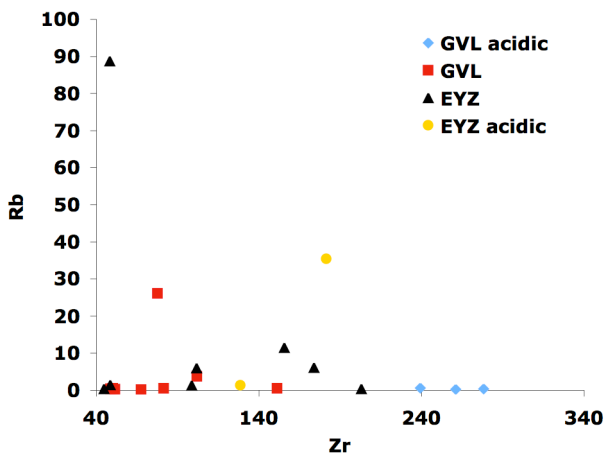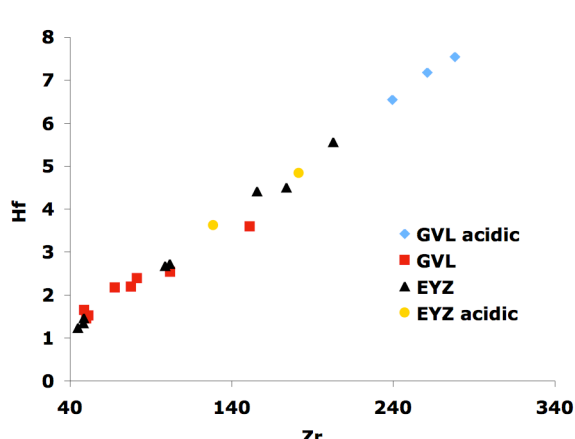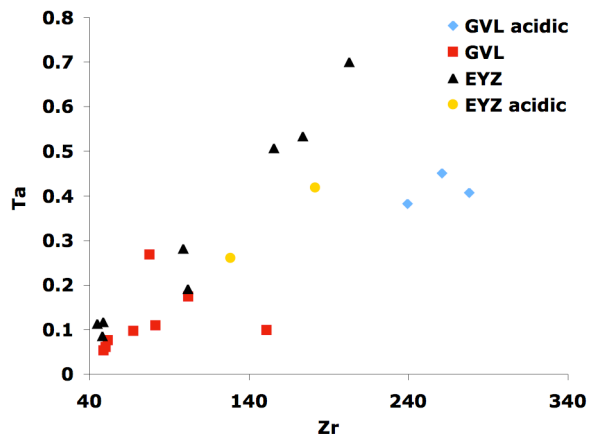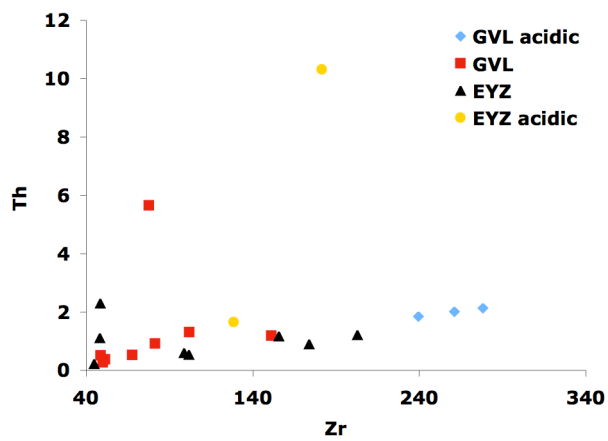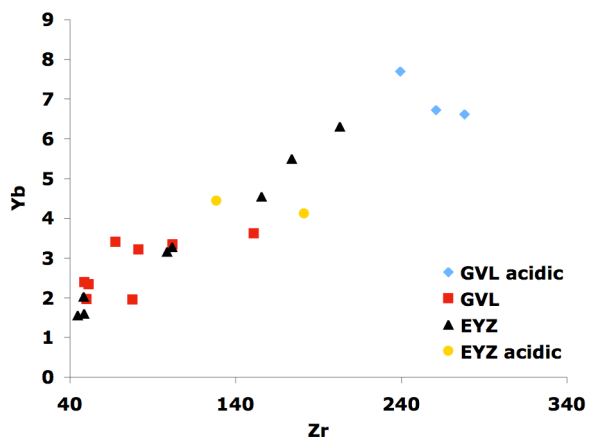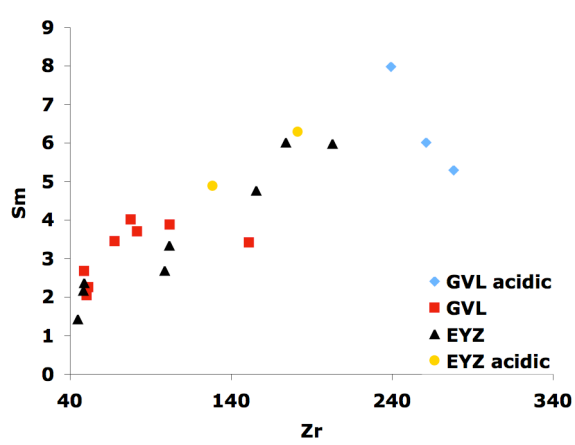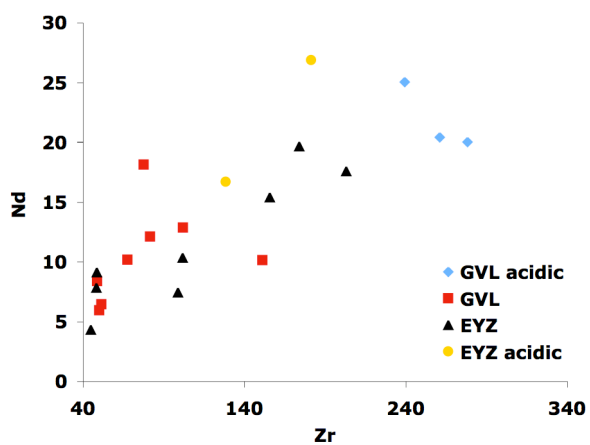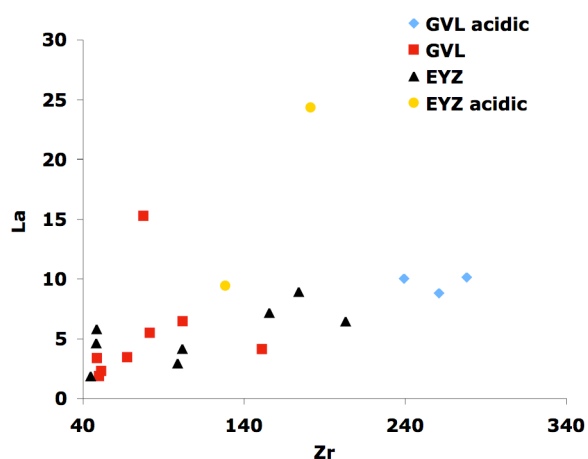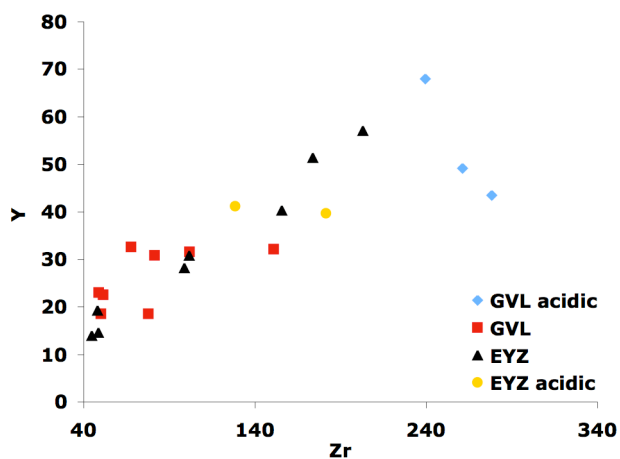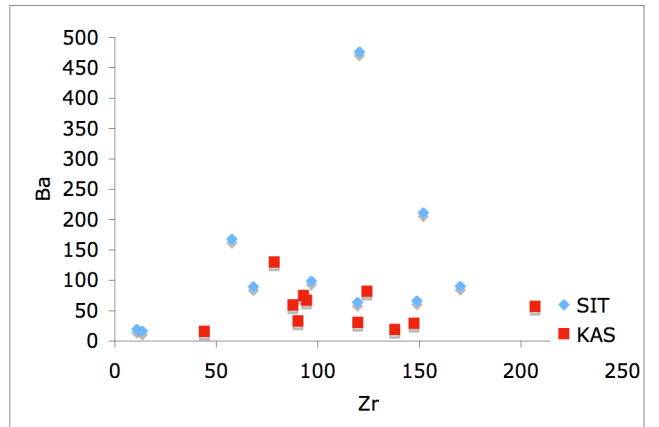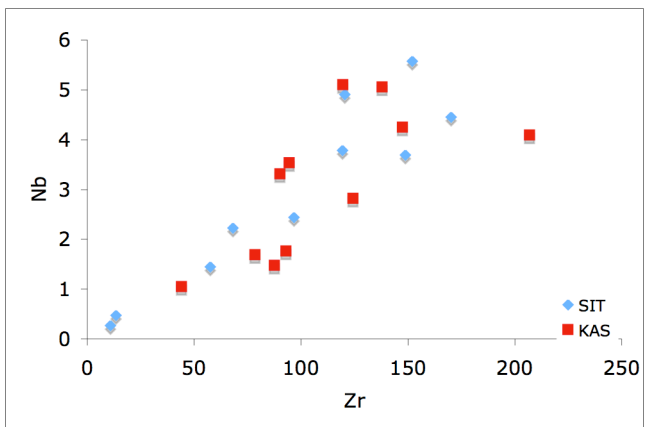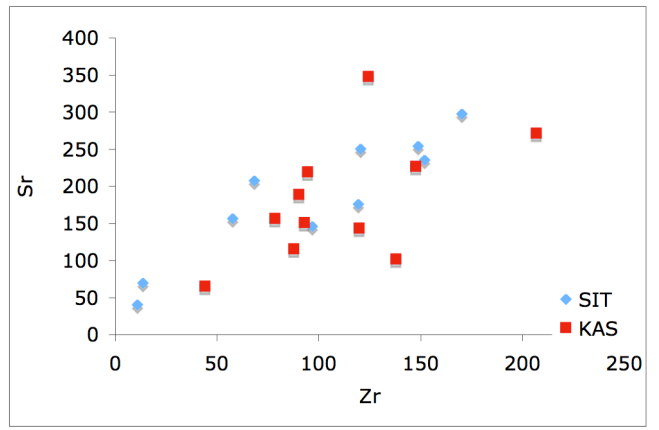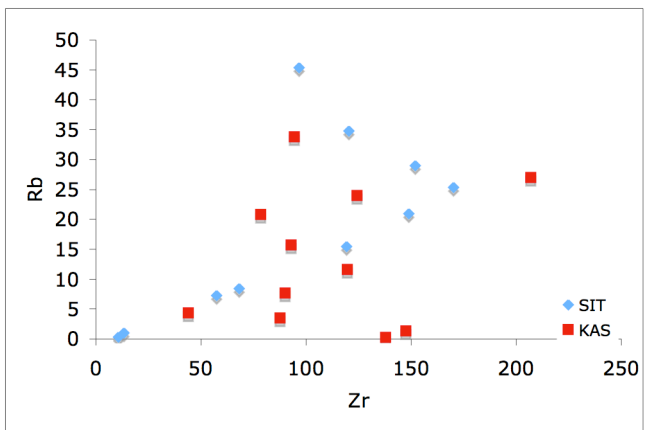
# Oraiokastro Ophiolite

## X.R.F
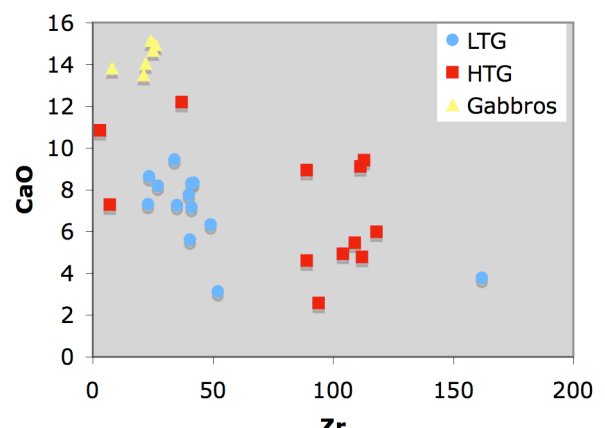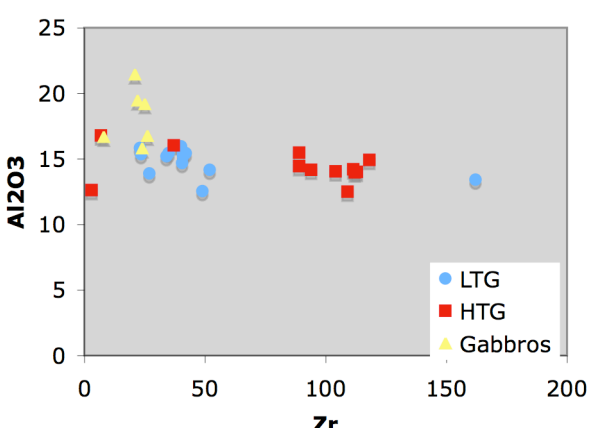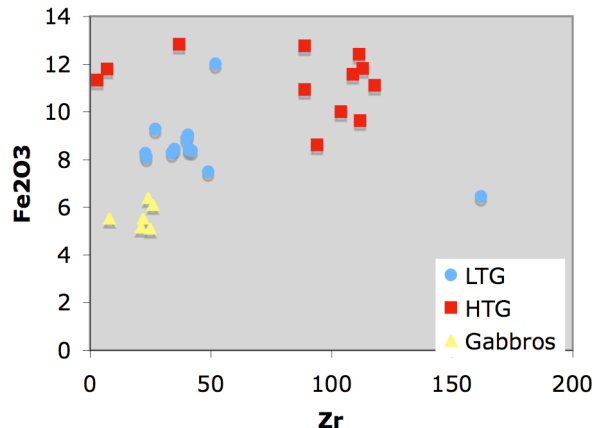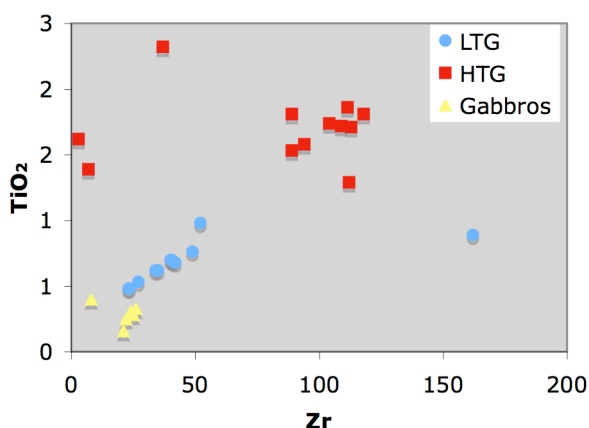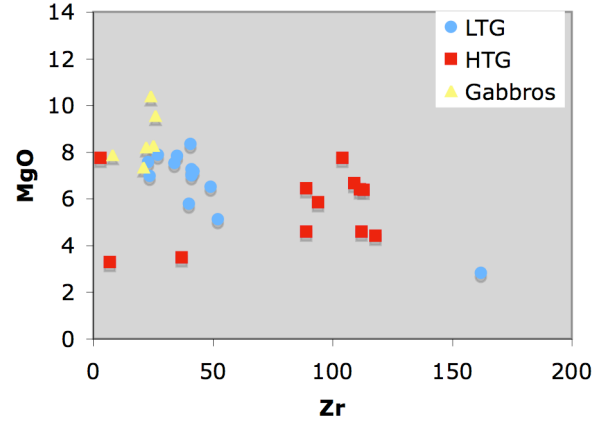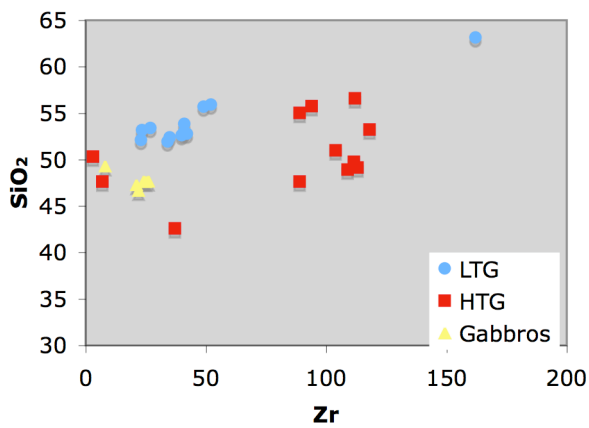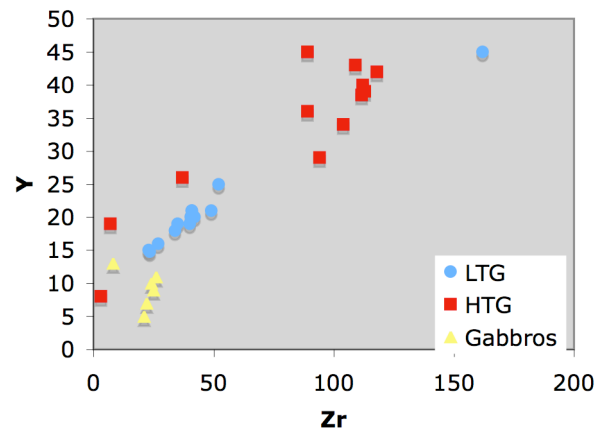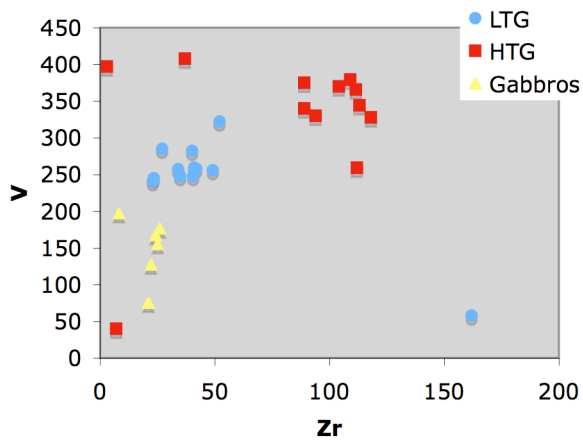
## LA-ICPMS
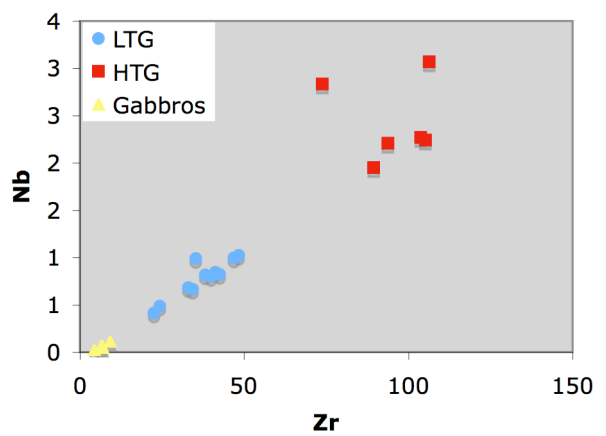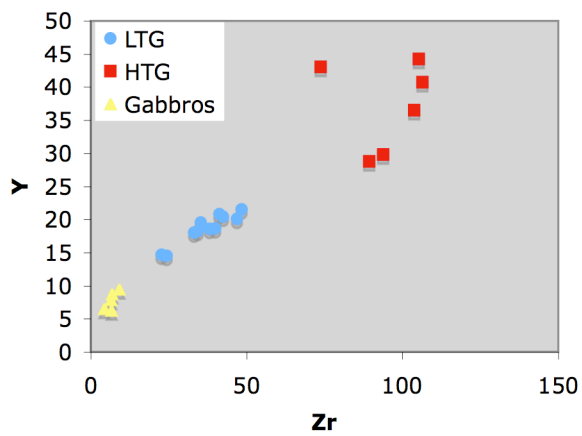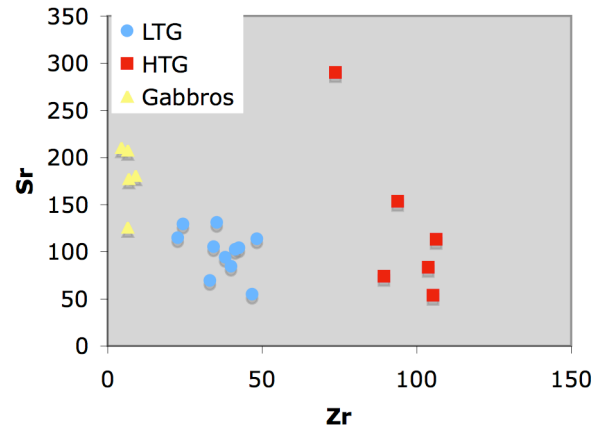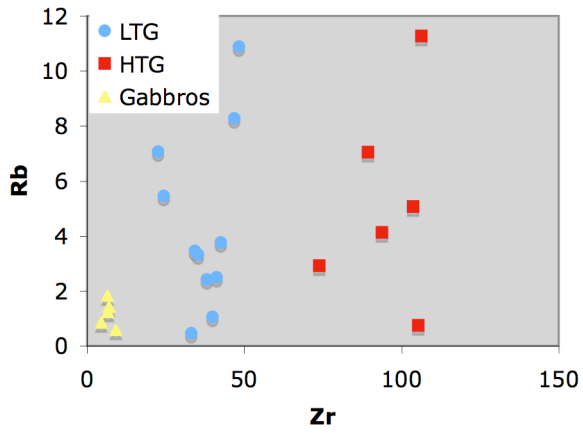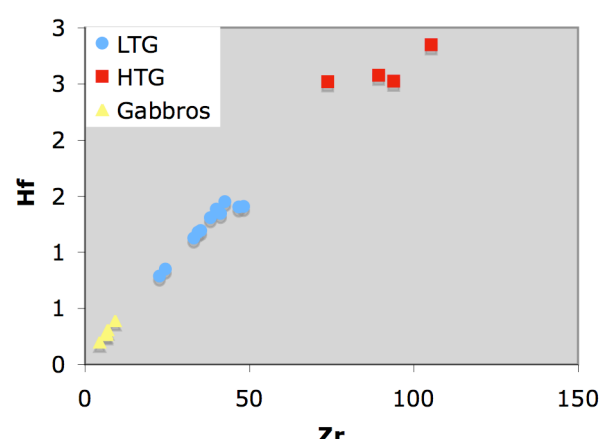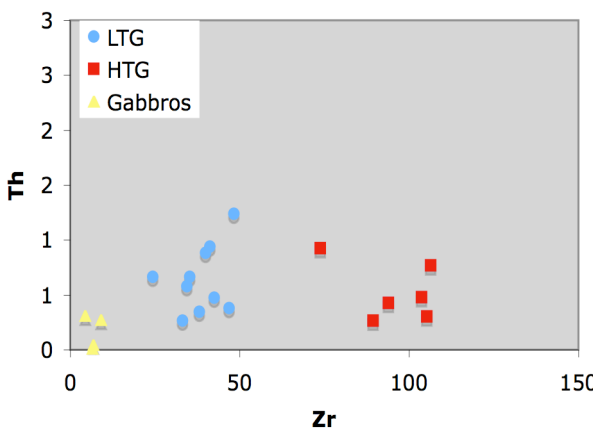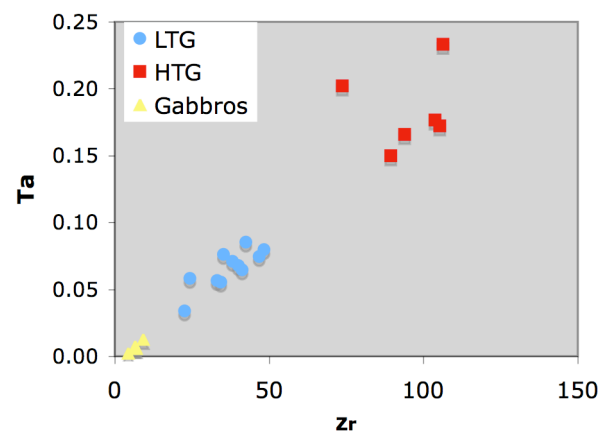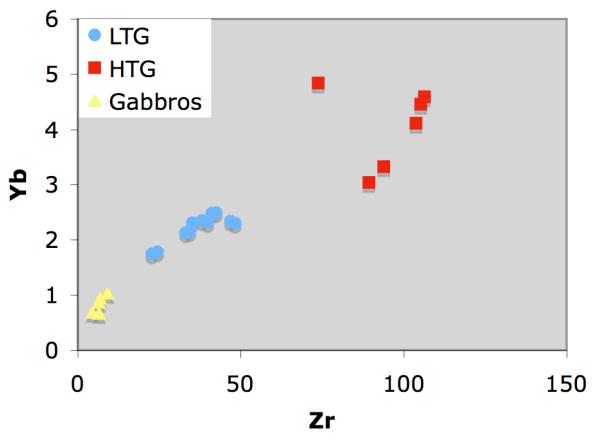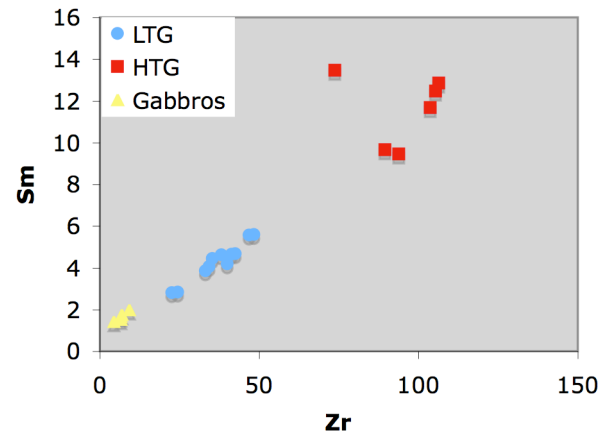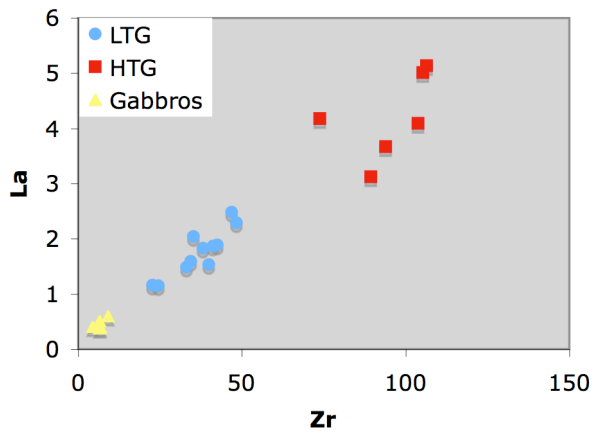
# Thessaloniki

## X.R.F.
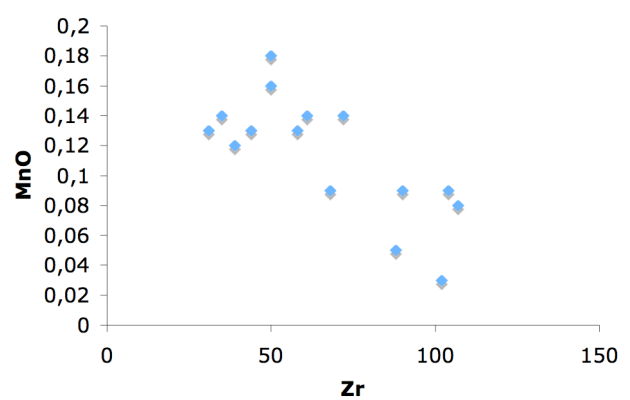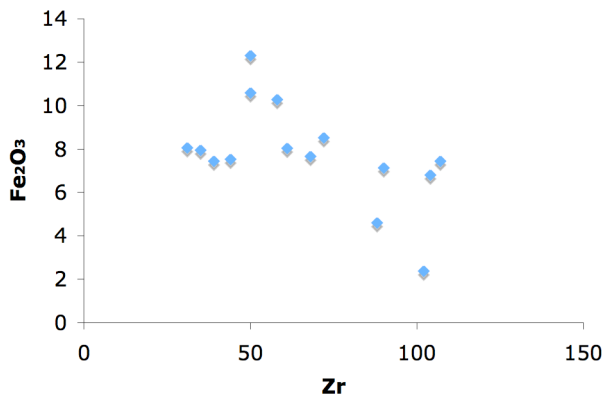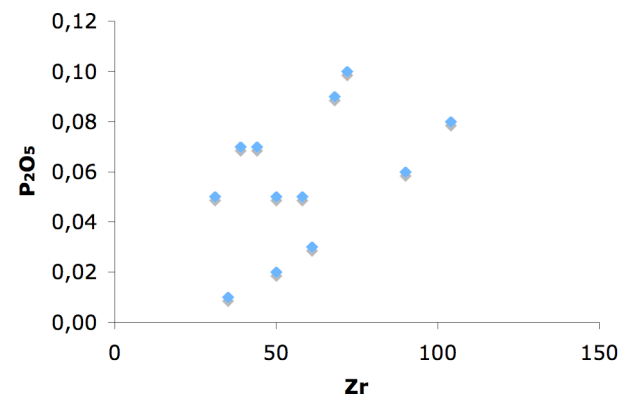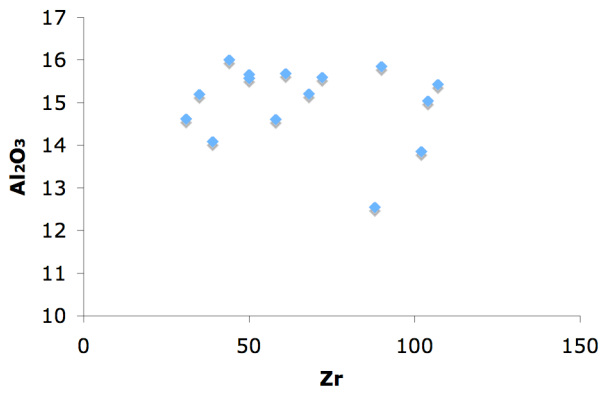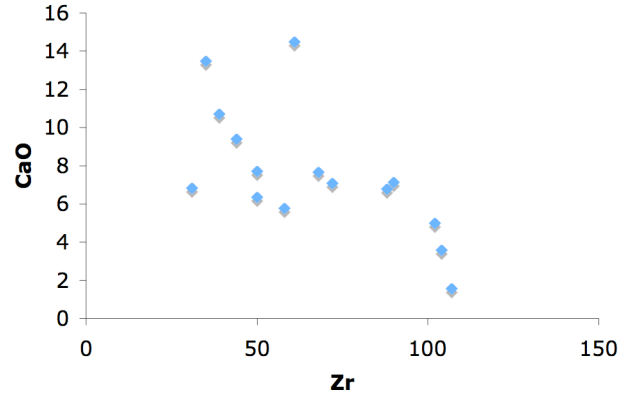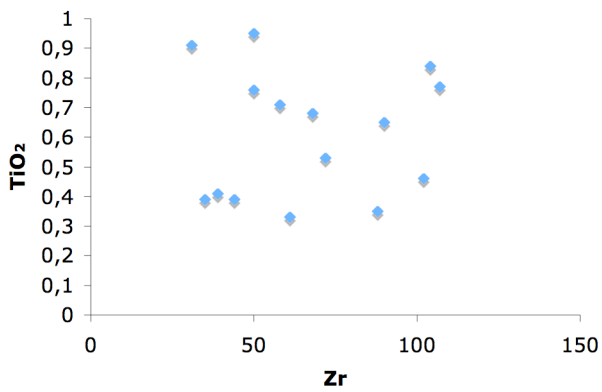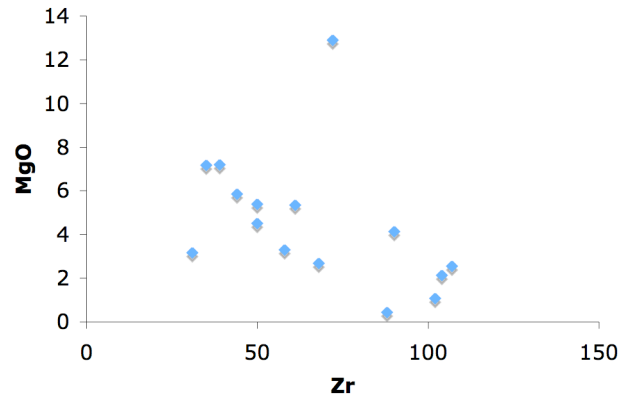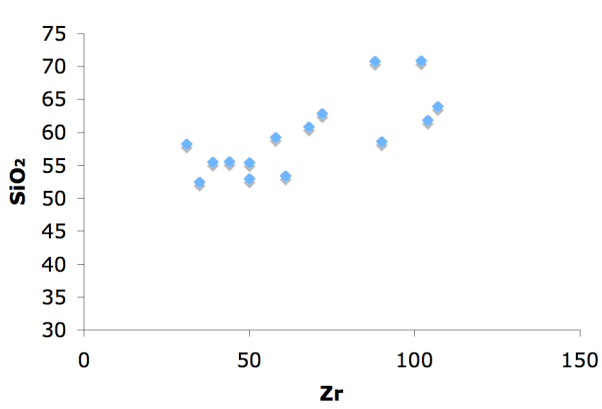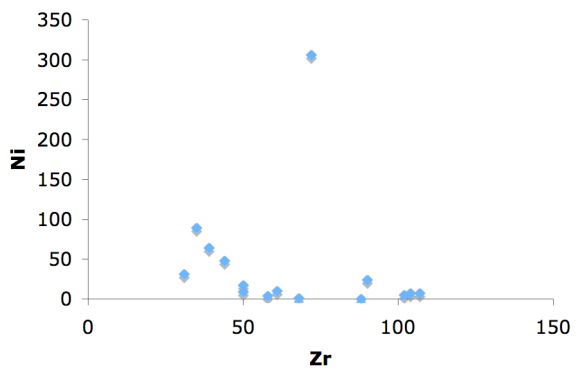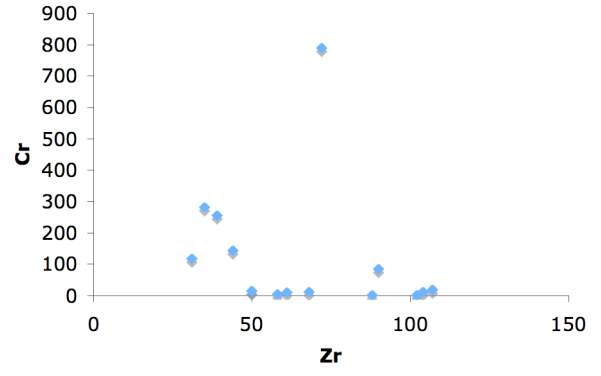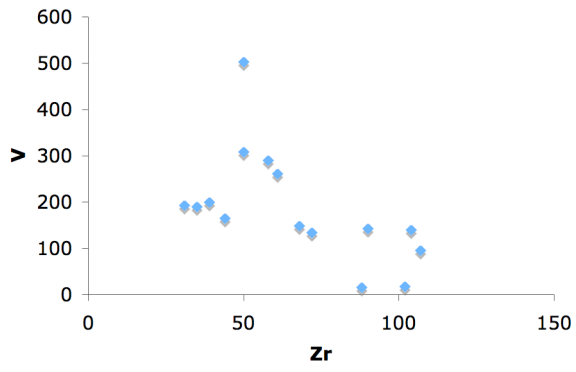
## LA-ICPMS
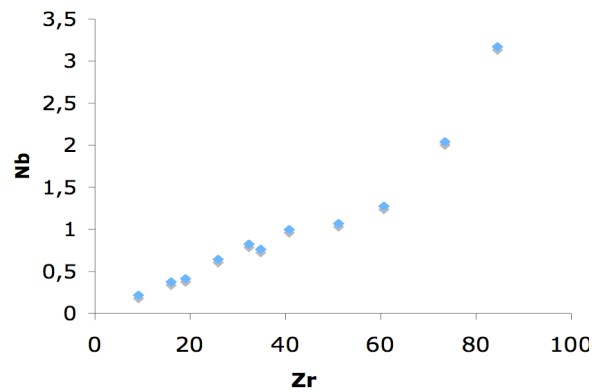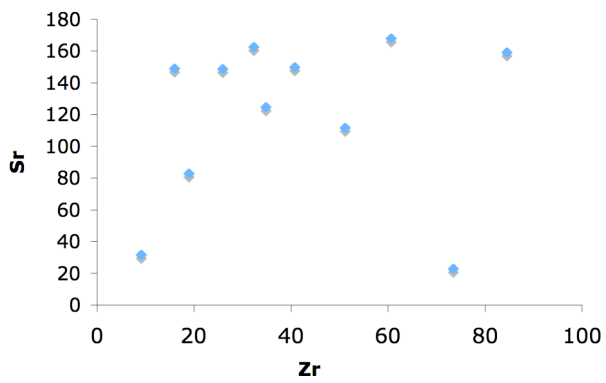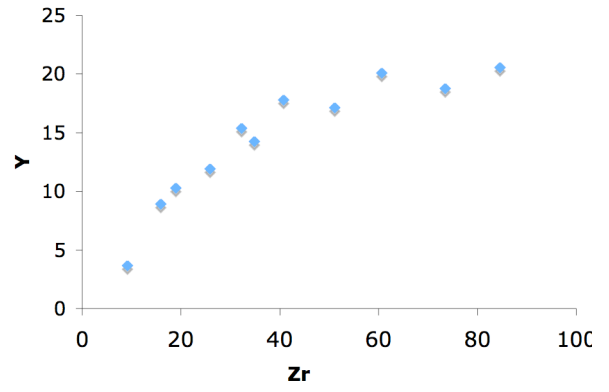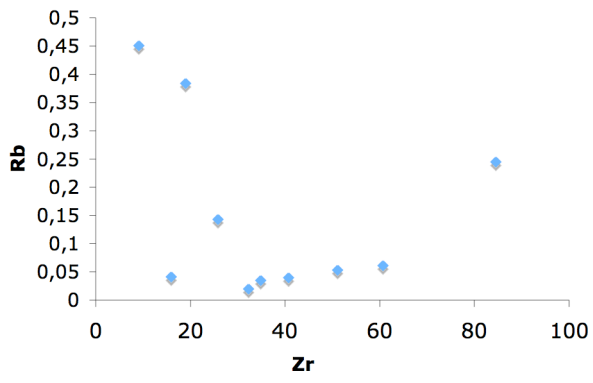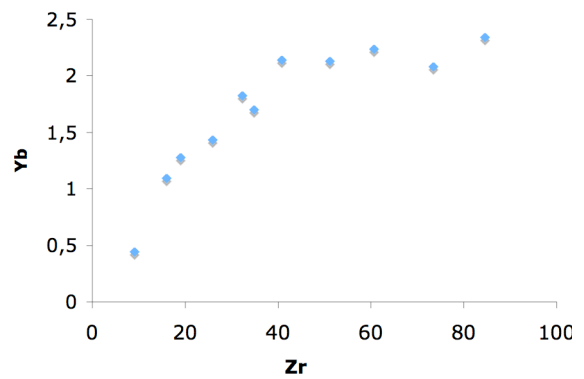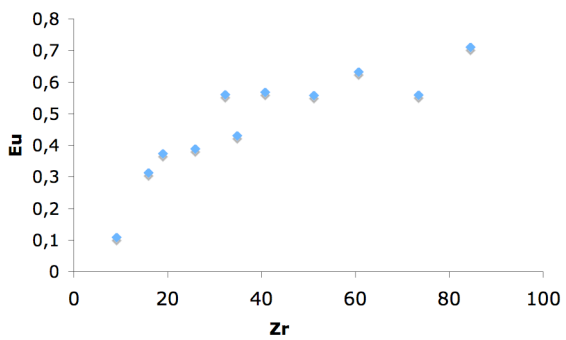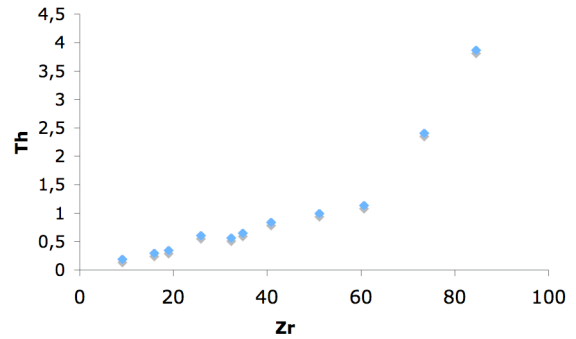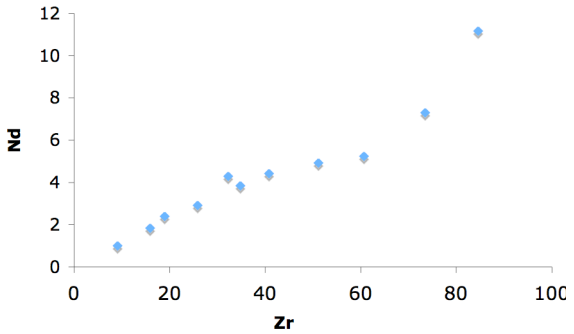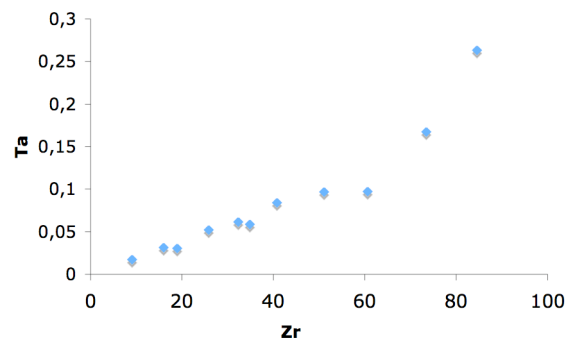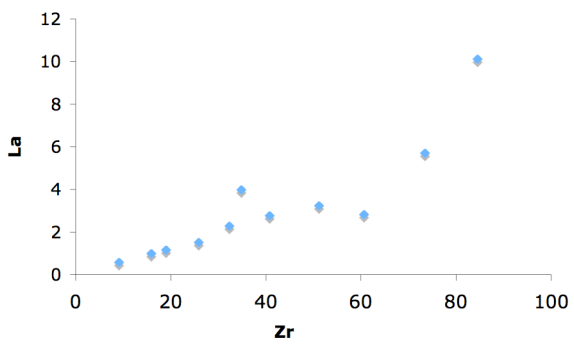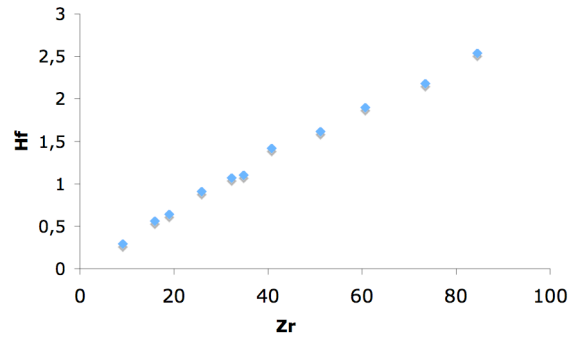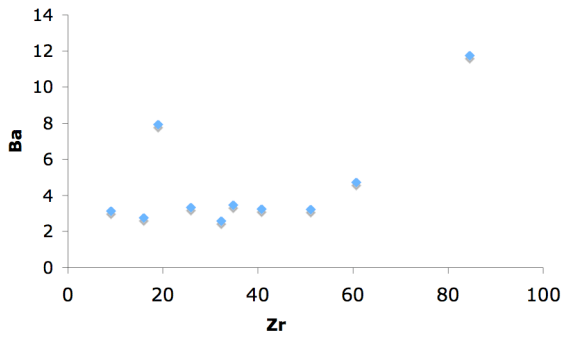
# Sithonia and Kassandra Ophiolite

## X.R.F.
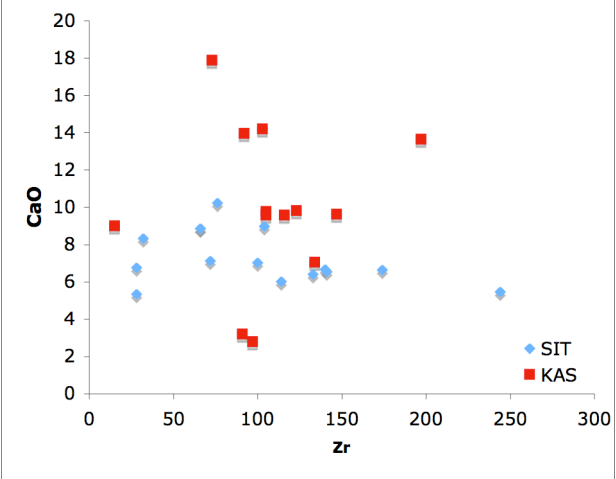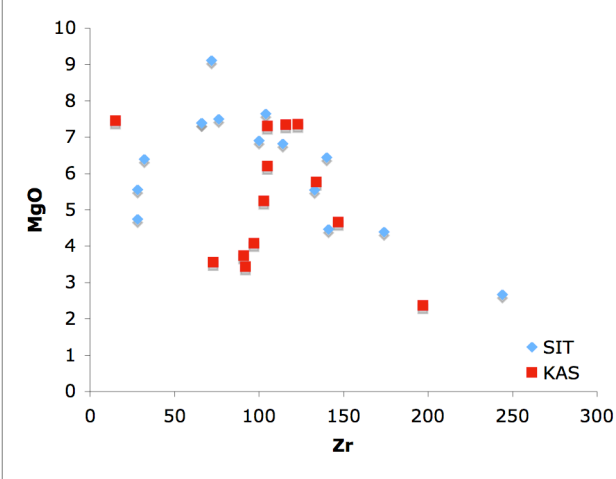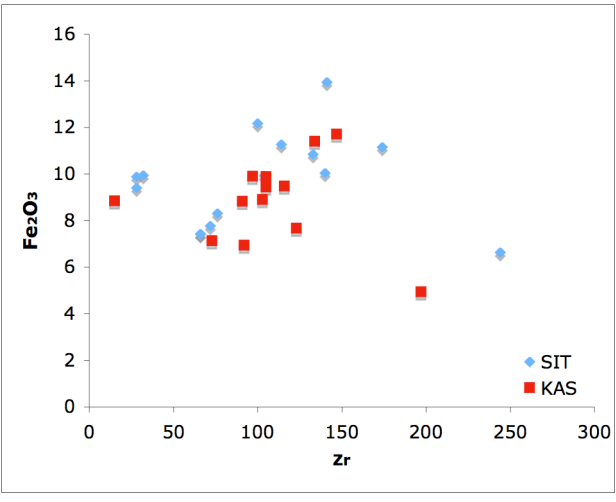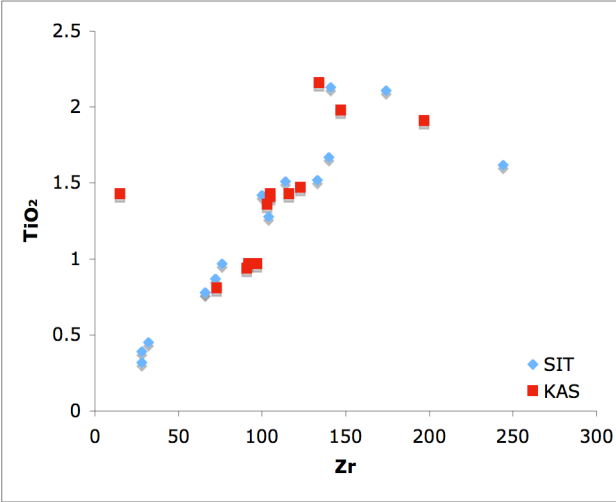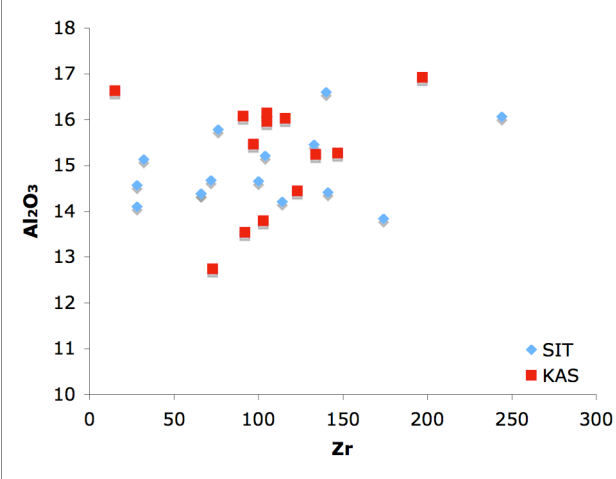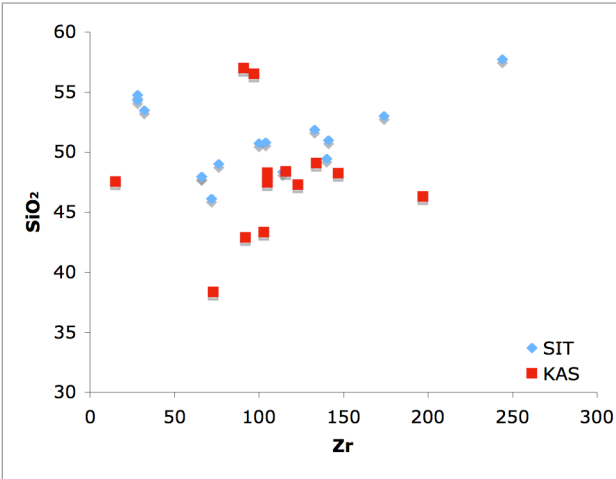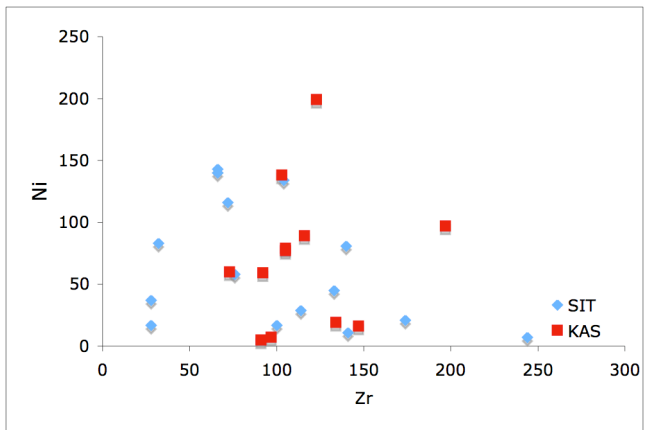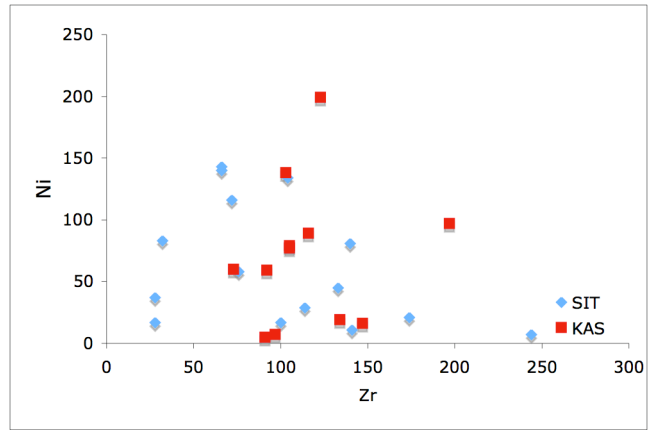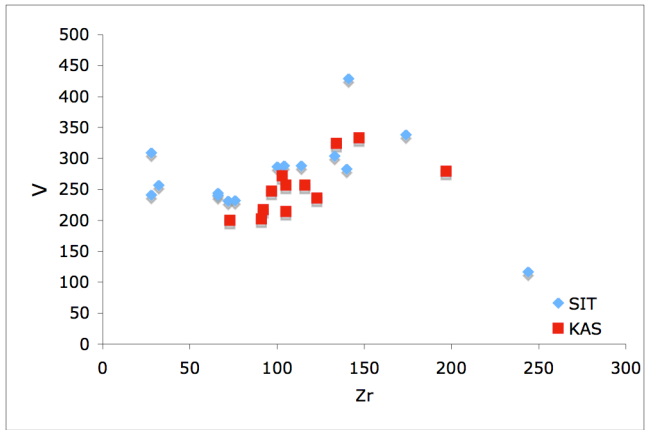
# LA-ICPMS

# Guevguely Ophiolite

Gabbro (Skra)

Gabbro (Skra)

Diorite

Gabbro (Skra)

Basaltic Dyke

Sheeted Dykes (Evzonoi)

Basaltic Dyke (Evzonoi)

Chilled margin

Pillow - lavas (Evzonoi)

Mafic xenolith in Rhyolite (Eyzonoi)

Rhyolitic Dykes

Mafic Dykes (Eyzonoi)

# Oraeokastro Ophiolite



limestones

phyllites

Oraeokastro Ophiolite

Contact between the Ophiolite and the limestones

Quartenary deposits

limestones

phyllites

Lavas

pillow-like lavas

sheeted dykes

leucocratic differenciates

Gabbro

Basaltic Dyke

epidosite network

# Thessaloniki



excavation front

typical outcrop of the sheeted dykes



ponds of leucocratic differenciates

Thessaloniki



foliated diorite

Chortiatis Magmatic Suite
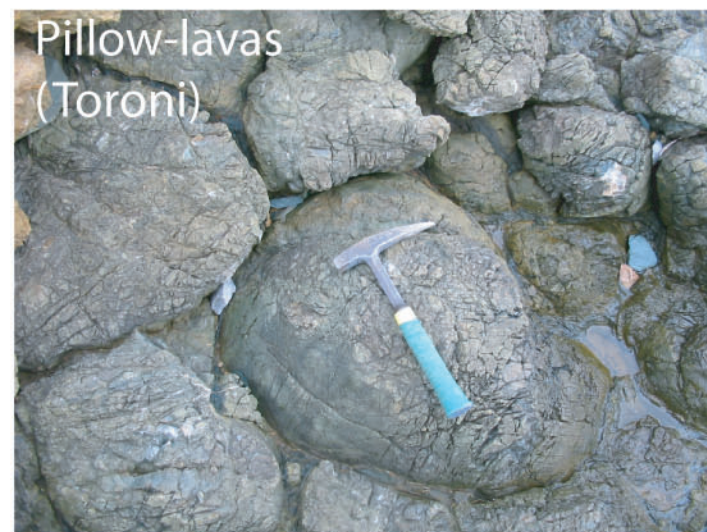
Sheeted dyke complex in Pounta

Pillow-lavas
(Toroni)

Sithonia
and
Kassandra
Ophiolites

Pillow-lavas (Kassandra)

massive-lavas (Kassandra)

weathered pillow-lavas

(Kassandra)

massive-lavas (Kassandra)

# Curriculum Vitae

---

**Name**                                : **Panagiotis**

**Surname**                             : **Zachariadis**

**Father's name and surname**   : **Theodoros Zachariadis**

**Mother's name and surname**  : **Soultana Masoura**

---

**14 September 1976**     Born in Thessaloniki, Hellas.

**1982-1988**     Primary School, Thessaloniki, Hellas.

**1988-1994**     Secondary School, Thessaloniki, Hellas.

**1995-2000**     Geology studies, School of Geology, Faculty of  Sciences, Aristotle University of Thessaloniki, Hellas.

**2000-2002**     Postgraduate Studies in Petrology and Geochemistry, School of Geology, Faculty of Sciences, Aristotle University of Thessaloniki, Hellas.

**2002-2007**     Ph.D. studies, Institut für Geowissenschaften, Johannes Gutenberg Universität, Mainz, Germany.